



**GUILAINE MARQUES
JARIA**

**PRODUÇÃO DE ADSORVENTES À BASE DE
RESÍDUOS PARA A REMOÇÃO DE FÁRMACOS DA
ÁGUA: ATIVAÇÃO QUÍMICA E MODIFICAÇÃO**

**PRODUCTION OF WASTE-BASED ADSORBENTS
FOR THE REMOVAL OF PHARMACEUTICALS FROM
WATER: CHEMICAL ACTIVATION AND
MODIFICATION**



Universidade de Aveiro
2020

**GUILAINE MARQUES
JARIA**

PRODUÇÃO DE ADSORVENTES À BASE DE RESÍDUOS PARA REMOÇÃO DE FÁRMACOS DA ÁGUA: ATIVAÇÃO QUÍMICA E MODIFICAÇÃO

PRODUCTION OF WASTE-BASED ADSORBENTS FOR THE REMOVAL OF PHARMACEUTICALS FROM WATER: CHEMICAL ACTIVATION AND MODIFICATION

Tese apresentada à Universidade de Aveiro para cumprimento dos requisitos necessários à obtenção do grau de Doutor em Química, realizada sob a orientação científica do Doutor Valdemar Inocêncio Esteves, Professor Auxiliar do Departamento de Química da Universidade de Aveiro, da Doutora Vânia Maria Amaro Calisto, Investigadora Auxiliar do Departamento de Química da Universidade de Aveiro, e da Doutora Marta Otero Cabero, Investigadora Principal do Departamento de Ambiente e Ordenamento da Universidade de Aveiro.

FCT Fundação para a Ciência e a Tecnologia
MINISTÉRIO DA CIÊNCIA, TECNOLOGIA E ENSINO SUPERIOR



UNIÃO EUROPEIA
Fundo Social Europeu



REPÚBLICA
PORTUGUESA

Apoio financeiro da FCT através de Fundos Nacionais, FSE e União Europeia, no âmbito do POCH – Programa Operacional Capital Humano. Apoio via Bolsa de Doutoramento (SFRH/BD/138388/2018).

Cofinanciado por:



PROGRAMA OPERACIONAL COMPETITIVIDADE E INTERNACIONALIZAÇÃO



UNIÃO EUROPEIA
Fundo Europeu
de Desenvolvimento Regional

FCT Fundação para a Ciência e a Tecnologia
MINISTÉRIO DA CIÊNCIA, TECNOLOGIA E ENSINO SUPERIOR

Apoio financeiro dos projetos PTDC/AAG-TEC/1762/2014 (RemPharm) e POCI-01-0145-FEDER-028598 (WasteMAC), financiados pelo FEDER, através do PT2020 Partnership Agreement e Compete 2020, e por fundos nacionais (OE), através da FCT/MCTES.

Dedico este trabalho aos meus pais, à minha irmã e ao meu sobrinho

o júri

presidente

Doutor Vítor António Ferreira da Costa
Professor Catedrático, Universidade de Aveiro

Doutora Maria Arminda Costa Alves
Professora Catedrática, Universidade do Porto

Doutora Ana Sofia Dias Mestre
Investigadora Auxiliar, Universidade de Lisboa

Doutora Angelina Lopes Simões Pena
Professora Associada com Agregação, Universidade de Coimbra

Doutor João António Baptista Pereira de Oliveira
Professor Associado, Universidade de Aveiro

Doutora Vânia Maria Amaro Calisto
Equiparada a Investigadora Auxiliar, Universidade de Aveiro (coorientadora)

agradecimentos

Agradeço aos meus orientadores pela orientação científica, ajuda e confiança que sempre mostraram. Ao Professor Valdemar agradeço por me ter acolhido no seu grupo de investigação como bolsista e aluna de doutoramento e também pela motivação, inteira disponibilidade de ajuda e apoio durante todo o meu percurso. À Doutora Marta Otero, agradeço a sua grande e valiosa ajuda e motivação em todos os trabalhos, e também a sua amizade. À Doutora Vânia Calisto, um agradecimento especial porque foi quem esteve mais diretamente comigo no laboratório, ajudando-me e apoiando-me sempre que precisei. Agradeço, ainda, pela oportunidade de trabalhar nos seus projetos de investigação e também toda a confiança, motivação e amizade.

Agradeço ao projeto RemPharm (PTDC/AAG-TEC/1762/2014), com o qual iniciei e realizei a maior parte deste projeto de doutoramento. Agradeço o financiamento da Fundação para a Ciência e a Tecnologia, via bolsa de doutoramento (SFRH/BD/138388/2018), apoiado por Fundos Nacionais, Fundo Social Europeu (FSE), Programa Operacional de Capital Humano (POCH) e União Europeia. Agradeço, ainda, ao projeto WasteMAC (POCI-01-0145-FEDER-028598).

Um agradecimento a todas as pessoas e instituições que colaboraram na, e para, a concretização deste projeto. Ao Professor Doutor João Oliveira, à Doutora Mirtha Lourenço e à Doutora Paula Ferreira pelas colaborações e valiosa ajuda na realização dos trabalhos experimentais da otimização da produção e da funcionalização de carvão ativado. À Doutora Patrícia Silva pela colaboração nos trabalhos laboratoriais. À Doutora Maria Victoria Gil e ao Doutor Sérgio Santos pela colaboração nas análises para a caracterização física e química dos materiais. Ao Engenheiro Milton Fontes e aos seus colaboradores pela disponibilidade na recolha de águas de efluente.

Agradeço aos meus colegas de grupo e de laboratório pelos bons tempos que passámos no laboratório, onde imperou sempre a boa disposição e o espírito de cooperação e de entreaajuda.

Agradeço aos meus amigos, aos que sempre o foram, e continuam a ser, e aos que se tornaram ao longo deste período, pelos bons e divertidos momentos e por todo o apoio e amizade.

Um agradecimento muito especial à minha família, pai, mãe, irmã, cunhado e sobrinho, pelo carinho, apoio e confiança que sempre me transmitiram ao longo da vida.

Muito obrigada.

palavras-chave

valorização de resíduos industriais; lamas da indústria da pasta e do papel; carvão ativado; pirólise; ativação química; adsorção; adsorção em colunas de leito-fixo; funcionalização; termodinâmica de adsorção; contaminantes emergentes

resumo

O desenvolvimento sustentável da sociedade implica a adoção de estratégias ligadas à gestão dos resíduos e sua valorização (numa perspectiva de economia circular) e ao tratamento de efluentes (nomeadamente, para a remoção de fármacos da água). Sendo o processo de adsorção por carvão ativado (CA) um método bem estabelecido para o tratamento de águas, este trabalho incide sobre a produção de CA a partir de resíduos, nomeadamente lamas da indústria da pasta e do papel, para a remoção de fármacos da água. Esta abordagem pretende proporcionar uma solução integrada nos dois desafios ambientais anteriormente referidos.

Comparativamente com as lamas biológicas (LB), as lamas primárias (LP) da indústria da pasta e do papel, mostraram ter um grande potencial para a produção de adsorventes à base de carvão. A partir de LP, e usando um processo de ativação química e pirólise, foi possível produzir CA, quer na forma de pó, quer na forma granular (usando um agente aglomerante) com elevadas áreas superficiais (S_{BET}) (comparáveis às de CA comerciais da mesma granulometria). Os CA produzidos em pó apresentaram, em sistemas descontínuos de adsorção, capacidades de adsorção para os fármacos carbamazepina (CBZ), sulfametoxazol (SMX) e paroxetina (PAR), da mesma ordem de grandeza que os CA comerciais. Contudo, quando aplicados em matrizes de efluente real, observam-se variações na capacidade de adsorção dos CA produzidos para os fármacos em estudo, principalmente no caso do SMX, que diminuiu, e da PAR, que aumentou.

O CA granular produzido apresentou, em sistemas descontínuos de adsorção, menor capacidade de adsorção para os três fármacos CBZ, SMX e PAR, do que o CA granular comercial de referência. Também neste caso, se verificou uma redução da capacidade de adsorção da CBZ e do SMX em matrizes de efluente real. Estudos realizados em colunas de leito-fixo (modo contínuo) mostraram que o CA granular produzido apresentou maior volume de rutura e maior capacidade de adsorção da CBZ para o menor fluxo. Verificou-se, ainda, a redução da capacidade de adsorção com o aumento da complexidade da matriz aquosa (água destilada > efluente real > soluções multicomponente - com os três fármacos - em efluente).

A aplicação de diferentes metodologias de modificação ou funcionalização da superfície dos CA em pó mostrou ser uma abordagem interessante, observando-se um aumento de seletividade de alguns CA funcionalizados para alguns dos fármacos em estudo, apesar da redução geral da S_{BET} destes. Em suma, este trabalho demonstra o potencial das LP da indústria papelreira para a produção de CA alternativos aos CA comerciais, em particular para a formulação em pó, e para a sua aplicação na remoção de fármacos das águas.

keywords

Valorization of industrial residues; paper mill sludge; activated carbon; pyrolysis; chemical activation; adsorption; fixed-bed adsorption systems; functionalization; adsorption thermodynamics; emerging contaminants

abstract

The sustainable development of society implies the adoption of strategies related to waste management and valorization (in a circular economy perspective) and to effluent treatment (namely for the removal of pharmaceuticals from water). Being adsorption by activated carbon (AC) a well-established method for water treatment, this work focuses on the production of AC using residues, namely sludge from pulp and paper industry, for the removal of pharmaceuticals from water. This approach aims to foster an integrated solution for the two environmental issues involved in this work.

Primary pulp and paper mill sludge (PS) showed a great potential to produce carbon-based adsorbents, relatively to biological sludge (BS). Through the use of PS and a production process involving chemical activation and pyrolysis, it was possible to produce AC in both powdered and granular (using a binder agent) forms, with high surface areas (S_{BET}) (similar to those of commercial AC with the same granulometry). The produced powdered AC presented, in batch adsorption systems, adsorption capacities for the pharmaceuticals carbamazepine (CBZ), sulfamethoxazole (SMX) and paroxetine (PAR), in the same magnitude of commercial AC. However, when applied in wastewater matrix, variations in the adsorption capacity of the produced AC for the studied pharmaceutical was observed, namely in the case of SMX, which decreased, and PAR, that increased.

The produced granular AC showed, in batch adsorption systems, lower adsorption capacity for the three pharmaceuticals CBZ, SMX, and PAR, than the commercial granular AC used as reference. Also, in this case, a reduction in the adsorption capacity for CBZ and SMX was observed for wastewater matrices. In fixed-bed column studies (continuous mode) the produced granular AC presented a higher breakthrough volume and adsorption capacity for CBZ for the lower flow-rate. Also, it was observed a reduction of the adsorption capacity with the increase of the complexity of the aqueous matrix (distilled water > wastewater > multicomponente solutions – with the three pharmaceuticals – in wastewater).

The application of different functionalization methods to the powdered AC surface showed to be an interesting approach, evidencing an increase in the selectivity of some functionalized AC for some of the pharmaceuticals under study, despite the general reduction in their S_{BET} .

Concluding, this work demonstrates the potential of PS from pulp and paper mill industry to produce alternative AC, particularly in the powdered form, to be applied in the removal of pharmaceuticals from water.

CONTENTS

Chapter 1

<i>Overview</i>	1
1.1. Motivation	3
1.2. Objectives.....	4
1.3. Thesis layout	6
1.4. References	8

Chapter 2

<i>Introduction</i>	11
2.1. Pulp and paper mills and the challenges of waste management.....	13
2.2. Activated Carbon	14
2.2.1. Activated carbon production	14
2.2.2. Structure and surface chemistry	16
2.2.2.1. Porosity.....	16
2.2.2.2. Surface chemistry of carbon adsorbents.....	17
2.2.3. Alternative raw materials used in the production of activated carbon	19
2.3. Pharmaceuticals occurrence and removal from wastewater.....	22
2.4. References	27

Chapter 3

<i>Viability of using pulp and paper mill sludge to produce carbon-based adsorbents</i>	37
3.1. Contextualization	39
3.2. Materials and Methods	41
3.2.1. Factory description and sludge production	41
3.2.2. Sludge collection and conditioning	41
3.2.3. Carbon adsorbents production.....	42
3.2.3.1. Pyrolysis	42
3.2.3.2. Washing.....	42

3.2.4. Methods for characterization of raw materials and carbon adsorbents	42
3.2.5. Variability of the carbon adsorbents production process	43
3.3. Results and Discussion	43
3.3.1. Characterization of raw materials and carbon adsorbents	43
3.3.1.1. Total organic carbon (TOC) and inorganic carbon (IC)	43
3.3.1.2. Fourier transform infrared spectroscopy with attenuated total reflectance (ATR-FTIR)	46
3.3.1.3. Specific surface area (S_{BET})	48
3.3.1.4. Proximate analysis	50
3.3.2. Production of adsorbent materials from paper mill sludge: practical implications	51
3.3.2.1. Variability of the carbon adsorbents production process	51
3.3.2.2. Impact of the raw material characteristics in the production of carbon adsorbents	52
3.4. Conclusions	53
3.5 References	55

Chapter 4

<i>Optimization of the production of activated carbon using paper mill sludge as raw material</i>	59
4.1. Contextualization	61
4.2. Materials and Methods	62
4.2.1. Chemicals and reagents	62
4.2.2. Preparation of activated carbons – Full factorial design and statistical analysis	62
4.2.3. Adsorption tests	64
4.2.4. Methods for physicochemical characterization of the activated carbons	64
4.3. Results and Discussion	65
4.3.1. Full factorial design: responses	65
4.3.2. Full factorial design: model fitting and statistical analysis	66
4.3.3. Physical and chemical characterization of the selected activated carbons	72
4.3.3.1. Proximate and ultimate analysis	72
4.3.3.2. Point of zero charge (pH_{pzc}) and surface functional groups	73
4.3.3.3. Specific surface area (S_{BET})	74
4.3.3.4. Scanning electron microscopy (SEM)	75
4.4. Conclusions	75

4.5. References	77
-----------------------	----

Chapter 5

<i>Performance of primary paper mill sludge-based powdered activated carbon in the removal of pharmaceuticals from wastewater</i>	79
---	----

5.1. Contextualization	81
------------------------------	----

5.2. Materials and Methods	82
----------------------------------	----

5.2.1. Chemical and reagents	82
------------------------------------	----

5.2.2. Preparation of the alternative activated carbon (AC3)	82
--	----

5.2.3. Methods for characterization of the alternative activated carbon (AC3) and the commercial activated carbon (CAC)	82
---	----

5.2.4. Wastewater sampling	83
----------------------------------	----

5.2.5. Adsorption experiments	83
-------------------------------------	----

5.2.5.1. Adsorption kinetics	83
------------------------------------	----

5.2.5.2. Adsorption equilibrium	84
---------------------------------------	----

5.3. Results and Discussion	85
-----------------------------------	----

5.3.1. Activated carbons characterization	85
---	----

5.3.2. Wastewater samples' characterization	86
---	----

5.3.3. Adsorption kinetics	87
----------------------------------	----

5.3.4. Adsorption equilibrium	90
-------------------------------------	----

5.4. Conclusions	97
------------------------	----

5.5. References	98
-----------------------	----

Chapter 6

<i>Development of a primary paper mill sludge-based a granular activated carbon and its application in the removal of pharmaceuticals from water</i>	103
--	-----

6.1. Contextualization	105
------------------------------	-----

6.2. Materials and Methods	106
----------------------------------	-----

6.2.1. Chemicals and reagents	106
-------------------------------------	-----

6.2.2. Production of a granular activated carbon from primary paper mill sludge and a binder agent	107
--	-----

6.2.3. Methods for physicochemical characterization of the produced granular activated carbon (PSA-PA) and the commercial granular activated carbon (GACN)	107
--	-----

6.2.4. Wastewater sampling	108
6.2.5. Batch adsorption experiments with the produced granular activated carbon (PSA-PA) and the commercial granular activated carbon (GACN)	109
6.3. Results and Discussion	110
6.3.1. Physicochemical characterization of the produced granular activated carbon (PSA-PA) and the commercial granular activated carbon (GACN)	110
6.3.1.1. Chemical characterization	110
6.3.1.2. Physical characterization	115
6.3.2. Batch adsorption experiments with the produced granular activated carbon (PSA-PA) and the commercial granular activated carbon (GACN)	117
6.3.2.1. Wastewater samples' characterization.....	117
6.3.2.2. Kinetic studies	117
6.3.2.3. Equilibrium studies.....	119
6.4. Conclusions	124
6.5. References	125

Chapter 7

<i>Fixed-bed performance of primary paper mill sludge-based granular activated carbon for the removal of pharmaceuticals from water.....</i>	127
7.1. Contextualization.....	129
7.2. Materials and Methods	130
7.2.1. Chemicals and reagents.....	130
7.2.2. Wastewater sampling	130
7.2.3. Adsorption studies in fixed-bed systems using the granular activated carbon PSA-PA as adsorbent	130
7.2.3.1. Fixed-bed adsorption of pharmaceuticals.....	131
7.2.3.2. Regeneration of exhausted granular activated carbon PSA-PA	131
7.2.3.3. Fixed-bed column data analysis and mathematical breakthrough fitting models.....	132
7.3. Results and Discussion	134
7.3.1. Wastewater sample's characterization	134
7.3.2. Fixed-bed adsorption experiments with the granular activated carbon PSA-PA	134
7.3.2.1. Adsorption of carbamazepine from distilled water and wastewater at different flow rates.....	134

7.3.2.2. Adsorption of carbamazepine, sulfamethoxazole, and paroxetine from single and ternary solutions in wastewater	139
7.3.3. Regeneration and adsorption onto granular activated carbon PSA-PA	141
7.3.4. Comparison with other studies assessing the removal of carbamazepine, sulfamethoxazole, and paroxetine in fixed-bed reactors.....	144
7.4. Conclusions	145
7.5. References	146

Chapter 8

<i>Surface functionalization of waste-based activated carbon and its effect on the removal of six pharmaceuticals from water</i>	149
8.1. Contextualization	151
8.2. Materials and Methods	152
8.2.1. Chemical and reagents	152
8.2.2. Material synthesis	153
8.2.2.1. Waste-based activated carbon (AC3) synthesis.....	153
8.2.2.2. Functionalization of the alternative activated carbon (AC3).....	153
8.2.3. Methods for characterization of the synthesized materials	156
8.2.4. Adsorptive removal of pharmaceuticals from water	156
8.3. Results and Discussion.....	158
8.3.1. Characterization of the synthesized materials	158
8.3.2. Adsorptive removal of pharmaceuticals from water	166
8.4. Conclusions	172
8.5. References	174

Chapter 9

<i>Effects of thiol functionalization of a waste-derived activated carbon on the adsorption of sulfamethoxazole from water: kinetic, equilibrium and thermodynamics studies</i>	179
9.1. Contextualization	181
9.2. Materials and Methods	181
9.2.1. Chemical and reagents	181
9.2.2. Material synthesis and characterization	182

9.2.2.1. Production of the alternative activated carbon (AC3) and thiol functionalized AC3 (AC-MPTMS).....	182
9.2.2.2. Methods for physicochemical characterization of the synthesized materials	182
9.2.3. Adsorption experiments	183
9.2.3.1. Kinetic studies	183
9.2.3.2. Equilibrium studies.....	184
9.2.3.3. Adsorption activation energy and thermodynamic parameters	184
9.3. Results and Discussion.....	186
9.3.1. Physicochemical characterization of the alternative activated carbon (AC3) and thiol functionalized AC3 (AC-MPTMS)	186
9.3.1.1. Specific surface area (S_{BET})	186
9.3.1.2. Scanning electron microscopy (SEM).....	187
9.3.1.3. X-Ray photoelectron spectroscopy (XPS).....	187
9.3.2. Adsorption of sulfamethoxazole onto the alternative activated carbon (AC3) and thiol functionalized AC3 (AC-MPTMS) - studies in buffered solutions at pH8 prepared in ultrapure water	190
9.3.2.1. Kinetic and equilibrium studies.....	190
9.3.2.2. Estimation of the activation energy and thermodynamic parameters	195
9.3.3. Evaluation of the functionalized activated carbon (AC-MPTMS) performance in the adsorption of sulfamethoxazole from wastewater.....	199
9.4. Conclusions	201
9.5. References	203

Chapter 10

<i>Final remarks and future work</i>	207
10.1. Final remarks.....	209
10.2. Future work	211

Appendix	213
-----------------------	-----

List of figures

Chapter 2

Figure 2.1. Schematic representation of the possible sources of water contamination by pharmaceuticals (based on Ebele et al. (2017) and Patel et al. (2019))..... 24

Chapter 3

Figure 3.1. Representation of total organic (TOC) and inorganic (IC) carbon for raw, pyrolysed and pyrolyzed and washed materials for all batches of both factories. 44

Figure 3.2. ATR-FTIR spectra of primary sludge (PS) and biological sludge (BS) and carbon adsorbents (P and PW materials) produced from them for both factories..... 46

Figure 3.3. Specific surface area (S_{BET}) for pyrolyzed (P) and pyrolysed and washed (PW) materials produced from the four batches of both primary (PS) and biological sludge (BS) of both factories. Mean values for each type of material are also shown. 49

Figure 3.4. Proximate analysis (*wr%*, dry basis) for raw, pyrolysed (P) and washed materials (PW). Presented values correspond to the mean from the four batches collected for each factory and type of sludge (MC – Moisture Content; A – Ash; VM – Volatile Matter; FC – Fixed Carbon). 50

Chapter 4

Figure 4.1. a) Cumulative percentages of adsorption for the three pharmaceuticals (SMX, CBZ, and PAR) and b) S_{BET} values for the produced AC and the commercial AC (PBFG4). 65

Figure 4.2. Probability plots for a) yield of production; b) the adsorption percentage of SMX; c) the adsorption percentage of CBZ; d) the adsorption percentage of PAR; e) TOC; and f) S_{BET} 68

Figure 4.3. Response surfaces for: a) yield of production; b) adsorption percentages for SMX (b1), CBZ (b2), and PAR (b3); c) S_{BET} (c1 – for the activating agent KOH, and c2 – for the activating agent K_2CO_3); and d) TOC. 69

Figure 4.4. Biplot of the principal component analysis (PCA). 71

Figure 4.5. a) Plot of pH_{pzc} values *versus* amount of total acidic surface groups for AC 3, 4, 6 and 7; b) Graphical representation of the amounts of the acidic and basic surface groups for AC 3, 4, 6 and 7. 73

Figure 4.6. SEM images at different magnifications (3 000x, 10 000x, 30 000x, and 50 000x): a) AC3; b) AC4; c) AC6; d) AC7. 75

Chapter 5

Figure 5.1. XPS analysis for AC3: a) survey spectrum; b) high-resolution spectrum of C1s; c) high-resolution spectrum of N1s; d) high-resolution spectrum of O1s. 87

Figure 5.2. Kinetic study of the adsorption of CBZ, SMX and PAR onto AC3 (■) and CAC (Δ) in a) ultrapure water and b) wastewater. Results were fitted to pseudo-first (full line) and pseudo-second (dash line) order kinetic models. 88

Figure 5.3. Equilibrium study of the adsorption of CBZ, SMX and PAR onto AC3 (■) and CAC (Δ) in a) ultrapure water and b) wastewater. Results were fitted to Langmuir (full line) and Freundlich (dash line) equilibrium models. 91

Chapter 6

Figure 6.1. ATR-FTIR spectra of a) PSA-PA and b) GACN. 111

Figure 6.2. XPS survey spectra and high-resolution spectra for C1s, O1s, and N1s, of a) PSA-PA and b) GACN. 114

Figure 6.3. Pore size distribution of PSA-PA and GACN. 115

Figure 6.4. Scanning electron microscopy (SEM) images for a) PSA-PA and b) GACN at magnifications of 300x, 3 000x, 10 000x and 50 000x. 116

Figure 6.5. Kinetic study of the adsorption of CBZ, SMX and PAR onto PSA-PA (■) and GACN (Δ) in a) ultrapure water and in b) wastewater. Results were fitted to pseudo-first (full line) and pseudo-second (dash line) order kinetic models. 118

Figure 6.6. Equilibrium study of the adsorption of CBZ, SMX and PAR onto PSA-PA (■) and GACN (Δ) in a) ultrapure water and in b) wastewater. Results considering the fitting to Langmuir (full line) and Freundlich (dash line) models are presented. 120

Chapter 7

- Figure 7.1.** Breakthrough curves and fittings of the experimental data to the Yan model for the adsorption of CBZ onto PSA-PA at flow rates of 4.3 L d⁻¹, 8.6 L d⁻¹, and 13 L d⁻¹, in a) distilled water and b) wastewater. 135
- Figure 7.2.** Breakthrough curves and fittings of the experimental data to the Yan model for the adsorption of CBZ, SMX, and PAR onto PSA-PA at flow rates of 4.3 L d⁻¹ from a) single and b) ternary solutions in wastewater. 139
- Figure 7.3.** Breakthrough curves and fittings of the experimental data to the Yan model for the fixed-bed adsorption of CBZ from distilled water for 3 cycles of PSA-PA utilization: cycle 0 – virgin PSA-PA; cycle 1 – after first regeneration; and cycle 2 – after second regeneration..... 142

Chapter 8

- Figure 8.1.** Schematic representation of the functionalization procedures: A – Direct amination; B – Organosilane grafting with APTES; C – Organosilane grafting with MPTMS; and D – functionalization with an organic polymer (COP-19, based on Mines et al. (2017)). 155
- Figure 8.2.** Pore size distribution of AC3 and functionalized AC. Pore width was obtained from the non-linear density functional theory (NLDFT). 159
- Figure 8.3.** SEM images of crushed samples of a) AC, b) AC-NH₂, and c) AC-MPTMS..... 160
- Figure 8.4.** ATR-FTIR spectra of AC3 and functionalized AC. 160
- Figure 8.5.** Raman spectra of AC3 and functionalized AC. X can be C, S, N, or O atoms. 161
- Figure 8.6.** XPS survey spectra and high-resolution XPS spectra of C1s, N1s, S2p+Si2s, and O1s for: a) AC-NH₂, b) AC-MPTMS, and c) AC3* (results from chapter 5)..... 163
- Figure 8.7.** TGA and DrTGA of a) AC3, b) AC-NH₂, c) AC-APTES, d) AC-MPTMS, and e) AC-COP. Note: Different scales in the secondary yy axis (DrTGA) were chosen in each figure for a better visualization of results..... 165
- Figure 8.8.** Adsorption of the six studied pharmaceuticals (CBZ, LOR, SMX, PIR, PAR and VEN) in different matrices (ultrapure water, ultrapure water at pH 7.6 and wastewater) onto the AC3 and the functionalized AC. Error bars correspond to the standard deviation (n=3)..... 167

Figure 8.9. PCA for the normalized adsorption percentages of pharmaceutical onto the five AC and the physicochemical properties of the pharmaceuticals (PC1 vs PC2 vs PC3 plots account for 95.56%, 95.22%, and 92.17% of the variability, for ultrapure water, ultrapure water with adjusted pH 7.6, and wastewater, respectively).....	168
Figure 8.10. Adsorption of the six studied pharmaceuticals in different matrices onto the AC3 and the functionalized AC, normalized to the S_{BET} for each AC. Error bars correspond to standard deviations ($n = 3$)......	170
Figure 8.11. PCA plots for the principal components PC1, PC2 and PC3. Ultrapure water, ultrapure water with adjusted pH 7.6 and wastewater are represented by the colored solid lines, dash lines and dotted lines, respectively. Black lines correspond to the physicochemical characteristics considered in this analysis.	171
 <i>Chapter 9</i>	
Figure 9.1. Pore size distribution determined for AC3 (grey line) and AC-MPTMS (dash black line).....	186
Figure 9.2. SEM images obtained for a) AC3 and b) AC-MPTMS at different magnifications (3 000x, 10 000x, 30 000x and 50 000x)......	187
Figure 9.3. XPS survey spectra and high-resolution spectra (with deconvolution) of C1s, O1s, N1s and Si2s+S2p determined for a) AC3 and b) AC-MPTMS.....	189
Figure 9.4. Fitting results from the kinetic studies on the adsorption of SMX onto AC3 and AC-MPTMS from buffered solution prepared in ultrapure water (pH 8) at three different temperatures: a) 15 °C, b) 25 °C, and c) 35 °C. Results were fitted to pseudo-first (full line) and pseudo-second (dash line) order kinetic models.....	191
Figure 9.5. Fitting results from the equilibrium studies on the adsorption of SMX onto AC3 and AC-MPTMS from buffered solution prepared in ultrapure water (pH 8) at three different temperatures a) 15 °C, b) 25 °C, and c) 35 °C. Results were fitted to Langmuir (full line) and Freundlich (dash line) models.	193
Figure 9.6. Plots of k_2 versus $1/T$ for the adsorption of SMX onto a) AC3 and b) AC-MPTMS.....	195
Figure 9.7. Plots of K_e versus $1/T$ for the adsorption of SMX onto a) AC3 and b) AC-MPTMS.....	199

Figure 9.8. Experimental results from the a) kinetic and b) equilibrium studies on the adsorption of SMX onto AC-MPTMS from wastewater (at 25 °C) together with the fittings to the considered models. 200

List of Tables

Chapter 1

Table 1.1. Physicochemical properties of the studied pharmaceuticals (based on PubChem (accessed in February 2019) and Calisto et al. (2015)).	5
---	---

Chapter 2

Table 2.1. Examples of wastes used as precursors in the production of alternative carbon adsorbents.	20
---	----

Chapter 3

Table 3.1. Total (TC, %) and inorganic carbon (IC, %) values (n=3) for raw, pyrolysed (P) and pyrolysed and washed (PW) materials. TOC was obtained by difference.	45
Table 3.2. Textural parameters of pyrolysed (P) and pyrolysed and washed (PW) materials.	49
Table 3.3. Proximate analysis (wt%, dry basis) for raw and pyrolysed and washed (PW) materials.	51

Chapter 4

Table 4.1. Analysis of variance (ANOVA) used for the fitted models to the experimental data.	63
Table 4.2. Codified variables and responses obtained for each of the sixteen activated carbons (AC) produced from paper mill sludge and for the commercial AC.	66
Table 4.3. Analysis of variance (ANOVA) of the obtained responses (least square method).	67
Table 4.4. General overview of the optimization results of full factorial design.	69
Table 4.5. Proximate and ultimate analysis of the precursor (PS) and the selected activated carbons (AC).	72
Table 4.6. Boehm's titrations and point of zero charge (pH_{pzc}) results.	73

Table 4.7. Textural parameters of the activated carbons AC3, AC4, AC6, and AC7. 74

Chapter 5

Table 5.1. Kinetic adsorption models considered for the fitting of the experimental kinetics. 84

Table 5.2. Adsorption isotherm models considered for the fitting of the experimental isotherms. 85

Table 5.3. pH, conductivity and TOC values for the effluent samples..... 86

Table 5.4. Fitting parameters of pseudo-first and pseudo-second order kinetic models to the experimental data for both carbons (AC3 and CAC) and the three pharmaceuticals (CBZ, SMX, and PAR) in ultrapure water and wastewater. 89

Table 5.5. Fitting parameters of Langmuir and Freundlich isotherm models to the experimental data for both carbons (AC3 and CAC) and the three pharmaceuticals (CBZ, SMX, and PAR) in ultrapure water and wastewater. 92

Table 5.6. Adsorption capacity of alternative waste-based adsorbents reported in literature for the removal of CBZ, SMX, and PAR. 95

Chapter 6

Table 6.1. Experimental conditions tested to produce a granular activated carbon (GAC) using primary papermill sludge (PS) as precursor, ammonium lignosulfonate (AL) as binder agent and different chemical activating agents (AA). 108

Table 6.2. Proximate and ultimate analyses for the produced (PSA-PA) and commercial (GACN) granular activated carbons. 111

Table 6.3. Amount of acidic and total basic functional groups of both granular activated carbons (PSA-PA and GACN) determined by Boehm’s titration. 112

Table 6.4. X-Ray photoelectron spectroscopy (XPS) results for PSA-PA and GACN. 113

Table 6.5. Textural characterization of PSA-PA and GACN. 115

Table 6.6. Properties of the wastewater samples. 117

Table 6.7. Fitting parameters of pseudo-first and pseudo-second order kinetic models to the experimental data for both carbons (PSA-PA and GACN) and the three pharmaceuticals (CBZ, SMX, and PAR) in ultrapure water and wastewater. 119

Table 6.8. Fitting parameters of Langmuir, Freundlich, and Sips isotherm models to the experimental data for both carbons (PSA-PA and GACN) and the three pharmaceuticals (CBZ, SMX, and PAR) in ultrapure water and wastewater. 121

Chapter 7

Table 7.1. Breakthrough models considered for the description of fixed-bed column studies..... 133

Table 7.2. Properties of the wastewater samples. 134

Table 7.3. Efficiency and mass transfer parameters determined from the breakthrough curves corresponding to the fixed-bed adsorption of pharmaceuticals onto PSA-PA in distilled water and wastewater. 137

Table 7.4. Fitting parameters of the Thomas, Yoon-Nelson, and Yan models to the experimental data of the fixed-bed adsorption of CBZ onto PSA-PA, at different flow rates. 138

Table 7.5. Fitting parameters of the Thomas, Yoon-Nelson and Yan models to the experimental data of the fixed-bed adsorption of CBZ, SMX and PAR onto PSA-PA from single and ternary solutions in wastewater at a flow rate of 4.3 L d^{-1} 141

Table 7.6. Textural parameters of PSA-PA used in the subsequent fixed-bed adsorption cycles: cycle 0 (virgin PSA-PA), cycle 1 (after first regeneration) and cycle 2 (after second regeneration) and of PSA-PA after use in the cycle 2..... 142

Table 7.7. Fitting parameters of the Thomas, Yoon-Nelson and Yan models to the experimental data of the fixed-bed adsorption of CBZ onto PSA-PA from distilled water after regeneration stages 1 and 2, at a flow rate of 4.3 L d^{-1} 143

Chapter 8

Table 8.1. Physicochemical properties of the additional studied pharmaceuticals (based on PubChem, accessed in February 2019). 157

Table 8.2. Textural properties of AC3 and functionalized AC..... 159

Table 8.3. Elemental analysis and point of zero charge (pH_{pzc}) results for AC3 and functionalized AC. 162

Table 8.4. X-Ray photoelectron spectroscopy (XPS) results for AC3*, AC-NH₂ and AC-MPTMS. 164

Chapter 9

Table 9.1. Textural properties of AC3 and AC-MPTMS. 186

Table 9.2. Fitting results from the kinetic studies on the adsorption of SMX onto AC3 and AC-MPTMS from buffered solutions prepared in ultrapure water (pH 8) at three different temperatures (15 °C, 25 °C and 35 °C). 192

Table 9.3. Fitting results from the equilibrium studies on the adsorption of SMX onto AC3 and AC-MPTMS from buffered solution prepared in ultrapure water (pH 8) at three different temperatures (15 °C, 25 °C and 35 °C). 194

Table 9.4. Studies involving the adsorption of sulfamethoxazole (SMX) onto powdered (PAC) or granular (GAC) activated carbons. 196

Table 9.5. Thermodynamic parameters calculated for the adsorption of SMX onto AC3 and AC-MPTMS. 198

Table 9.6. Fitting results for the kinetic and equilibrium studies on the adsorption of SMX onto AC-MPTMS from wastewater (at 25 °C). 200

Abbreviations

A	Ash
AA	Activating agent
AC	Activated carbon
AC3	Activated carbon produced from PS using the conditions of activating agent (KOH):PS ratio of 1:1 and maximum temperature of 800 °C during 150 min
AL	Ammonium lignosulfonate
ANOVA	Analysis of variance
AOP	Advanced oxidation processes
APTES	(3-aminopropyl)triethoxysilane
ATR-FTIR	Fourier transform infrared with attenuated total reflectance
BS	Biological paper mill sludge
BHJ	Barret-Joyned-Halenda
CAC	Commercial powdered activated carbon from Norit (SAE SUPER 8003.6)
CBZ	Carbamazepine
CEC	Contaminants of emerging concern
CELPA	Associação da Indústria Papeleira
CEPI	Confederation of European Paper Industries
COP	Covalent organic polymer
DA	Dubinin-Astakhov
DIPEA	Diisopropylethylamine
DMSO	Dimethyl sulfoxide
DR	Dubinin-Radushkevich
EBCT	Empty bed contact time
F1	Factory 1
F2	Factory 2
FBU	Fraction of bed utilization
FC	Fixed carbon
FFD	Full factorial design
GAC	Granular activated carbon
GACN	Commercial granular activated carbon from Norit
IC	Inorganic carbon
IR	Impregnation ratio
LOR	Lorazepam

Abbreviations

MC	Moisture content
MEKC	Micellar electrokinetic chromatography
MPTMS	(3-Mercaptopropyl)trimethoxysilane
MW	Molecular weight
NLDFT	Non-linear density functional theory
OC	Organic carbon
P	Pyrolyzed
PAC	Powdered activated carbon
PAR	Paroxetine
PBFG4	Powdered commercial AC from Chemviron (reference)
PC	Principal component
PCA	Principal component analysis
PIB	Produto Interno Bruto
PIR	Piroxicam
PS	Primary paper mill sludge
PSA	Polar surface area
PSA-PA	Granular activated carbon produced from primary paper mill sludge (PS)
PSD	Pore size distribution
PW	Pyrolyzed and washed
RSD	Relative standard deviation
RSM	Response surface methodology
SEM	Scanning electron microscopy
SMX	Sulfamethoxazole
TGA	Thermogravimetric analysis
TOC	Total organic carbon
UV-Vis	Ultraviolet-visible
VEN	Venlafaxine
VM	Volatile matter
WWTP	Wastewater treatment plant
XPS	X-Ray photoelectron spectroscopy

Symbols

A	Area above the breakthrough curve (d)
C_0	Initial concentration of adsorbate (mg L^{-1})
C_e	Residual concentration of adsorbate at equilibrium (mg L^{-1})
D	Average pore diameter (nm)
D_o	Overall desirability
d_i	Individual desirability
E_a	Activation energy (J mol^{-1})
F	Frequency factor
h	Bed height (cm)
h_{MTZ}	Height of mass transfer zone (cm)
k	Adsorption rate constant
k_{TH}	Thomas model rate constant ($\text{L d}^{-1} \text{mg}^{-1}$)
k_{YN}	Yoon-Nelson model rate constant (d^{-1})
k_1	Rate constant of pseudo-first order model (min^{-1})
k_2	Rate constant of pseudo-second order model ($\text{g mg}^{-1} \text{min}^{-1}$)
K_e^o	Thermodynamic equilibrium constant (dimensionless)
K_g	Isotherm equilibrium constant
K_F	Freundlich adsorption constant ($\text{mg}^{1-1/n} \text{L}^{1/n} \text{g}^{-1}$)
K_L	Langmuir equilibrium constant (L mg^{-1})
K_{ow}	Octanol-water partition coefficient
K_S	Sips isotherm constant (L mg^{-1}) ^N
L	Average micropore width (nm)
m	Mass of adsorbent (g)
n	Constant related to the degree of non-linearity of the Freundlich isotherm model
N	Parameter associated to the heterogeneity of the surface of the Sips isotherm model
pH_{pzc}	pH of the point of zero charge
pK_a	Acid dissociation constant
Q	Flow-rate (L d^{-1})
q_b	Adsorption capacity at breakthrough time (mg g^{-1})
q_e	Adsorption capacity at equilibrium (mg g^{-1})
q_m	Maximum adsorption capacity (mg g^{-1})
q_t	Adsorption capacity at time t (mg g^{-1})
q_{total}	Adsorption capacity at saturation time (mg g^{-1})

Symbols

q_{TH}	Saturation adsorption capacity (mg g^{-1}) from Thomas model
q_Y	Amount of solute adsorbed (mg g^{-1}) from Yan model
$q_{10\%}$	Adsorption capacity at breakthrough fraction of 10% (mg g^{-1})
R	Universal gas constant ($8.314 \text{ J K}^{-1} \text{ mol}^{-1}$)
S_{BET}	BET (Brunauer, Emmett and Teller) surface area ($\text{m}^2 \text{ g}^{-1}$)
S_{micro}	Microporous area ($\text{m}^2 \text{ g}^{-1}$)
S_w	Solubility (mg L^{-1})
t_b	Breakthrough time (d)
$t_{10\%}$	Time at breakthrough fraction of 10% (d)
$t_{50\%}$	Time required for 50% of adsorbate breakthrough (d)
T	Temperature (K or $^{\circ}\text{C}$)
U_r	Adsorbent usage rate (g L^{-1})
V_b	Breakthrough volume (volume treated at breakthrough fraction of 10%) (L)
V_c	Fixed-bed volume (L)
W_0	Micropore volume ($\text{cm}^3 \text{ g}^{-1}$)
V_P	Pore volume ($\text{cm}^3 \text{ g}^{-1}$)
Z	Bed depth (cm)
α^Y	Yan model parameter
ΔG°	Gibbs energy ($\text{J mol}^{-1} \text{ K}^{-1}$)
ΔH°	Enthalpy of adsorption ($\text{J mol}^{-1} \text{ K}^{-1}$)
ΔS°	Entropy of adsorption ($\text{J mol}^{-1} \text{ K}^{-1}$)
ρ_{Hg}	Apparent density (g cm^{-3})
γ	Coefficient of activity (dimensionless)

1

OVERVIEW

In this chapter is presented the thesis framework, namely, the motivation of the work carried out as well as the proposed objectives and the layout of the chapters included in the document.

1.1. Motivation

Science is more than academic studies associated to the different research fields. Its main purpose is to understand how natural world works, helping the humanity to progress, but it must also contribute to the sustainability of this world and its resources. Two great environmental problems existing nowadays, whose mitigation is essential, are: a) the exploration of natural resources together with the generation of industrial residues (Gaur et al., 2020); and b) the presence of pharmaceuticals (Taheran et al., 2018) in water systems.

The problematic associated to the industrial residues generated from the production of the different products that are essential to the modern society, presents an important environmental issue. One example is the case of paper industry, which produces high amounts of industrial residues that cannot be infinitely supported without serious environmental consequences (Mandeep et al., 2020). Therefore, in the past few years, the world has recognized the importance of passing from the *linear economy* model, which entails the production, utilization and elimination (residues) of materials, to a *circular economy* model, which proposes the recycling/upcycling of the materials and their continuous return into the industry or market, with great emphasis on a zero-waste approach (Silva et al., 2018). This is clearly recommended in the Directive 2018/851/EC where are defined the goals concerning sustainable waste management, with the aim of increasing the efficiency in the use of new sources. On this wise, the use of residues as raw materials (secondary raw materials) instead of virgin raw materials contributes to the main goal of reducing the depletion of natural resources.

The presence of pharmaceuticals in the aquatic environment has been a widely studied issue in the recent years, confirming the growing concern related to their occurrence/detection in the aquatic environment (Ebele et al., 2017; Sousa et al., 2018; Majumder et al., 2019; Patel et al., 2019). Actually, wastewater treatment plants (WWTP) are important sources of these contaminants (Taheran et al., 2018; Couto et al., 2019) since they were not designed for their removal (Rivera-Utrilla et al., 2013; Taheran et al., 2018; Couto et al., 2019). Hence, the application of cost effective tertiary treatments that guarantee the removal of these emerging contaminants is of outmost importance to prevent their influx into surface and ground waters and to mitigate the effects that they can have in aquatic life (Sui et al., 2015; Jeirani et al., 2017).

Using residues to produce waste-based adsorbents, such as activated carbon (AC), and their application for removal of pharmaceuticals from water is an interesting approach to find an integrated

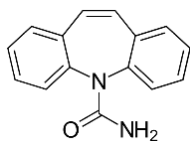
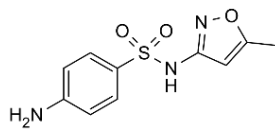
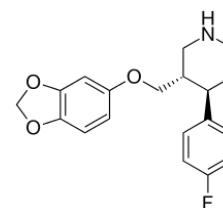
solution for the two environmental problems that were above referred. Additionally, by using residues as AC precursors, pressure on natural resources, that may be used in the production of this type of material, and costs associated to raw materials are minimized (Dias et al., 2007; Kim et al., 2019; Silva et al., 2018; Stavropoulos and Zabaniotou, 2009). In this sense, the production of alternative adsorbents using industrial residues as parent material, for instance residues resulting from the paper industry, namely, primary and secondary or biological sludge, can be an alternative to commercial AC to be applied in wastewater treatment systems for the removal of pharmaceuticals from wastewaters.

1.2. Objectives

The main objective of this work was the production of alternative carbon adsorbents through pyrolysis and chemical activation of solid residues resulting from wastewater treatment in paper mill industries and their use for removal of pharmaceuticals from aquatic systems. Paper mill sludge was subjected to a thermal treatment under inert atmosphere (pyrolysis) and an activation and/or functionalization procedure was applied to improve the adsorptive performance of the material. The produced adsorbents were applied in the removal of pharmaceuticals from different classes, focusing on the antiepileptic carbamazepine (CBZ), the antibiotic sulfamethoxazole (SMX) and the antidepressant paroxetine (PAR). CBZ is a psychiatric drug frequently detected in groundwater, rivers, and lagoons, at relatively high concentrations (Clara et al., 2004; Almeida et al., 2014; Sui et al., 2015) and there are even reports of its detection in drinking and tap waters (Patel et al., 2019). Additionally, according to Ebele et al. (2017), CBZ was already identified as an anthropogenic pollution marker (Clara et al., 2004) and may be a possible future candidate for emerging priority substance (Sousa et al., 2018). SMX is an antibiotic with high antibacterial capacity and resistance to degradation (Moral-Rodríguez et al., 2016) and is frequently found in wastewater effluents (Hoffmann et al., 2016). Paroxetine is a selective serotonin re-uptake inhibitor (SSRI) acting in the central nervous system (Calisto and Esteves, 2009; Calisto et al., 2015). The study of paroxetine in the environment as well as its removal from water is less exhaustive than the other two compounds. Nevertheless, it is a pharmaceutical widely consumed and has been detected in wastewaters (Patel et al., 2019) and in superficial waters (Duarte et al., 2019). Some physicochemical properties of the target pharmaceuticals are presented in Table 1.1.

Table 1.1. Physicochemical properties of the studied pharmaceuticals (based on PubChem (accessed in February 2019) and Calisto et al. (2015)).

<i>Pharmaceutical</i>	<i>MW</i> (<i>g mol⁻¹</i>)	<i>S_w</i> (<i>mg L⁻¹</i>)	<i>pK_a</i>	<i>log K_{ow}</i>	<i>Polar surface area /Å²</i>	<i>H bond acceptors</i>
Carbamazepine (1)	236.27	18 (25 °C)	2.3; 13.9	2.67	46.3	3
Sulfamethoxazole (2)	253.28	500 (25 °C)	1.8; 5.7	0.89	107	6
Paroxetine (3)	374.8	5400	9.9	3.89	39.7	4

**(1)**C₁₅H₁₂N₂O**(2)**C₁₀H₁₁N₃O₃S**(3)**C₁₉H₂₀FNO₃

Regarding the specific objectives of the work, they consisted of:

- Evaluation of the viability of primary (PS) and biological (BS) sludges from pulp and paper industry to produce carbon adsorbents;
- Producing an efficient AC using PS as precursor and evaluating its adsorption performance for pharmaceuticals from different therapeutic classes;
- Production of a granular activated carbon using PS and testing its performance in batch and fixed-bed systems;
- Application of the developed materials for the removal of pharmaceuticals in wastewater matrices;
- Evaluation of the impact of modification/functionalization of the AC on the adsorption of pharmaceuticals, in relation to the AC without modification.

1.3. Thesis layout

This thesis is composed by 10 chapters comprising the description of the methodology and the results obtained regarding the study of the production of AC, using PS as raw material, and their application in the removal of pharmaceuticals from water.

Chapter 1

Overview.

Chapter 2

In chapter 2 is presented a brief introduction to the main topics addressed in the thesis, specifically regarding the problematic of paper mill sludge (residues); AC adsorbents and the use of wastes as raw materials for their production; and the presence of pharmaceuticals in the environment.

Chapter 3

Chapter 3 presents the evaluation of the potential of different paper mill sludges (namely, PS and BS from two pulp and paper mill factories) as raw materials to produce non-activated carbon adsorbents. The study in this chapter allowed to select PS as the more viable precursor.

Chapter 4

Chapter 4 describes an optimization study on the production of AC (in the powdered form) by chemical activation and conventional pyrolysis under different conditions, using PS as precursor. A full factorial design was applied to determine the most adequate conditions to produce AC intended for the removal of pharmaceuticals. These were defined after statistical analysis of the selected responses (namely, product yield, adsorption percentages for CBZ, SMX and PAR, specific surface area (S_{BET}), and total organic carbon (TOC)) and optimization by response surface methodology (RSM). Physicochemical characterization of the carbons produced under optimized conditions was also performed.

Chapter 5

Chapter 5 is dedicated to the evaluation of the adsorptive performance of the AC selected from the optimization study in chapter 4, toward the removal of CBZ, SMX, and PAR, in ultrapure water and wastewater, through kinetic and equilibrium studies in batch system. The results were compared with the ones obtained for a commercial powdered AC (CAC) whose performance was also assessed.

Chapter 6

In this chapter, the production of a PS-based granular AC (PSA-PA) is addressed. PSA-PA was characterized and its adsorptive performance, in ultrapure water and wastewater, toward the removal of CBZ, SMX, and PAR, in batch systems was evaluated. In addition, parallel studies on a commercial granular AC (GACN) were also executed for comparison purposes.

Chapter 7

Chapter 7 presents the application of PSA-PA in fixed-bed column systems. The studies involved the analysis of the effects of the system operational parameters and the adsorption behavior both in mono and multicomponent solutions of CBZ, SMX, and PAR, and in wastewater matrices.

Chapter 8

In chapter 8, the functionalization of the powdered AC (selected according to chapter 4 results and tested in chapter 5) is addressed. Four functionalization's methodologies were applied to observe if the introduction of specific surface functional groups interferes in the adsorption of different pharmaceuticals. Adsorption tests were performed for the three chosen pharmaceutical (CBZ, SMX, and PAR) and for other three compounds, lorazepam (LOR), piroxicam (PIR), and venlafaxine (VEN). These tests were realized in three different matrices, ultrapure water, ultrapure water with adjusted pH 7.6, and in wastewater.

Chapter 9

In chapter 9, the powdered AC produced according to the selected conditions in chapter 4 was functionalized with thiol groups (AC-MPTMS) and the adsorption of SMX, considering three different temperatures, 15 °C, 25 °C and 35 °C, in buffered solutions with adjusted pH 8, onto the parent AC and AC-MPTMS, is evaluated. The thermodynamic parameters of the adsorption process were estimated. Additionally, adsorption studies involving SMX and AC-MPTMS using a wastewater matrix at constant temperature of 25 °C were performed.

Chapter 10

Chapter 10 report the final remarks of the overall work and presents some suggestions for future work.

1.4. References

- Almeida, A., Calisto, V., Esteves, V.I., Schneider, R.J., Soares, A.M., Figueira, E., Freitas, R., 2014. Presence of the pharmaceutical drug carbamazepine in coastal systems: effects on bivalves. *Aquat. Toxicol.* 156, 74-87.
- Calisto, V., Esteves, V.I., 2009. Psychiatric pharmaceuticals in the environment. *Chemosphere* 77, 1257-1274.
- Calisto, V., Ferreira, C.I., Oliveira, J.A., Otero, M., Esteves, V.I., 2015. Adsorptive removal of pharmaceuticals from water by commercial and waste-based carbons. *J. Environ. Manage.* 152, 83-90.
- Clara, M., Strenn, B., Kreuzinger, N., 2004. Carbamazepine as a possible anthropogenic marker in the aquatic environment: investigations on the behaviour of carbamazepine in wastewater treatment and during groundwater infiltration. *Water Res.* 38, 947-954.
- Couto, C.F., Lange, L.C., Amaral, M.C.S., 2019. Occurrence, fate and removal of pharmaceutically active compounds (PhACs) in water and wastewater treatment plants—A review. *Journal of Water Process Engineering* 32, 100927.
- Dias, J.M., Alvim-Ferraz, M.C., Almeida, M.F., Rivera-Utrilla, J., Sanchez-Polo, M., 2007. Waste materials for activated carbon preparation and its use in aqueous-phase treatment: a review. *J. Environ. Manage.* 85, 833-846.
- Directive (EU) 2018/851 of the European Parliament and of the Council of 30 May 2018 amending Directive 2008/98/EC on waste. *Off. J. Eur. Union.* 150, 109-140
- Duarte, P., Almeida, C.M.R., Fernandes, J.P., Morais, D., Lino, M., Gomes, C.R., Carvalho, M.F., Mucha, A.P., 2019. Bioremediation of bezafibrate and paroxetine by microorganisms from estuarine sediment and activated sludge of an associated wastewater treatment plant. *Sci. Total Environ.* 655, 796-806.
- Ebele, A.J., Abou-Elwafa Abdallah, M., Harrad, S., 2017. Pharmaceuticals and personal care products (PPCPs) in the freshwater aquatic environment. *Emerging Contaminants* 3, 1-16.
- Gaur, V.K., Sharma, P., Sirohi, R., Awasthi, M.K., Dussap, C.-G., Pandey, A., 2020. Assessing the impact of industrial waste on environment and mitigation strategies: A comprehensive review. *J. Hazard. Mater.* 398, 123019.
- Hoffmann, H., Baldofski, S., Hoffmann, K., Flemig, S., Silva, C.P., Esteves, V.I., Emmerling, F., Panne, U., Schneider, R.J., 2016. Structural considerations on the selectivity of an immunoassay for sulfamethoxazole. *Talanta* 158, 198-207.
- Jeirani, Z., Niu, C.H., Soltan, J., 2017. Adsorption of emerging pollutants on activated carbon. *Rev. Chem. Eng.* 33, 491-522.
- Kim, M.H., Jeong, I.T., Park, S.B., Kim, J.W., 2019. Analysis of environmental impact of activated carbon production from wood waste. *Environ. Eng. Res.* 24, 117-126.

- Majumder, A., Gupta, B., Gupta, A.K., 2019. Pharmaceutically active compounds in aqueous environment: A status, toxicity and insights of remediation. *Environ. Res.* 176, 108542.
- Mandeep, Gupta, G.K., Shukla, P., 2020. Insights into the resources generation from pulp and paper industry wastes: Challenges, perspectives and innovations. *Bioresource Technol.* 297, 122496.
- Moral-Rodríguez, A.I., Leyva-Ramos, R., Ocampo-Pérez, R., Mendoza-Barron, J., Serratos-Alvarez, I.N., Salazar-Rabago, J.J., 2016. Removal of ronidazole and sulfamethoxazole from water solutions by adsorption on granular activated carbon: equilibrium and intraparticle diffusion mechanisms. *Adsorption* 22, 89-103.
- Patel, M., Kumar, R., Kishor, K., Mlsna, T., Pittman, C. U., Mohan, D., 2019. Pharmaceuticals of Emerging Concern in Aquatic Systems: Chemistry, Occurrence, Effects, and Removal Methods. *Chem. Rev.* 119, 3510–3673.
- PubChem online data base at <https://pubchem.ncbi.nlm.nih.gov>, accessed in February 7, 2019.
- Rivera-Utrilla, J., Sánchez-Polo, M., Ferro-García, M.Á., Prados-Joya, G., Ocampo-Pérez, R., 2013. Pharmaceuticals as emerging contaminants and their removal from water. A review. *Chemosphere* 93, 1268-1287.
- Silva, C.P., Jaria, G., Otero, M., Esteves, V.I., Calisto, V., 2018. Waste-based alternative adsorbents for the remediation of pharmaceutical contaminated waters: Has a step forward already been taken? *Bioresource Technol.* 250, 888–901.
- Sousa, J.C.G., Ribeiro, A.R., Barbosa, M.O., Pereira, M.F.R., Silva, A.M.T., 2018. A review on environmental monitoring of water organic pollutants identified by EU guidelines. *J. Hazard. Mater.* 344, 146-162.
- Stavropoulos, G.G., Zabaniotou, A.A., 2009. Minimizing activated carbons production cost. *Fuel Process. Technol.* 90, 952-957.
- Sui, Q., Cao, X., Lu, S., Zhao, W., Qiu, Z., Yu, G., 2015. Occurrence, sources and fate of pharmaceuticals and personal care products in the groundwater: A review. *Emerging Contaminants* 1, 14-24.
- Taheran, M., Naghdi, M., Brar, S.K., Verma, M., Surampalli, R.Y., 2018. Emerging contaminants: Here today, there tomorrow! *Environ. Nanotechnol. Monit. Manag.* 10, 122-126.

2

INTRODUCTION

This chapter presents an introductory summary of the main subjects addressed in this thesis, namely, the challenge of industrial wastes management, particularly sludges produced by paper mill industries; the preparation of alternative activated carbons (AC), and wastes used as raw materials for their production; and, the problematic of the presence of pharmaceuticals in the aquatic environment.

2.1. Pulp and paper mills and the challenges of waste management

Pulp and paper industry is one of the most important industrial sectors in the world (Molina-Sánchez et al., 2018; Gaur et al., 2020). In Portugal, this is a well-established industry where, according to CELPA (“Associação da Indústria Papeleira”), in 2016, the production of the sector of the Industry of wood, pulp, paper, paperboard and their printing articles represented 4.3 % of the national PIB (“Produto Interno Bruto”), 7.8 % of the production of the sectors of “Industry, energy, water and sanitation”, and 2.5 % of the national production (CELPA, 2018).

Pulp and paper mill industry faces an important environmental challenge concerning waste management (Mandeep et al., 2020). This industry requires large quantities of water to operate and produces large amounts of solid residues from their wastewater treatment (Soucy et al., 2014; Faubert et al., 2016; CELPA, 2018; Molina-Sánchez et al., 2018). Considering that, in 2018, the total production of paper and paperboard, in Portugal, was of 2060 thousand tonnes, this implies not only a huge quantity of water used, but also large volumes of effluents produced and, therefore, a high quantity of solid residues (sludge) arising from the treatment of such effluents (CELPA, 2018). According to Molina-Sánchez et al. (2018), per each ton of paper produced, 40 kg to 50 kg of sludge are generated. This sludge derives from primary and biological or secondary treatments, and, therefore, there are two types of sludge: primary sludge (PS) and secondary or biological sludge (BS). PS, which constitutes about 70 % of the total sludge obtained from the clarification process of wastewater treatment (Monte et al., 2009; Molina-Sánchez et al., 2018), is derived from the mechanical treatment for the removal of certain fine particles, being constituted mostly by organic matter (cellulose fibers) (Calisto et al., 2014; Simão et al., 2018). After the primary treatment, the wastewater is sent to a secondary treatment plant, for bacterial digestion of the remaining suspended solids, and the resulting mixture of the lasting suspended solids and biosolids is called BS (Soucy et al., 2014; Simão et al., 2018), which corresponds to 30% of the total sludge (Molina-Sánchez et al., 2018). Some studies indicate that this type of sludge may have lignin in its constitution (because of its low biodegradability) and no cellulose or hemicelluloses (Calisto et al., 2014). The generated volumes of BS are lower than those of PS, since most of the heavy, fibrous and/or inorganic solids are removed in the primary treatment (Monte et al., 2009).

Considering the large volumes of sludge generated along the production of pulp and paper (Faubert et al., 2016; CELPA, 2018), the management of such residues is an important issue for the paper industry. Landfill and other ways of disposal are the major routes of discarding these types of solid

residues, followed by energetic valorization, agriculture and composting and, finally, valorization by other industries (CELPA, 2018). However, landfill of organic residuals has been discouraged, being recommended the reduction or elimination of this practice and its substitution by most efficient methods of use and recycling of the residues (Faubert et al., 2016). Hence, it is important to find new ways of reducing this kind of residues and minimize their impact in the environment.

2.2. Activated Carbon

2.2.1. Activated carbon production

Activated carbon (AC) is one of the most popular adsorbents used for the removal of contaminants from water and wastewater due to its well-developed porous structure and high internal surface area, which confer it great adsorption characteristics (Calvete et al., 2009; Kyzas et al., 2013; Yu et al., 2013; Arena et al., 2016).

Carbon materials are usually obtained by a carbonization process under inert atmosphere, also known as pyrolysis, in which, the carbonaceous precursor (biomass, fossil, or waste carbon source) is transformed in a material constituted essentially by carbon (Pierson, 1993; Hagemann et al., 2018). From this thermochemical process, charcoal, biochar, or AC can be obtained, depending on the precursor and production process (Hagemann et al., 2018). The production of AC introduces an additional step of activation applied during or after the carbonization step. This supplementary step improves the specific surface area (S_{BET}) of the materials, one of the main features of AC, essential for the adsorption processes (Rouquerol et al., 2014; Hagemann et al., 2018).

The production process of carbon materials, such as biochar or AC, consists of the slow thermal treatment of the precursor at high temperature, generally reaching 700 °C to 1300 °C (Pierson, 1993; Marsh and Rodríguez-Reinoso, 2006). At the temperatures below 700 °C, the release of water (around 100 °C), carbon dioxide and organic molecules occurs (Rouquerol et al., 2014) as the decomposition of cellulose, hemicelluloses and lignin components takes place, resulting in the devolatilization of the material (Wang et al., 2016). Hence, the organic precursor is decomposed into a carbon residue while volatile compounds are released, and the final solid product is a material with a high content of carbon and a low content in heteroatoms such as oxygen (O), hydrogen (H), chlorine (Cl), nitrogen (N), sulfur (S), and others (Pierson, 1993; Marsh and Rodríguez-Reinoso, 2006). The diffusion of volatile compounds is a crucial step and must occur slowly to avoid disruption and rupture of the carbon network. At the early stages of the heat-treatment temperature (HTT), polyaromatic ring structures are developed

(Marsh and Rodríguez-Reinoso, 2006; Rouquerol et al., 2014). The progressive heating increases the carbon/hydrogen (C/H) and carbon/oxygen (C/O) ratios, but some heteroatoms remain chemically bonded at the edges of the aromatic macromolecules in an infinite number of ways, forming surface functional groups (Moreno-Castilla, 2004; Marsh and Rodríguez-Reinoso, 2006; Barroso-Bogeat et al., 2014; Rouquerol et al., 2014).

During the carbonization process, pores are developed and tend to be filled with tar-like substances that block the pore entrances, conferring relative low porosity to the materials (Pierson, 1993). To unclog pores, an activation procedure is employed in the production of AC (Hagemann et al., 2018) which, together with the type of precursor and conditions of carbonization, define the type and range of porosity of the material (Rouquerol et al., 2014; Thakur and Thakur, 2016; Kwiatkowski and Broniek, 2017; Hagemann et al., 2018). The activation process can be performed by two different ways, physical or chemical, both being influenced by the operation conditions of the pyrolysis step (maximum temperature, heating ramp, residence time, and atmosphere) (Alcañiz-Monge and Illan-Gomez, 2008; Azargohar and Dalai, 2008). Physical activation is the oldest method of activation and it involves the application of steam, carbon dioxide (CO₂), oxygen (O₂), or a mixture of them, under controlled conditions (González-García, 2018; Hagemann et al., 2018). It is considered a two-step process, with the second step (activation) being performed at high temperature (usually between 700 – 1100 °C), after a first pyrolysis of the precursor (Nahil and Williams, 2012; Ukanwa et al., 2019). In the activation process, some carbon atoms react with the fluid activating agent, releasing carbon monoxide, carbon dioxide, hydrogen or methane and developing a porous structure in the solid residue (Thakur and Thakur, 2016; González-García, 2018; Hagemann et al., 2018; Ukanwa et al., 2019). In the case of the chemical activation process, this implies the use of chemical activating agents (inorganic additives) such as zinc chloride (ZnCl₂), alkali hydroxides (generally, potassium hydroxide, KOH, and sodium hydroxide, NaOH), phosphoric acid (H₃PO₄), sulfuric acid (H₂SO₄), and potassium carbonate (K₂CO₃) (Tzvetkov et al., 2016; Hagemann et al., 2018; Heidarinejad et al., 2020). The activating agents act as dehydrating and/or oxidizing agents and also prevent shrinkage during carbonization, and the production process is, in general, performed by mixing the activating agent with the precursor, by physical mixing or by impregnation, followed by carbonization (Marsh and Rodríguez-Reinoso, 2006; González-García, 2018; Ukanwa et al., 2019). In the chemical activation process, the type of precursor, chemical used as activating agent, ratio of activating agent/precursor and temperature affect the pore size distribution and the S_{BET} of the final material (González-García, 2018; Heidarinejad et al., 2020). For instance, H₃PO₄ is widely used for lignocellulosic precursors (Heidarinejad et al., 2020) and promotes meso- and macroporosity González-García (2018). In the case of the alkali agents, narrow to wide micropores can

be generated and, in the particular case of KOH, high ratios of KOH/precursor are also responsible for the disintegration of the material (González-García, 2018). The main disadvantage of chemical activation is the use of chemical agents, which may introduce impurities in the material and produces a higher amount of inorganic components (Zhou et al., 2018). This implies a further step of washing that may pose an additional environmental issue (Zhou et al., 2018). However, chemical activation is considered to produce AC with higher yields and higher S_{BET} , and, in average, lower temperatures are required (usually between 400 °C and 800 °C) comparing to physical activation (which also requires longer times of production and hence higher energy demand) (Yahya et al., 2015; Bergna et al., 2018; Ukanwa et al., 2019; Heidarinejad et al., 2020).

The enhancement of AC porosity by activation, and, thus, the increase in their S_{BET} (González-García, 2018), together with the surface chemistry of the AC, are key features for the adsorption process (Moreno-Castilla, 2004; Barroso-Bogeat et al., 2014; Thakur and Thakur, 2016), one of the main applications of these materials. AC are versatile materials able to adsorb a wide variety of substances. However, the use of commercial AC in large scale, at industrial level, presents a high economic cost, which is a major disadvantage of these materials (Calvete et al., 2009; Girods et al., 2009; Selvaraju and Bakar, 2017). In that matter, the production of alternative adsorbents with good adsorption capacities and at the same time at lower costs is a very important challenge.

2.2.2. Structure and surface chemistry

2.2.2.1. Porosity

AC are often classified as microporous or mesoporous materials. These designations comes from the classification of pores according to their size into three main groups: micropores (size < 2 nm), mesopores (size between 2-50 nm) and macropores (size > 50 nm) (Dabrowski, 2001; Marsh and Rodríguez-Reinoso, 2006; Rouquerol et al., 2014; Thakur and Thakur, 2016). Porosity is an important parameter for the adsorption process, since this occurs in the meso and micropores of the AC, with macroporosity facilitating the transport of the adsorbate molecules into them, assisting the adsorption process (Dabrowski, 2001; Marsh and Rodríguez-Reinoso, 2006; Rouquerol et al., 2014). According to Marsh and Rodríguez-Reinoso (2006), “*porosity is a function of structure*” and *vice-versa*, therefore the assessment of the porous structure of the carbon materials, and particularly AC, is of utmost importance.

Exception made to diamond (sp^3 atomic structure), all known carbon structures present a degree of order between the hexagonal graphite (sp^2 atomic structure) and the most disordered porous carbon

(Marsh and Rodríguez-Reinoso, 2006). Graphite is the most stable and the most common form of elemental carbon at ambient temperature and normal atmospheric pressure (Marsh and Rodríguez-Reinoso, 2006; Rouquerol et al., 2014). Graphite is constituted by graphene layers that have an interplanar spacing around 0.335 nm and no chemical bonds between the layers, only van der Waals attractive forces (Marsh and Rodríguez-Reinoso, 2006; Rouquerol et al., 2014). An important property of graphite is the fact that it is easy to be cleaved along the basal plane and easily form intercalation compounds (Rouquerol et al., 2014). Carbon materials produced by carbonization (pyrolysis) of carbonaceous parent materials can be considered as smaller segments of graphene layers that no longer have the ABABAB stacking or parallel layers of graphite (Pierson, 1993; Marsh and Rodríguez-Reinoso, 2006). Hence, the final product of carbonization is a network of carbon atoms with residual hydrogen, that may be seen as small segments of graphene sheets of different sizes, possessing cavities (molecular spaces) that define the porosity of the structure (Marsh and Rodríguez-Reinoso, 2006; Thakur and Thakur, 2016). These segments, aggregates of small crystallites with some graphitic order but randomly oriented, possess defects and imperfections such as stacking faults, holes, non-planarity, linear carbons (*dangling* bonds) and also heteroatoms (Pierson, 1993; Marsh and Rodríguez-Reinoso, 2006; Thakur and Thakur, 2016). In the case of the structure of AC, and according to Marsh and Rodríguez-Reinoso (2006), “*the defective micro-graphene layer is totally central to the structure of activated carbon*”.

It is important to know the structure of carbon materials to understand their porosity, however, for carbon materials such as AC (non-graphitizable and isotropic carbons) it is difficult, if even possible, to make considerations related to their structure (Marsh and Rodríguez-Reinoso, 2006). Nevertheless, nowadays, it is easier to understand the structure of materials such as AC using spectroscopic techniques, namely X-ray diffraction and Raman spectroscopy, and also microscopic techniques as scanning and transmission electron microscopy (SEM and TEM, respectively) (Thakur and Thakur, 2016).

2.2.2.2. *Surface chemistry of carbon adsorbents*

Along with porosity, surface chemistry is a very important feature for the adsorption capacity of carbon adsorbents. Both constitute the *active sites* for the adsorption process, with microporosity possessing the *sites*, within the micropores, where physisorption occurs and, for instance, the surface oxygen complexes being the *site* where chemisorption occurs (Marsh and Rodríguez-Reinoso, 2006).

As referred before, during carbonization, although several heteroatoms are removed, some of them remain in the structure, forming the surface chemistry, through functional groups, of the carbon material. These heteroatoms are largely present at the edges of the non-planar and defective graphene

layers of the carbon material and at defect positions (*dangling bonds*), which are sites that present high reactivity due to the high densities of unpaired electrons (Thakur and Thakur, 2016). They play an important role in the adsorption from aqueous solutions since the functional groups constituted by these heteroatoms, principally oxygen-groups, determine to a great extent the properties of the carbon material (Thakur and Thakur, 2016). These functional groups can be acidic and basic carbon-oxygen groups, with the acidic groups being mainly carbonyls, carboxyls, phenols and lactones, while the basic groups are mostly pyrones, chromenes and quinones structures (Li et al., 2002; Dabrowski et al., 2005; Stavropoulos et al., 2008).

An interesting point related to the surface chemistry of carbon-based materials is the possibility of its modification/functionalization by the introduction of specific functional groups for the enhancement of the uptake of specific compounds (Li et al., 2002; Rivera-Utrilla et al., 2011; Thakur and Thakur, 2016). Therefore, several methods have been reported in the literature concerning modification and/or functionalization methods of AC. Modification/functionalization methods can be classified into three categories: chemical modification (acidic treatment, base treatment, impregnation, ozone treatment), physical modification (microwave treatment, plasma treatment) and biological modification (Bhatnagar et al., 2013; Thakur and Thakur, 2016). These modifications generally involve oxidative and non-oxidative treatments, that is, the AC passes through oxidation and then is subjected to grafting by chemical, electrochemical, plasma and/or microwave (Dongil et al., 2011; Bhatnagar et al., 2013).

Oxidation, one of the most used methods to introduce carbon-oxygen functional groups in the surface of the AC, is accomplished using oxidizing gases (oxygen, steam, carbon dioxide) or oxidizing solutions (nitric acid, hydrogen peroxide, sulfuric acid, chlorine water) (Jaramillo et al., 2010; Dongil et al., 2011; Rivera-Utrilla et al., 2011; Figueiredo, 2013; Zhang, 2013). The use of acid solutions is also classified as an acidic treatment (Bhatnagar et al., 2013). Generally, aqueous oxidation increases the concentration of carboxylic acid while gaseous oxidation increases the concentration of hydroxyl surface groups (Velo-Gala et al., 2014). Oxidation is an important method for modification/functionalization of the AC surface, because the carbon-oxygen radicals result in important functional groups that influence the acid-base characteristics of the carbon materials through their point of zero charge (pH_{pzc}), electron acceptor/donor character, and hydrophobicity (Velo-Gala et al., 2014). The introduction of oxygen-containing groups make the surface of the carbon less hydrophobic and less inert, and oxidation may, in most cases, reduce the surface area of the material (Dongil et al., 2011; Rivera-Utrilla et al., 2011; Singha et al., 2013; Zhang, 2013). Nevertheless, oxygenated functional groups are important because they can

be used to introduce new functional groups at the surface of the carbon materials through their modification (Stein et al., 2009; Velo-Gala et al., 2014).

Other modification methods can be applied, for instance, to introduce nitrogen and sulfur functionalities to the surface of the material (Bhatnagar et al., 2013; Rivera-Utrilla et al., 2011; Thakur and Thakur, 2016). The introduction of nitrogen functional groups (nitrogenation) may involve a basic treatment of the carbon material using nitrogen compounds such as ammonia, urea and melamine, generally, applying high temperatures and after the oxidation of the carbon with nitric acid or NO_x (Bhatnagar et al., 2013; Thakur and Thakur, 2016). This treatment induces a positively charged surface useful to the adsorption of negatively charged species (acidic molecules) and/or organic species through, for instance, dipole-dipole forces, H-bonding, and covalent bonding (Bhatnagar et al., 2013). The introduction of sulfur containing groups (sulfuration) onto the carbon surface can be accomplished using sulfurous gases as CS_2 , H_2S and SO_2 (Figueiredo, 2013; Thakur and Thakur, 2016). These methods might enhance the adsorptive properties of AC for organic and polar compounds, once they can increase the basicity and polarity of the carbon surface, which may favor the adsorbent-adsorbate interactions (Rivera-Utrilla et al., 2011).

The functionalization of AC has already been performed for different purposes, for instance, for catalytic applications (Radkevich et al., 2008; Figueiredo, 2013) and carbon electrodes (Pognon et al., 2011; Lebègue et al., 2013a), to get some insights on reaction mechanisms (Lebègue et al., 2011; Lebègue et al., 2013b). Yet, although the functionalization of AC to be applied in the removal of organic contaminants, through the different methodologies described above, is uncommon, it can be a way of enhancing the specificity of these materials.

2.2.3. Alternative raw materials used in the production of activated carbon

Commercial AC are mainly produced using as raw materials coals (anthracite, bituminous, sub-bituminous and lignite), peat, woods, fruit stones and nutshells, namely coconut shell, as well as synthetic polymers (Marsh and Rodríguez-Reinoso, 2006). Along with pyrolysis and activation conditions, the raw material is an important factor, influencing the characteristics of the AC (Yahya et al., 2015; Bergna et al., 2018; González-García, 2018). It is desirable that the raw materials possess a high content in carbon and a low content in inorganic compounds, high density, and sufficient volatile content (Bergna et al., 2018). Also, low degradation on storage and low cost are desirable factors (Bergna et al., 2018). In Table 2.1 are presented some studies concerning the use of different wastes (agricultural and industrial) as precursors in the production of AC, using different activation methodologies. It can be

observed that agricultural wastes tend to present a lower ash content than industrial wastes, which may constitute a challenge in the use of the latter as raw materials to produce AC.

Table 2.1. Examples of wastes used as precursors in the production of alternative carbon adsorbents.

Raw material	Raw material initial characteristics					Production conditions	S_{BET} ($m^2 g^{-1}$)	Adsorbate	Reference
	MC (%)	VM (%)	FC (%)	Ash (%)	%C				
Rattan sawdust	–	–	–	–	–	1- Carbonization at 700 °C; 2- Chemical activation of the char with KOH at 850 °C IR:1	1083	Methylene blue	Hameed et al. (2007)
Waste biomass (Sunflower oil cake)	9.8	67.4	17.6	5.2	46.6	Chemical activation with H_2SO_4 at 600 °C IR: 0.85 IR: 1.9	240 115	Methylene blue	Karagoz et al. (2008)
Wood particles wastes	–	–	–	–	–	1- Carbonization at 300 °C 2- Physical activation of the char with steam at 800 °C	1367	Phenol	Girods et al. (2009)
Walnut shells	3.4	78.4	17.6	0.5	48.1	Vacuum chemical activation with $ZnCl_2$ at 450 °C and at 30 kPa IR: 0.5 IR: 0.75 IR: 1 IR: 1.5 IR: 2	909 1180 1462 1750 1800	Methylene blue	Yang and Qiu (2010)
Paper mill sludge	–	57.6	8.29	41.98	–	1- carbonization at 300 °C; 2- physical activation with steam at 850 °C	131	Methylene blue	Li et al. (2011a)
Grape seeds	6.5	67.4	–	1.6	56.5	Chemical activation with H_3PO_4 at 500 °C IR: 3	1139	Diuron	Al Bahri et al. (2012)
Waste paper sludge	–	–	–	43.8	20.2	1- carbonization at 600 °C; 2- physical activation with CO_2 at 600 °C	17	–	Hofmann and Pietrzak (2012)

MC – moisture content; VM – volatile matter; FC – fixed carbon; %C – elemental carbon content
IR – impregnation ratio activating agent:precursor or char

Table 2.1. (Continued)

Raw material	Raw material initial characteristics					Production conditions	S_{BET} ($m^2 g^{-1}$)	Adsorbate	Reference
	MC (%)	VM (%)	FC (%)	Ash (%)	%C				
Cherry stones	6.8	82.3	–	0.3	–	Chemical activation with NaOH at 600 °C IR: 2	343-932	–	Pietrzak et al. (2014)
Primary paper mill sludge	14.4	38.12	24.97	22.56	24.2	1- carbonization at 700 °C; 2- chemical activation with potassium fluoride (KF) at 810 °C IR 0.95	640	Reactive orange 16, Reactive blue 19	Auta and Hameed (2014)
Industrial paper sludge	2.2	74.8	10.1	12.9	–	1- carbonization at 700 °C; 2- chemical activation with H ₃ PO ₄ IR:1.5	6493	enrofloxacin	Chowdhury et al. (2019)
Avocado seed	–	–	–	–	–	chemical activation: ZnCl ₂ ; 500 °C	1584	propranolol, paracetamol, diclofenac, tetracycline, amoxicillin	Lima et al. (2019)
Corn cob	10.5	62.9	24.9	1.7	–	1- carbonization: 500 °C; 2- chemical activation with NaOH at 800 °C IR: 4	2381 2532	Pb ²⁺	Zhang et al. (2020)
Wheat bran	14.3	55.9	26.2	3.6	–	IR: 4	2532		
Rice husk	11.4	51.6	24.5	12.5	–	IR: 3	2786		
Soybean shell	12.6	58.2	23.8	5.4	–	IR:4	2628		
Eucalyptus residue (branches)	–	–	–	–	47	chemical activation: H ₃ PO ₄ at 400 °C IR: 2.5	1545	methylene blue	Han et al. (2020)
Spent brewery grains						chemical activation at 800 °C		carbamazepine	Sousa et al. (2020)
Barley wine (BW)	3.3	74.1	22.0	4.0	–	IR: 1	1090		
Pilsener (PL)	2.9	75.8	19.3	5.0	–	IR: 1	1120		

MC – moisture content; VM – volatile matter; FC – fixed carbon; %C – elemental carbon content
IR – impregnation ratio activating agent:precursor or char

The high amount of research focused on the production of AC using residue-based raw materials is not only associated to a way of waste valorization and a possible waste management solution, but also to reducing the cost of carbon adsorbents (Thakur and Thakur, 2016; González-García, 2018). As referred, AC are known to be very good adsorbents due to their extremely high S_{BET} (in the range of 800–1800 $\text{m}^2 \text{g}^{-1}$) (Krahnstöver and Wintgens, 2018); yet, their use for water treatment is considerably expensive (Selvaraju and Bakar, 2017). According to Selvaraju and Bakar (2017) the cost of a commercial AC varies, according to its quality, between USD 2.2 and 5 per kg of material. Yunus et al. (2020) referred that the price of the commercial AC also depends on the coal range and may vary from 1190 USD/ton to 18 267 USD/ton. Also, the consumption of AC can be relatively high; for instance, González-García (2018) referred that, in 2015, 12,804,000 tonnes of AC were consumed worldwide.

The use of pulp and paper mill sludge as raw material to produce AC can be an innovative strategy for their management by the pulp and paper industry, avoiding conventional waste management practices, which are being discouraged (Calisto et al., 2014). This allows using wastes to produce an added value material to be used in wastewater treatment, approaching a circular economy concept. Moreover, in previous studies, both primary and biological sludge have already showed good potential to be considered as parent materials to produce carbon adsorbents, namely biochars (Calisto et al., 2014; Calisto et al., 2015; Ferreira et al., 2015). There are some literature involving the use of this type of residues to produce AC, namely, the studies by Khalili et al. (2000); Khalili et al. (2002); Li et al. (2011a); Li et al. (2011b); Auta and Hameed (2014); Jaria et al. (2015); and Chowdhury et al. (2019). From these studies, it is important to highlight the study by Khalili et al. (2000), that obtained an AC with a S_{BET} of 1249 $\text{m}^2 \text{g}^{-1}$, using a chemical activation with ZnCl_2 and a ZnCl_2 :sludge ratio of 2.5. However, using ZnCl_2 is less environmentally friendly than other activating agents, such as H_3PO_4 (Heidarinejad et al., 2020). Another interesting study is the one by Chowdhury et al. (2019) that produced a char using paper mill sludge as precursor and, then, applied a chemical activation with H_3PO_4 to the produced char (Table 2.1).

2.3. Pharmaceuticals occurrence and removal from wastewater

Pharmaceuticals represent an important group of chemical compounds for the society, allowing to enhance the quality of the human and animal life towards the mitigation of diseases and/or infections (Kaczala and Blum, 2016; Ebele et al., 2017; Ferreira et al., 2017; Patel et al., 2019). However, the increase in their consumption (Sangion and Gramatica, 2016), and the development of more sensitive

analytical techniques, has led to their detection in the environment, namely in aquatic compartments (Kaczala and Blum, 2016; Ebele et al., 2017; Majumder et al., 2019; Jaria et al., 2020). Even considering that some of these compounds are not persistent or bioaccumulated, their continuous entrance into the environment can pose a great stress, mostly to aquatic life, due the effect of “pseudo-persistency” (Ebele et al., 2017; Courtier et al., 2019; Patel et al., 2019). Currently, the concentrations found in que aquatic environment are in the range of the nanograms per liter (ng L^{-1}) to micrograms per liter ($\mu\text{g L}^{-1}$), however, there are a few reports of the presence of some pharmaceuticals, like the antibiotic ciprofloxacin, present in the range of mg L^{-1} (Petrie et al., 2015; Majumder et al., 2019). Despite that, there exist already some evidences that, even at such small concentrations, pharmaceuticals can affect ecosystems (Ebele et al., 2017; Courtier et al., 2019; Majumder et al., 2019). Examples of this are the occurrence of antibiotic-resistance in bacteria or the disruption of endocrine systems of living organisms (Gurke et al., 2015; Jagiello et al., 2015; Comber et al., 2018). Also, it is known that antidepressant drugs may affect invertebrates even at environmentally relevant concentrations (Sangion and Gramatica, 2016). For instance, Brodin et al. (2013) showed that dilute concentrations of oxazepam (psychiatric pharmaceutical) can affect fish behavior; and, the work of Foster et al. (2010) reported the influence of fluoxetine, a selective serotonin reuptake inhibitor (SSRI), in amphibian development.

The continuous and increasing presence of pharmaceuticals in the environment has resulted in their inclusion within the group of the emerging contaminants, also known as contaminants of emerging concern (CEC), which are compounds that are detected in the environment but are not covered by existing regulations (for instance, water-quality policies) (Sousa et al., 2018; Taheran et al., 2018). Although there is no regulation for pharmaceuticals, in 2000, the European Union published the Water Framework Directive (Directive 2000/60/EC) directed to water protection, and a list of priority substances for monitorization was included in Directive 2008/105/EC (Ebele et al., 2017; Sousa et al., 2018). Later, Decision 2015/495/EU was published including a first watch list, which contained 10 substances considered as CEC. This list was then revised in Decision 2018/840/EU (second watch list) (Loos et al., 2018; Courtier et al., 2019). In these watch lists, some pharmaceuticals such as diclofenac, azithromycin, clarithromycin, erythromycin, amoxicillin, and ciprofloxacin were integrated (Decision 2015/495/EU; Decision 2018/840/EU), with the last two (antibiotics) being added in the list of 2018 (Decision 2018/840/EU). Despite the inexistence of regulations for the allowable limits of pharmaceuticals in water, these directives evidence the increasing concern associated to this problematic. This is also noticeable by the large number of recent publications, including review papers, regarding the presence of pharmaceuticals in the environment and different strategies for their removal from water systems (e.g. Sangion and Gramatica (2016); Seo et al. (2016); Wang and Wang (2016); Ebele et al.

(2017); Richmond et al. (2017); Yang et al. (2017); Comber et al. (2018); De Andrade et al. (2018); Mansour et al. (2018); Silva et al. (2018); Courtier et al. (2019); Majumder et al. (2019); and Patel et al. (2019)).

Most of the pharmaceutical substances are polar compounds with a molecular weight ranging from 200 to 1000 Da, hydrophilic, and present low volatility (Kümmerer, 2008; Ebele et al., 2017; De Andrade et al., 2018; Majumder et al., 2019; Patel et al., 2019), which increase the probability of pharmaceuticals to be transported to surface waters (Ebele et al., 2017). The physicochemical characteristics of pharmaceuticals largely influence their action as chemical contaminants: they can present themselves as large and chemically complex molecules with different structures, functionalities, shape, and molecular weight; they can present more than one ionizable group depending on the medium pH; they are moderately soluble in water; some can persist in the environment for years and can be accumulated and become biologically active (Rivera-Utrilla et al., 2013; Patel et al., 2019). Additionally, the presence of pharmaceutical metabolites, derived from the several transformations that may occur during metabolism, may conserve biologic activity, and express a different environmental behavior than the pharmaceutical, increasing the complexity of this problematic (Patel et al., 2019). Pharmaceuticals enter the environment through several sources, namely, wastes from industrial activities, hospital effluents, private households and landfills (Kümmerer, 2008; Rivera-Utrilla et al., 2013; Frederic and Yves, 2014; Gadipelly et al., 2014; Chonova et al., 2016; Kaczala and Blum, 2016; Sangion and Gramatica, 2016; Ebele et al., 2017; Courtier et al., 2019) (Figure 2.1).

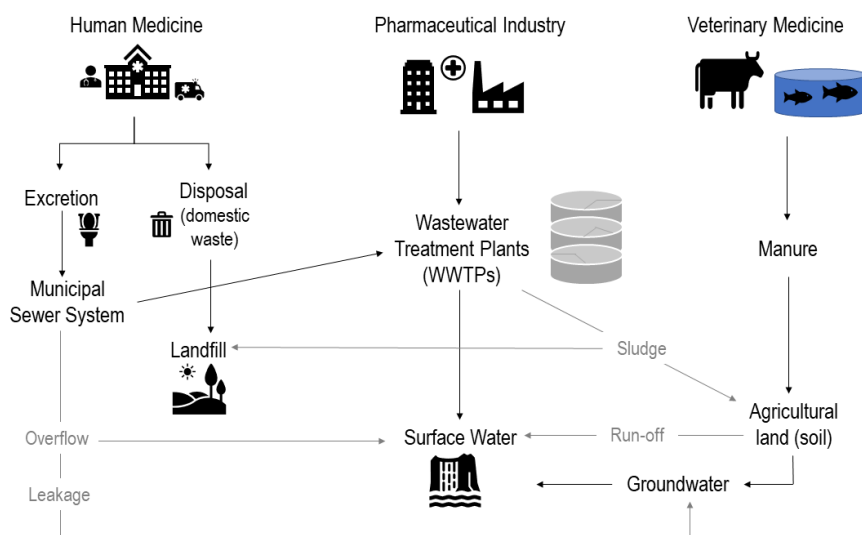


Figure 2.1. Schematic representation of the possible sources of water contamination by pharmaceuticals (based on Ebele et al. (2017) and Patel et al. (2019)).

The presence of pharmaceuticals in the aquatic environment is mainly attributed to the inefficiency of the wastewater treatment plants (WWTP) in the removal of these compounds, mostly because the applied conventional treatments were not designed for that purpose (Majumder et al., 2019; Patel et al., 2019). Therefore, effluents of these plants are a primary concern since they are the main pathway of the introduction of pharmaceuticals into water bodies due to the discharged contaminated effluents and the application of sludge in soils (Evgenidou et al., 2015; Barbosa et al., 2016; Ebele et al., 2017; De Andrade et al., 2018; Majumder et al., 2019; Patel et al., 2019).

In general, the removal percentages of pharmaceuticals in WWTP are very distinct, depending on the compound/metabolite and, therefore, on its physicochemical properties, namely, water solubility and octanol/water coefficient ($\log K_{ow}$), tendency to volatilize or to adsorb, and degradation half-life, along with the specific treatment processes of the WWTP (Zhang et al., 2008; Rivera-Utrilla et al., 2013; Evgenidou et al., 2015; Gurke et al., 2015; Ebele et al., 2017; Courtier et al., 2019; Majumder et al., 2019; Patel et al., 2019). For instance, hydrophilic pharmaceuticals tend to be less adsorbed onto the settling particles in primary treatment, therefore, presenting low removal percentages in this treatment stage (Majumder et al., 2019; Patel et al., 2019). Also, pharmaceuticals may be harmful for microorganisms implying the inhibition of microbiological activity and therefore of the degradation process in biological treatment (Majumder et al., 2019; Patel et al., 2019). Furthermore, the possible transformation of some metabolites into the parent compound may lead to the detection of higher concentrations of the pharmaceutical product in the effluent of the WWTP compared to the influent (Patel et al., 2019). All this together with other external factors, such as pH and seasonality, also cause variations in the removal efficiency of the different pharmaceuticals (Wang and Wang, 2016; Patel et al., 2019).

Besides conventional treatments, other processes can be applied in WWTP, namely, ozonation and other advanced oxidation processes (AOP) (such photolysis and Fenton oxidation), membrane filtration, reverse osmosis, and adsorption via AC (Chong et al., 2010; Rivera-Utrilla et al., 2013; Gogoi et al., 2018; Patel et al., 2019). These treatments allow to enhance the removal efficiency of pharmaceuticals, however, they are also influenced by the physicochemical properties of the compounds, as well as by the operation conditions of the respective treatment (Patel et al., 2019). Among these methods, adsorption by AC (physical method) and ozonation (chemical method) are referred as the main alternatives to achieve an efficient removal of organic micropollutants (Kårelid et al., 2017). Ozonation is considered an efficient method and widely used for the removal of pharmaceuticals from water and wastewater (Wang and Wang, 2016; Patel et al., 2019). However, one of the main problems of ozonation

is the generation of by-products that may be toxic and, particularly in wastewater, this method may not be completely efficient due to matrix effects on the formation of hydroxyl radicals (Wang and Wang, 2016; De Andrade et al., 2018).

AC adsorption is, likewise, considered a versatile method to the treatment of wastewaters (Rakić et al., 2015; Wang and Wang, 2016). In general, adsorption processes present good performance in water treatment systems; however, they also face some limitations mostly related to technical challenges (for instance, post-separation, agglomeration), short-life, influence of organic matter, and also high economical costs (Chong et al., 2010; Chon et al., 2015). Nevertheless, adsorption processes have shown to efficiently remove pharmaceuticals from water, being also a relatively passive process, performed in mild operation conditions, with low energy consumption and do not release by-products for the treated water (De Andrade et al., 2018). Different mechanisms have been proposed to explain the adsorption of pharmaceuticals onto AC, namely, dispersive interactions between π electrons of the aromatic ring and π electrons of the graphene planes of the AC surface; formation of a donor-acceptor complex involving carbonyl type surface groups (donors) and the aromatic rings (acceptors); electrostatic/dispersion interactions and hydrogen bonds (Moreno-Castilla, 2004; Terzyk, 2004; Villaescusa et al., 2011; Rivera-Utrilla et al., 2013). These mechanisms are affected by numerous variables that ultimately affect adsorption efficiency such as solubility of the adsorbate, hydrophobicity of both adsorbate and adsorbent, pH of the medium, polarity and molecular size of the adsorbate (Moreno-Castilla, 2004; Dabrowski et al., 2005; Nabais et al., 2008; Rivera-Utrilla et al., 2013). In any case, important advantages of AC based treatments for the removal of pharmaceuticals are that they do not generate toxic or pharmacologically active products; the surface of AC can be modified in order to strengthen π - π interactions or to be specific to a pharmaceutical or a group of pharmaceuticals; and AC possesses a high adsorption capacity towards a huge variety of pharmaceutical compounds (Rivera-Utrilla et al., 2013).

In that sense, it is important to deepen effective and specific treatments, such as adsorption, in order to reduce the environmental impact of pharmaceutical compounds that are present in effluents (Rivera-Utrilla et al., 2013).

2.4. References

- Al Bahri, M.; Calvo, L.; Gilarranz, M. A.; Rodriguez, J. J. Activated carbon from grape seeds upon chemical activation with phosphoric acid: Application to the adsorption of diuron from water. *Chem. Eng. J.* 2012, 203, 348.
- Alcañiz-Monge, J., Illan-Gomez, M.J., 2008. Insight into hydroxides-activated coals: chemical or physical activation? *J. Colloid Interf. Sci.* 318, 35-41.
- Arena, N., Lee, J., Clift, R., 2016. Life Cycle Assessment of activated carbon production from coconut shells. *J. Clean. Prod.* 125, 68-77.
- Auta, M., Hameed, B.H., 2014. Optimized and functionalized paper sludge activated with potassium fluoride for single and binary adsorption of reactive dyes. *J. Ind. Eng. Chem.* 20, 830-840.
- Barbosa, M.O., Moreira, N.F., Ribeiro, A.R., Pereira, M.F., Silva, A.M., 2016. Occurrence and removal of organic micropollutants: An overview of the watch list of EU Decision 2015/495. *Water Res.* 94, 257-279.
- Barroso-Bogeat, A., Alexandre-Franco, M., Fernández-González, C., Gómez-Serrano, V., 2014. FT-IR Analysis of Pyrone and Chromene Structures in Activated Carbon. *Energy & Fuels* 28, 4096-4103.
- Bergna, D., Varila, T., Romar, H., Lassi, U., 2018. Comparison of the Properties of Activated Carbons Produced in One-Stage and Two-Stage Processes. *Journal of Carbon Research* 4, 41.
- Bhatnagar, A., Hogland, W., Marques, M., Sillanpää, M., 2013. An overview of the modification methods of activated carbon for its water treatment applications. *Chem. Eng. J.* 219, 499-511.
- Brodin, T., Fick, J., Jonsson, M., Klaminder, J., 2013. Dilute Concentrations of Psychiatric Drug Alter Behavior of Fish from Natural Populations. *Science* 339.
- Calisto, V., Ferreira, C.I., Oliveira, J.A., Otero, M., Esteves, V.I., 2015. Adsorptive removal of pharmaceuticals from water by commercial and waste-based carbons. *J. Environ. Manage.* 152, 83-90.
- Calisto, V., Ferreira, C.I., Santos, S.M., Gil, M.V., Otero, M., Esteves, V.I., 2014. Production of adsorbents by pyrolysis of paper mill sludge and application on the removal of citalopram from water. *Bioresour. Technol.* 166, 335-344.
- Calvete, T., Lima, E.C., Cardoso, N.F., Dias, S.L.P., Pavan, F.A., 2009. Application of carbon adsorbents prepared from the Brazilian pine-fruit-shell for the removal of Procion Red MX 3B from aqueous solution—Kinetic, equilibrium, and thermodynamic studies. *Chem. Eng. J.* 155, 627-636.
- CELPA, 2018. Boletim Estatístico Indústria Papeleira Portuguesa. In <http://www.celipa.pt/wp-content/uploads/2020/01/Boletim_WEB_Final_Dez2019.pdf>.
- Chen, D., Xie, S., Chen, C., Quan, H., Hua, L., Luo, X., Guo, L., 2017. Activated biochar derived from pomelo peel as a high-capacity sorbent for removal of carbamazepine from aqueous solution. *RSC Advances* 7, 54960-54979.

- Chon, K., Salhi, E., von Gunten, U., 2015. Combination of UV absorbance and electron donating capacity to assess degradation of micropollutants and formation of bromate during ozonation of wastewater effluents. *Water Res.* 81, 388-397.
- Chong, M.N., Jin, B., Chow, C.W., Saint, C., 2010. Recent developments in photocatalytic water treatment technology: a review. *Water Res.* 44, 2997-3027.
- Chonova, T., Keck, F., Labanowski, J., Montuelle, B., Rimet, F., Bouchez, A., 2016. Separate treatment of hospital and urban wastewaters: A real scale comparison of effluents and their effect on microbial communities. *Sci. Total Environ.* 542, 965-975.
- Chowdhury, S., Sikder, J., Mandal, T., Halder, G., 2019. Comprehensive analysis on sorptive uptake of enrofloxacin by activated carbon derived from industrial paper sludge. *Sci. Total Environ.* 665, 438-452.
- Comber, S., Gardner, M., Sörme, P., Leverett, D., Ellor, B., 2018. Active pharmaceutical ingredients entering the aquatic environment from wastewater treatment works: A cause for concern? *Sci. Total Environ.* 613-614, 538-547.
- Courtier, A., Cadiere, A., Roig, B., 2019. Human pharmaceuticals: Why and how to reduce their presence in the environment. *Current Opinion in Green and Sustainable Chemistry* 15, 77-82.
- Dabrowski, A., 2001. Adsorption - from theory to practice. *Adv. Colloid Interfac.* 93, 135-224.
- Dabrowski, A., Podkoscielny, P., Hubicki, Z., Barczak, M., 2005. Adsorption of phenolic compounds by activated carbon-a critical review. *Chemosphere* 58, 1049-1070.
- De Andrade, J.R., Oliveira, M.F., Da Silva, M.G.C., Vieira, M.G.A., 2018. Adsorption of Pharmaceuticals from Water and Wastewater Using Nonconventional Low-Cost Materials: A Review. *Ind. Eng. Chem. Res.* 57, 3103-3127.
- Decision 2015/495/EU of 20 March 2015 establishing a watch list of substances for Union-wide monitoring in the field of water policy pursuant to Directive 2008/105/EC of the European Parliament and of the Council, *Off. J. Eur. Union* 78 (2015) 40-42.
- Decision 2018/840/EU of 5 June 2018 establishing a watch list of substances for Union-wide monitoring in the field of water policy pursuant to Directive 2008/105/EC of the European Parliament and of the Council and repealing Commission Implementing Decision (EU) 2015/495 *Off. J. Eur. Union* 141 (2015) 9-12.
- Devi, P., Saroha, A.K., 2016. Improvement in performance of sludge-based adsorbents by controlling key parameters by activation/modification: A critical review. *Crit. Rev. Env. Sci. Tec.* 46, 1704-1743.
- Directive 2000/60/EC of the European Parliament and of the Council of 23 October 2000 establishing a framework for Community action in the field of water policy. *Official Journal* 327, 0001 – 0073.
- Directive 2008/105/EC of the European Parliament and of the Council of 16 December 2008 on environmental quality standards in the field of water policy, amending and subsequently repealing

- Council Directives 82/176/EEC, 83/513/EEC, 84/156/EEC, 84/491/EEC, 86/280/EEC and amending Directive 2000/60/EC of the European Parliament and of the Council.
- Dongil, A.B., Bachiller-Baeza, B., Guerrero-Ruiz, A., Rodriguez-Ramos, I., Martinez-Alonso, A., Tascon, J.M., 2011. Surface chemical modifications induced on high surface area graphite and carbon nanofibers using different oxidation and functionalization treatments. *J. Colloid Interf. Sci.* 355, 179-189.
- Ebele, A.J., Abou-Elwafa Abdallah, M., Harrad, S., 2017. Pharmaceuticals and personal care products (PPCPs) in the freshwater aquatic environment. *Emerging Contaminants* 3, 1-16.
- Evgenidou, E.N., Konstantinou, I.K., Lambropoulou, D.A., 2015. Occurrence and removal of transformation products of PPCPs and illicit drugs in wastewaters: a review. *Sci Total Environ.* 505, 905-926.
- Faubert, P., Barnabé, S., Bouchard, S., Côté, R., Villeneuve, C., 2016. Pulp and paper mill sludge management practices: What are the challenges to assess the impacts on greenhouse gas emissions? *Resour. Conserv. Recycl.* 108, 107-133.
- Ferreira, C.I.A., Calisto, V., Otero, M., Nadais, H., Esteves, V.I., 2017. Removal of tricaine methanesulfonate from aquaculture wastewater by adsorption onto pyrolysed paper mill sludge Catarina. *Chemosphere* 139, 139-146.
- Ferreira, C.I.A., Calisto, V., Santos, S.M., Cuerda-Correa, E.M., Otero, M., Nadais, H., Esteves, V.I., 2015. Application of pyrolysed agricultural biowastes as adsorbents for fish anaesthetic (MS-222) removal from water. *J. Anal. Appl. Pyrol.* 112, 313-324.
- Figueiredo, J.L., 2013. Functionalization of porous carbons for catalytic applications. *J. Mater. Chem. A* 1, 9351-9364.
- Foster, H.R., Burton, G.A., Basu, N., Werner, E.E., 2010. Chronic exposure to fluoxetine (Prozac) causes developmental delays in *Rana pipiens* larvae. *Environ. Toxicol. Chem.* 29, 2845-2850.
- Frederic, O., Yves, P., 2014. Pharmaceuticals in hospital wastewater: their ecotoxicity and contribution to the environmental hazard of the effluent. *Chemosphere* 115, 31-39.
- Gadipelly, C., Pérez-González, A., Yadav, G.D., Ortiz, I., Ibáñez, R., Rathod, V.K., Marathe, K.V., 2014. Pharmaceutical Industry Wastewater: Review of the Technologies for Water Treatment and Reuse. *Ind. Eng. Chem. Res.* 53, 11571-11592.
- Gaur, V.K., Sharma, P., Sirohi, R., Awasthi, M.K., Dussap, C.-G., Pandey, A., 2020. Assessing the impact of industrial waste on environment and mitigation strategies: A comprehensive review. *J. Hazard. Mater.* 398, 123019.
- Gavrilescu, M., Demnerova, K., Aamand, J., Agathos, S., Fava, F., 2015. Emerging pollutants in the environment: present and future challenges in biomonitoring, ecological risks and bioremediation. *New Biotechnol.* 32, 147-156.

- Girods, P., Dufour, A., Fierro, V., Rogaume, Y., Rogaume, C., Zoulalian, A., Celzard, A., 2009. Activated carbons prepared from wood particleboard wastes: characterisation and phenol adsorption capacities. *J. Hazard. Mater.* 166, 491-501.
- Girods, P.; Dufour, A.; Fierro, V.; Rogaume, Y.; Rogaume, C.; Zoulalian, A.; Celzard, A. Activated carbons prepared from wood particleboard wastes: characterisation and phenol adsorption capacities. *J. Hazard. Mater.* 2009, 166 (1), 491.
- Gogoi, A., Mazumder, P., Tyagi, V.K., Chaminda, G.G.T., An, A.K., Kumar, M., 2018. Occurrence and fate of emerging contaminants in water environment: A review. *Groundw. Sustain. Dev.* 6, 169-180.
- González-García, P., 2018. Activated carbon from lignocellulosics precursors: A review of the synthesis methods, characterization techniques and applications. *Renew. Sustain. Energ. Rev.* 82, 1393-1414.
- Gros, M., Petrovic, M., Ginebreda, A., Barcelo, D., 2010. Removal of pharmaceuticals during wastewater treatment and environmental risk assessment using hazard indexes. *Environ. Int.* 36, 15-26.
- Gurke, R., Rossler, M., Marx, C., Diamond, S., Schubert, S., Oertel, R., Fauler, J., 2015. Occurrence and removal of frequently prescribed pharmaceuticals and corresponding metabolites in wastewater of a sewage treatment plant. *Sci. Total Environ.* 532, 762-770.
- Hagemann, N., Spokas, K., Schmidt, H.-P., Kägi, R., Böhler, M.A., Bucheli, T.D., 2018. Activated Carbon, Biochar and Charcoal: Linkages and Synergies across Pyrogenic Carbon's ABCs. *Water* 10.
- Hameed, B. H.; Ahmad, A. L.; Latiff, K. N. A., 2007. Adsorption of basic dye (methylene blue) onto activated carbon prepared from rattan sawdust. *Dyes and Pigments* 75 (1), 143.
- Han, Q., Wang, J., Goodman, B.A., Xie, J., Liu, Z., 2020. High adsorption of methylene blue by activated carbon prepared from phosphoric acid treated eucalyptus residue. *Powder Technol.* 366, 239-248.
- Heidarinejad, Z., Dehghani, M.H., Heidari, M., Javedan, G., Ali, I., Sillanpää, M., 2020. Methods for preparation and activation of activated carbon: a review. *Environ. Chem. Lett.* 18, 393-415.
- Hofman, M., Pietrzak, R., 2012. NO₂ removal by adsorbents prepared from waste paper sludge. *Chem. Eng. J.*, 183, 278-283.
- Jagiello, K., Mostrag-Szlichtyng, A., Gajewicz, A., Kawai, T., Imaizumi, Y., Sakurai, T., Yamamoto, H., Tatarazako, N., Mizukawa, K., Aoki, Y., Suzuki, N., Watanabe, H., Puzyn, T., 2015. Towards modelling of the environmental fate of pharmaceuticals using the QSPR-MM scheme. *Environ. Modell. Softw.* 72, 147-154.
- Jaramillo, J., Álvarez, P.M., Gómez-Serrano, V., 2010. Oxidation of activated carbon by dry and wet methods. *Fuel Process. Technol.* 91, 1768-1775.
- Jaria, G., Calisto, V., Gil, M.V., Otero, M., Esteves, V.I., 2015. Removal of fluoxetine from water by adsorbent materials produced from paper mill sludge. *J. Colloid Interf. Sci.* 448, 32-40.

- Jaria, G., Calisto, V., Otero, M., Esteves, V.I., 2020. Monitoring pharmaceuticals in the aquatic environment using enzyme-linked immunosorbent assay (ELISA) - a practical overview. *Anal. Bioanal. Chem.* 412, 3983-4008.
- Kaczala, F., Blum, S.E., 2016. The Occurrence of Veterinary Pharmaceuticals in the Environment: A Review. *Curr. Anal. Chem.* 12, 169-182.
- Karagoz, S.; Tay, T.; Ucar, S.; Erdem, M., 2008. Activated carbons from waste biomass by sulfuric acid activation and their use on methylene blue adsorption. *Bioresour. Technol.* 2008, 99 (14), 6214.
- Kårelid, V., Larsson, G., Björleinius, B., 2017. Pilot-scale removal of pharmaceuticals in municipal wastewater: Comparison of granular and powdered activated carbon treatment at three wastewater treatment plants. *J. Environ. Manage.* 193, 491-502.
- Khalili, N.R., Campbell, M., Sandi, G., Golas, J., 2000. Production of micro- and mesoporous activated carbon from paper mill sludge - I. Effect of zinc chloride activation. *Carbon* 38, 1905-1915.
- Khalili, N.R., Vyas, J.D., Weangkaew, W., Westfall, S.J., Parulekar, S.J., Sherwood, R., 2002. Synthesis and characterization of activated carbon and bioactive adsorbent produced from paper mill sludge. *Sep. Purif. Technol.* 26, 295-304.
- Krahnstöver, T., Wintgens, T., 2018. Separating powdered activated carbon (PAC) from wastewater – Technical process options and assessment of removal efficiency. *J. Environ. Chem. Eng.* 6, 5744–5762.
- Kümmerer, K., 2008. *Pharmaceuticals in the Environment - Sources, Fate, Effects and Risks*, Third ed. Springer, Heidelberg.
- Kwiatkowski, M., Broniek, E., 2017. An analysis of the porous structure of activated carbons obtained from hazelnut shells by various physical and chemical methods of activation. *Colloids Surf. A Physicochem. Eng. Asp.* 529, 443-453.
- Kyzas, G., Fu, J., Matis, K., 2013. The Change from Past to Future for Adsorbent Materials in Treatment of Dyeing Wastewaters. *Materials* 6, 5131-5158.
- Lebègue, E., Brousse, T., Gaubicher, J., Cougnon, C., 2013a. Chemical functionalization of activated carbon through radical and diradical intermediates. *Electrochem. Commun.* 34, 14-17.
- Lebègue, E., Brousse, T., Gaubicher, J., Cougnon, C., 2013b. Spontaneous arylation of activated carbon from aminobenzene organic acids as source of diazonium ions in mild conditions. *Electrochim. Acta* 88, 680-687.
- Lebègue, E., Madec, L., Brousse, T., Gaubicher, J., Levillain, E., Cougnon, C., 2011. Modification of activated carbons based on diazonium ions in situ produced from aminobenzene organic acid without addition of other acid. *J. Mater. Chem.* 21, 12221-12223.
- Li, L., Quinlivan, P.A., Knappe, D.R.U., 2002. Effects of activated carbon surface chemistry and pore structure on the adsorption of organic contaminants from aqueous solution. *Carbon* 40, 2085-2100.
- Li, T., Huang, B., Wang, S., Chen, C., Tang, L., Lu, Q., Lin, W., 2013. Covalent Grafting of Organic Molecules onto Activated Carbon by a Single Step. *BioResources* 8, 2300-2309.

- Li, W., Yue, Q., Tu, P., Ma, Z., Gao, B., Li, J., Xu, X., 2011b. Adsorption characteristics of dyes in columns of activated carbon prepared from paper mill sewage sludge. *Chem. Eng. J.* 178, 197-203.
- Li, W.C., 2014. Occurrence, sources, and fate of pharmaceuticals in aquatic environment and soil. *Environ. Pollut.* 187, 193-201.
- Li, W.-H., Yue, Q.-Y., Gao, B.-Y., Wang, X.-J., Qi, Y.-F., Zhao, Y.-Q., Li, Y.-J., 2011a. Preparation of sludge-based activated carbon made from paper mill sewage sludge by steam activation for dye wastewater treatment. *Desalination* 278, 179-185.
- Lima, D.R., Gomes, A.A., Lima, E.C., Umpierres, C.S., Thue, P.S., Panzenhagen, J.C.P., Dotto, G.L., El-Chaghaby, G.A., de Alencar, W.S., 2019. Evaluation of efficiency and selectivity in the sorption process assisted by chemometric approaches: Removal of emerging contaminants from water. *Spectrochim. Acta A Mol. Biomol. Spectrosc.* 218, 366-373.
- Loos, R., Marinov, D., Sanseverino, I., Napierska, D., Lettieri, T., 2018. Review of the 1st Watch List under the Water Framework Directive and recommendations for the 2nd Watch List, EUR 29173 EN, Publications Office of the European Union, Luxembourg, ISBN 978-92-79-81839-4, doi:10.2760/614367, JRC111198.
- Majumder, A., Gupta, B., Gupta, A.K., 2019. Pharmaceutically active compounds in aqueous environment: A status, toxicity and insights of remediation. *Environ. Res.* 176, 108542.
- Mandeep, Gupta, G.K., Shukla, P., 2020. Insights into the resources generation from pulp and paper industry wastes: Challenges, perspectives and innovations. *Bioresour. Technol.* 297, 122496.
- Mansour, F., Al-Hindi, M., Yahfoufi, R., Ayoub, G.M., Ahmad, M.N., 2018. The use of activated carbon for the removal of pharmaceuticals from aqueous solutions: a review. *Rev. Environ. Sci. Biotechnol.* 17, 109-145.
- Marsh, H., Rodríguez-Reinoso, F., 2006. Activated Carbon, First ed. Elsevier, England.
- Molina-Sánchez, E., Leyva-Díaz, J., Cortés-García, F., Molina-Moreno, V., 2018. Proposal of Sustainability Indicators for the Waste Management from the Paper Industry within the Circular Economy Model. *Water* 10, 1014.
- Monte, M.C., Fuente, E., Blanco, A., Negro, C., 2009. Waste management from pulp and paper production in the European Union. *Waste Manage.* 29, 293-308.
- Moreno-Castilla, C., 2004. Adsorption of organic molecules from aqueous solutions on carbon materials. *Carbon* 42, 83-94.
- Nabais, J.M.V., Mouquinho, A., Galacho, C., Carrott, P.J.M., Ribeiro Carrott, M.M.L., 2008. In vitro adsorption study of fluoxetine in activated carbons and activated carbon fibres. *Fuel Process. Technol.* 89, 549-555.
- Nahil, M.A., Williams, P.T., 2012. Characterisation of Activated Carbons with High Surface Area and Variable Porosity Produced from Agricultural Cotton Waste by Chemical Activation and Co-activation. *Waste Biomass Valori.* 3, 117-130.

- Patel, M., Kumar, R., Kishor, K., Mlsna, T., Jr., Pittman, C.U., Mohan, D., 2019. Pharmaceuticals of Emerging Concern in Aquatic Systems: Chemistry, Occurrence, Effects, and Removal Methods. *Chem. Rev.* 119, 3510–3673.
- Petrie, B., Barden, R., Kasprzyk-Hordern, B., 2015. A review on emerging contaminants in wastewaters and the environment: Current knowledge, understudied areas and recommendations for future monitoring. *Water Res.* 72, 3-27.
- Pierson, H.O., 1993. Handbook of Carbon, Graphite, Diamond and Fullerenes - Properties, Processing and Applications. Noyes Publications, New Jersey.
- Pietrzak, R.; Nowicki, P.; Kazmierczak, J.; Kuszynska, I.; Goscianska, J.; Przepiorski, J. Comparison of the effects of different chemical activation methods on properties of carbonaceous adsorbents obtained from cherry stones. *Chem. Eng. Res. Des.* 2014, 92 (6), 1187.
- Pognon, G., Brousse, T., Bélanger, D., 2011. Effect of molecular grafting on the pore size distribution and the double layer capacitance of activated carbon for electrochemical double layer capacitors. *Carbon* 49, 1340-1348.
- Radkevich, V.Z., Senko, T.L., Wilson, K., Grishenko, L.M., Zaderko, A.N., Diyuk, V.Y., 2008. The influence of surface functionalization of activated carbon on palladium dispersion and catalytic activity in hydrogen oxidation. *Applied Catalysis A: General* 335, 241-251.
- Rakić, V., Rac, V., Krmar, M., Otman, O., Auroux, A., 2015. The adsorption of pharmaceutically active compounds from aqueous solutions onto activated carbons. *J. Hazard. Mater.* 282, 141-149.
- Richmond, E.K., Grace, M.R., Kelly, J.J., Reisinger, A.J., Rosi, E.J., Walters, D.M., 2017. Pharmaceuticals and personal care products (PPCPs) are ecological disrupting compounds (EcoDC). *Elem. Sci. Anth.* 5, 66.
- Rivera-Utrilla, J., Sánchez-Polo, M., Ferro-García, M.Á., Prados-Joya, G., Ocampo-Pérez, R., 2013. Pharmaceuticals as emerging contaminants and their removal from water. A review. *Chemosphere* 93, 1268-1287.
- Rivera-Utrilla, J., Sanchez-Polo, M., Gomez-Serrano, V., Alvarez, P.M., Alvim-Ferraz, M.C., Dias, J.M., 2011. Activated carbon modifications to enhance its water treatment applications. An overview. *J. Hazard. Mater.* 187, 1-23.
- Rouquerol, F., Rouquerol, J., Sing, K.S.W., Llewellyn, P., Maurin, G., 2014. Adsorption by Powders and Porous Solids - Principles, Methodology and Applications, Second ed. Academic Press, Poland.
- Sangion, A., Gramatica, P., 2016. Hazard of pharmaceuticals for aquatic environment: Prioritization by structural approaches and prediction of ecotoxicity. *Environ. Int.* 95, 131-143.
- Selvaraju, G., Bakar, N.K.A., 2017. Production of a new industrially viable green-activated carbon from *Artocarpus integer* fruit processing waste and evaluation of its chemical, morphological and adsorption properties. *J. Clean. Prod.* 141, 989-999.

- Seo, P.W., Bhadra, B.N., Ahmed, I., Khan, N.A., Jhung, S.H., 2016. Adsorptive Removal of Pharmaceuticals and Personal Care Products from Water with Functionalized Metal-organic Frameworks: Remarkable Adsorbents with Hydrogen-bonding Abilities. *Sci. Rep.* 6, 34462-34462.
- Silva, C.P., Jaria, G., Otero, M., Esteves, V.I., Calisto, V., 2018. Waste-based alternative adsorbents for the remediation of pharmaceutical contaminated waters: Has a step forward already been taken? *Bioresource Technol.* 250, 888–901.
- Simão, L., Hotza, D., Raupp-Pereira, F., Labrincha, J.A., Montedo, O.R.K., 2018. Wastes from pulp and paper mills - a review of generation and recycling alternatives. *Cerâmica* 64, 443-453.
- Singha, S., Sarkar, U., Luharuka, P., 2013. Functionalized granular activated carbon and surface complexation with chromates and bi-chromates in wastewater. *Sci. Total. Environ.* 447, 472-487.
- Soucy, J., Koubaa, A., Migneault, S., Riedl, B., 2014. The potential of paper mill sludge for wood–plastic composites. *Ind. Crop. Prod.* 54, 248-256.
- Sousa, A.F.C., Gil, M.V. & Calisto, V., 2020. Upcycling spent brewery grains through the production of carbon adsorbents - application to the removal of carbamazepine from water. *Environ. Sci. Pollut. R.* 27, 36463–36475.
- Sousa, J.C.G., Ribeiro, A.R., Barbosa, M.O., Pereira, M.F.R., Silva, A.M.T., 2018. A review on environmental monitoring of water organic pollutants identified by EU guidelines. *J. Hazard. Mater.* 344, 146-162.
- Stavropoulos, G.G., Samaras, P., Sakellaropoulos, G.P., 2008. Effect of activated carbons modification on porosity, surface structure and phenol adsorption. *J. Hazard. Mater.* 151, 414-421.
- Stein, A., Wang, Z., Fierke, M.A., 2009. Functionalization of Porous Carbon Materials with Designed Pore Architecture. *Adv. Mater.* 21, 265-293.
- Taheran, M., Naghdi, M., Brar, S.K., Verma, M., Surampalli, R.Y., 2018. Emerging contaminants: Here today, there tomorrow! *Environ. Nanotechnol. Monit. Manag.* 10, 122-126.
- Terzyk, A.P., 2004. Molecular properties and intermolecular forces--factors balancing the effect of carbon surface chemistry in adsorption of organics from dilute aqueous solutions. *J. Colloid Interf. Sci.* 275, 9-29.
- Thakur, V.K., Thakur, M.K., 2016. Chemical Functionalization of Carbon Nanomaterials - Chemistry and Applications. CRC Press, New York.
- Tzvetkov, G., Mihaylova, S., Stoitchkova, K., Tzvetkov, P., Spassov, T., 2016. Mechanochemical and chemical activation of lignocellulosic material to prepare powdered activated carbons for adsorption applications. *Powder Technol.* 299, 41-50.
- Ukanwa, K.S., Patchigolla, K., Sakrabani, R., Anthony, E., Mandavgane, S., 2019. A Review of Chemicals to Produce Activated Carbon from Agricultural Waste Biomass. *Sustainability* 11, 6204.
- Velo-Gala, I., López-Peñalver, J.J., Sánchez-Polo, M., Rivera-Utrilla, J., 2014. Surface modifications of activated carbon by gamma irradiation. *Carbon* 67, 236-249.

- Villaescusa, I., Fiol, N., Poch, J., Bianchi, A., Bazzicalupi, C., 2011. Mechanism of paracetamol removal by vegetable wastes: The contribution of π - π interactions, hydrogen bonding and hydrophobic effect. *Desalination* 270, 135-142.
- Wang, J., Wang, S., 2016. Removal of pharmaceuticals and personal care products (PPCPs) from wastewater: A review. *J. Environ. Manage.* 182, 620-640.
- Wang, X., Hu, M., Hu, W., Chen, Z., Liu, S., Hu, Z., Xiao, B., 2016. Thermogravimetric kinetic study of agricultural residue biomass pyrolysis based on combined kinetics. *Bioresource Technol.* 219, 510-520.
- Yahya, M.A., Al-Qodah, Z., Ngah, C.W.Z., 2015. Agricultural bio-waste materials as potential sustainable precursors used for activated carbon production: A review. *Renew. Sust. Energ. Rev.* 46, 218-235.
- Yang, J.; Qiu, K. Preparation of activated carbons from walnut shells via vacuum chemical activation and their application for methylene blue removal. *Chem. Eng. J.* 2010, 165 (1), 209.
- Yang, Y., Ok, Y.S., Kim, K.H., Kwon, E.E., Tsang, Y.F., 2017. Occurrences and removal of pharmaceuticals and personal care products (PPCPs) in drinking water and water/sewage treatment plants: A review. *Sci. Total Environ.* 596-597, 303-320.
- Yu, M., Gong, H., Chen, Z., Zhang, M., 2013. Adsorption characteristics of activated carbon for siloxanes. *J. Environ. Chem. Eng.* 1, 1182-1187.
- Yunus, Z.M., Al-Gheethi, A., Othman, N., Hamdan, R., Ruslan, N.N., 2020. Removal of heavy metals from mining effluents in tile and electroplating industries using honeydew peel activated carbon: A microstructure and techno-economic analysis. *J. Clean. Prod.* 251, 119738.
- Zhang, J., 2013. Phenol Removal from Water with Potassium Permanganate Modified Granular Activated Carbon. *Journal of Environmental Protection* 4, 411-417.
- Zhang, Y., Geissen, S.U., Gal, C., 2008. Carbamazepine and diclofenac: removal in wastewater treatment plants and occurrence in water bodies. *Chemosphere* 73, 1151-1161.
- Zhang, Y., Song, X., Zhang, P., Gao, H., Ou, C., Kong, X., 2020. Production of activated carbons from four wastes via one-step activation and their applications in Pb²⁺ adsorption: Insight of ash content. *Chemosphere* 245, 125587.
- Zhou, J., Luo, A., Zhao, Y., 2018. Preparation and characterisation of activated carbon from waste tea by physical activation using steam. *J. Air Waste Manage.* 68, 1269-1277.

3

VIABILITY OF USING PULP AND PAPER MILL SLUDGE TO PRODUCE CARBON-BASED ADSORBENTS

Abstract

Pulp and paper industry produces massive amounts of sludge from wastewater treatment, which constitute an enormous environmental challenge. A possible management option is the conversion of sludge into carbon-based adsorbents to be applied in water remediation. For such utilization, it is important to investigate if sludge is a consistent raw material originating reproducible final materials (either over time or from different manufacturing processes), which is the main goal of this work. For that purpose, different primary (PS) and biological sludge (BS) batches from two factories with different operation modes were sampled and subjected to pyrolysis (P materials) and to pyrolysis followed by acid washing (PW materials). All the materials were characterized by proximate analysis, total organic carbon (TOC) and inorganic carbon (IC), attenuated total reflectance Fourier transform infrared spectroscopy (ATR-FTIR) and N_2 adsorption isotherms (specific surface area (S_{BET}) and porosity determination). Sludge from the two factories proved to have distinct physicochemical properties, mainly in what concerns IC. After pyrolysis, the washing step was essential to reduce IC and to considerably increase S_{BET} , yet with high impact in the final product yield. Among the produced materials, PW materials from PS were those having the highest S_{BET} values (387-488 $m^2 g^{-1}$). Overall, it was found that precursors from different factories might originate final materials with distinct characteristics, being essential to take into account this source of variability when considering pulp and paper mill sludge as a raw material. Nevertheless, for PS, low variability was found between batches, which points out to the reliability of such residues to be used as precursors of carbon adsorbents.

This chapter was based on the published article:

Jaria, G., Silva, C.P., Ferreira, C.I., Otero, M., Calisto, V., 2017. Sludge from paper mill effluent treatment as raw material to produce carbon adsorbents: An alternative waste management strategy. *J. Environ. Manage.* 188, 203-211.

3.1. Contextualization

Pulp and paper industry is considered to be one of the most important industrial segments in the world. The enormous water requirements of this industry results in the generation of huge volumes of wastewater (on average, in a typical paper mill, between 1.5 m³ and 60 m³ of effluent is generated for each ton of paper) (Soucy et al., 2014; Adhikari and Bhattacharyya, 2015). As a consequence of the effluent treatment, a large quantity of sludge is produced (see more detailed information in chapter 2, section 2.1), which represents a massive environmental burden. Biological (BS) and primary sludge (PS) are amongst the produced solid wastes and their properties depend on the manufacturing process, namely wood preparation, pulp and paper manufacture, chemical recovery, recycled paper processing and wastewater treatment (Monte et al., 2009; Buruberry et al., 2015; Pervaiz and Sain, 2015; Vochozka et al., 2016).

In recent years, and considering that environmental legislation is increasingly stringent, the pulp and paper industry has been facing some challenges with respect to the management of the resulting wastes. This aspect must be linked to economic aspects in order to apply feasible solutions for waste management/valorization (Buruberry et al., 2015; Kamali and Khodaparast, 2015; Pervaiz and Sain, 2015). In the case of sludge from wastewater treatment, management options include incineration (approximately 19 % of sludge is incinerated on-site) for energy recovery, land application to enhance soil fertility on agricultural and forest areas, and production of ethanol (Likon and Trebše, 2012; Bajpai, 2015; Pervaiz and Sain, 2015). However, the most common practice has always been the landfill disposal of sludge (Likon and Trebše, 2012; Pervaiz and Sain, 2015). Landfills can be owned and operated by the industry itself or can be independently maintained, implying a significant cost for the mills. In any case, landfills should comply with the requirements of the European Landfill Directive (1999/31/EC) (Likon and Trebše, 2012). Nevertheless, landfilling is not recommended and is being discouraged since it causes environmental problems related with leaching and greenhouse gas production (Reckamp et al., 2014). The Confederation of European Paper Industries (CEPI) supports a complete ban of landfilling and incineration in the European Union in agreement with the Waste Framework Directive (2008/98/EC), which lays down some basic waste management principles, prioritizing recycling over energy recovery and disposal. Also, the European Commission Roadmap to a Resource Efficient Europe (COM (2011) 571) foresees the sustainability of the Europe's economy by 2050, proposing milestones to be reached by 2020 in which waste will be managed as a resource and energy recovery will be limited to non-

recyclable materials (CEPI, 2016; European Commission, 2016a, 2016b). Therefore, sustainable practices must be developed, involving the valorization of wastes, by using them as raw materials for distinct purposes (Buruberri et al., 2015). In this context, some innovative approaches for the conversion of sludge from the pulp and paper industry into new materials have been explored in the past two decades. Promising innovations include the use of such sludge as heat insulation material, paper and wood adhesive, dried mixture for use as pesticides or fertilizers carriers in agriculture and as building material (Likon and Trebše, 2012; Buruberri et al., 2015; Pervaiz and Sain, 2015). Also, given the carbonaceous nature of pulp and paper mill sludge, their conversion into activated carbon (AC) with application for water remediation has been proposed by several authors (Khalili et al., 2000; Khalili et al., 2002; Devi and Saroha, 2014; Pirzadeh and Ghoreyshi, 2014; Reckamp et al., 2014; Ferreira et al., 2016a). This conversion, besides reducing the environmental problems associated with the disposal of wastes, also enhances wastewater treatment by using materials from industrial waste itself, and helps the preservation of naturally-existing resources usually applied in the production of AC (Khalili et al., 2002). Adsorbents originated from pulp and paper mill sludge have already been applied in the adsorption of phenolic compounds (Devi and Saroha, 2014; Pirzadeh and Ghoreyshi, 2014; Devi and Saroha, 2015; Masomi et al., 2015), dyes (Li et al., 2011; Auta and Hameed, 2014), heavy metals (Battaglia et al., 2003) or pharmaceuticals (Calisto et al., 2014; Calisto et al., 2015; Ferreira et al., 2015; Jaria et al., 2015; Ferreira et al., 2016b) from contaminated waters.

There is a relationship between the properties of an adsorbent material and its effectiveness, these properties being importantly determined by the used precursor and the production process (Gonzalez et al., 1995; Namazi et al., 2010). Therefore, in order to evaluate the appropriateness of pulp and paper mill sludge as precursor for the production of carbon adsorbents, it is essential to know if these wastes are a consistent and reliable raw material, guaranteeing the repeatability of the final product through time. However, no attention is given to this aspect when studying the production of alternative adsorbents from pulp and paper mill sludge (and other residues in general).

This work aimed to assess, for the very first time, the consistency of carbon adsorbents produced by the pyrolysis of sludge from the pulp and paper industry. With this purpose, four PS and BS batches collected from two factories with different operation characteristics were used. Moreover, in order to conclude about the potential of the obtained materials as adsorbents, key physicochemical properties were determined and the influence of the raw materials on these properties evaluated. All the materials (raw sludge and resulting carbons) were characterized by proximate analysis, N₂ adsorption isotherms (specific surface area (S_{BET}) and porosity determination), total organic carbon (TOC) and inorganic carbon (IC), and attenuated total reflectance Fourier transform infrared spectroscopy (ATR-FTIR).

3.2. *Materials and Methods*

3.2.1. *Factory description and sludge production*

Sludge from two paper industries, hereafter named Factory 1 (F1) and Factory 2 (F2), were used in this work. Both factories use a kraft elemental chlorine free pulp production process and operate using *Eucalyptus globulus* wood. Factory 1 has more than 6 decades of existence and was the first one, worldwide, to produce paper pulp from eucalyptus wood by the kraft process. Its production reaches 320,000 tons of bleached pulp per year, while the Factory 2 production reaches approximately 570,000 tons of bleached eucalyptus kraft pulp and 800,000 tons of uncoated wood free printing paper. Therefore, Factory 2 combines the production of pulp and paper, while Factory 1 produces only pulp.

On average, in both factories, PS and BS are produced at a rate of 20 kg and 10 kg per ton of air dried pulp, respectively. These solid wastes are generated during the effluent treatment. PS results from fibers rejected after the cooking/digestion of the pulp and losses of fibers and other solids which occur when liquid effluents are involved (for example, washing and bleaching). The composition of PS is very similar to the pulp, consisting essentially of organic matter (mostly composed of fibrous materials) (Calisto et al., 2014; Soucy et al., 2014). BS is generated in the secondary or biological treatment and is considered as being constituted mostly by biomass (after dehydration) (chapter 2) (Calisto et al., 2014; Soucy et al., 2014). The process generates a large amount of sludge due to the microbial growth, however, as referred in chapter 2, the generated volume of BS is lower than that of PS (Monte et al., 2009).

3.2.2. *Sludge collection and conditioning*

PS and BS were collected four times from each F1 and F2 in campaigns separated by 15 days from each other (between October 2015 and February 2016). After collection, PS and BS were firstly dried at room temperature, followed by a 24 h period at 105 °C in an oven. BS was grinded with a mortar grinder and sieved (the 0.5-1.0 mm fraction was used in this work). In the case of PS, a blade mill was used after drying, resulting in an extremely light net of fibrous material which was not possible to sieve.

Sludge samples are referred as F1PS1, F1PS2, F1PS3 and F1PS4, for the four PS batches from Factory 1 (F1PS); F2PS1, F2PS2, F2PS3 and F2PS4, for the four PS batches from Factory 2 (F2PS). An

equivalent nomenclature was defined for BS samples, using, for example, F1BS1 for the first batch of BS from Factory 1.

3.2.3. Carbon adsorbents production

3.2.3.1. Pyrolysis

After sludge collection and conditioning, PS and BS samples were separately pyrolyzed into porcelain crucibles in a muffle (Nüve, series MF 106, Turkey). The pyrolysis was carried out under inert atmosphere (nitrogen flow), at 800 °C and a residence time of 150 min (heating rate of 10 °C min⁻¹). The referred production conditions were selected according to the results obtained in a previous work (Calisto et al., 2014). Pyrolyzed materials (P materials) are referred by adding “P” to the nomenclature used for the respective raw material (as defined in section 3.2.2) using, for example, F1PS1-P.

3.2.3.2. Washing

After pyrolysis, carbons were washed with 1.2 M HCl followed by distilled water until the washing solution reached neutral pH. The purpose of this procedure was to remove ashes and other inorganic matter, in order to improve microporosity and surface area by unblocking obstructed pores. Finally, the produced carbons were dried in an oven at 105 °C for 24 h. When referring materials subjected to washing after pyrolysis (PW materials), “PW” is added to the terminology of the respective raw material (as defined in section 3.2.2) using, for example, F1PS1-PW.

3.2.4. Methods for characterization of raw materials and carbon adsorbents

The physicochemical characterization of materials was obtained by determining the content in total organic carbon (TOC) and inorganic carbon (IC); Fourier transform infrared spectroscopy with attenuated total reflectance (ATR-FTIR); specific surface area (S_{BET}); and proximate analysis. The description of these methods is presented in Appendix A, sections A1; A2.3; A3.1; and A4.

Proximate analysis was only performed on the raw materials and the corresponding PW materials. P materials were not analyzed since it was concluded by the S_{BET} determination that they do not present attractive surface areas and micropore volumes and therefore would not present adsorptive potential.

3.2.5. Variability of the carbon adsorbents production process

In order to guarantee that the observed variability between factories and batches is not due to the carbon production process (pyrolysis and acid washing), it is important to assure the consistency of those procedures. The repeatability of the pyrolysis process was evaluated by performing replicates of the pyrolysis for the first batch of PS from Factory 1 (F1PS1-P). Moreover, due to the major influence of the acid washing in the characteristics of the final material, this step was also evaluated. Both the effect of the washing time (60 and 300 min) and the repeatability of the washing process were assessed by performing 3 replicates of each washing time for materials produced from the first batch of PS and BS from Factory 1 (F1PS1-PW and F1BS1-PW). All the resulting materials were analyzed by IC, TOC and S_{BET} .

3.3. Results and Discussion

3.3.1. Characterization of raw materials and carbon adsorbents

3.3.1.1. Total organic carbon (TOC) and inorganic carbon (IC)

The TOC and IC results (Figure 3.1 and respective Table 3.1) revealed that the raw materials from Factory 1, for both PS and BS, presented higher levels of IC than those from Factory 2 and TOC was significantly lower for the raw materials from Factory 1 than from Factory 2. Overall, the pyrolysis process resulted in a decrease of TOC, except for BS from Factory 2, with TOC increasing after pyrolysis. After the HCl washing step of the P materials, a significant increase in the percentage of TOC was verified while the IC fell to negligible values, showing that the acid washing was effective in the removal of the inorganic carbon. Further changes due to the washing procedure will be addressed in the subsequent sections.

Considering the consistency of the materials, the highest variability between sludge batches was observed for the TOC contents of raw materials from Factory 1 (relative standard deviation (RSD) for PS and BS of 36 % and 32 %, respectively) and for pyrolyzed PS from Factory 1 (RSD of 44 %). These three described cases of high variability are characterized by a high content in IC. The highest RSD are a consequence of the relatively low values of TOC (for the raw materials from Factory 1) and do not reflect meaningful fluctuations in the values of this parameter. Lower variability (RSD in the range 3-14 %) was observed for all the other batches (raw materials, P and PW materials from Factory 2 and PW materials from Factory 1).

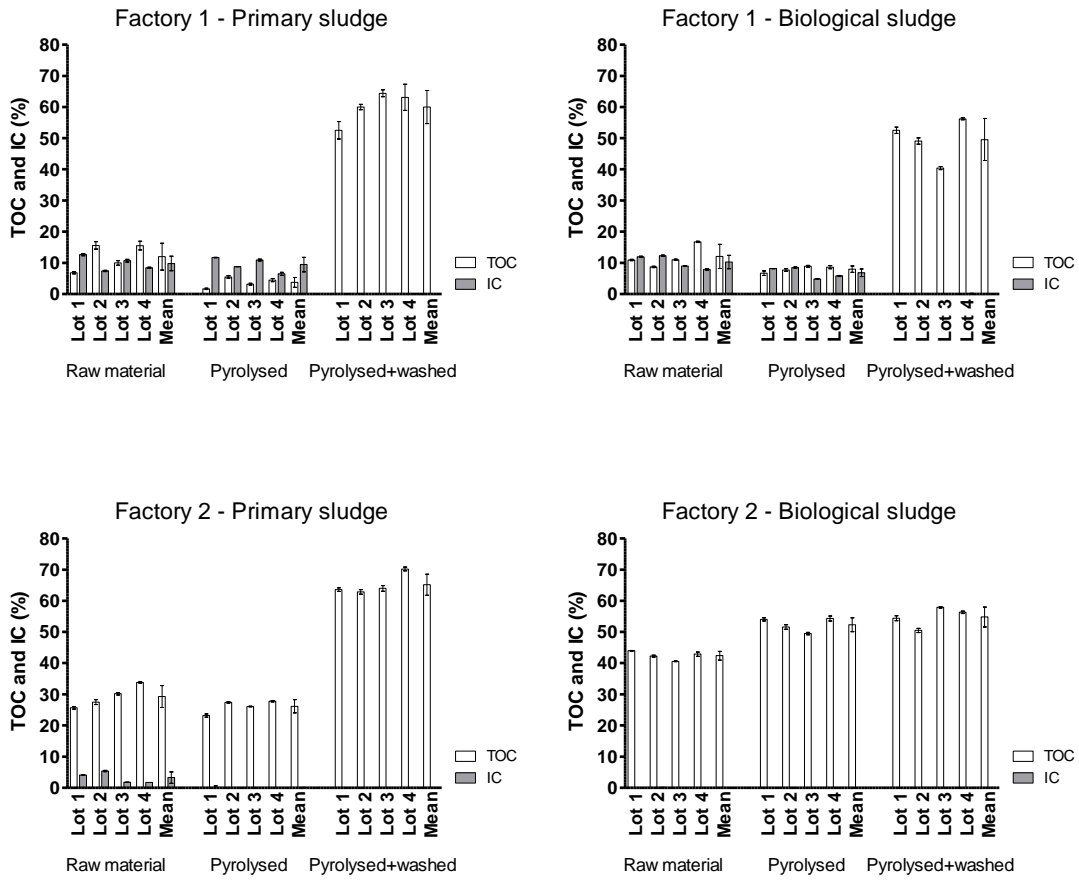


Figure 3.1. Representation of total organic (TOC) and inorganic (IC) carbon for raw, pyrolysed (P) and pyrolyzed and washed (PW) materials for all batches of both factories.

Table 3.1 - Total (TC, %) and inorganic carbon (IC, %) values (n = 3) for raw, pyrolysed (P) and pyrolysed and washed (PW) materials. TOC was obtained by difference.

Raw Materials	P Materials				PW Materials						
	TC (%)	IC (%)	TOC (%)	Materials	TC (%)	IC (%)	TOC (%)	Materials			
F1PS1	19.5 ± 0.2	12.6 ± 0.3	6.8 ± 0.3	F1PS1-P	13.4 ± 0.1	11.7 ± 0.1	1.7 ± 0.2	F1PS1-PW	53 ± 3	0.140 ± 0.001	53 ± 3
F1PS2	23 ± 1	7.4 ± 0.2	16 ± 1	F1PS2-P	14.3 ± 0.4	8.80 ± 0.04	5.5 ± 0.4	F1PS2-PW	59.0 ± 0.9	0.014 ± 0.003	60.0 ± 0.9
F1PS3	20.8 ± 0.7	10.7 ± 0.4	10.0 ± 0.7	F1PS3-P	14.1 ± 0.2	10.9 ± 0.3	3.2 ± 0.3	F1PS3-PW	64 ± 1	0.024 ± 0.001	64 ± 1
F1PS4	24 ± 1	8.4 ± 0.2	15 ± 1	F1PS4-P	11.0 ± 0.2	6.5 ± 0.5	4.5 ± 0.5	F1PS4-PW	63 ± 4	0.10 ± 0.02	63 ± 4
F2PS1	29.8 ± 0.3	4.1 ± 0.1	25.7 ± 0.4	F2PS1-P	23.3 ± 0.1	0.05 ± 0.53	23.2 ± 0.5	F2PS1-PW	63.6 ± 0.6	0.019 ± 0.002	63.6 ± 0.6
F2PS2	32.9 ± 0.8	5.4 ± 0.2	27.5 ± 0.8	F2PS2-P	27.4 ± 0.2	0.021 ± 0.002	27.4 ± 0.2	F2PS2-PW	63.0 ± 0.7	0.013 ± 0.001	62.9 ± 0.7
F2PS3	32 ± 2	1.77 ± 0.03	30.2 ± 0.4	F2PS3-P	26.4 ± 0.1	0.22 ± 0.01	26.1 ± 0.1	F2PS3-PW	64.0 ± 0.9	0.013 ± 0.003	64.0 ± 0.9
F2PS4	35 ± 2	1.752 ± 0.002	33.8 ± 0.2	F2PS4-P	27.9 ± 0.2	0.03 ± 0.05	27.8 ± 0.2	F2PS4-PW	70.2 ± 0.6	0.010 ± 0.001	70.2 ± 0.6
F1BS1	22.9 ± 0.1	11.9 ± 0.2	10.9 ± 0.2	F1BS1-P	14.8 ± 0.7	8.18 ± 0.01	6.7 ± 0.7	F1BS1-PW	53 ± 1	0.088 ± 0.001	52 ± 1
F1BS2	21.1 ± 0.1	12.3 ± 0.2	8.7 ± 0.2	F1BS2-P	16.2 ± 0.2	8.5 ± 0.3	7.7 ± 0.4	F1BS2-PW	49 ± 1	0.025 ± 0.001	49 ± 1
F1BS3	20.1 ± 0.1	9.0 ± 0.1	11.0 ± 0.2	F1BS3-P	13.7 ± 0.3	4.83 ± 0.04	8.9 ± 0.3	F1BS3-PW	40.4 ± 0.5	0.016 ± 0.002	40.4 ± 0.5
F1BS4	25.6 ± 0.2	7.9 ± 0.2	17.7 ± 0.2	F1BS4-P	14.3 ± 0.5	5.8 ± 0.2	8.6 ± 0.5	F1BS4-PW	56.3 ± 0.3	0.141 ± 0.06	56.2 ± 0.3
F2BS1	44.0 ± 0.1	0.024 ± 0.001	44.0 ± 0.1	F2BS1-P	54.0 ± 0.5	0.03 ± 0.01	54.0 ± 0.5	F2BS1-PW	54.4 ± 0.8	0.023 ± 0.001	54.4 ± 0.8
F2BS2	42.4 ± 0.3	0.10 ± 0.02	42.3 ± 0.3	F2BS2-P	51.7 ± 0.7	0.050 ± 0.002	51.6 ± 0.7	F2BS2-PW	50.5 ± 0.7	0.03 ± 0.02	50.5 ± 0.7
F2BS3	40.6 ± 0.1	0.02 ± 0.01	40.6 ± 0.1	F2BS3-P	49.5 ± 0.4	0.025 ± 0.005	49.5 ± 0.4	F2BS3-PW	57.9 ± 0.2	0.016 ± 0.002	57.9 ± 0.2
F2BS4	42.9 ± 0.7	0.022 ± 0.001	42.9 ± 0.7	F2BS4-P	54.3 ± 0.8	0.022 ± 0.001	54.3 ± 0.8	F2BS4-PW	56.3 ± 0.4	0.014 ± 0.001	56.3 ± 0.4

3.3.1.2. Fourier transform infrared spectroscopy with attenuated total reflectance (ATR-FTIR)

The ATR-FTIR spectra obtained for PS, BS, and the carbon adsorbents (P and PW materials) obtained from them are depicted in the Appendix C3, Figures C3.1 and C3.2. Considering that spectra of different batches of the same material did not present noticeable differences, only one batch is exemplified in Figure 3.2 (the first batch of PS, BS, and resulting carbons for both factories).

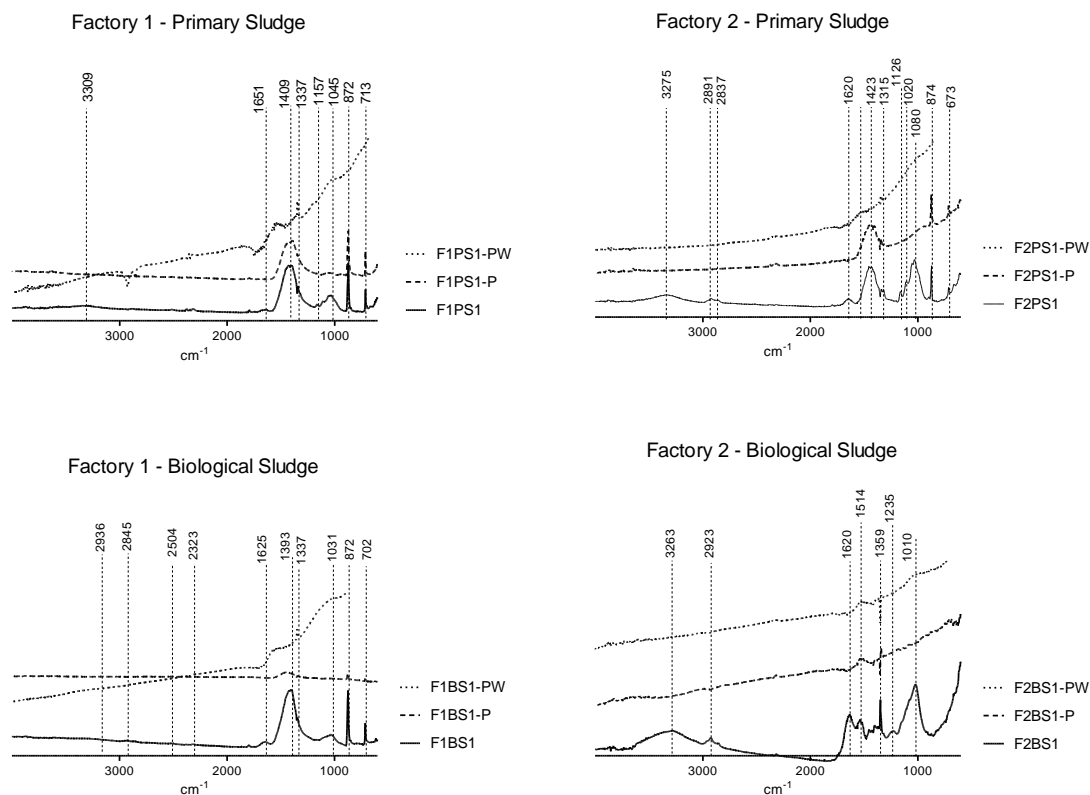


Figure 3.2. ATR-FTIR spectra of primary sludge (PS) and biological sludge (BS) and carbon adsorbents (P and PW materials) produced from them for both factories.

The results (Figure 3.2, and Figures C3.1 and C3.2) show that the precursor materials (both PS and BS) have a much more complex chemical composition than the P materials and even more than the PW materials.

In the case of raw PS (Figure 3.2. and Figures C3.1) from both factories, the FTIR spectra evidenced the presence of two main peaks at $\sim 1400\text{ cm}^{-1}$ and $\sim 850\text{ cm}^{-1}$ which, in conjugation, point out to the presence of carbonates (Coates, 2000). The relative intensity of these peaks (when compared with

other peaks/bands of the spectra) is higher for raw materials from Factory 1 than from Factory 2, which indicates that the first presented a higher content in inorganic matter. This fact can be easily confirmed by IC results (Figure 3.1 and Table 3.1). In these spectra of Figure 3.2 and Figure C3.1, one can also identify broad bands between 3200 cm^{-1} and 3600 cm^{-1} , attributed to O-H stretching from hydroxyl groups of cellulose and water (Calisto et al., 2014). This can be observed in almost all the batches from both factories, although in the raw materials from Factory 1 this band is not so evident, possibly due to the high intensity of the carbonate peaks. In the *fingerprint* region, several peaks are present between 1650 cm^{-1} and 1150 cm^{-1} . These peaks can be associated, for instance, to C–O–C stretching vibration of pyranose ring ($\sim 1150\text{ cm}^{-1}$) and to C–H bending vibrations ($\sim 1300\text{ cm}^{-1}$) (Calisto et al., 2014; Jaria et al., 2015). In both Factory 1 and Factory 2, several peaks/bands around 1200 cm^{-1} and 1000 cm^{-1} can be observed and can be related to alcohol groups (around 1050 cm^{-1} it corresponds to primary alcohols C–O stretch; around 1100 cm^{-1} it corresponds to secondary alcohols C–O stretch; around 1150 cm^{-1} to tertiary alcohols C–O stretch; and around 1200 cm^{-1} to phenol C–O stretch) (Coates, 2000). Also, peaks in the ranges $1150\text{--}1050\text{ cm}^{-1}$ and $1140\text{--}1070\text{ cm}^{-1}$ might be derived from the presence of alkyl-substituted ether and cyclic ethers (large rings (C–O–C stretch)), respectively (Coates, 2000). The peak around 1650 cm^{-1} is associated to carbonyl groups (Coates, 2000; Calisto et al., 2014); the peaks in the range $750\text{--}450\text{ cm}^{-1}$ correspond to in-plane and out-plane aromatic ring deformation vibrations, C–H and C–C stretching (Jaria et al., 2015). Overall, the spectra obtained for PS are similar to the cellulose spectrum (Méndez et al., 2009).

Regarding BS, the spectra obtained for raw materials from Factory 1 are similar to those obtained for PS (Figure 3.2, and Figures C3.1 and C3.2 in Appendix C3) from the same factory. However, the spectra determined for BS from the two factories are very different (Figure 3.2). Once again, there is a high relative intensity of the peaks related to carbonates, which may difficult the identification of other characteristic peaks. Relatively to BS from Factory 2, the occurrence of several peaks identified for PS, namely, the broad band between 3100 cm^{-1} and 3600 cm^{-1} and weak and medium absorption peaks/bands in the range $1670\text{--}1620\text{ cm}^{-1}$, can be observed. Other bands such as the ones around 1000 , 1200 and 1500 cm^{-1} are indicative of the presence of aromatic groups and absorption at $\sim 1200\text{ cm}^{-1}$ can be attributed to phenol C–O stretch or to aryl–O stretch in aromatic ethers (Coates, 2000; Calisto et al., 2014). In these raw material spectra (BS from Factory 2; Figures 3.2 and C3.2) the peaks related to the carbonate groups ($\sim 1400\text{ cm}^{-1}$ and 850 cm^{-1}) appear to be absent. The overall spectra are very similar to that of lignin (Beyer et al., 1997; Calisto et al., 2014).

In the case of P materials (Figure 3.2, Figures C3.1. and C3.2), the presence of carbonate ions continues to be evident. In pyrolysed PS (Figure C3.1), it can be observed that these peaks appeared

almost in all cases, but are more pronounced in the case of Factory 1; for pyrolyzed BS (Figure C3.2), only those from Factory 1 present this combination of characteristic peaks. The washing of the P materials resulted in the disappearance of the majority of the bands (implying the absence of the main functional groups identified in the raw materials) and, in general, there was a low variability in the ATR-FTIR spectra between batches and between factories, for all the materials produced from both PS and BS. The most evident inference is the disappearance of the peaks related to the presence of carbonates. Moreover, a peak in the region $1615\text{-}1495\text{ cm}^{-1}$ was observed, indicating the presence of aromatics. A peak around 1300 cm^{-1} was also identified and can be associated to different groups, including carboxylic acids or aryl-amines (Pavia et al., 2001), or to the alcohols O–H stretch or to aromatic ring stretches (Calisto et al., 2014).

Overall, it can be said that, using ATR-FTIR, no significant differences were observed between batches.

3.3.1.3. Specific surface area (S_{BET})

The S_{BET} determined for the carbon adsorbents herein produced are shown in Figure 3.3 and in Table 3.2. From the displayed results, it is clear that the acid washing step resulted in a remarkable increase of the S_{BET} of P materials. Overall, this increase was also observed for microporous volume (W_0) (Table 3.2), traditionally regarded as a key factor for optimum removal efficiencies in carbon adsorbents (Cabrita et al., 2010). These results point to acid washing as an essential step for unblocking occluded pores after the pyrolysis of PS and BS and, therefore, to produce carbon adsorbents from them. In any case, quite low S_{BET} values were determined for BS-PW from Factory 2 as compared with the other PW materials. It can be also observed that materials from Factory 1 (either PS or BS) presented higher S_{BET} than materials from Factory 2. The largest S_{BET} values determined ($(424 \pm 45)\text{ m}^2\text{ g}^{-1}$) were those of the PS-PW.

In general, BS-PW presented higher variability between batches (RSD of 37 % and 58 % for Factory 1 and 2, respectively) in comparison with the corresponding materials obtained from PS (RSD of 11 % and 16 % for Factory 1 and 2, respectively). This higher variability may be related to the larger heterogeneity of the raw material, since the generation of BS includes the bacterial digestion of the organic content of the sludge. Then, PS-PW from both factories not only presented consistent S_{BET} values but also relatively high S_{BET} , which are key features for the production of carbon adsorbents.

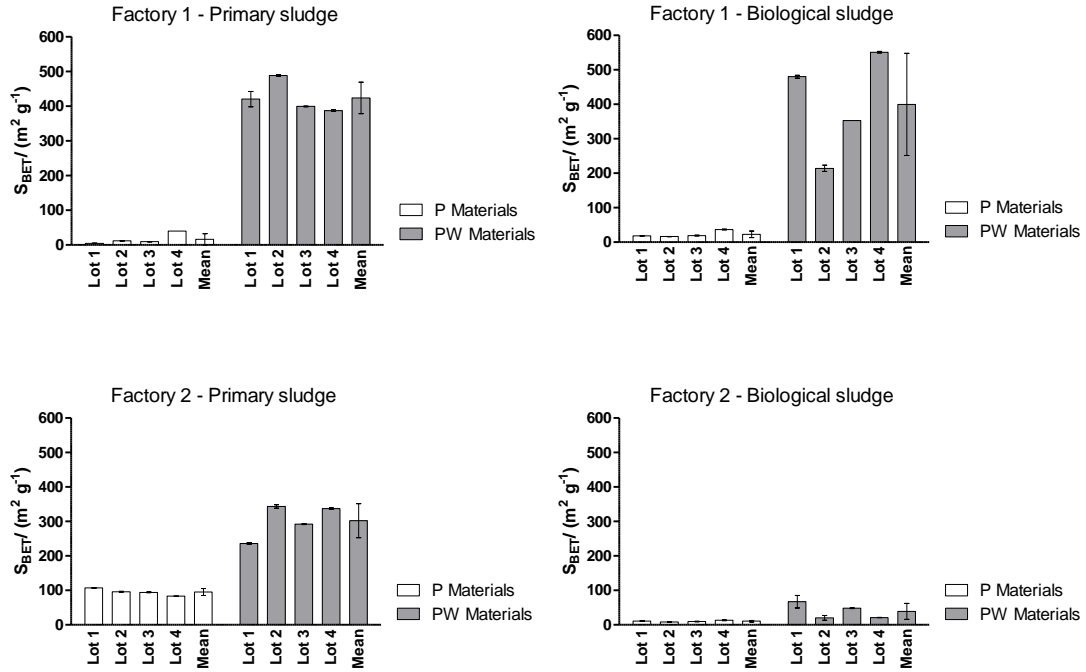


Figure 3.3. Specific surface area (S_{BET}) for pyrolyzed (P) and pyrolyzed and washed (PW) materials produced from the four batches of both primary (PS) and biological sludge (BS) of both factories. Mean values for each type of material are also shown.

Table 3.2. Textural parameters of the pyrolyzed (P) and pyrolyzed and washed (PW) materials.

Primary sludge					Biological sludge				
Sample	P materials		PW materials		Sample	P materials		PW materials	
	S_{BET} ($m^2 g^{-1}$)	W_0 ($cm^3 g^{-1}$)	S_{BET} ($m^2 g^{-1}$)	W_0 ($cm^3 g^{-1}$)		S_{BET} ($m^2 g^{-1}$)	W_0 ($cm^3 g^{-1}$)	S_{BET} ($m^2 g^{-1}$)	W_0 ($cm^3 g^{-1}$)
F1PS1	4.2 ± 0.4	0.0000	413 ± 3	0.0149	F1BS1	18.5 ± 0.2	0.0000	476 ± 2	0.0407
F1PS2	11.8 ± 0.4	0.0000	488 ± 2	0.0336	F1BS2	16.5 ± 0.3	0.0000	214.9 ± 0.9	0.0192
F1PS3	9.1 ± 0.3	0.0000	399 ± 1	0.0529	F1BS3	19.4 ± 0.7	0.0000	352.53 ± 0.01	0.0138
F1PS4	39.7 ± 0.2	0.0059	387 ± 3	0.0837	F1BS4	36.8 ± 0.8	0.0000	551 ± 2	0.0811
F2PS1	107 ± 1	0.0154	236 ± 2	0.0454	F2BS1	11 ± 1	0.0000	67 ± 18	0.0000
F2PS2	96 ± 1	0.0233	343 ± 5	0.0000	F2BS2	8.7 ± 0.8	0.0000	20 ± 7	0.0000
F2PS3	94 ± 1	0.0147	292 ± 1	0.0460	F2BS3	9.8 ± 0.4	0.0000	48 ± 1	0.0000
F2PS4	83.0 ± 0.5	0.0226	337 ± 2	0.0290	F2BS4	13.2 ± 0.8	0.0000	21.1 ± 0.4	0.0000

W_0 – micropore volume

3.3.1.4 Proximate analysis

Proximate analysis results are depicted in Figure 3.4 and Table 3.3. For the raw materials, the ash content of Factory 1 is much higher compared to that of Factory 2 (approximately twice the value, in the case of PS, and thrice the value in the case of BS). These results are in accordance with the ones from TOC (Figure 3.1 and Table 3.1) and ATR-FTIR spectra (Figure 3.2 and Figures C3.1 and C3.2 in Appendix C3). Also, Factory 1 has, in general and for both PS and BS, lower values of fixed carbon and volatile matter than Factory 2. Considering the described variations, the factories presented a distinct profile in what concerns proximate analysis.

Concerning the effects of pyrolysis and washing, PW materials registered a considerable increase in the fixed carbon and a decrease in the volatile matter. This tendency was observed for PW materials obtained from both PS and BS of the two factories. Despite the verified differences between factories for the raw materials, the resulting PW materials presented a similar pattern indicating that the variability in the proximate analysis profile of the precursors did not imply PW materials with distinct characteristics. The ash content of the PW materials was in line with these findings: while, as previously referred, raw materials from Factory 1 had two to three times the ash content of the Factory 2, the ash content of PW materials was similar for both factories.

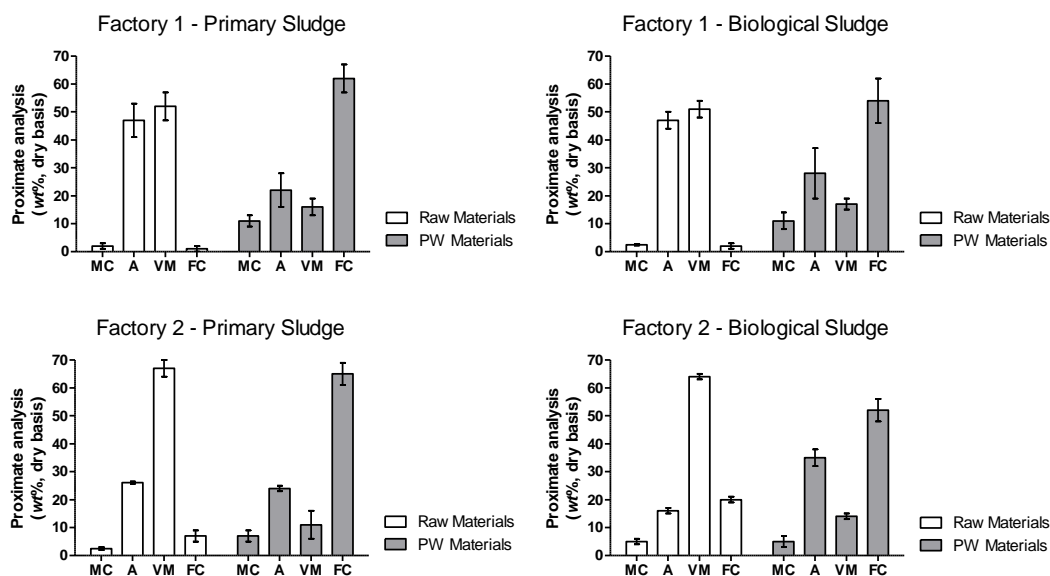


Figure 3.4. Proximate analysis (wt%, dry basis) for raw, pyrolyzed (P) and washed materials (PW). Presented values correspond to the mean of the four batches collected for each factory and type of sludge (MC – Moisture Content; A – Ash; VM – Volatile Matter; FC – Fixed Carbon).

Table 3.3 – Proximate analysis (wt %, dry basis) for raw and pyrolyzed and washed (PW) materials.

Sample	Raw Materials				PW Materials			
	Moisture content	Ash	Volatile Matter	Fixed Carbon	Moisture content	Ash	Volatile Matter	Fixed Carbon
F1PS1	0.9	55.5	44.8	0.0	12.0	22.4	18.0	59.5
F1PS2	3.1	42.6	56.9	0.5	9.6	26.2	16.6	57.2
F1PS3	1.5	47.3	52.3	0.4	8.0	25.4	12.4	62.2
F1PS4	1.5	42.4	55.3	2.30	13.5	12.7	18.7	68.7
<i>Mean ± SD</i>	<i>2 ± 1</i>	<i>47 ± 6</i>	<i>52 ± 5</i>	<i>1 ± 1</i>	<i>11 ± 2</i>	<i>22 ± 6</i>	<i>16 ± 3</i>	<i>62 ± 5</i>
F2PS1	4.4	25.6	67.1	7.3	7.2	24.7	7.6	67.7
F2PS2	4.4	25.9	70.6	3.5	4.4	24.8	7.2	68.0
F2PS3	4.9	26.3	64.7	8.9	9.5	23.7	11.2	65.2
F2PS4	3.6	26.6	66.0	7.5	5.1	22.6	18.0	59.3
<i>Mean ± SD</i>	<i>2.5 ± 0.5</i>	<i>26.1 ± 0.4</i>	<i>67 ± 3</i>	<i>7 ± 2</i>	<i>7 ± 2</i>	<i>24 ± 1</i>	<i>11 ± 5</i>	<i>65 ± 4</i>
F1BS1	2.8	46.0	52.9	1.1	10.0	22.9	18.4	58.7
F1BS2	2.2	49.2	49.1	1.6	8.8	28.5	15.5	56.0
F1BS3	2.7	50.3	47.6	2.1	9.4	40.9	16.4	42.6
F1BS4	2.5	44.1	52.6	3.3	14.7	21.3	19.0	59.8
<i>Mean ± SD</i>	<i>2.5 ± 0.3</i>	<i>47 ± 3</i>	<i>51 ± 3</i>	<i>2 ± 1</i>	<i>11 ± 3</i>	<i>28 ± 9</i>	<i>17 ± 2</i>	<i>54 ± 8</i>
F2BS1	4.0	15.2	64.3	20.4	6.5	37.8	14.4	47.8
F2BS2	3.5	16.2	63.4	20.4	4.8	37.2	13.0	49.8
F2BS3	6.8	17.4	63.5	19.1	7.2	34.5	13.5	52.0
F2BS4	4.9	14.8	64.9	20.3	2.2	30.3	13.1	56.6
<i>Mean ± SD</i>	<i>5 ± 1</i>	<i>16 ± 1</i>	<i>64 ± 1</i>	<i>20 ± 1</i>	<i>5 ± 2</i>	<i>35 ± 3</i>	<i>14 ± 1</i>	<i>52 ± 4</i>

3.3.2. Production of adsorbent materials from paper mill sludge: practical implications

3.3.2.1. Variability of the carbon adsorbents production process

The evaluation of the repeatability of the pyrolysis process revealed no major differences with values of the different replicates ranging from $(10.4 \pm 0.3) \%$ to $(11.7 \pm 0.4) \%$ for IC, $(1.8 \pm 0.3) \%$ to $(1.7 \pm 0.2) \%$ for TOC and $(1.36 \pm 0.02) \text{ m}^2 \text{ g}^{-1}$ to $(4.2 \pm 0.4) \text{ m}^2 \text{ g}^{-1}$ for S_{BET} . Concerning possible variations due to the acid washing, washing times of 60 min and 300 min were both found to produce reproducible materials in what concerns S_{BET} ($S_{\text{BET}} \text{RSD}_{60 \text{ min}} = 0.75 \%$ and $S_{\text{BET}} \text{RSD}_{300 \text{ min}} = 0.56 \%$; $n = 3$). Also, it was found that the longer washing time (300 min) had no advantages in obtaining a higher S_{BET} ($S_{\text{BET} 60 \text{ min}} = (480 \pm 4) \text{ m}^2 \text{ g}^{-1}$ and $S_{\text{BET} 300 \text{ min}} = (443 \pm 2) \text{ m}^2 \text{ g}^{-1}$). The same conclusions were obtained

by IC and TOC determination ($IC_{60 \text{ min}} = (0.088 \pm 0.001) \%$ and $IC_{300 \text{ min}} = (0.040 \pm 0.005) \%$; $TOC_{60 \text{ min}} = (52 \pm 1) \%$ and $TOC_{300 \text{ min}} = (54 \pm 2) \%$). Therefore, the time of 60 min was selected for the washing of the materials subsequently used in the evaluation of the adequacy of PS and BS as precursors.

Overall, these results confirm that the pyrolysis and washing (including washing time) are not a relevant source of variability in the production of the carbon adsorbents from pulp and paper industry sludge.

3.3.2.2. Impact of the raw material characteristics in the production of carbon adsorbents

Obtaining final materials with interesting physicochemical characteristics (high S_{BET} , high TOC, and low ash content) is a key step for considering the valorization of paper mill sludge for the production of carbon adsorbents. However, the feasibility of such application should be also evaluated considering the consistency of the produced materials over time and it is also crucial to be aware if factories with different production processes result in carbon materials with distinct properties. Only with the evaluation of such variability, conclusions about the reliability of the produced materials for large scale and/or continuous production and application can be drawn.

The results here described show that sludge collected from Factory 1 has very high IC contents (Figure 3.1; Table 3.1), most certainly calcium carbonate used in the bleaching process in the pulp and paper manufacturing. This fact is evidenced by ATR-FTIR spectra (which present peaks/bands typical of carbonates; Figures 3.2, and C3.1 and C3.2 in Appendix C), IC determination (Figure 3.1; Table 3.1), and proximate analyses (Figure 3.4; Table 3.3). A high IC content is generally not desirable for raw materials intended for the production of carbon adsorbents. In fact, after pyrolysis, sludge from Factory 1 continues to have relatively large IC content (Figure 3.1; Table 3.1), which was effectively reduced by the subsequent acid washing. However, in the case of sludge from Factory 1, despite the effectiveness of the washing step in the reduction of IC, increase of TOC and high improvement of the S_{BET} (Figure 3.3; Table 3.2), the final yield of production (pyrolysis and washing) of the corresponding carbon material is very low (around 4 % and 13 % for PS and BS, respectively). On the other hand, both PS and BS from Factory 2 have very low IC content with direct impact in the global yield of production (around 10 % and 35% for PS and BS, respectively). The high IC content also had consequences in the hardness and resistance of the produced materials. Carbons derived from PS, from both factories, are necessarily powdered carbons, considering that PS is fibrous in nature. Yet, in the case of BS from Factory 1, it was, in fact, possible to obtain granular carbons by pyrolysis but grains did not resist to the acid washing. Contrarily, BS from Factory 2, which had a low IC content, was appropriate for the production of a

granular adsorbent by pyrolysis which was resistant to the acid washing. Overall, the high IC content of raw materials resulted in two major drawbacks: *a)* low production yields and *b)* reduced hardness/strength of the materials to withstand use as granular carbon adsorbents. Nevertheless, the presence of carbonates might also have positive implications in the S_{BET} . Sludge from Factory 2, with low IC (particularly in the case of BS), consistently resulted in carbon materials with lower S_{BET} values. Considering that alkali metal carbonates are used as activating agents for inducing the development of microporosity and surface areas (Viswanathan et al., 2009), the carbonates naturally present in the sludge from Factory 1 might have triggered some kind of chemical activation process. In any case, the high S_{BET} values obtained for the materials produced by the pyrolysis and acid washing of PS from both factories, together with the uniformity between batches, point to the possible applicability of these carbon adsorbents for wastewater treatment. Moreover, these findings are encouraging for further investigation concerning the improvement of such properties, namely through activation procedures.

3.4. Conclusions

In this work the consistency of carbon adsorbents derived from the pyrolysis (followed or not by acid washing) of sludge from the paper industry was evaluated considering *(i)* the variability between different sludge batches, and *(ii)* the variability between two factories operating with different production processes. The results showed that the major difference between raw materials from different factories was the IC content, which was much higher in the sludge from Factory 1 than in the one from Factory 2. Yet, IC was effectively reduced by an acid washing step after pyrolysis, which also increased the corresponding TOC and considerably improved the S_{BET} . The high IC had important implications in the production yield and in the hardness of the produced materials (relatively high IC meant lower production yields and lower materials' hardness). However, despite high IC content, higher S_{BET} were observed for both PS and BS materials from Factory 1, which presented very interesting properties in terms of surface area, especially considering that they were not subjected to chemical activation. Still considering S_{BET} , P and PW materials produced from BS presented relative high variability between batches, while the S_{BET} of materials from different batches of PS did not differ in more than 16 %. Overall, it can be concluded that precursors from factories with different operation mode might originate final materials with distinct characteristics. Therefore, it is essential to take into account this source of variability when considering paper mill sludge as a raw material. On the other hand, low variability was found between materials produced from different batches of sludge for each factory, which is a good

indicator of the reliability of such residues to be used as new precursors/raw materials for the production of carbon adsorbents.

3.5. References

- Adhikari, G., Bhattacharyya, K.G., 2015. Impact of pulp and paper mill effluents and solid wastes on soil mineralogical and physicochemical properties. *Environ. Monit. Assess.* 187, 1-13.
- Auta, M., Hameed, B.H., 2014. Optimized and functionalized paper sludge activated with potassium fluoride for single and binary adsorption of reactive dyes. *J. Ind. Eng. Chem.* 20, 830-840.
- Bajpai, P., 2015. Management of pulp and paper mill waste, 1st ed., Springer International Publishing, pp. 104.
- Battaglia, A., Calace, N., Nardi, E., Petronio, B.M., Pietroletti, M., 2003. Paper mill sludge–soil mixture: kinetic and thermodynamic tests of cadmium and lead sorption capability. *Microchem. J.* 75, 97-102.
- Beyer, L., Fründ, R., Mueller, K., 1997. Short-term effects of a secondary paper mill sludge application on soil properties in a Psammentic Haplumbrept under cultivation. *Sci. Total Environ.* 197, 127-137.
- Buruberri, L.H., Seabra, M.P., Labrincha, J.A., 2015. Preparation of clinker from paper pulp industry wastes. *J. Hazard. Mater.* 286, 252-260.
- Cabrita, I., Ruiz, B., Mestre, A.S., Fonseca, I.M., Carvalho, A.P., Ania, C.O., 2010. Removal of an analgesic using activated carbons prepared from urban and industrial residues. *Chem. Eng. J.* 163, 249-255.
- Calisto, V., Ferreira, C.I., Oliveira, J.A., Otero, M., Esteves, V.I., 2015. Adsorptive removal of pharmaceuticals from water by commercial and waste-based carbons. *J. Environ. Manage.* 152, 83-90.
- Calisto, V., Ferreira, C.I., Santos, S.M., Gil, M.V., Otero, M., Esteves, V.I., 2014. Production of adsorbents by pyrolysis of paper mill sludge and application on the removal of citalopram from water. *Bioresource Technol.* 166, 335-344.
- CEPI, 2016. Confederation of European Paper Industries. <http://www.cepi-sustainability.eu/forestry> (Accessed on April 2016).
- Choy, K.K.H., Barford, J.P., McKay, G., 2005. Production of activated carbon from bamboo scaffolding waste - process design, evaluation and sensitivity analysis. *Chem. Eng. J.* 109, 147-165.
- Coates, J., 2000. Interpretation of Infrared Spectra, A Practical Approach. John Wiley & Sons Ltd, Chichester.
- Devi, P., Saroha, A.K., 2014. Risk analysis of pyrolyzed biochar made from paper mill effluent treatment plant sludge for bioavailability and eco-toxicity of heavy metals. *Bioresource Technol.* 162, 308-315.
- Devi, P., Saroha, A.K., 2015. Simultaneous adsorption and dechlorination of pentachlorophenol from effluent by Ni–ZVI magnetic biochar composites synthesized from paper mill sludge. *Chem. Eng. J.* 271, 195-203.

- European Commission, 2016a. Directive 2008/98/EC on Waste (Waste Framework Directive). <http://ec.europa.eu/environment/waste/framework/> (accessed on April 2016).
- European Commission, 2016b. Roadmap to a Resource Efficient Europe. http://ec.europa.eu/environment/resource_efficiency/about/roadmap/index_en.htm (accessed on April 2016).
- Ferreira, C.I., Calisto, V., Cuerda-Correa, E.M., Otero, M., Nadais, H., Esteves, V.I., 2016a. Comparative valorisation of agricultural and industrial biowastes by combustion and pyrolysis. *Bioresource Technol.* 218, 918-925.
- Ferreira, C.I.A., Calisto, V., Otero, M., Nadais, H., Esteves, V.I., 2016b. Comparative adsorption evaluation of biochars from paper mill sludge with commercial activated carbon for the removal of fish anaesthetics from water in Recirculating Aquaculture Systems. *Aquacult. Eng.* 74, 76-83.
- Ferreira, C.I.A., Calisto, V., Santos, S.M., Cuerda-Correa, E.M., Otero, M., Nadais, H., Esteves, V.I., 2015. Application of pyrolysed agricultural biowastes as adsorbents for fish anaesthetic (MS-222) removal from water. *J. Anal. Appl. Pyrol.* 112, 313-324.
- Gonzalez, J.C., Gonzalez, M.T., Molina-Sabio, M., Rodriguez-Reinoso, F., Sepulveda-Escribano, A., 1995. Porosity of activated carbons prepared from different lignocellulosic materials. *Carbon* 33, 1175-1177.
- Jaria, G., Calisto, V., Gil, M.V., Otero, M., Esteves, V.I., 2015. Removal of fluoxetine from water by adsorbent materials produced from paper mill sludge. *J. Colloid Interf. Sci.* 448, 32-40.
- Kamali, M., Khodaparast, Z., 2015. Review on recent developments on pulp and paper mill wastewater treatment. *Ecotox. Environ. Safe.* 114, 326-342.
- Khalili, N.R., Campbell, M., Sandi, G., Golas, J., 2000. Production of micro- and mesoporous activated carbon from paper mill sludge - I. Effect of zinc chloride activation. *Carbon* 38, 1905-1915.
- Khalili, N.R., Vyas, J.D., Weangkaew, W., Westfall, S.J., Parulekar, S.J., Sherwood, R., 2002. Synthesis and characterization of activated carbon and bioactive adsorbent produced from paper mill sludge. *Sep. Purif. Technol.* 26, 295-304.
- Li, W.-H., Yue, Q.-Y., Gao, B.-Y., Wang, X.-J., Qi, Y.-F., Zhao, Y.-Q., Li, Y.-J., 2011. Preparation of sludge-based activated carbon made from paper mill sewage sludge by steam activation for dye wastewater treatment. *Desalination* 278, 179-185.
- Likon, M., Trebše, P., 2012. Recent advances in paper mill sludge management, in *Industrial Waste*, edited by Show, K.-Y., InTech, pp. 73-90.
- Masomi, M., Ghoreyshi, A.A., Najafpour, G.D., Mohamed, A.R.B., 2015. Dynamic adsorption of phenolic compounds on activated carbon produced from pulp and paper mill sludge: experimental study and modeling by artificial neural network (ANN). *Desalination Water Treat.* 55, 1453-1466.
- Méndez, A., Fidalgo, J.M., Guerrero, F., Gascó, G., 2009. Characterization and pyrolysis behaviour of different paper mill waste materials. *J. Anal. Appl. Pyrol.* 86, 66-73.

- Monte, M.C., Fuente, E., Blanco, A., Negro, C., 2009. Waste management from pulp and paper production in the European Union. *Waste Manag.* 29, 293-308.
- Namazi, A.B., Jia, C.Q., Allen, D.G., 2010. Production and characterization of lignocellulosic biomass-derived activated carbon. *Water Sci. Technol.* 62, 2637-2646.
- Ng, C., Marshall, W.E., Rao, R.M., Bansode, R.R., Losso, J.N., 2003. Activated carbon from pecan shell: process description and economic analysis. *Ind. Crop. Prod.* 17, 209-217.
- Pavia, D.L., Lampman, G.M., Kriz, G.S., 2001. Introduction to Spectroscopy – A guide for students of organic chemistry, 3rd ed., Vondeling, J. (Ed.), Thomson Learning, Inc.
- Pervaiz, M., Sain, M., 2015. Recycling of paper mill biosolids: A review on current practices and emerging biorefinery initiatives. *Clean* 43, 919-926.
- Pirzadeh, K., Ghoreyshi, A.A., 2014. Phenol removal from aqueous phase by adsorption on activated carbon prepared from paper mill sludge. *Desalination and Water Treat.* 52, 6505-6518.
- Reckamp, J.M., Garrido, R.A., Satrio, J.A., 2014. Selective pyrolysis of paper mill sludge by using pretreatment processes to enhance the quality of bio-oil and biochar products. *Biomass and Bioenergy* 71, 235-244.
- Soucy, J., Koubaa, A., Migneault, S., Riedl, B., 2014. The potential of paper mill sludge for wood–plastic composites. *Ind. Crop. Prod.* 54, 248-256.
- Viswanathan, B., Neel, P.I., Varadarajan, T.K., 2009. Methods of activation and specific applications of carbon materials, National Centre for Catalysis Research, Indian Institute of Technology Madras (https://www.researchgate.net/publication/299393936_Methods_of_Activation_and_Specific_Applications_of_Carbon_Materials).
- Vochozka, M., Maroušková, A., Váchal, J., Straková, J., 2016. Reengineering the paper mill waste management. *Clean Technol. Environ.* 18, 323-329.

4

OPTIMIZATION OF THE PRODUCTION OF ACTIVATED CARBON USING PRIMARY PAPER MILL SLUDGE AS RAW MATERIAL

Abstract

In this chapter, primary paper mill sludge was used as a precursor to produce activated carbon (AC) aiming at the removal of pharmaceuticals from water. A full factorial design of four factors (pyrolysis temperature, residence time, precursor:activating agent ratio, and type of activating agent) at two levels, 650 °C and 800 °C, 60 minutes and 150 minutes, 10:1 and 1:1, and K₂CO₃ and KOH, respectively, was applied to the production of AC using paper mill sludge as precursor. The responses analyzed were the yield of production, the percentage of adsorption of three pharmaceuticals (sulfamethoxazole (SMX), carbamazepine (CBZ), and paroxetine (PAR)), BET surface area (S_{BET}), and total organic carbon (TOC). A Principal Component Analysis (PCA) was applied to determine similarities between the produced AC and then a desirability function was used to select the optimum production conditions to produce AC. Four AC were pointed as appropriate for the adsorption of pharmaceuticals by the PCA and characterized by means of point of zero charge (pH_{pzc}), acidic and basic functional groups, proximate and ultimate analysis, Hg porosimetry, and scanning electron microscopy (SEM). These four AC presented very good adsorption percentages for the three pharmaceuticals, around 78 % in average, and S_{BET} between 1350 m² g⁻¹ and 1650 m² g⁻¹. Among them, the desirability function pointed to the conditions 800 °C, 60 minutes, 1:1, and KOH as the optimum to produce AC from primary paper mill sludge (PS).

This chapter was based on the published article:

Jaria, G., Silva, C.P., Oliveira, J.A.B.P., Santos, S.M., Gil, M.V., Otero, M., Calisto, V., Esteves, V.I., 2019. Production of highly efficient activated carbons from industrial wastes for the removal of pharmaceuticals from water-A full factorial design. *J. Hazard. Mater.* 370, 212-218.

4.1. Contextualization

Activated carbons (AC) are materials presenting high specific surface areas (S_{BET}), and their production involve an activation process (chemical or physical) which allow to enhance their porosity (more detailed information in chapter 2). Also, it is well known that, together with the precursor properties, the production process has a great influence in the final characteristics of the carbon adsorbent (e.g. S_{BET} and pore size distribution), also affecting the yield of production (Bergna et al., 2018) and the adsorption effectiveness toward some target compounds (Rajapaksha, 2014). For the optimization of AC production, the use of experimental designs is an interesting approach to systematically observe how the production conditions impact the characteristics of the material, allowing to select the best set of conditions for producing an AC with desirable characteristics. This approach was addressed by some authors (Tan et al., 2008; Kwagheger and Adejoh, 2012; Ennaciri et al., 2014; Ahmad et al., 2017); however, to the best of the author's knowledge, there are no studies considering the optimization of the production of AC using primary paper mill sludge (PS) as precursor.

In the previous chapter (chapter 3) it was shown that PS is a reliable precursor for AC production, resulting in carbon materials with consistent physicochemical characteristics, even when different batches of precursor are considered. In this sense, this chapter aims at the optimization of AC production using PS as raw material and applying chemical activation together with a thermal treatment under inert atmosphere (one-step pyrolysis). In order to achieve optimal conditions for the production of the PS-based AC, an optimization study was carried out to assess the influence of some production parameters in key characteristics and adsorption efficiency of the produced materials. In that way, a full factorial design was applied to the production of a PS-based AC, considering as variables the pyrolysis temperature, pyrolysis residence time, precursor:activating agent ratio, and activating agent. The responses evaluated were the yield of production (η %), the percentage of adsorption of the AC towards pharmaceuticals from three different classes – the anti-epileptic carbamazepine, CBZ (%AdsCBZ), the antibiotic sulfamethoxazole, SMX (%AdsSMX), and the antidepressant paroxetine, PAR (%AdsPAR) – S_{BET} , and total organic (TOC) and inorganic (IC) carbon content.

4.2. Materials and Methods

4.2.1. Chemicals and reagents

The reagents used for the activation process were potassium hydroxide (KOH) (EKA PELLETS, $\geq 86\%$) and potassium carbonate (K_2CO_3) (AnalaR NORMAPUR, 99.8%). For the washing step hydrochloric acid (HCl; AnalaR NORMAPUR, 37%) was used. The pharmaceuticals used for the adsorption tests were CBZ (Sigma Aldrich, 99%); SMX (TCI, $> 98\%$); and PAR (TCI, $> 98\%$). All the solutions were prepared in ultrapure water obtained from a Milli-Q Millipore system (Milli-Q plus 185). The commercial AC (PBF4) was used as reference and was kindly provided by Chemviron.

4.2.2. Preparation of activated carbons – Full factorial design and statistical analysis

To produce the alternative AC, PS from Factory 2 was used as precursor after being dried and grinded (preparation of PS described in chapter 3, section 3.2.2). Despite the satisfactory results obtained for PS collected in both Factory 1 and 2, Factory 2 was the one selected to pursue with studies as its operational characteristics led to higher simplicity in the sludge collection process.

AC were prepared by chemical activation, using KOH or K_2CO_3 , followed by a one-step pyrolysis. In order to conclude about optimal production conditions, a full factorial design was applied using four factors at two levels, namely, the pyrolysis temperature (650 °C and 800 °C), x_1 , the residence time (60 minutes and 150 minutes), x_2 , the precursor:activating agent ratio (10:1 and 1:1), x_3 , and the type of activating agent (K_2CO_3 and KOH), x_4 . PS was impregnated with the activating agent, stirred during 1 h, and left to dry at room temperature. The dried materials were put in porcelain crucibles and pyrolysed, under N_2 atmosphere, in a muffle (Nüve, series MF 106, Turkey). Overall, sixteen AC were obtained (AC 1-16), which were subjected to a washing step with a 1.2 M solution of HCl to remove ashes. The responses considered to perform the statistical analysis were the yield of production (η), calculated by (equation 4.1), the percentage of adsorption for CBZ, SMX, and PAR, the S_{BET} , and the TOC.

$$\eta(\%) = \frac{\text{final mass of AC (g)}}{\text{mass of precursor (g)}} \times 100 \quad (\text{equation 4.1})$$

The behavior of the responses was described by a second-order interaction models (equation 4.2),

$$y = \beta_0 + \sum_{i=1}^k \beta_i x_i + \sum_{1 \leq i < j}^k \beta_{ij} x_i x_j + \varepsilon \quad (\text{equation 4.2})$$

where k is the number of variables, β_0 is a constant, β_i represents the coefficients of the linear parameters, β_{ij} represents the coefficients of the interaction parameters, x_i and x_j are the variables, and ε is the random error term (Bezerra et al., 2008). The significant factors influencing each response were determined by means of the normal probability distribution plots, where the effects outside the normal distribution were those considered for the model, since their estimates are the ones that most influenced the responses. Then, the regression models were obtained by the least squares method and statistically evaluated by an analysis of variance (ANOVA) (Table 4.1) (Bezerra et al., 2008). This statistical analysis allowed to determine the most favorable operational conditions for each response.

Table 4.1. Analysis of variance (ANOVA) used for the fitted models to the experimental data.

Variance source	Sum of squares (SS)	Degrees of freedom (v)	Mean Square (MS)
<i>Regression (model)</i>	$SS_{REG} = \sum_i^m \sum_j^{n_i} (\hat{y}_i - \bar{y})^2$	$p-1$	$MS_{REG} = \frac{SS_{REG}}{p-1}$
<i>Residuals</i>	$SS_{res} = \sum_i^m \sum_j^{n_i} (y_{ij} - \hat{y}_i)^2$	$n-p$	$MS_{res} = \frac{SS_{res}}{n-p}$
<i>Total</i>	$SS_{Total} = \sum_i^m \sum_j^{n_i} (y_{ij} - \bar{y})^2$	$n-1$	

n_i – number of observations; m - total number of levels in the design; p - number of parameters of the model (coefficients); \hat{y}_i - estimated value by the model for the level i ; \bar{y} - overall mean; y_{ij} - mean of replicates performed in the same set of experimental conditions

Additionally, a principal component analysis (PCA) was used to observe the distribution of the produced AC according to the responses, and a multiple response analysis was applied to determine the set of conditions that simultaneously satisfied all responses, corresponding to the best balance among different response variables. This was achieved by applying a Derringer function, also called desirability function (equations 4.3 and 4.4), which is a multicriteria methodology based on the construction of a desirability function for each individual response, where the measured properties of each response are transformed into a dimensionless individual desirability (d_i) scale ranging between 0 and 1 (Derringer and Suich, 1980; Bezerra et al., 2008). Individual desirabilities were calculated using equation 4.3, representing a one-side transformation and where \hat{y}_i is the polynomial function obtained for responses,

y_{i*} and y_i^* are the minimum and maximum acceptable values, respectively, and r will define the shape of d_i and the importance/weight of each response (Derringer and Suich, 1980; Ennaciri et al., 2014).

$$d_i = \left[\frac{\hat{y}_i - y_{i*}}{y_i^* - y_{i*}} \right]^r \quad (\text{equation 4.3})$$

Therefore, the polynomial function obtained for the responses (fitted response values) were used and the individual desirabilities combined by a geometric mean (equation 4.4).

$$D_o = (d_\eta \times d_{AdsSMX} \times d_{AdsCBZ} \times d_{AdsPAR} \times d_{S_{BET}} \times d_{TOC})^{1/6} \quad (\text{equation 4.4.})$$

The D_o value gives the overall assessment of the desirability of the combined response levels. In this study a one-sided transformation was applied, and the r value was assumed to be 1 (Derringer and Suich, 1980).

4.2.3. Adsorption tests

Batch experiments under agitation were carried out to determine the adsorption of the selected pharmaceuticals onto the sixteen produced AC and to evaluate their adsorptive performance. Pharmaceutical solutions of CBZ, SMX, and PAR with an initial concentration of 5 mg L⁻¹ were prepared separately. Each pharmaceutical solution was placed in contact with each of the 16 AC and shaken overnight in an overhead shaker (Heidolph, Reax 2) at 80 rpm under controlled temperature ((25.0 ± 0.1) °C). The concentration of AC was 0.015 g L⁻¹ and was chosen accordingly to the results obtained in preliminary tests.

After shaking, the adsorption samples were filtered through 0.22 µm PVDF filters (Whatman) and immediately analyzed for the residual concentration of the corresponding pharmaceutical. The adsorption samples were filtered through 0.22 µm PVDF filters (Whatman) and immediately analyzed by UV-vis spectrophotometry, according to the procedure described in Appendix B, section B1).

4.2.4. Methods for physicochemical characterization of the activated carbons

For all the produced and reference AC, S_{BET} and TOC were determined. Four AC were selected, based on their high ability to remove the studied pharmaceuticals from water, and were further characterized by point of zero charge (pH_{pzc}), the amount of surface acidic and basic functional groups (Boehm's titrations), proximate and ultimate analyses and scanning electron microscopy (SEM). The methodologies used for each technique are described in Appendix A, sections A1; A2.2; A3; A4; A5, and A6.

4.3. Results and Discussion

4.3.1. Full factorial design: responses

The design matrix (codified variables) and the response values for the yield, percentage of adsorption (for SMX, CBZ, and PAR), TOC, and S_{BET} are presented in Table 4.2. Also, the cumulative percentage of adsorption of the three pharmaceuticals and S_{BET} of the AC are graphically represented in Figure 4.1.

The results indicate that the highest temperature (x_1) and the highest impregnation ratio (x_3) were the most favorable conditions. The AC from AC1 to AC8 simultaneously present the largest percentages of adsorption and highest S_{BET} . These AC have in common being produced with the maximum pyrolysis temperature here considered (800 °C), showing that this temperature positively influences the development of porosity. AC 3, 4, 6 and 7 present the highest S_{BET} and the largest percentages of adsorption for CBZ, SMX, and PAR. It is noteworthy that these waste-based AC removed significantly higher pharmaceutical percentages than the commercial AC (PBF4) used as reference. Considering the results of TOC, all the produced carbons possess a high TOC content. Despite not being considered as a response of the full factorial design, it is also interesting to refer that all AC present very low percentage of IC (below 2 %). Amongst the 16 experiments, AC 3, 4, 6, and 7 present the highest TOC contents, which are very close to the TOC of the commercial AC used as reference.

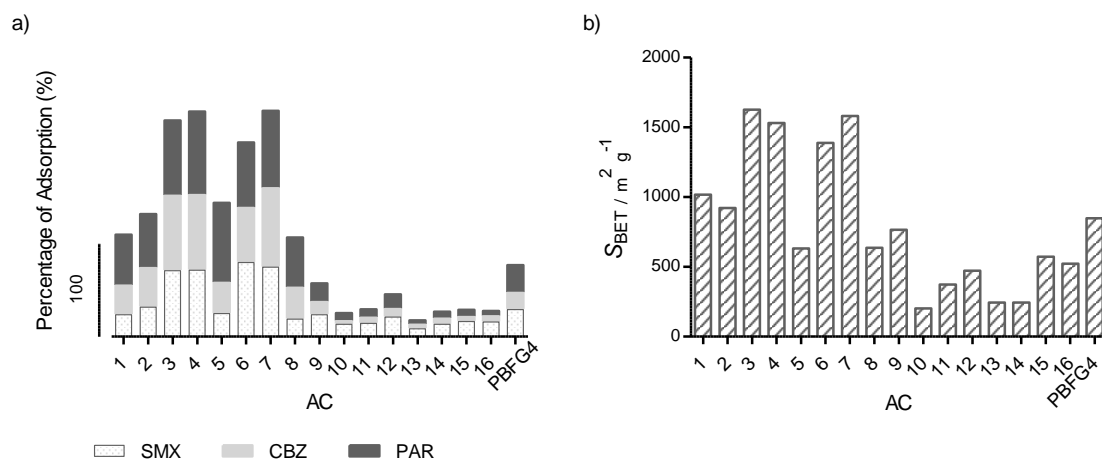


Figure 4.1. a) Cumulative percentages of adsorption for the three studied pharmaceuticals (SMX, CBZ, and PAR) and b) S_{BET} values, for the produced AC and the commercial AC (PBF4).

Table 4.2. Codified variables and responses obtained for each of the sixteen activated carbons (AC) produced from paper mill sludge and for the commercial AC.

EXP	Variables				Responses					
	x_1	x_2	x_3	x_4	η (%)	Ads (%) SMX	Ads (%) CBZ	Ads (%) PAR	S_{BET} ($m^2 g^{-1}$)	TOC %
1	+	+	-	-	26.4	23±3	31±3	55±3	1017	42.5±0.2
2	+	+	-	+	23.5	32±2	42±3	58±1	923	52±2
3	+	+	+	+	2.7	71±1	81±3	81±1	1627	67±1
4	+	-	+	+	2.8	71±3	81±1	90.0±0.2	1531	66±2
5	+	-	-	-	30.9	25±5	33±3	53±5	630	41.3±0.2
6	+	-	+	-	3.7	80±2	59±2	70±4	1389	62.8±0.2
7	+	+	+	-	3.4	75±2	85±1	84±5	1583	59±1
8	+	-	-	+	30.0	19±5	34±2	54±2	637	40±1
9	-	+	+	-	5.2	23±6	13.8±0.3	20±5	766	54±1
10	-	-	-	+	23.7	13±3	3±2	9±5	200	58.1±0.2
11	-	+	-	+	21.6	14±3	6±2	9±2	372	59±1
12	-	+	+	+	5.7	21±2	8.8±0.1	16±5	473	54.8±0.4
13	-	+	-	-	22.6	8±2	4±1	4.5±0.1	244	57±1
14	-	-	-	-	27.5	13±2	6±1	8±2	244	58.0±0.4
15	-	-	+	-	7.8	16±2	5±1	8±6	573	55.2±0.3
16	-	-	+	+	7.0	16±1	6±1	6±2	523	54.9±0.5
Commercial AC as reference										
PBF4 (Chemviron)						29±4	18±5	30±2	848 ^a	77.5 ± 0.1 ^a

x_1 – Pyrolysis temperature (650 °C (-) and 800 °C (+)); x_2 – Residence time (60(-) minutes or 150 (+) minutes); x_3 – precursor:activating:agent ratio (10:1 (-) and 1:1(+)); x_4 – Activating agent (K_2CO_3 (-) and KOH (+))

^a data published in *Jaria et al. (2015)*

4.3.2. Full factorial design: model fitting and statistical analysis

The normal probability distribution plots of the factors influencing each response are depicted in Figure 4.2. The regression models (equations 4.5 to 4.10) were statistically evaluated as present in Table 4.3. The P -value for all models is less than 0.05, indicating that the models satisfactorily fit the experimental data.

$$\hat{y}_{\text{yield}} = 15.28 - 1.38 x_2 - 10.50 x_3 - 1.77 x_1 x_3 \quad (4.5)$$

$$\hat{y}_{\text{SMX}} = 32.47 + 16.89 x_1 + 14.09 x_3 + 10.70 x_1 x_3 \quad (4.6)$$

$$\hat{y}_{\text{CBZ}} = 31.11 + 24.46 x_1 + 11.17 x_3 + 9.45 x_1 x_3 \quad (4.7)$$

$$\hat{y}_{PAR} = 39.07 + 29.06 x_1 + 7.75 x_3 + 5.36 x_1 x_3 \quad (4.8)$$

$$\hat{y}_{TOC} = 55.05 - 1.25 x_1 + 4.12 x_3 + 5.78 x_1 x_3 \quad (4.9)$$

$$\hat{y}_{BET} = 795.76 + 371.44 x_1 + 262.40 x_3 - 25.83 x_2 x_3 x_4 \quad (4.10)$$

The results on the optimization of the experimental data, performed using a surface response methodology, are presented in Table 4.4. The surfaces concerning the dependence of the response in terms of the residence time (x_2) versus the temperature of pyrolysis (x_1); precursor:activating agent ratio (x_3) versus the temperature of pyrolysis (x_1); and/or precursor:activating agent ratio (x_3) versus the residence time (x_2) are presented in Figure 4.3.

Table 4.3. Analysis of variance (ANOVA) of the obtained responses (least square method).

Response	Source	Simple linear regression				
		ν	SS	MS	F value	P value
Yield (%)	Regression	3	1.84x10 ³	613.3	256.9	3.78x10 ⁻¹¹
	Error	12	28.71	2.33		
	Total	15				
Ads(%) SMX	Regression	3	9.57x10 ³	3.19x10 ³	194.43	1.95x10 ⁻¹⁰
	Error	12	196.97	16.41		
	Total	15				
Ads(%) CBZ	Regression	3	1.30x10 ⁴	4.33x10 ³	96.21	1.16x10 ⁻⁸
	Error	12	540.44	45.04		
	Total	15				
Ads(%) PAR	Regression	3	1.49x10 ⁴	4.97x10 ³	167.06	4.75x10 ⁻¹⁰
	Error	12	357.44	29.79		
	Total	15				
S _{BET} (m ² g ⁻¹)	Regression	3	3.32x10 ⁶	1.11x10 ⁶	35.4	3.07x10 ⁻⁶
	Error	12	3.75x10 ⁵	3.13x10 ³		
	Total	15				
TOC (%)	Regression	3	830.59	276.86	24.51	2.09x10 ⁻⁵
	Error	12	135.5	11.29		
	Total	15				

ν – degrees of freedom; SS – sum of squares; MS – mean squares ($MS=SS/\nu$)

Table 4.4. General overview of the optimization results of full factorial design.

<i>Optimization results</i>						
<i>Responses</i>	<i>Yield</i>	<i>Ads (%) SMX</i>	<i>Ads (%) CBZ</i>	<i>Ads (%) PAR</i>	<i>TOC (%)</i>	<i>S_{BET} (m² g⁻¹)</i>
<i>Maximum</i>	28.9	74.2	76.2	81.2	63.7	1455
<i>x₁</i>	800 °C	800 °C	800 °C	800 °C	800 °C	800 °C
<i>x₂</i>	60 min	a	a	a	a	60 min
<i>x₃</i>	10:1	1:1	1:1	1:1	1:1	1:1
<i>x₄</i>	a	a	a	a	a	KOH

x₁ – Pyrolysis temperature; *x₂* – Residence time; *x₃* – Precursor:activating agent ratio; *x₄* – Activating agent.

^a Not significant.

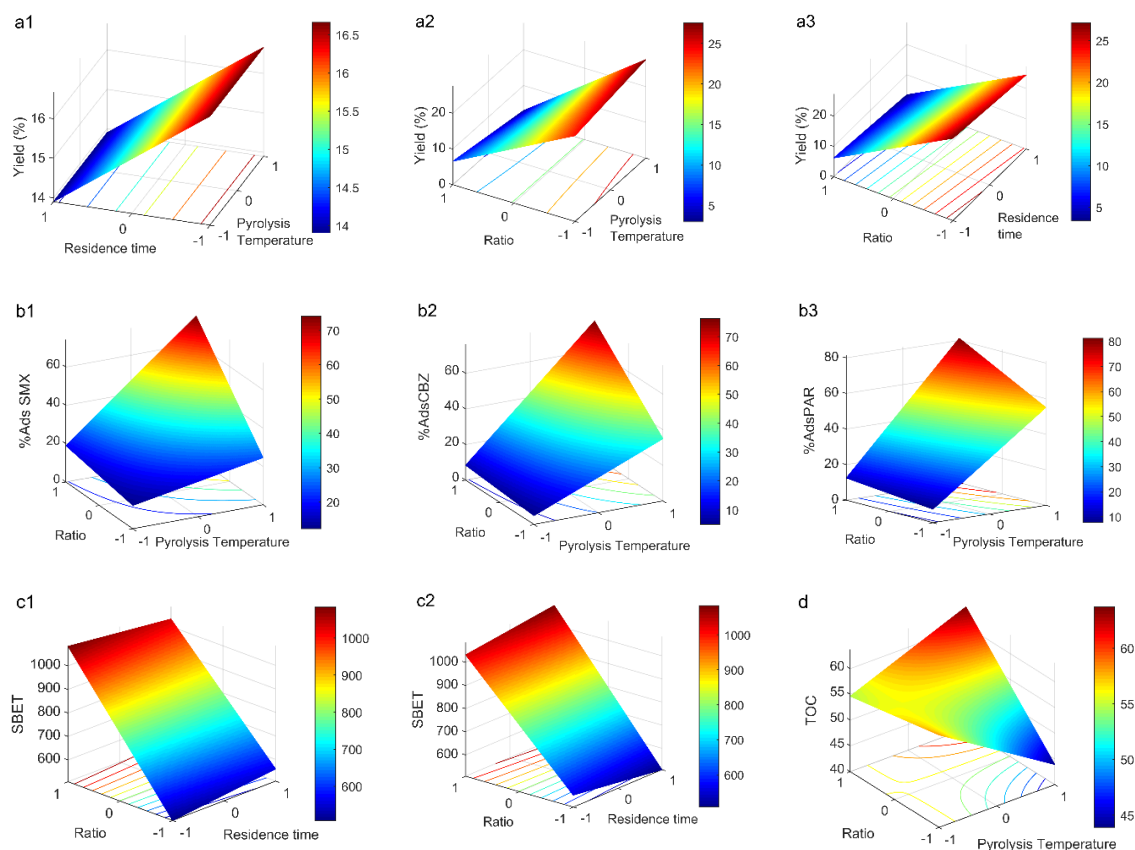


Figure 4.3. Response surfaces for: a) yield of production; b) adsorption percentages for SMX (b1), CBZ (b2), and PAR (b3); c) S_{BET} (c1 – for the activating agent KOH, and c2 – for the activating agent K_2CO_3); and d) TOC.

Figure 4.3a evidences that the yield of production is affected by the three effects, x_2 , x_3 , and x_1x_3 , with x_3 having the strongest influence. The better results are obtained for the highest pyrolysis temperature (800 °C) together with the lowest values of residence time (60 min) and precursor:activating agent ratio (10:1). Relatively to the adsorption of pharmaceuticals, Figure 4.3b1, b2 and b3 representing the response surfaces for SMX, CBZ, and PAR respectively, show that the highest percentages of adsorption occur for the highest values x_1 and x_3 (800 °C and 1:1). However, in the case of PAR, the influence of the precursor:activating agent ratio for higher temperatures is less pronounced than for the other two pharmaceuticals. In the case of the S_{BET} , this response is also mainly affected by the pyrolysis temperature (x_1) and by the precursor:activating agent ratio (x_3), with the response increasing for the highest values of both factors, 800 °C and 1:1, respectively (equation 4.10 and Table 4.4). However, residence time together with the precursor:activating agent ratio and the type of activating agent also have some impact in the response (Figure 4.3c). Hence, for higher precursor:activating agent ratios and considering the use of KOH as activating agent, one can observe that the response is higher for lower residence time (60 min) while in the case of using K_2CO_3 as activating agent, the response increase for a higher residence time. For lower precursor:activating agent ratios, the inverse occurs. Despite the little influence of the type of activating agent in the responses for S_{BET} , in general, this factor has not showed to significantly influence the responses. In fact, both activating agents are potassium-based reagents, which is the element considered to be the responsible for the development of porosity. Metallic potassium formed during the gasification process acts as a template due to its intercalation in the graphite-like structure, creating new porosities which highly increase the surface area of the produced carbon material (Marsh and Rodríguez-Reinoso, 2006; Ahmed and Theydan, 2012). Although Ahmed and Theydan (2012) considered that the amount of potassium atoms released during KOH activation is higher than with K_2CO_3 activation, leading to a higher surface area of the carbons produced by KOH activation, in this study, this was not evident, with both activating agents resulting in very similar S_{BET} (Table 4.2). At last, for the TOC (Figure 4.3d), the results are very interesting, with the interaction of pyrolysis temperature and precursor:activating agent ratio, not showing an apparent linear relationship, but evidencing highest values of response for the highest temperature of pyrolysis and for the highest precursor:activating agent ratio.

Overall, factors x_1 and x_3 have the highest influence, presenting better results for the higher level, corresponding to 800 °C and 1:1 ratio of precursor:activating agent, respectively (Table 4.4). The type of activating agent showed to have little influence in the values of S_{BET} . An important aspect of this study is that the chemical activation was performed at a precursor:activating agent ratio of 1:1 when, mostly in the case of KOH, the chemical activation usually uses a precursor:KOH ratio between 1:2 and 1:4

(Bandosz, 2006; Lillo-Ródenas et al., 2007; Alcañiz-Monge and Illan-Gomez, 2008). Also, it is important to highlight that the heat treatment (pyrolysis) and activation were performed in one step only, reducing the environmental impact of the production and also the production costs.

The PCA biplot analysis (Figure 4.4) clearly shows that the AC 3, 4, 6 and 7 are grouped, with very similar responses in what concerns S_{BET} and percentage of adsorption for SMX, CBZ, and PAR. This group is separated from the other produced carbons by the TOC and is clearly more distant from the yield of production, which is confirmed by the low yield values that AC 3, 4, 6 and 7 presented. This group presents the highest S_{BET} and adsorption percentages, and therefore, these materials were chosen to perform further physicochemical characterization, which is presented in section 4.3.3.

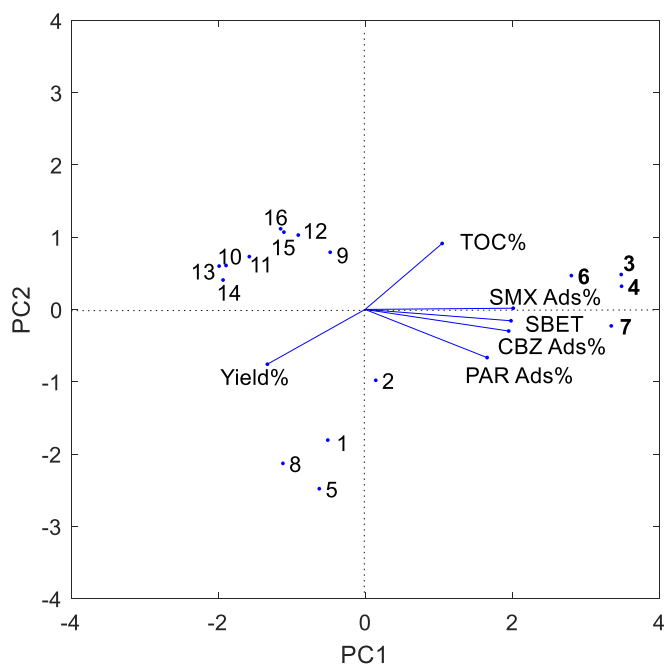


Figure 4.4. Biplot of the principal component analysis (PCA).

Concerning the application of the desirability function to analyze the optimization of all responses simultaneously, the results show that the AC with the best responses was the one produced with a temperature pyrolysis of 800 °C, a residence time of 60 min, a precursor:activating agent ratio close to 1:1 (0.6 in the codified variables between -1 and 1, meaning a precursor:activating ratio around 2:1 to 3:1), and using KOH as activating agent. The desirability, D, value obtained was 0.643, indicating a favorable balance of the responses.

4.3.3. Physical and chemical characterization of the selected activated carbons

All the produced AC were analyzed through TOC and S_{BET} analyses. The AC 3, 4, 6 and 7, indicated by the PCA as the carbons with the highest S_{BET} and adsorption percentage towards the three studied pharmaceuticals, were selected for further physical and chemical characterization to deepen the knowledge on their properties, namely, in what concerns their surface chemistry. These characteristics are also important for the future analysis of the interactions between the adsorbents and the adsorbates.

4.3.3.1. Proximate and ultimate analysis

The proximate and ultimate analyses (Table 4.5) showed that the carbon materials possess a high content in fixed carbon, which is consistent with the TOC determination (Table 4.2). Correspondingly, these AC possess low content in ashes (below 15 %), which is also in accordance with the low IC content of the samples.

Table 4.5. Proximate and Ultimate Analysis of the precursor (PS) and the selected activated carbons (AC).

Materials	PS	AC3	AC4	AC6	AC7
<i>Proximate Analysis (db)</i>					
Moisture (wt%)	4.78	6.85	19.71	16.38	16.55
Volatile Matter (wt%)	63.75	23.26	21.34	25.46	25.52
Fixed Carbon Content	8.30	63.12	65.54	62.57	63.74
Ash (wt%)	27.94	13.62	13.12	11.97	10.74
<i>Ultimate Analysis (dab)</i>					
% C	46.69	72.27	73.82	81.32	78.45
% H	5.42	1.35	2.56	1.48	1.60
% N	1.51	0.69	0.67	0.87	1.14
% S	0.00	0.38	0.00	0.00	0.46
%O ^a	46.38	25.31	22.95	16.33	18.36
O/C	0.993	0.350	0.311	0.201	0.234
H/C	0.116	0.019	0.035	0.018	0.020

Except for moisture, all values in proximate analysis are presented in a dry basis (db).

The values of FC were determined by difference.

Ultimate analysis values are presented in a dry and ash free basis (dab).

^aThe values of %O were estimated by difference: %O=100-C-H-N-S.

It is well known that AC contain several heteroatoms, being hydrogen, oxygen, nitrogen, and sulfur, the most abundant. All the heteroatoms are important to the properties of the AC, but oxygen-containing functional groups, particularly the ones at the edges of the structure, are considered to be particularly relevant in the surface chemistry of the materials (Thakur and Thakur, 2016). The four AC possess a high content in oxygen and the high O/C atomic ratio indicates the high incidence of

oxygenated functional groups such as hydroxyl, carboxylate, and carbonyl. The low values of H/C atomic ratios indicate a high degree of aromaticity of the AC (Ahmed et al., 2016), relatively to the raw material (PS).

4.3.3.2. Point of zero charge (pH_{pzc}) and surface functional groups

The results obtained for pH_{pzc} and surface functionalities of the four selected AC among those here produced are presented in Figure 4.5 and in Table 4.6.

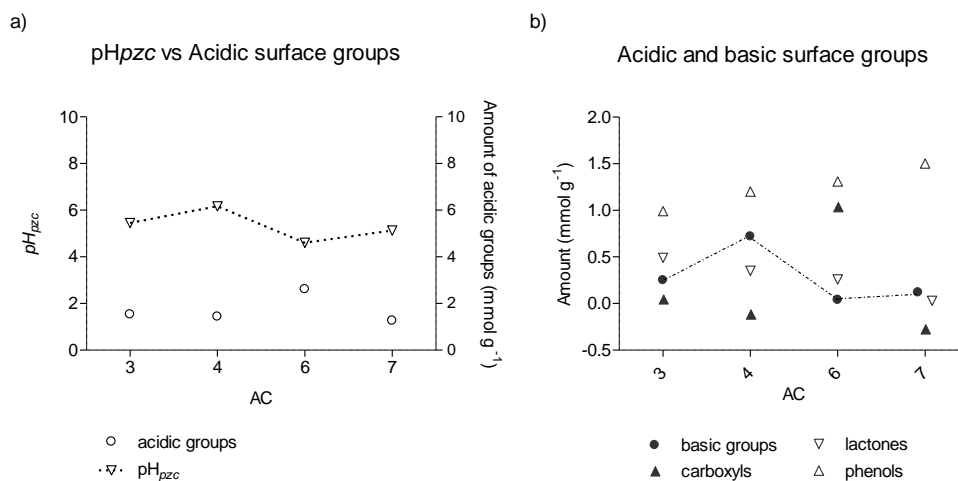


Figure 4.5. a) Plot of pH_{pzc} values *versus* amount of total acidic surface groups for AC 3, 4, 6 and 7; b) Graphical representation of the amounts of the acidic and basic surface groups for AC 3, 4, 6 and 7.

Table 4.6. Boehm's titrations and point of zero charge (pH_{pzc}) results.

Materials	<i>Amount of functional groups (mmol g⁻¹)</i>				pH_{pzc}	
	<i>pK_a < 6.37</i>	<i>6.37 < pK_a < 10.25</i>		<i>Total</i>		
	<i>carboxyls</i>	<i>phenol</i>	<i>lactones</i>	<i>acid</i>		
AC3	0.05	0.99	0.49	1.53	0.25	5.45
AC4	-0.11	1.20	0.35	1.44	0.72	6.16
AC6	1.04	1.31	0.26	2.61	0.04	4.60
AC7	-0.27	1.50	0.03	1.26	0.12	5.12

Some values obtained for carboxylic groups, namely for AC 4 and 7, are slightly negative, which cannot be considered as valid. These negative values can be explained by the inexistence or very low

amounts of carboxyl groups, associated with some sources of ambiguity in the results of this methodology that have already been pointed out by several authors: a) simple titration ratios are not always attained on the uptake of bases; b) the bases uptake can be affected by the equilibration time in a porous carbon; c) restrictions on the accessibility of the bases to inner pores can occur; and d) side reactions may exist on the carbon surface or with the reactants (Bandosz, 2006). Furthermore, the stereochemical proximity between functional groups can alter the properties of each one, since it is known that the properties of the functional groups are strongly related to their local environment (Bandosz, 2006; Thakur and Thakur, 2016). It can also be observed that AC7 has less lactones than the other three AC. Moreover, AC4 is the one that possesses the highest content of total basic groups combined with a low content of total acidic groups, which is in accordance with the pH_{pzc} as it is the carbon with the highest pH_{pzc} (when compared with AC 3, 6, and 7). This is clear in the graphs a) and b) in Figure 4.5, where it is interesting to observe that the values of pH_{pzc} show the same pattern (dotted lines) than the content in basic groups, although not so pronounced. AC6 possesses a slightly higher amount of acidic groups, which is also in accordance with the pH_{pzc} values.

4.3.3.3. Specific surface area (S_{BET})

The results concerning the N_2 adsorption isotherms for AC 3, 4, 6, and 7 (Tables 4.2 and 4.7) show that the four AC with higher S_{BET} present larger prevalence of micropores (around 68 % of the total pore volume). Also, the apparent densities are very low, which is consistent with the high microporosity degree of the materials and also with the low production yields here obtained.

Table 4.7. Textural parameters of the activated carbons AC3, AC4, AC6, and AC7.

Materials	ρ_{Hg} (g cm^{-3})	N_2 adsorption at -196°C		
		V_p ($\text{cm}^3 \text{g}^{-1}$)	Dubinin-Astakhov (DA)	
			W_0 ($\text{cm}^3 \text{g}^{-1}$)	L (nm)
AC3	0.09	1.07	0.73	1.74
AC4	0.10	0.96	0.69	1.73
AC6	0.10	0.83	0.64	1.66
AC7	0.09	1.00	0.71	1.74

ρ_{Hg} – apparent density; V_p - total pore volume; W_0 - micropore volume; L - average micropore width

4.3.3.4. Scanning electron microscopy (SEM)

SEM was used to analyze the surface morphology of AC 3, 4, 6 and 7. From the SEM images (Figure 4.6), it can be observed that the produced AC possess a high level of porosity. The structure is irregular and the presence of pores is well defined, as it was expected according to the results obtained by the N₂ adsorption isotherms (Table 4.2). However, the magnifications used in SEM mostly revealed the macroporosity (> 50 nm) of the AC, while microporosity cannot be evaluated at the obtained magnifications (Figure 4.6).

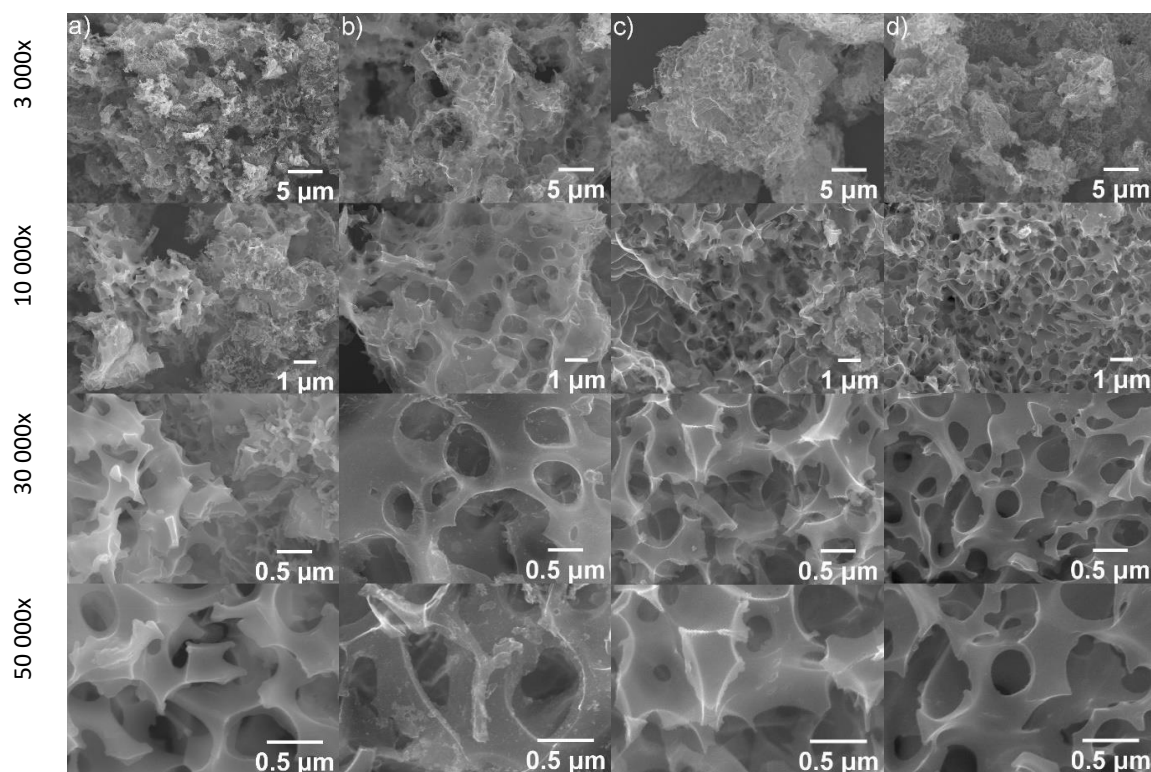


Figure 4.6. SEM images at different magnifications (3 000x, 10 000x, 30 000x, and 50 000x): a) AC3; b) AC4; c) AC6; d) AC7.

4.4. Conclusions

In this work, a full factorial design was applied to produce AC using PS as precursor, with optimal conditions to remove three pharmaceuticals (SMX, CBZ, and PAR) from water. Four factors

(pyrolysis temperature, residence time, precursor:activating agent ratio, and type of activating agent) were studied at two levels and their influence in six responses (yield of production, percentage of adsorption for SMX, CBZ, and PAR, TOC, and S_{BET}) were evaluated. The main factors affecting S_{BET} and the percentage of adsorption of the selected pharmaceuticals were found to be the pyrolysis temperature and the precursor:activating agent ratio. The highest temperature (800 °C) and highest precursor:activating agent ratio (1:1) resulted in S_{BET} between 1380 m² g⁻¹ and 1630 m² g⁻¹ and percentages of adsorption for the three pharmaceuticals of 78 % (in average), only using 0.015 mg L⁻¹ of AC. A desirability function allowed to make a multivariate analysis of all the responses and to select the best produced AC. Overall, the results obtained showed that the AC produced according to the optimal selected conditions are suitable for the removal of CBZ, SMX and PAR from water, with adsorption percentages significantly higher than those of a reference commercial AC. Thus, using PS as precursor, the full factorial design was proven to be an effective approach for selecting the most appropriate conditions to produce a highly efficient AC probably capable to compete with the performance of commercial AC in the market.

4.5. References

- Ahmad, M.A., Afandi, N.S., Bello, O.S., 2017. Optimization of process variables by response surface methodology for malachite green dye removal using lime peel activated carbon. *Appl. Water Sci.* 7, 717-727.
- Ahmed, M.B., Zhou, J.L., Ngo, H.H., Guo, W., 2016. Insight into biochar properties and its cost analysis. *Biomass and Bioenergy* 84, 76-86.
- Ahmed, M.J., Theydan, S.K., 2012. Adsorption of cephalexin onto activated carbons from Albizia lebeck seed pods by microwave-induced KOH and K₂CO₃ activations. *Chem. Eng. J.* 211-212, 200-207.
- Alcañiz-Monge, J., Illan-Gomez, M.J., 2008. Insight into hydroxides-activated coals: chemical or physical activation? *J. Colloid. Interf. Sci.* 318, 35-41.
- Bandosz, T.J., 2006. Activated Carbon Surfaces in Environmental Remediation, first ed. Elsevier, New York.
- Bergna, D., Varila, T., Romar, H., Lassi, U., 2018. Comparison of the Properties of Activated Carbons Produced in One-Stage and Two-Stage Processes. *Journal of Carbon Research* 4, 41.
- Bezerra, M.A., Santelli, R.E., Oliveira, E.P., Villar, L.S., Escalera, L.A., 2008. Response surface methodology (RSM) as a tool for optimization in analytical chemistry. *Talanta* 76, 965-977.
- Derringer, G., Suich, R., 1980. Simultaneous Optimization of Several Response Variables. *J. Qual. Technol.* 12.
- Ennaciri, K., Baçaoui, A., Sergent, M., Yaacoubi, A., 2014. Application of fractional factorial and Doehlert designs for optimizing the preparation of activated carbons from Argan shells. *Chemometr. Intell. Lab.* 139, 48-57.
- Jaria, G., Calisto, V., Gil, M.V., Otero, M., Esteves, V.I., 2015. Removal of fluoxetine from water by adsorbent materials produced from paper mill sludge. *J. Colloid Interf. Sci.* 448, 32-40.
- Kwaghger, A., Adejoh, E., 2012. Optimization of conditions for the preparation of activated carbon from mango nuts using ZnCl₂. *International Journal of Engineering Research and Development* 1, 01-07.
- Lillo-Ródenas, M.A., Marco-Lozar, J.P., Cazorla-Amorós, D., Linares-Solano, A., 2007. Activated carbons prepared by pyrolysis of mixtures of carbon precursor/alkaline hydroxide. *J. Anal. Appl. Pyrol.* 80, 166-174.
- Marsh, H., Rodríguez-Reinoso, F., 2006. Activated Carbon, First ed. Elsevier, England.
- Rajapaksha, A.U.V., M.; Zhang, M.; Ahmad, M.; Mohan, D.; Chang, S. X.; Ok, Y. S. , 2014. Pyrolysis condition affected sulfamethazine sorption by tea waste biochars. *Bioresource Technol.* 166, 303-308.

Tan, I., Ahmad, A., Hameed, B., 2008. Optimization of preparation conditions for activated carbons from coconut husk using response surface methodology. *Chem. Eng. J.* 137, 462-470.

Thakur, V.K., Thakur, M.K., 2016. Chemical Functionalization of Carbon Nanomaterials: Chemistry and Applications. CRC Press, New York.

5

PERFORMANCE OF PRIMARY PAPER MILL SLUDGE-BASED POWDERED ACTIVATED CARBON IN THE REMOVAL OF PHARMACEUTICALS FROM WASTEWATER

Abstract

A primary paper mill sludge (PS)-based powdered activated carbon (AC), AC3, was produced aiming the single adsorption of three pharmaceuticals (carbamazepine (CBZ), sulfamethoxazole (SMX), and paroxetine (PAR)) from ultrapure and wastewater. Kinetic and equilibrium adsorption experiments were run in batch operation conditions and for comparison purposes, they were also performed using a high-performance commercial powdered AC (CAC). Adsorption kinetics was fast for the three pharmaceuticals and similar onto AC3 and CAC in either wastewater or ultrapure water. However, matrix effects were observed in equilibrium results, and were more remarkably noted for AC3. These effects were evidenced by Langmuir maximum adsorption capacities (q_m , mg g^{-1}): for AC3, the lowest and highest q_m were 194 ± 10 (SMX) and 287 ± 9 (PAR), in ultrapure water, and 47 ± 1 (SMX) and 407 ± 14 (PAR), in wastewater, while for CAC, the lowest and highest q_m were of 118 ± 7 (SMX) and 190 ± 16 (PAR) in ultrapure water, and 123 ± 5 (SMX) and 160 ± 7 (CBZ) in wastewater. It was found that the matrix pH played a key role in these differences by controlling the surface electrostatic interactions between pharmaceutical and AC. Overall, it was evidenced the need of adsorption results in real matrices and demonstrated that AC3 is a promising option to be implemented in tertiary wastewater treatment for pharmaceutical's removal.

This chapter was based on the published article:

Silva, C.P., Jaria, G., Otero, M., Esteves, V.I., Calisto, V., 2019. Adsorption of pharmaceuticals from biologically treated municipal wastewater using paper mill sludge-based activated carbon. *Environ. Sci. Pollut. R.* 26, 13173-13184.

5.1. Contextualization

As referred in chapter 2, although the presence of pharmaceuticals in water is still unregulated, it is expected a stricter legislation on the discharge of pharmaceuticals into the environment in the near future so upgraded wastewater treatments will be necessary to cope with new regulations. For this reason, a great research effort has been carried out on alternative or additional treatments to those usually applied in wastewater treatment plants (WWTP). The incorporation of adsorption processes as tertiary treatments into current WWTP is quite feasible, which is essential from a practical point of view (Coimbra et al. 2015). In this sense, the utilization and application of waste-based adsorbents has emerged as a sustainable alternative to conventional activated carbons (AC) from non-renewable precursors (Silva et al., 2018), being a growing research field along the years (González-García, 2018). However, it is often observed in literature that two important aspects of the performance assessment of adsorbents are lacking or poorly addressed: the removal efficiency of the produced adsorbents in real water samples, namely wastewater samples, and the comparison of the produced adsorbents with commercial AC to evaluate if they are, in fact, a valid alternative.

In the previous chapter, a full factorial design experiment evidenced that primary paper mill sludge (PS) can be successfully used as precursor of AC. From the sixteen studied experimental conditions, four resulted in AC with high specific surface areas (S_{BET}) and high adsorption removal percentages for carbamazepine (CBZ), sulfamethoxazole (SMX) and paroxetine (PAR), in ultrapure water. One of these materials, AC3, was the AC presenting the highest S_{BET} ($1627 \text{ m}^2 \text{ g}^{-1}$) and very good responses in terms of adsorption percentage for the pharmaceuticals studied.

Considering these facts, this work aimed at assessing the practical utilization of the previously optimized powdered AC3 in the removal of CBZ, SMX, and PAR from wastewater, evaluating its potential for its application in tertiary treatment of wastewater for the removal of pharmaceuticals. Also, the performance of a commercial activated carbon (CAC) was evaluated under the same conditions for comparison.

5.2. Materials and Methods

5.2.1. Chemicals and reagents

The chemical activation process was performed using potassium hydroxide (KOH) (EKA PELLETS, $\geq 86\%$), while the washing step used HCl (AnalaR NORMAPUR, 37%). Pharmaceuticals used for the adsorption studies were CBZ (Sigma Aldrich, 99%), SMX (TCI, $> 98\%$) and PAR (paroxetine-hydrochloride; TCI, $> 98\%$). All the solutions were prepared in ultrapure water (obtained from a Milli-Q Millipore system Milli-Q plus 185) or in wastewater collected at a wastewater treatment plant (WWTP). The CAC used for comparison purposes was a high-performance commercial powdered AC from Norit (SAE SUPER 8003.6), kindly supplied by Salmon & CIA.

5.2.2. Preparation of the alternative activated carbon (AC3)

The AC3 was produced according to the conditions used for the experiment 3 described in chapter 4 and using PS as precursor. Briefly, the dried PS was grinded with a blade mill and impregnated with KOH in a 1:1 activating agent/precursor ratio. The mixture was stirred in an ultrasonic bath during 1 h and left to dry at room temperature. The dried material was subjected to pyrolysis into porcelain crucibles in a muffle (Nüve, series MF 106, Turkey), under controlled N_2 atmosphere, at $800\text{ }^\circ\text{C}$ and 150 min of residence time. After pyrolysis, AC3 was washed with 1.2 M HCl, to remove ashes and other inorganic material (aiming to improve both the microporosity and the S_{BET} by unblocking obstructed pores), and then washed with distilled water until reaching a neutral pH. Finally, the produced AC3 was dried in an oven for 24 h at $105\text{ }^\circ\text{C}$.

5.2.3. Methods for characterization of the alternative activated carbon (AC3) and the commercial activated carbon (CAC)

In this work, AC3 was characterized by X-ray Photoelectron Spectroscopy (XPS). S_{BET} and microporosity, total organic and inorganic carbon (TOC and IC, respectively), point of zero charge (pH_{pzc}), the main surface acidic and basic functional groups (Boehm's titrations), proximate and ultimate analysis and scanning electron microscopy (SEM) analysis were previously determined and are presented in the chapter 4 (section 4.3.3). For comparison, in this work, CAC was also subjected to characterization by means of nitrogen adsorption isotherms for the determination of S_{BET} and microporosity, TOC and

IC, pH_{pzc} , proximate and ultimate analysis and SEM analysis. The methods applied in these techniques are detailed in Appendix A, sections A1; A2.1; A2.2; A3; A4; and A5.

5.2.4. Wastewater sampling

Wastewater for the adsorption experiments was collected at three collection campaigns (between May and September 2017) from a local WWTP (Aveiro's WWTP, Águas do Centro Litoral). This WWTP treats domestic sewage and was designed to serve 159,700 population equivalents and receives an average daily flow of $39,278 \text{ m}^3 \text{ day}^{-1}$. In the WWTP, wastewater is subjected to primary and then biological treatment. Wastewater was collected after the biological decanter, which corresponds to the final treated effluent that is discharged into the environment (in this case, into the sea, at $\sim 3 \text{ km}$ from the coast). Immediately after collection, wastewater was filtered through $0.45 \text{ }\mu\text{m}$, 293 mm Supor® membrane disk filters (Gelman Sciences) and stored at $4 \text{ }^\circ\text{C}$ until use, which occurred within a maximum of 15 days. Wastewater collected in each campaign was characterized by measuring conductivity (WTW meter), pH (pH/mV/ $^\circ\text{C}$ meter pHenomenal® pH 1100 L, VWR), and TOC (Shimadzu, model TOC-V_{CPH}, SSM-5000A). The results of the characterization of wastewater samples are present in Table 5.3 (section 5.3.2)

5.2.5. Adsorption experiments

Batch adsorption experiments were performed by contacting single pharmaceutical solutions (CBZ, SMX, or PAR), with an initial concentration (C_0) of 5 mg L^{-1} , with a known mass (m) of adsorbent (AC3 and CAC) in polypropylene tubes. The tubes were stirred in a head-over-head shaker (Heidolph, Reax 2) at 80 rpm, under controlled temperature ($(25.0 \pm 0.1) \text{ }^\circ\text{C}$). Control experiments, i.e., the pharmaceutical solution in absence of adsorbent, were run in parallel and all experiments were run in triplicate. After shaking, solutions were filtered through $0.2 \text{ }\mu\text{m}$ PVDF filters (Whatman) and analyzed by micellar electrokinetic chromatography (MEKC) as described on Appendix B, section B2.

5.2.5.1 Adsorption kinetics

The time needed to attain the adsorption equilibrium was determined by shaking single pharmaceutical solutions (prepared in ultrapure or wastewater) with the corresponding adsorbent (AC3 or CAC) for different time intervals (between 5 min and 360 min). In ultrapure water, for both AC, the adsorbent concentration (g L^{-1}) in all experiments was 0.020 g L^{-1} . Meanwhile, when using wastewater,

adsorbent dosage was 0.020 g L⁻¹ for experiments on the adsorption of CBZ and PAR and 0.10 g L⁻¹ for experiments on the adsorption of SMX. Then, the amount of pharmaceutical adsorbed per mass unit of adsorbent at each time (q_t , mg g⁻¹), was calculated using equation 5.1:

$$q_t = \frac{(C_0 - C_t)V}{m} \quad (\text{equation 5.1})$$

where C_0 is the initial concentration of pharmaceutical (mg L⁻¹), C_t is the residual pharmaceutical concentration in the solution at time t (mg L⁻¹), V is the volume of solution (L), and m is the mass of adsorbent (g) (Limousin et al., 2007). The obtained experimental data were fitted to pseudo-first and pseudo-second order kinetic models (Table 5.1).

Table 5.1. Kinetic adsorption models considered for the fitting of the experimental kinetics.

Model	Non-linear equation	Assumptions	References
<i>Pseudo-first order model</i>	$q_t = q_e[1 - \exp(-k_1 t)]$ (equation 5.2)	reaction model; high initial concentrations of adsorptive; active sites are not the main rate controlling step, which in some cases may be the external or the internal diffusions	Lagergren (1898); Wang and Guo (2020)
<i>Pseudo-second order model</i>	$q_t = \frac{k_2 q_e^2 t}{1 + k_2 q_e t}$ (equation 5.3)	reaction model; associated to adsorption into active sites	Ho and McKay (1999); Wang and Guo (2020)

q_t – quantity of adsorbate removed at time t per unit mass of adsorbent (mg g⁻¹); q_e – amount of adsorbate adsorbed at equilibrium (mg g⁻¹); k_1 – rate constant of pseudo-first order (min⁻¹); k_2 – rate constant of pseudo-second order (g mg⁻¹ min⁻¹); t – stirring time (min).

5.2.5.2 Adsorption equilibrium

Equilibrium adsorption experiments were performed by shaking single pharmaceuticals' solutions (CBZ, SMX, or PAR) in either ultrapure water or wastewater with a known adsorbent concentration (0.008 g L⁻¹ to 0.050 g L⁻¹, for CBZ, SMX and PAR in ultrapure water; 0.008 g L⁻¹ to 0.050 g L⁻¹, for CBZ and PAR in wastewater; and 0.02 g L⁻¹ to 0.2 g L⁻¹ for SMX in wastewater) of AC3 and CAC during the time needed to attain the equilibrium, as determined in previous section. Then, the amount of pharmaceutical adsorbed per mass unit of adsorbent at equilibrium (q_e , mg g⁻¹), was calculated using equation 5.4:

$$q_e = \frac{(C_0 - C_e)V}{m} \quad (\text{equation 5.4})$$

where C_e (mg L^{-1}) is the residual pharmaceutical concentration after shaking during the equilibrium time. The obtained experimental data were fitted to non-linear models commonly used to describe the adsorption equilibrium isotherms, namely Langmuir and Freundlich models (Table 5.2).

Table 5.2. Adsorption isotherm models considered for the fitting of the experimental isotherms.

Model	Isotherm equation	Assumptions	Reference
<i>Langmuir</i>	$q_e = \frac{q_m K_L C_e}{1 + K_L C_e}$ (equation 5.5)	Monolayer adsorption; homogeneous surface	Langmuir (1918); Ahmed and Dhedan (2012)
<i>Freundlich</i>	$q_e = K_F C_e^{1/n}$ (equation 5.6)	Heterogeneous surface	Freundlich (1906); Ahmed and Dhedan (2012)

q_e – amount of solute adsorbed at equilibrium (mg g^{-1}); C_e – amount of solute in the aqueous phase at equilibrium (mg L^{-1}); q_m – maximum adsorption capacity (mg g^{-1}); K_L – Langmuir equilibrium constant related to the rate of adsorption (L mg^{-1}); K_F – Freundlich adsorption constant ($\text{mg}^{1-1/n} \text{L}^{1/n} \text{g}^{-1}$); n – constant related with the degree of non-linearity of the equation (for $n=1$, linear adsorption; $n<1$, non-favorable adsorption and $n>1$, favorable adsorption).

5.3. Results and Discussion

5.3.1. Activated carbons characterization

Regarding S_{BET} and microporosity, the AC3 presented a S_{BET} of $1627 \text{ m}^2 \text{g}^{-1}$, which was considered an excellent S_{BET} value comparing with the high-performance CAC used in the present study ($S_{\text{BET}} 996 \text{ m}^2 \text{g}^{-1}$) and also comparing with other alternative adsorbents used in literature (alternative AC with S_{BET} between $891 \text{ m}^2 \text{g}^{-1}$ and $1060 \text{ m}^2 \text{g}^{-1}$ (Mestre et al., 2007, 2014; Cabrita et al., 2010)). The AC3 presented also high prevalence of micropores (~68 % of the total pore volume).

In chapter 4 it was shown that, in what respects proximate and ultimate analyses, AC3 presented high content in fixed carbon (~63 %) and low content in ashes (~14 %). CAC presented similar ash content (~10 %), but higher fixed carbon content (~86 %). These results were consistent with the high TOC ($(67 \pm 1) \%$, for AC3 (chapter 4) and $(80.9 \pm 0.4) \%$, for CAC) and low IC (lower than 2 % for both carbons) results. CAC presented a pH_{pzc} of ~7, while the pH_{pzc} of ~5 determined for AC3 (chapter 4) indicated that it presented an acidic surface which was confirmed by the determination of the acidic oxygen-containing functional groups (carboxyl, lactones, and phenols) by the Boehm's titrations.

From the SEM images, it was observed that the produced AC3 presented a high level of porosity, with an irregular surface and a well-defined presence of porous (which was in accordance with the N_2

adsorption isotherms) (chapter 4); CAC presented some degree of porosity, but, for the same magnification, less roughness was observed in comparison with the AC3.

In what concerns XPS analysis (Figure 5.1), analyzing the survey spectrum (Figure 5.1a), it was possible to verify the high content in carbon (80.5 %) and oxygen (18.5 %) heteroatom in the surface of AC3. By deconvolution of the C1s region (Figure 5.1b) of the AC3 spectrum, the presence of the graphitic Csp^2 (peak 1 – 284.4 eV, which was the one presenting the highest intensity), the C–C sp^3 bond of the edge of the graphene layer (peak 2 – 285.3 eV), the C–O single bond, assigned to ether and alcohol groups (peak 3 – 286.1 eV), the O–C=O bond of carboxylic acids and/or carboxylic anhydride (peak 5 – 289.2 eV), and the $\pi-\pi^*$ transition in C1 (peak 6 – 290.5 eV) was evident (Velo-Gala et al., 2014). The N1s spectra (Figure 5.1c) presented four main peaks: around 397.7 eV (peak 1), which may be attributed to pyridine nitrogen functional groups; around 399.6 eV (peak 2), that may be related to pyrrole or pyridine functional groups; around 401.5 eV (peak 3), that may be assigned to quaternary nitrogen; and, finally, peak 4 (~402.9 eV) which may be attributed to the presence of oxidized forms of nitrogen (Lee et al., 2016). Concerning the O1s spectra (Figure 5.1d), AC3 presented a peak around 531.1 eV (peak 1) which may be assigned to the C=O group in quinones, and a peak around 532.6 (peak 2) which can be attributed to single bonded C–O–H (Abd-El-Aziz et al., 2008; Velo-Gala et al., 2014). There was also a peak at 533.9 eV (peak 3) that can be assigned to oxygen atoms in carboxyl groups (–COOH or COOR), and a peak around 536 eV (peak 4) that may be related to physisorbed water (Velo-Gala et al., 2014).

5.3.2. Wastewater samples' characterization

Results on the characterization of wastewater from the three collection campaigns, namely, pH, conductivity and TOC are depicted in Table 5.3.

Table 5.3. pH, conductivity and TOC values for the effluent samples.

	Sample 1	Sample 2	Sample 3
pH	7.7	7.8	7.9
Conductivity (mS cm⁻¹)	8.5	9.2	5.8
TOC (mg L⁻¹)	16.9	17.0	18.5

The analyzed parameters showed that the wastewater collected during different campaigns maintained similar properties. Therefore, the stability of the wastewater matrix for the adsorption experiments may be assumed.

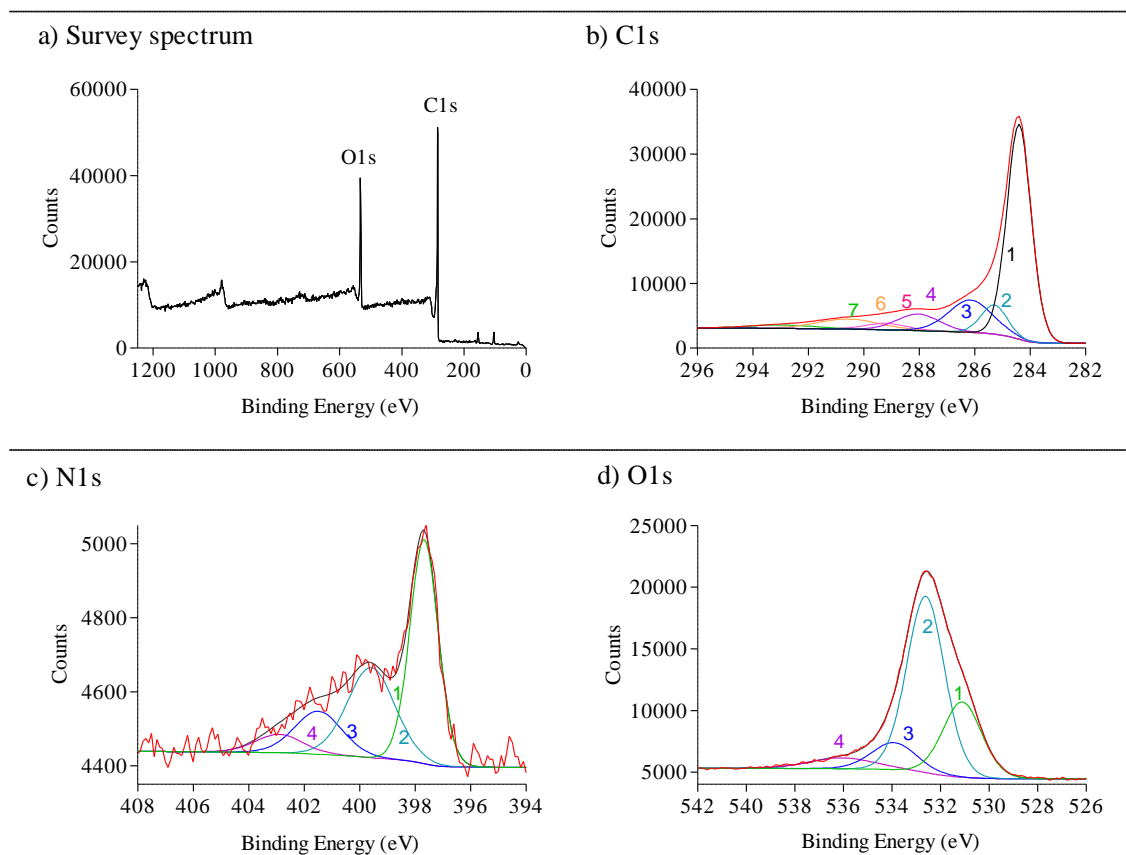


Figure 5.1. XPS analysis for AC3: a) survey spectrum; b) high-resolution spectrum of C1s; c) high-resolution spectrum of N1s; d) high-resolution spectrum of O1s.

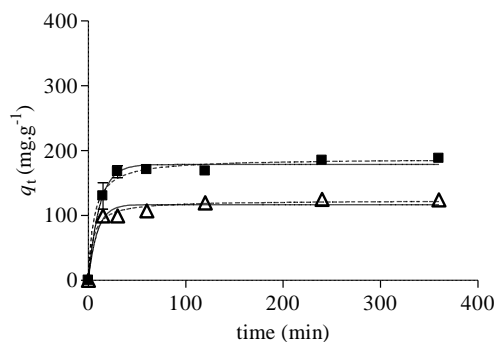
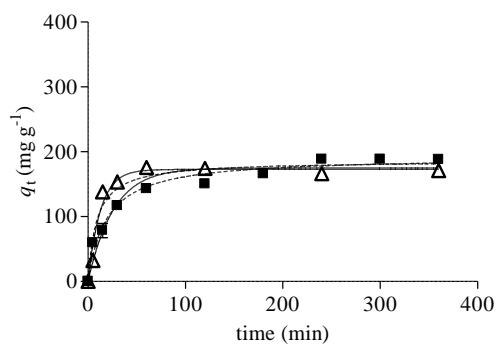
5.3.3. Adsorption kinetics

The assessment of the time needed for the pharmaceuticals to achieve the equilibrium in the bulk solution/carbon surface interface is an important parameter since, for the practical application of an adsorbent, it should not only present good adsorption capacities but also to adsorb in a suitable time scale. The results on the amount of each pharmaceutical adsorbed onto the AC3 or the CAC at time t (q_t , mg g^{-1}) versus time in ultrapure water and wastewater are represented in Figure 5.2 together with the corresponding fittings to pseudo-first and pseudo-second order kinetic models. The parameters obtained from the fittings of experimental results in ultrapure water and wastewater are summarized in Table 5.4.

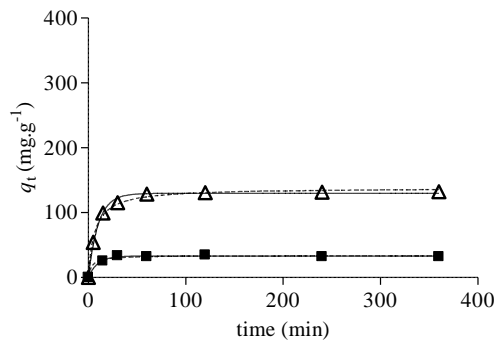
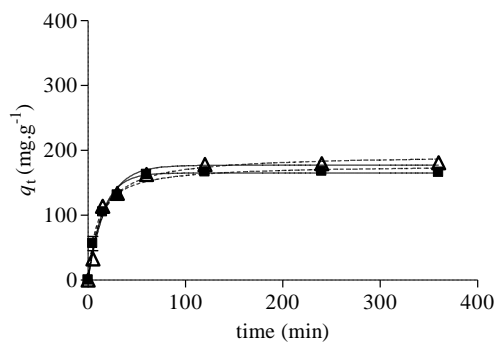
a) Ultrapure water

b) Wastewater

Carbamazepine



Sulfamethoxazole



Paroxetine

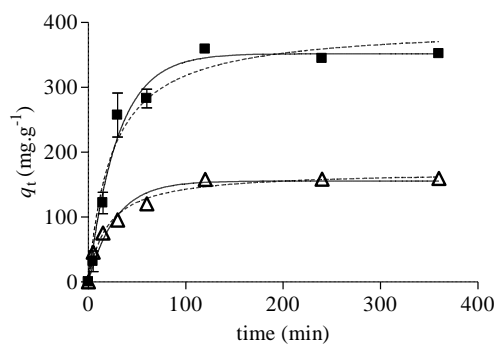
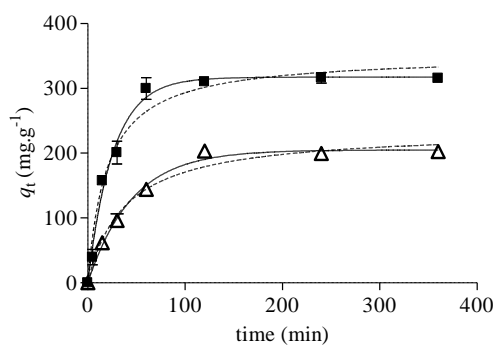


Figure 5.2. Kinetic study of the adsorption of CBZ, SMX and PAR onto AC3 (■) and CAC (Δ) in a) ultrapure water and b) wastewater. Results were fitted to pseudo-first (full line) and pseudo-second (dash line) order kinetic models.

Table 5.4. Fitting parameters of pseudo-first and pseudo-second order kinetic models to the experimental data for both carbons (AC3 and CAC) and the three pharmaceuticals (CBZ, SMX, and PAR) in ultrapure water and wastewater.

		<i>Pseudo-first order</i>		<i>Pseudo-second order</i>			
		q_e	k_1	R^2	q_e	k_2	R^2
<i>ultrapure water</i>							
CBZ	AC3	175 ± 7	0.038 ± 0.007	0.940	192 ± 7	0.00027 ± 0.00005	0.974
	CAC	173 ± 6	0.078 ± 0.013	0.971	186 ± 12	0.00060 ± 0.00024	0.934
SMX	AC3	165 ± 3	0.066 ± 0.006	0.991	178 ± 4	0.00056 ± 0.00007	0.993
	CAC	177 ± 5	0.054 ± 0.006	0.987	194 ± 7	0.00038 ± 0.00008	0.982
PAR	AC3	317 ± 7	0.039 ± 0.003	0.991	351 ± 17	0.00014 ± 0.00003	0.976
	CAC	205 ± 5	0.022 ± 0.002	0.993	236 ± 13	0.00011 ± 0.00003	0.979
<i>wastewater</i>							
CBZ	AC3	179 ± 4	0.09 ± 0.01	0.989	188 ± 5	0.0009 ± 0.0002	0.990
	CAC	117 ± 4	0.11 ± 0.03	0.964	123 ± 4	0.0017 ± 0.0005	0.986
SMX	AC3	32 ± 1	0.32 ± 0.09	0.949	33 ± 1	0.019 ± 0.007	0.969
	CAC	129 ± 2	0.098 ± 0.007	0.995	138 ± 2	0.0011 ± 0.0001	0.995
PAR	AC3	352 ± 12	0.033 ± 0.004	0.982	396 ± 25	0.00010 ± 0.00003	0.966
	CAC	156 ± 7	0.036 ± 0.006	0.962	171 ± 6	0.00030 ± 0.00006	0.984

q_e – amount of pharmaceutical adsorbed at equilibrium (mg g^{-1}); k_1 – rate constant of pseudo-first order (min^{-1}); k_2 – rate constant of pseudo-second order ($\text{g mg}^{-1} \text{min}^{-1}$); R^2 – coefficient of correlation

In ultrapure water, the kinetic experimental results regarding the adsorption of the pharmaceuticals onto AC3 were better described by the pseudo-second order model (with exception to PAR). Contrarily, the pseudo-first order model is the one that better described the pharmaceuticals' adsorption kinetics onto CAC. In any case, both models reasonably fitted experimental results ($R^2 \geq 0.93$), which means that both k_1 and k_2 can be used to compare the adsorption rate of CBZ, SMX and PAR onto AC3 and CAC. Comparing the adsorption of the three pharmaceuticals onto AC3 and CAC, it can be verified that the CAC presented a slightly faster kinetics for CBZ but slower for SMX and PAR. However, the kinetic rate constants obtained for all systems were in the same order of magnitude and the equilibrium is quickly reached (60 min to 240 min) onto both carbons, showing that they are kinetically adequate for the adsorption of the considered pharmaceuticals. In wastewater, except for PAR onto AC3, experimental results better fitted the pseudo-second than the pseudo-first order kinetic model. Still, both models may be considered adequate for the description of the experimental results onto both AC3 and CAC ($R^2 \geq 0.95$). On the other hand, the time needed to attain the equilibrium in wastewater was not affected by matrix effects and the AC3 continued to compare favorably with CAC. Still, in the case of

SMX, the adsorption was even faster in wastewater than in ultrapure water. Coimbra et al. (2019) had already observed that the matrix of an effluent from a WWTP, despite its complexity, did not affect the time needed to reach the equilibrium for other pharmaceuticals (salicylic acid, diclofenac, ibuprofen, and acetaminophen), which was equally short in both ultrapure and wastewater.

5.3.4. Adsorption equilibrium

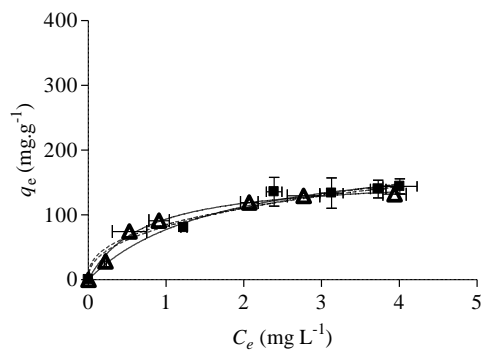
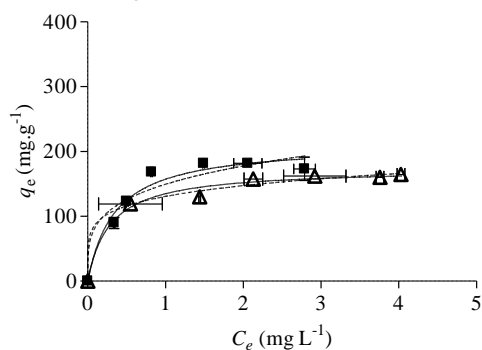
The adsorption isotherms, represented as the amount of each pharmaceutical adsorbed onto AC3 and CAC at equilibrium (q_e , mg g⁻¹) versus the amount of pharmaceutical remaining in solution (C_e , mg L⁻¹), are shown in Figure 5.3. Fitting parameters to Langmuir and Freundlich equilibrium models are summarized in Table 5.5, for isotherms determined in ultrapure water and wastewater. In ultrapure water (Figure 5.3), experimental data were well described either by Langmuir or Freundlich, with satisfactory correlation coefficients ($R^2 \geq 0.93$). As for Langmuir model, the AC3 presented higher adsorption capacities (q_m between 194 mg g⁻¹ and 287 mg g⁻¹) than CAC (between 118 mg g⁻¹ and 190 mg g⁻¹) for the three pharmaceuticals tested. This difference may be related with the S_{BET} (1627 m² g⁻¹ for AC3 and 996 m² g⁻¹ for CAC), which is one of the most important factors affecting the adsorption process. In any case, as for the relative low concentrations of CBZ, SMX and PAR in wastewater (Aydin et al., 2017; Shelver et al., 2008; Zhang et al., 2008), the q_m determined for both AC3 and CAC points to their capacity to treat large volumes before saturation. Equilibrium isotherms in wastewater (Figure 5.3) were also adequately fitted by both Langmuir and Freundlich models ($R^2 \geq 0.96$). Focusing on the Freundlich isotherm, it can be observed that the adsorption isotherm was favorable ($n > 1$) for both carbons and matrices (Table 5.5), which points to the fact that the adsorbents are efficient removing both high and low concentrations of the tested pharmaceuticals (Coimbra et al., 2019). Regardless, differences between equilibrium results in ultrapure water and wastewater were evident, which must be related to the fact of wastewater being a very complex matrix. For the adsorption of CBZ, either onto AC3 and CAC, the type of matrix did not affect negatively the adsorption capacities, with q_m values in wastewater being similar to those obtained in ultrapure water. Also, in both matrices, the adsorption capacity of CBZ onto AC3 was higher than onto CAC. In the case of PAR, the adsorption capacity onto either AC3 and CAC was higher in wastewater than in ultrapure water. This was especially evident for AC3 (q_m 29 % higher in wastewater than in ultrapure water), as for the comparison of the corresponding q_m in Table 5.5. Also, the great difference between the adsorbents regarding PAR adsorption capacity in wastewater has to be highlighted: PAR q_m onto AC3 was 62 % higher than onto CAC. Finally, in the case of SMX, the adsorption capacity onto AC3 was larger than onto CAC in ultrapure water, but in wastewater, the

contrary was observed (lower capacity onto AC3 than onto CAC). Furthermore, the q_m corresponding to SMX onto AC3 was 76 % lower in wastewater than in ultrapure water.

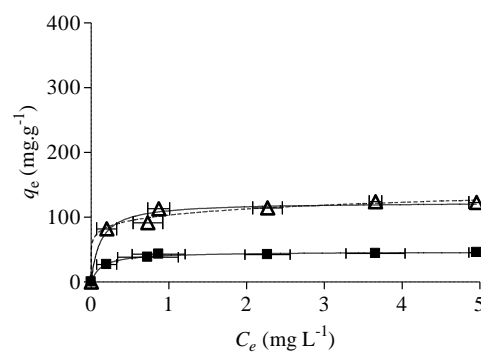
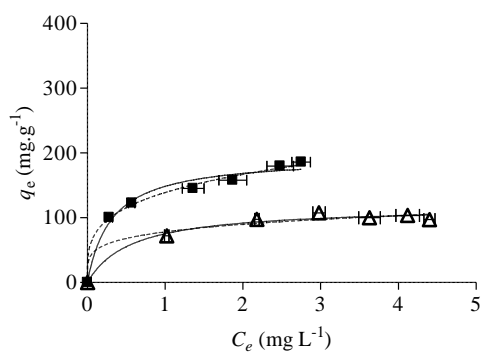
a) Ultrapure water

b) Wastewater

Carbamazepine



Sulfamethoxazole



Paroxetine

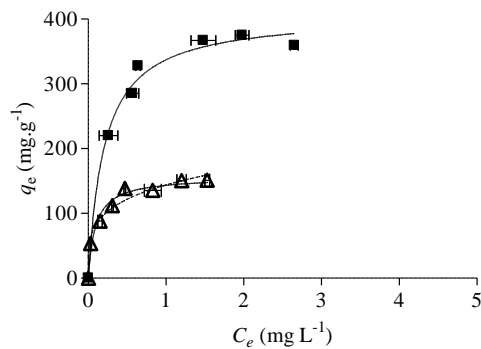
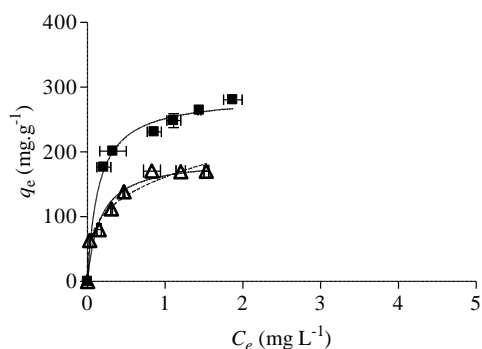


Figure 5.3. Equilibrium study of the adsorption of CBZ, SMX and PAR onto AC3 (■) and CAC (Δ) in a) ultrapure water and b) wastewater. Results were fitted to Langmuir (full line) and Freundlich (dash line) equilibrium models.

Table 5.5. Fitting parameters of Langmuir and Freundlich isotherm models to the experimental data for both carbons (AC3 and CAC) and the three pharmaceuticals (CBZ, SMX, and PAR) in ultrapure water and wastewater.

		<i>Langmuir</i>		<i>Freundlich</i>			
		q_m	K_L	R^2	K_F	n	R^2
<i>ultrapure water</i>							
CBZ	AC3	212 ± 16	2.8 ± 0.8	0.965	149 ± 8	4 ± 1	0.928
	CAC	174 ± 7	3.5 ± 0.9	0.986	131 ± 4	5.80 ± 0.97	0.990
SMX	AC3	194 ± 10	3.2 ± 0.7	0.979	139 ± 2	3.8 ± 0.2	0.996
	CAC	118 ± 7	1.8 ± 0.6	0.982	78 ± 6	5 ± 2	0.972
PAR	AC3	287 ± 9	7 ± 1	0.991	Not converged		
	CAC	190 ± 16	6 ± 2	0.941	161 ± 5	3.5 ± 0.4	0.972
<i>wastewater</i>							
CBZ	AC3	209 ± 27	0.6 ± 0.2	0.984	82 ± 10	2.3 ± 0.5	0.975
	CAC	160 ± 7	1.4 ± 0.2	0.991	85 ± 6	2.65 ± 0.45	0.956
SMX	AC3	47 ± 1	7.3 ± 1.2	0.992	Not converged		
	CAC	123 ± 5	8.4 ± 2.5	0.975	103 ± 3	7.9 ± 1.5	0.981
PAR	AC3	407 ± 14	4.8 ± 0.8	0.990	Not converged		
	CAC	156 ± 7	11.0 ± 2.6	0.975	144 ± 4	4.2 ± 0.5	0.975

q_m – maximum adsorption capacity (mg g^{-1}); K_L – Langmuir equilibrium constant related to the rate of adsorption (L mg^{-1}); K_F – Freundlich adsorption constant ($\text{mg}^{1-1/n} \text{L}^{1/n} \text{g}^{-1}$); n – constant related with the degree of non-linearity of the equation; R^2 – coefficient of correlation

Adsorption, which is a rather complex process, is strongly ruled by electrostatic and non-electrostatic interactions. The influence of these interactions is directly governed by the characteristics of both the adsorbent (key parameters of the carbon's surface chemistry comprise its pH, surface functional groups and uptake of specific adsorbates per unit S_{BET}) (Smith et al., 2009) and the adsorbate (essential characteristics of the adsorbate are the octanol/water coefficient ($\log K_{\text{ow}}$), the water solubility, the $\text{p}K_a$ and the molecular size) (Calisto et al., 2015). The complexity involving the balance between these variables makes it very difficult to infer the effectiveness of adsorption in wastewater from results in ultrapure water. Therefore, although most of the studies on alternative adsorbents in literature do not contain such information, for the practical application of any adsorbent, experimentation in real matrices are essential.

In this work, it was found that each pharmaceutical behaved differently in wastewater as compared with ultrapure water. The adsorbents' and pharmaceuticals' charges at wastewater pH may be

underneath these differences. In general, an acidic surface favors the uptake of alkaline adsorbates and vice-versa. In the case of AC3 and CAC, the pH_{pzc} was around 5 (chapter 4, section 4.3.3.2) and 7, respectively, which indicates that CAC is neutral while the AC3 presents an acidic surface. This was also observed by the determination of the acidic oxygen-containing functional groups by the Boehm's titrations: the surface chemistry of the AC3 was mostly dominated by phenols and lactones (chapter 4, section 4.3.3.2). Also, it is important to evaluate the main protonation state of the pharmaceuticals tested during the adsorption experiments. In wastewater ($\text{pH} \sim 7.8$), considering the $\text{p}K_a$ values of the pharmaceuticals ($\text{p}K_{a1\text{CBZ}} = 2.3$, $\text{p}K_{a2\text{CBZ}} = 13.9$; $\text{p}K_{a1\text{SMX}} = 1.8$, $\text{p}K_{a2\text{SMX}} = 5.7$; $\text{p}K_{a\text{PAR}} = 9.9$) (Table 1.1, in chapter 1), CBZ should be neutral, SMX negative and PAR positive. This may explain the marked decrease in the adsorption capacity of SMX for the AC3 in wastewater.

Given the two $\text{p}K_a$ values of SMX, for pH around 4, the non-protonated form is the predominant one, increasing pH to 7, most of the SMX molecules will be the deprotonated state, and for a $\text{pH} > 7$, the predominant form of SMX will be the deprotonated one by the complete dissociation of the hydrogen present in the $-\text{NH}-$ group (Qi et al., 2014). Therefore, SMX will be negatively charged in wastewater ($\text{pH} > 7$) and will be mostly electrostatically repulsed by the also negatively charged AC3 surface. Contrarily, CAC does not have a predominantly negatively charged surface, which may explain the non-decrease of SMX adsorption capacity. On the other hand, electrostatic interactions may be also responsible for the fact that, in ultrapure water, the differences between the adsorption capacities of AC3 and CAC are not so accentuated. In ultrapure water, pH is around 5.5-6 (much lower than that of wastewater) so changing the pharmaceuticals' speciation in comparison with wastewater.

Inversely to SMX, the adsorption of PAR onto AC3 was favored by the pH of the wastewater since PAR will be positively charged in that matrix. In the case of this pharmaceutical, the presence of one fluorine atom, which is the most electronegative halogen, may also count for strong hydrogen bonds with the AC3 functional groups (this carbon presented carboxyl groups compatible with hydrogen bonding as it was defined in its characterization), increasing the affinity between adsorbate and adsorbent.

Finally, as for CBZ, which is neutral at both the pH of ultrapure water and wastewater, no significant differences were observed between the q_m values of AC3 in the two studied matrices.

The above results highlighted the importance of electrostatic interactions for the adsorption of pharmaceuticals and evidenced that the adsorption capacity of AC3, as that of any other adsorbent, is highly dependent on the protonation state of the target pharmaceutical, which is turn is governed by the aqueous matrix. It may therefore be advanced that the implementation of AC3 will be especially favorable for cations, followed by neutrals and lastly anions.

To further assess the efficiency of AC3 in the removal of the three pharmaceuticals, a selection of the most relevant and recent literature on the utilization of alternative waste-based adsorbents for the removal of the considered pharmaceuticals, was done. Table 5.6 summarizes the maximum adsorption capacity determined by different authors for these pharmaceuticals. Overall, most of the alternative adsorbents used for the target purpose were produced from agrowastes and few from industrial wastes. Also, among the three pharmaceuticals here considered, SMX is the one that has received more attention in the literature, followed by CBZ and PAR. In any case, for the three pharmaceuticals, most of the studies have been carried out in ultrapure water. Very few works were carried out in real matrices or somehow evaluated matrix effects (e.g., Greiner et al. 2018; Naghdi et al. 2017; Shimabuku et al. 2014). Still, except for Oliveira et al. (2018), who used AC from paper pulp and compared the adsorption of these pharmaceuticals from ultrapure and wastewater, and Baghdadi et al. (2016), who used an optimally synthesized magnetic AC for the removal of CBZ, no results on the adsorption capacity of alternative adsorbents in wastewater were found. Safeguarding this important fact, data in Table 5.6 evidenced that, even in wastewater, the optimized AC3 displayed a larger CBZ adsorption capacity than the other alternative adsorbents, except for the AC produced from pomelo peel by Chen et al. (2017) under a two-step pyrolysis procedure. The latter is the waste-based adsorbent that, to the best of author's knowledge, possesses the largest CBZ adsorption capacity in ultrapure water, this value being only slightly higher than q_m values here determined for AC3 in wastewater. With respect to SMX, the adsorption capacity of AC3 here determined in ultrapure water is quite relevant as compared with results in the literature (Table 5.6). On the other hand, the adsorption capacity of AC3 in wastewater is higher than most of the values determined for other materials in ultrapure water and higher than the capacity of the AC from bleached paper pulp in wastewater (Oliveira et al. 2018). It must be pointed out that the largest SMX capacity in ultrapure water reported in the literature for an alternative adsorbent was determined by Zbair et al. (2018) for an AC produced from almond shell in a two-step pyrolysis and using hydrogen peroxide as activating agent in a ratio 1:10 (carbon from the first pyrolysis/hydrogen peroxide). This AC was used in adsorption experiments carried out under stirring in an ultrasonic bath, with no specification of the temperature at which the isotherms were determined. Finally, regarding PAR, scarce results on the adsorption capacity of waste-based adsorbents were found in the literature. Overall, Table 5.6 evidences that the optimized AC3 in this work displayed very remarkable capacities in ultrapure and, especially, in wastewater.

Table 5.6. Adsorption capacity of alternative waste-based adsorbents reported in literature for the removal of CBZ, SMX, and PAR.

Pharmaceutical	Waste-based adsorbent	Matrix	Isotherm conditions ^a	Adsorption capacity ^b (mg g ⁻¹)	Reference	
CBZ	AC from coconut shell	Ultrapure water	T = 23 °C	57.6	Yu et al. (2008)	
	Rice straw	Ultrapure water	T = 28 °C; pH = 6.5	28.6	Liu et al. (2013)	
	Biochar from paper mill sludge	Ultrapure water	T = 25 °C; pH = 10.5	12.6	Calisto et al. (2015)	
	Magnetic AC from coconut, pinenut and walnut shells	Ultrapure water	T = 25 °C; pH = 6	135.1	Shan et al. (2016)	
	Magnetic nanocomposite of AC	Wastewater	T = 25 °C; pH = 6.65	182.9	Baghdadi et al. (2016)	
	AC from pomelo peel	Ultrapure water	T = 25 °C; pH = 4.4	286.5	Chen et al. (2017)	
	Pine-wood derived nanobiochar		T = 25 °C; pH = 6	40	Naghdi et al. (2017)	
	AC from palm kernel shell	Ultrapure water	T = 25 °C; pH = 7	189	To et al. (2017)	
	AC from bleached paper pulp	Ultrapure water	T = 25 °C	93	Oliveira et al. (2018)	
		Wastewater	T = 25 °C; pH = 7.8	80		
		AC from spent brewery grains: -barley wine (BW)	Ultrapure water	T = 25 °C	190	Sousa et al. (2020)
			Wastewater	T = 25 °C; pH = 8.4	57.4	
		-pilsener (PL)	Ultrapure water	T = 25 °C	178	
		Wastewater	T = 25 °C; pH = 8.4	76		
	Optimized AC from paper mill sludge	Ultrapure water	T = 25 °C	212	This study	
		Wastewater	T = 25 °C; pH = 7.8	209		
SMX	Walnut shells	Ultrapure water	T = 20 °C; pH = 7	0.47	Teixeira et al. (2012)	
	Rice straw biochar	Ultrapure water	T = 25 °C; pH = 3	1.8	Han et al. (2013)	

^aThe temperature (T) at which isotherms were experimentally determined under batch stirred operation together with the pH of the aqueous matrix (if available).

^bMaximum adsorption capacity values resulting from the model fittings of the experimental isotherms.

Table 5.6. (Continued)

Pharmaceutical	Waste-based adsorbent	Matrix	Isotherm conditions ^a	Adsorption capacity ^b (mg g ⁻¹)	Reference
SMX	Biochar from paper mill sludge	Ultrapure water	T = 25 °C; pH = 10.5	1.69	Calisto et al. (2015)
	Rice straw biochar	Ultrapure water	T = 25 °C; pH = 6	4.2	Sun et al. (2016)
	Spent mushroom substrate	Ultrapure water	T = 15 °C; pH = 3	2.4	Zhou et al. (2016)
	Functionalized bamboo biochar	Ultrapure water	T = 25 °C; pH = 3.25	88.10	Ahmed et al. (2017)
	Hybrid clay nanosorbent	Ultrapure water	T = 25 °C; pH = 7	152	Martínez-Costa et al. (2018)
	AC from bleached paper pulp	Ultrapure water	T = 25 °C	110	Oliveira et al. (2018)
		Wastewater	T = 25 °C; pH = 7.8	13.3	
	Biochar from anaerobically digested bagasse	Ultrapure water	T = 25 °C; pH = 6.5	23.2	Regyyal and Sarmah, (2018)
	Modified organic vermiculites	Ultrapure water	T = 22 °C; pH ≈ 6	54.4	Yao et al. (2018)
	AC from almond shell	Ultrapure water	–	344.8	Zbair et al. (2018)
AC from almond shells	Ultrapure water	T = 30 °C; pH = 5.5 (optimized conditions)	106.9	Teixeira et al. (2019)	
Optimized AC from paper mill sludge	Ultrapure water	T = 25 °C	194	This study	
	Wastewater	T = 25 °C; pH = 7.8	47		
PAR	Biochar from paper mill sludge	Ultrapure water	T = 25 °C; pH = 10.5	38	Calisto et al. (2015)
	Optimized AC from paper mill sludge	Ultrapure water	T = 25 °C	287	This study
Wastewater		T = 25 °C; pH = 7.8	407		

^aThe temperature (T) at which isotherms were experimentally determined under batch stirred operation together with the pH of the aqueous matrix (if available).

^bMaximum adsorption capacity values resulting from the model fittings of the experimental isotherms.

5.4. Conclusions

The AC3 produced from PS displayed fast adsorption kinetics for the three pharmaceuticals considered (CBZ, PAR, and SMX), being as good as the high-performance CAC used for comparison. Furthermore, kinetic were equally fast in ultrapure and in wastewater. The equilibrium isotherms evidenced the better performance of AC3 than CAC in ultrapure water; however, in wastewater, equilibrium results onto AC3 were affected by matrix effects, which differed depending on the pharmaceutical. Thus, comparing adsorption onto AC3 from ultrapure water and wastewater, q_m of CBZ remained similar ($(212 \pm 16) \text{ mg g}^{-1}$ and $(209 \pm 27) \text{ mg g}^{-1}$, respectively), was larger for PAR ($(287 \pm 9) \text{ mg g}^{-1}$ and $(407 \pm 14) \text{ mg g}^{-1}$, respectively) and lower for SMX ($(194 \pm 10) \text{ mg g}^{-1}$ and $(47 \pm 1) \text{ mg g}^{-1}$, respectively). Matrix effects were not so evident in the case of adsorption onto CAC, which was related to differences in the surface charge of the carbons (neutral in the case of CAC and acidic in the case of AC3). Overall, it was demonstrated that the PS-based AC is a very good adsorbent for pharmaceuticals in water with high potential to be applied at a tertiary stage in wastewater treatment.

5.5. References

- Ahmed, M.B., Zhou, J.L., Ngo, H.H., Guo, W., Johir, M.A.H., Sornalingam, K., 2017. Single and competitive sorption properties and mechanism of functionalized biochar for removing sulfonamide antibiotics from water. *Chem. Eng. J.* 311, 348-358.
- Ahmed, M.J., Dhedan, S.K., 2012. Equilibrium isotherms and kinetics modeling of methylene blue adsorption on agricultural wastes-based activated carbons. *Fluid Phase Equilib.* 317, 9-14.
- Aydin, S., Aydin, M.E., Tekinay, A., Kiliç, H., 2017. Antidepressants in urban wastewater treatment plant: occurrence, removal and risk assessment. *Global Nest J.* 19, 100-106.
- Baghdadi, M., Ghaffari, E., Aminzadeh, B., 2016. Removal of carbamazepine from municipal wastewater effluent using optimally synthesized magnetic activated carbon: adsorption and sedimentation kinetic studies. *J. Environ. Chem. Eng.* 4, 3309-3321.
- Cabrita, I., Ruiz, B., Mestre, A.S., Fonseca, I.M., Carvalho, A.P., Ania, C.O., 2010. Removal of an analgesic using activated carbons prepared from urban and industrial residues. *Chem. Eng. J.* 163, 249-255.
- Calisto, V., Ferreira, C.I., Santos, S.M., Gil, M.V., Otero, M., Esteves, V.I., 2014. Production of adsorbents by pyrolysis of paper mill sludge and application on the removal of citalopram from water. *Bioresour. Technol.* 166, 335-344.
- Calisto, V., Ferreira, C.I.A., Oliveira, J.A.B.P., Otero, M., Esteves, V.I., 2015. Adsorptive removal of pharmaceuticals from water by commercial and waste-based carbons. *J. Environ. Manage.* 152, 83-90.
- Calisto, V., Jaria, G., Silva, C.P., Ferreira, C.I., Otero, M., Esteves, V.I., 2017. Single and multi-component adsorption of psychiatric pharmaceuticals onto alternative and commercial carbons. *J. Environ. Manage.* 192, 15-24.
- Chen, D., Xie, S., Chen, C., Quan, H., Hua, L., Luo, X., Guo, L., 2017. Activated biochar derived from pomelo peel as a high-capacity sorbent for removal of carbamazepine from aqueous solution. *RSC Adv* 7, 54969-54979.
- Coimbra, R.N., Calisto, V., Ferreira, C.I.A., Esteves, V.I., Otero, M., 2019. Removal of pharmaceuticals from municipal wastewater by adsorption onto pyrolyzed pulp mill sludge. *Arab. J. Chem.* 12, 3611-3620.
- Ferreira, C.I.A., Calisto, V., Otero, M., Nadais, H., Esteves, V.I., 2016. Comparative adsorption evaluation of biochars from paper mill sludge with commercial activated carbon for the removal of fish anaesthetics from water in Recirculating Aquaculture Systems. *Aquacult. Eng.* 74, 76-83.
- Ferreira, C.I.A., Calisto, V., Otero, M., Nadais, H., Esteves, V.I., 2017. Fixed-bed adsorption of Tricaine Methanesulfonate onto pyrolysed paper mill sludge. *Aquacult. Eng.* 77, 53-60.
- Freundlich, H., 1906. Über die Adsorption in Lösungen. *Z. Phys. Chem.* 57, 385-447.

- González-García, P., 2018. Activated carbon from lignocellulosics precursors: A review of the synthesis methods, characterization techniques and applications. *Renew. Sust. Energ. Rev.* 82, 1393-1414.
- Greiner, B.G., Shimabuku, K.K., Summers, R.S., 2018. Influence of biochar thermal regeneration on sulfamethoxazole and dissolved organic matter adsorption. *Environ. Sci.:Water Res. Technol.* 4, 169-174.
- Han, X., Liang, C., Li, T., Wang, K., Huang, H., Yang, X., 2013. Simultaneous removal of cadmium and sulfamethoxazole from aqueous solution by rice straw biochar. *J. Zhejiang Univ. Sci. B* 14, 640-649.
- Ho, I.S., McKay, G., 1999. Pseudo-second order model for sorption processes. *Process. Biochem.* 34, 451-465.
- Hou, L., Zhang, H., Wang, L., Chen, L., Xiong, Y., Xue, X., 2013. Removal of sulfamethoxazole from aqueous solution by sono-ozonation in the presence of a magnetic catalyst. *Sep. Purif. Technol.* 117, 46-52.
- Lagergren, S.Y., 1898. Zur Theorie der sogenannten Adsorption gelöster Stoffe. *K Sven Vetenskapsakademiens* 24, 1-3.
- Langmuir, I., 1918. The adsorption of gases on plane surfaces of glass, Mica and Platinum. *J. Am. Chem. Soc.* 40, 1361-1403.
- Lee, M.S., Park, M., Kim, H.Y., Park, S.J., 2016. Effects of microporosity and surface chemistry on separation performances of N-containing pitch-based activated carbons for CO₂/N₂ binary mixture. *Sci. Rep.* 6, 23224.
- Liu, Z., Zhou, X., Chen, X., Dai, C., Zhang, J., Zhang, Y., 2013. Biosorption of clofibric acid and carbamazepine in aqueous solution by agricultural waste rice straw. *J. Environ. Sci.* 25, 2384-2395.
- Martínez-Costa, J.I., Leyva-Ramos, R., Padilla-Ortega, E., Aragón-Piña, A., Carrales-Alvarado, D.H., 2018. Antagonistic, synergistic and non-interactive competitive sorption of sulfamethoxazole-trimethoprim and sulfamethoxazole-cadmium (ii) on a hybrid clay nanosorbent. *Sci. Total Environ.* 640-641, 1241-1250.
- Mestre, A.S., Pires, J., Nogueira, J.M.F., Carvalho, A.P., 2007. Activated carbons for the adsorption of ibuprofen. *Carbon* 45, 1979-1988.
- Mestre, A.S., Pires, R.A., Aroso, I., Fernandes, E.M., Pinto, M.L., Reis, R.L., Andrade, M.A., Pires, J., Silva, S.P., Carvalho, A.P., 2014. Activated carbons prepared from industrial pre-treated cork: sustainable adsorbents for pharmaceutical compounds removal. *Chem. Eng. J.* 253, 408-417.
- Naghdi, M., Taheran, M., Pulicharla, R., Rouissi, T., Brar, S.K., Verma, M., Surampalli, R.Y., 2017. Pine-wood derived nanobiochar for removal of carbamazepine from aqueous media: adsorption behavior and influential parameters. *Arab. J. Chem.* 12, 5292-5301.
- Oliveira, G., Calisto, V., Santos, S.M., Otero, M., Esteves, V.I., 2018. Paper pulp-based adsorbents for the removal of pharmaceuticals from wastewater: a novel approach towards diversification. *Sci. Total Environ.* 631-632, 1018-1028.

- Qi, C., Liu, X., Lin, C., Zhang, X., Ma, J., Tan, H., Ye, W., 2014. Degradation of sulfamethoxazole by microwave-activated persulfate: kinetics, mechanism and acute toxicity. *Chem. Eng. J.* 249, 6-14.
- Reguyal, F., Sarmah, A.K., 2018. Adsorption of sulfamethoxazole by magnetic biochar: effects of pH, ionic strength, natural organic matter and 17 α -ethinylestradiol. *Sci. Total Environ.* 628-629, 722-730.
- Shan, D., Deng, S., Zhao, T., Wang, B., Wang, Y., Huang, J., Yu, G., Winglee, J., Wiesner, M.R., 2016. Preparation of ultrafine magnetic biochar and activated carbon for pharmaceutical adsorption and subsequent degradation by ball milling. *J. Hazard. Mater.* 305, 156-163.
- Shelver, W.L., Shappell, N.W., Franek, M., Rubio, F., 2008. RELISA for sulfonamides and its application for screening in water contamination. *J. Agric. Food Chem.* 56, 6609-6615.
- Shimabuku, K.K., Cho, H., Townsend, E.B., Rosario-Ortiz, F.L., Summers, R.S., 2014. Modeling nonequilibrium adsorption of MIB and sulfamethoxazole by powdered activated carbon and the role of dissolved organic matter competition. *Environ. Sci. Technol.* 48, 13735-13742.
- Silva, C.P., Jaria, G., Otero, M., Esteves, V.I., Calisto, V., 2018. Waste-based alternative adsorbents for the remediation of pharmaceutical contaminated waters: Has a step forward already been taken? *Bioresource Technol.* 250, 888-901.
- Smith, K.M., Fowler, G.D., Pullket, S., Graham, N.J.D., 2009. Sewage sludge-based adsorbents: a review of their production, properties and use in water treatment applications. *Water Res.* 43, 2569-2594.
- Sousa, A.F.C., Gil, M.V., Calisto, V., 2020. Upcycling spent brewery grains through the production of carbon adsorbents - application to the removal of carbamazepine from water. *Environ. Sci. Pollut. R.* 27, 36463-36475.
- Sun, B., Lian, F., Bao, Q., Liu, Z., Song, Z., Zhu, L., 2016. Impact of low molecular weight organic acids (LMWOAs) on biochar micropores and sorption properties for sulfamethoxazole. *Environ. Pollut.* 214, 142-148.
- Teixeira, S., Delerue-Matos, C., Santos, L., 2012. Removal of sulfamethoxazole from solution by raw and chemically treated walnut shells. *Environ. Sci. Pollut. R.* 19, 3096-3106.
- Teixeira, S., Delerue-Matos, C., Santos, L., 2019. Application of experimental design methodology to optimize antibiotics removal by walnut shell based activated carbon. *Sci. Total Environ.* 646, 168-176.
- To, M-H., Hadi, P., Hui, C-W., Lin, C.S.K., McKay, G., 2017. Mechanistic study of atenolol, acebutolol and carbamazepine adsorption on waste biomass derived activated carbon. *J. Mol. Liq.* 241, 386-398.
- Velo-Gala, I., López-Peñalver, J.J., Sánchez-Polo, M., Rivera-Utrilla, J., 2014. Surface modifications of activated carbon by gamma irradiation. *Carbon* 67, 236-249.
- Wang, J., Guo, X., 2020. Adsorption kinetic models: Physical meanings, applications, and solving methods. *J. Hazard. Mater.* 390, 122156.

- Yao, Y., Zhang, Y., Gao, B., Chen, R., Wu, F., 2018. Removal of sulfamethoxazole (SMX) and sulfapyridine (SPY) from aqueous solutions by biochars derived from anaerobically digested bagasse. *Environ. Sci. Pollut. R.* 25, 25659-25667.
- Yu, Z., Peldszus, S., Huck, P.M., 2008. Adsorption characteristics of selected pharmaceuticals and an endocrine disrupting compound-naproxen, carbamazepine and nonylphenol-on activated carbon. *Water Res.* 42, 2873-2882.
- Zbair, M., Ait Ahsaine, H., Anfar, Z., 2018. Porous carbon by microwave assisted pyrolysis: an effective and low-cost adsorbent for sulfamethoxazole adsorption and optimization using response surface methodology. *J. Clean. Prod.* 202, 571-581.
- Zhang, Y., Geissen, S.U., Gal, C., 2008. Carbamazepine and diclofenac: removal in wastewater treatment plants and occurrence in water bodies. *Chemosphere* 73(8), 1151-1161.
- Zhou, A., Zhang, Y., Li, R., Su, X., Zhang, L., 2016. Adsorptive removal of sulfa antibiotics from water using spent mushroom substrate, an agricultural waste. *Desalin. Water Treat.* 57, 388-397.

6

DEVELOPMENT OF A PRIMARY PAPER MILL SLUDGE-BASED GRANULAR ACTIVATED CARBON AND ITS APPLICATION IN THE REMOVAL OF PHARMACEUTICALS FROM WATER

Abstract

In this work, a granular activated carbon (GAC) was produced using primary paper mill sludge (PS) as raw material and ammonium lignosulfonate (AL, a by-product of the cellulose pulp manufacture) as binder agent. For this purpose, a two-step pyrolysis production scheme was developed. The produced GAC (named PSA-PA) and a commercially available GAC (GACN), used as reference material, were physically and chemically characterized. Then, these materials were tested in batch experiments for the adsorption of carbamazepine (CBZ), sulfamethoxazole (SMX), and paroxetine (PAR) from ultrapure water and wastewater. Even though GACN and PSA-PA possess very similar specific surface areas (S_{BET}) ($629 \text{ m}^2 \text{ g}^{-1}$ and $671 \text{ m}^2 \text{ g}^{-1}$, respectively), PSA-PA displayed lower maximum adsorption capacities (q_m) than GACN for the pharmaceuticals here studied ($(6 \pm 1) \text{ mg g}^{-1}$ to $(44 \pm 5) \text{ mg g}^{-1}$ and $(49 \pm 6) \text{ mg g}^{-1}$ to $(106 \pm 40) \text{ mg g}^{-1}$, respectively). This may be related to the comparatively higher incidence of mesopores in GACN, which might have positively influenced its adsorptive performance. Moreover, the highest hydrophobic character and degree of aromaticity of GACN could also have contributed to its adsorption capacity. On the other hand, the performance of both GAC was significantly affected by the matrix in the case of CBZ and SMX, with lower q_m in wastewater than in ultrapure water. However, the adsorption of PAR was not affected by the matrix. Electrostatic interactions and pH effects might also have influenced the adsorption of the pharmaceutical compounds in wastewater.

This chapter was based on the published article:

Jaria, G., Calisto, V., Silva, C.P., Gil, M.V., Otero, M., Esteves, V.I., 2019. Obtaining granular activated carbon from paper mill sludge – A challenge for application in the removal of pharmaceuticals from wastewater. *Sci. Total Environ.* 653, 393-400.

6.1. Contextualization

Activated carbons (AC) can be found in the powdered form (PAC) or in the granular form (GAC), both used in water treatment. The main advantage of PAC is that, generally, it possesses higher specific surface area (S_{BET}) than GAC (Kårelid et al., 2017). However, the application of PAC as a tertiary treatment requires a separation step (for its removal from the treated water) that implies two main stages: sedimentation (through coagulation and/or flocculation and including a mixing process) and filtration (deep bed filtration; membrane filtration; cloth filtration) (Krahnstöver and Wintgens, 2018). In the case of GAC, its main advantage relies on the possibility of its application in fixed-bed column systems (continuous mode) and its capability of regeneration by thermal or chemical treatment and, therefore, its reuse (Marsh and Rodríguez-Reinoso, 2006; Kårelid et al., 2017). In fact, continuous fixed-bed systems are considered to be suitable for water treatment, presenting a more practical operation mode and easiness to scale-up to industrial level (Ferreira et al., 2017; Franco et al., 2017). Some raw materials used to produce commercial GAC include agricultural wastes, such as coconut shells, peach stones, and also walnut shells, due to their relatively high density, hardness and volatile content (Heschel and Klose, 1995; Kim et al., 2001; Aygün et al., 2003; Marsh and Rodríguez-Reinoso, 2006; Bae et al., 2014). Also, Ferreira et al. (2017) and Calisto et al. (2014) have shown the potential of biological paper mill sludge (BS) to produce granular adsorbent materials (biochars) with suitable granulometry and mechanical resistance to apply in fixed-bed-systems. However, as observed in chapter 3, BS presents high variability between sample batches from the same factory, being a raw material with low consistency. Hence, considering the promising results obtained for PS to produce PAC, the possibility of obtaining a GAC from PS was assessed. PS present a fibrous and brittle structure (mostly constituted by cellulose) and attempts to use wastes with similar constitution to produce GAC have failed. In fact, a main problem of waste-derived GAC is usually the low attrition resistance of the resulting materials, which may inhibit their use in adsorption beds (Smith et al., 2012). Different strategies have already been proposed to produce hardened GAC with high attrition resistance, namely, by pelletization and/or the utilization of binder agents (Carvalho et al., 2006). The introduction of a pelletization step is usually the approach when the AC are produced by physical activation, while the utilization of binders is usually the strategy in the case of chemical activation (Carvalho et al., 2006). Several patents have been published on the production of GAC employing binders such as urea-lignosulfonate (Blackmore, 1988) or ammonium lignosulfonate (Kovach, 1975). Also, in the literature, the utilization of binders such as humic acids

(Lozano-Castelló et al., 2002) or clays (Carvalho et al., 2006) has been proposed. A comparison of different binders was carried out by Lozano-Castelló et al. (2002), who used a humic acid derived sodium salt, polyvinyl alcohol, a phenolic resin, Teflon and an adhesive cellulose-based binder for the preparation of AC monoliths. Also, Smith et al. (2012) compared the utilization of ammonium lignosulphonate, polyvinyl alcohol, phenolic resin, araldite resin, lignosulphonic acid, calcium salt, and carboxymethyl cellulose sodium salt to produce GAC from sewage sludge. The authors of both studies (Lozano-Castelló et al., 2002; Smith et al., 2012) highlighted the importance of the selection of an appropriate binder so to avoid the deterioration of the adsorption performance of the final material.

This work aimed to give a step forward in the production of AC from PS and take on the challenge of obtaining a cellulosic waste-based GAC to be used in the removal of pharmaceuticals from water. For this purpose, ammonium lignosulfonate (AL), which, along with PS, is a by-product derived from the sulphite process applied in the manufacture of cellulose pulp, was used as binder agent. The physicochemical characterization of the produced GAC (PSA-PA) and of a commercial GAC (GACN) was performed and both adsorbents were tested under batch operation conditions for the adsorption of pharmaceuticals from ultrapure water and from wastewater. The versatility of the produced GAC was tested by studying the uptake of the three pharmaceuticals carbamazepine (CBZ), sulfamethoxazole (SMX), and paroxetine (PAR).

6.2. *Materials and Methods*

6.2.1. *Chemicals and reagents*

AL was used as binder agent and was kindly provided by Rayonier Advanced Materials. KOH (EKA PELLETS, $\geq 86\%$) was used as chemical activating agent. For the washing step, HCl (AnalaR NORMAPUR, 37%) was used. The pharmaceuticals used for the adsorption experiments were CBZ (carbamazepine, Sigma-Aldrich, 99%), SMX (sulfamethoxazole, TCI, $> 98\%$) and PAR (paroxetine-hydrochloride, TCI, $> 98\%$). The method used for the analytical quantification of the pharmaceuticals is described in Appendix B2. The GAC used as reference (GACN, DARCO 12 \times 20, particle size between 0.8 mm and 1 mm) was kindly provided by Norit. All solutions were prepared in ultrapure water obtained from a Milli-Q Millipore system (Milli-Q plus 185) or in wastewater (details on sampling and characterization are presented in section 6.2.4).

6.2.2. Production of a granular activated carbon from primary paper mill sludge and a binder agent

To produce a GAC using PS as raw material, several experimental approaches were tested until obtaining a material with suitable hardness to withstand the target application. In this context, the following factors were tested: type of activating agent; impregnation ratio between the precursor, the activating agent and the binder agent; impregnation order (activating agent followed by the binder agent or *vice versa*); and one- or two-step pyrolysis (detailed procedures are shown in Table 6.1). The optimized production methodology was achieved by a two-stage process (test N in Table 6.1). All the other tested conditions failed to produce a granular material. Accordingly, in the first stage, 30 g of PS was mixed with 70 mL of AL aqueous solution (at 35 %), resulting in a final PS:AL ratio (*w/w*) of 6:5. The mixture was stirred overnight in a head-over-head shaker (80 rpm) and left drying at room temperature followed by overnight oven-drying at 105 °C. The dried mixture was pyrolyzed under inert atmosphere (N₂) at 500 °C for 10 min. In a second stage, each 10 g of the resultant carbon (named PSA) was activated with 20 mL of a solution of KOH (at 50 %), resulting in a PSA:KOH final ratio (*w/w*) of 1:1. The mixture was stirred for 1 h in an ultrasonic bath and oven-dried at 105 °C overnight. This material was then pyrolyzed at 800 °C for 150 min, then washed with 1.2 M HCl and finally rinsed with distilled water until neutral pH was reached. The produced GAC, named PSA-PA, was crushed, grounded, and sieved to obtain a particle diameter between 0.5 mm and 1.0 mm.

6.2.3. Methods for physicochemical characterization of the produced granular activated carbon (PSA-PA) and the commercial granular activated carbon (GACN)

The physicochemical analysis of PSA-PA and GACN was performed by means of the determination of the total organic carbon (TOC) and inorganic carbon (IC); proximate and ultimate analysis; S_{BET} and Hg porosimetry; determination of the surface functionality by Boehm's titration; determination of the point of zero charge (pH_{pzc}); Fourier Transform Infrared spectroscopy with Attenuated Total Reflectance (ATR-FTIR); X-Ray Photoelectron Spectroscopy (XPS); and Scanning Electron Microscopy (SEM). The detailed procedures are explained in appendix A (sections A1, A2.1, A2.2, A2.3, A3, A4, A5, and A6).

Table 6.1. Experimental conditions tested to produce a granular activated carbon (GAC) using primary paper mill sludge (PS) as precursor, ammonium lignosulfonate (AL) as binder agent and different chemical activating agents (AA).

Test	Activating agent (AA)	Ratio (w:w:w)	Procedure
A	K ₂ CO ₃	10:10:1 ^a	AL was mixed in different proportions with PS and with the AA solution. It was left to dry and pyrolyzed at 800 °C for 150 min. From tests A to C, AL was added as an aqueous solution; from tests D to H, AL was added as a powder.
B	K ₂ CO ₃	4:4:1 ^a	
C	K ₂ CO ₃	2:2:1 ^a	
D	K ₂ CO ₃	10:10:1 ^a	
E	K ₂ CO ₃	4:4:1 ^a	
F	K ₂ CO ₃	2:2:1 ^a	
G	KOH	2:2:1 ^a	
H	H ₃ PO ₄	2:2:1 ^a	
I	KOH	2:2:1 ^a	PS was firstly washed with HCl 1.2 M and then with distilled water until neutral pH was reached, for the removal of ashes. Next, washed PS was mixed with AL (in powder) and AA, left to dry and pyrolyzed at 800 °C for 150 min.
J	KOH	2:2:1 ^a	PS was mixed with AL (in solution) in an overhead shaker for 12 h. After drying at room temperature, it was added to AA, left to dry and pyrolyzed at 800 °C for 150 min.
K	KOH	2:2:1 ^a	PS was mixed with AA and left to dry at room temperature. Next, AL (in solution) was added and the mixture was dried and pyrolyzed at 800 °C for 150 min.
L	K ₂ CO ₃	2:2:1 ^a	
M	K ₂ CO ₃	6:5 ^b ; 1:1 ^c	PS was mixed with the AL (in solution), dried and pyrolyzed at 500 °C for 10 min. The obtained carbon (PSA) was then mixed with the AA at a 1:1 ratio (PSA:AA, w:w). This mixture was shaken during 1 h in an ultrasonic bath, dried and pyrolyzed at 800 °C for 150 min. The final carbon (PSA-PA) was then washed with HCl 1.2 M and distilled water until neutral pH was reached.
N	KOH	6:5 ^b ; 1:1 ^c	

^aPS:AA:AL ratio; ^bPS:AL ratio; ^cPSA:AA ratio

Note: In all the above tests, pyrolysis was carried out under N₂ atmosphere.

6.2.4. Wastewater sampling

The performance of PSA-PA and GACN was evaluated in a real wastewater matrix for the three considered pharmaceuticals. Wastewater samples were collected between May 2017 and January 2018 (5 sampling campaigns) at the local wastewater treatment plant (WWTP) described in chapter 5 (section 5.2.4). After collection, wastewater was filtered and characterized as described in chapter 5 (section 5.2.4). The properties of wastewater samples used in this work are presented in Table 6.6 (section 6.3.2.1).

6.2.5. Batch adsorption experiments with the produced granular activated carbon (PSA-PA) and the commercial granular activated carbon (GACN)

Kinetic and equilibrium batch experiments were performed to determine the adsorption of CBZ, SMX, and PAR onto PSA-PA and GACN. For each pharmaceutical, solutions with a known initial concentration were prepared in both ultrapure water and wastewater and stirred together with PSA-PA or GACN in an overhead shaker (Heidolph, Reax 2) at 80 rpm and under controlled temperature ($(25.0 \pm 0.1) ^\circ\text{C}$). After stirring, solutions' aliquots were filtered through $0.22 \mu\text{m}$ PVDF filters (Whatman) and then analyzed for the remaining concentration of pharmaceutical. For all the pharmaceuticals, different initial concentrations controls (containing the pharmaceutical solution, but not GAC) were run simultaneously with experiments, which were carried out in triplicate. The solutions were analyzed by Micellar Electrokinetic Chromatography (MEKC) as described in Appendix B (Section B2).

For the kinetic studies, a predefined mass of each GAC was placed in polypropylene tubes and put in contact with 40 mL of a 5 mg L^{-1} aqueous single solution of each pharmaceutical. The concentrations of both PSA-PA and GACN were: in ultrapure water, 0.070 g L^{-1} for CBZ, 0.050 g L^{-1} for SMX, and 0.080 g L^{-1} for PAR; in wastewater, 0.150 g L^{-1} for CBZ and PAR, and 0.200 g L^{-1} for SMX. The solutions were shaken for different time intervals between 0.5 h and 72 h. The adsorbed concentration of pharmaceutical onto each GAC at time t , q_t (mg g^{-1}), was calculated using equation 5.1 (in chapter 5, section 5.2.5.1). The kinetic models used for fitting the experimental data were the pseudo-first and pseudo-second order models, presented in Table 5.1 in chapter 5 (equations 5.2 and 5.3, section 5.2.5.1).

Equilibrium experiments were performed by varying the initial concentration of the pharmaceutical and keeping the adsorbent mass constant. Hence, 40 mL of single solutions of each pharmaceutical, with concentrations varying between 5.0 mg L^{-1} and 0.5 mg L^{-1} (a minimum of 6 concentrations were considered for each system), were added to a predefined mass of carbon. In ultrapure water, the concentrations of PSA-PA were 0.050 g L^{-1} , 0.040 g L^{-1} and 0.060 g L^{-1} for the adsorption of CBZ, SMX, and PAR, respectively; and the concentrations of GACN were 0.050 g L^{-1} , 0.040 g L^{-1} and 0.040 g L^{-1} for the adsorption of CBZ, SMX, and PAR, respectively. In wastewater, the PSA-PA concentrations were of 0.125 g L^{-1} , 0.150 g L^{-1} and 0.100 g L^{-1} for the adsorption of CBZ, SMX, and PAR, respectively, while 0.125 g L^{-1} , 0.150 g L^{-1} and 0.080 g L^{-1} of GACN were used for the adsorption of CBZ, SMX, and PAR, respectively.

The adsorbed concentration of each pharmaceutical onto each GAC at the equilibrium, q_e (mg g^{-1}) was calculated using equation 5.4 (in chapter 5, section 5.2.5.2). The experimental results were fitted to Langmuir and Freundlich isotherm models (equations 5.5 and 5.6 in Table 5.2, chapter 5, section 5.2.5.2), and also to Sips isotherm model (Sips, 1948), presented in equation 6.1.

$$q_e = \frac{q_m K_S C_e^{1/N}}{1 + K_S C_e^{1/N}} \quad (\text{equation 6.1})$$

Where q_m is the maximum adsorption capacity (mg g^{-1}), K_S is the Sips constant (affinity parameter) (L mg^{-1})^N and N is the parameter associated to the heterogeneity of the surface (Ahmed and Dhedan, 2012).

6.3. Results and Discussion

6.3.1. Physicochemical characterization of the produced granular activated carbon (PSA-PA) and the commercial granular activated carbon (GACN)

6.3.1.1. Chemical characterization

PSA-PA and GACN present a high value of TOC, (72 ± 2) % and (79.7 ± 0.8) %, respectively, and a very low value of IC, (0.029 ± 0.003) % and (0.0204 ± 0.0002) %, respectively. Thus, the results obtained for TOC and IC were very similar for the produced and reference GAC. Comparing the values for PSA-PA with those for the precursor (TOC = (29 ± 1) % and IC = (3.3 ± 0.2) %) (Table 3.1 in chapter 3, section 3.3.1.1), the increase in the TOC content of the produced carbon compared with the precursor is clear.

The results of proximate and ultimate analyses are presented in Table 6.2 and show that both materials possess a high content in fixed carbon (77 % and 81 % for PSA-PA and GACN, respectively). The percentage in heteroatoms is higher for PSA-PA, namely in oxygen (13 % and 6 % for PSA-PA and GACN, respectively). Also, the H/C ratio indicates that GACN possesses a higher degree of aromaticity (lower H/C ratio) than PSA-PA.

Regarding ATR-FTIR analysis, the spectra for PSA-PA and for GACN are depicted in Figure (Figure 6.1). The spectrum of PSA-PA shows a peak at 1530 cm^{-1} , which is characteristic of aromatic compounds and can be also associated to secondary amide N–H and C–N bending ($1560\text{-}1530 \text{ cm}^{-1}$) (Stuart, 2004). The bands at 1100 cm^{-1} and 1180 cm^{-1} might be associated with secondary alcohols C–O stretch and the bands between 3800 cm^{-1} and 3600 cm^{-1} can be assigned to alcohol/phenol O–H stretching (Coates, 2000; Stuart, 2004). GACN spectrum revealed a broad band at 1125 cm^{-1} and a band at 1530

cm^{-1} , which can be associated to secondary alcohols C–O stretch and to the aromaticity of the material, respectively. Bands at 3605 cm^{-1} and 3720 cm^{-1} evidence the presence of alcohol/phenol O–H stretching (Coates, 2000).

Table 6.2. Proximate and ultimate analyses for the produced (PSA-PA) and commercial (GACN) granular activated carbons.

	PSA-PA	GACN
Proximate Analysis (db)		
Moisture (wt%)	8	8
Volatile Matter (wt%)	13	6
Fixed Carbon (FC)	77	81
Ash (wt%)	9	13
FC/VM	6	14
Ultimate Analysis (dab)		
%C	81.2	92.4
%H	1.9	0.75
%N	3.0	0.75
%S	0.80	0.05
%O	13.1	6.0
H/C	0.02	0.008
O/C	0.16	0.06

Notes:

Except for moisture, all values in proximate analysis are presented in a dry basis (db).

FC values were determined by difference.

Ultimate analysis is presented in a dry and ash free basis (dab).

The values of %O were estimated by difference: $\%O = 100\% - (\%C + \%H + \%N + \%S)$.

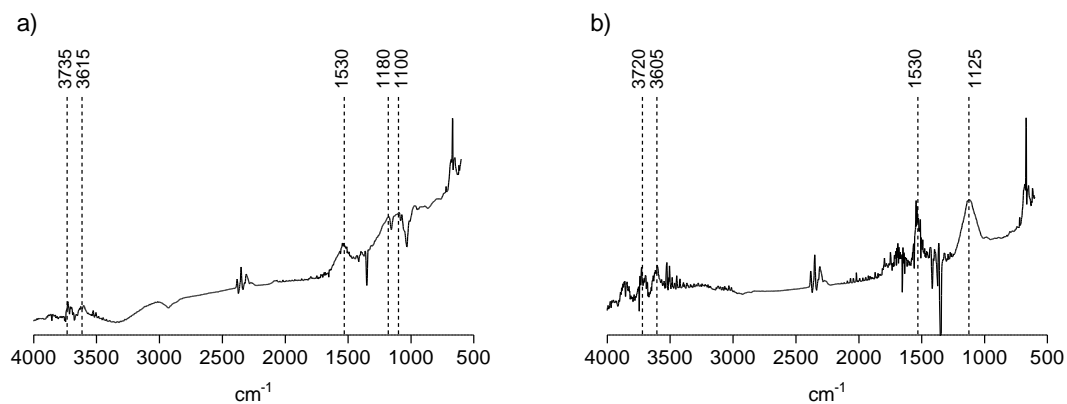


Figure 6.1. ATR-FTIR spectra of a) PSA-PA and b) GACN.

The determination of surface functional groups (Table 6.3) indicated that both GAC have an acidic nature, which was confirmed by the values of pH_{pzc} . Also, from the results in Table 6.3, it is possible to infer that the oxygen atoms present in both GAC are likely present in the form of carboxyl (particularly for GACN) and phenol groups, with lower incidence in lactones.

Table 6.3. Amount of acidic and total basic functional groups of both granular activated carbons (PSA-PA and GACN) determined by Boehm's titration.

Material	Amount of functional groups (mmol g^{-1})				pH_{pzc}
	<i>Carboxylics</i>	<i>Lactones</i>	<i>Phenols</i>	<i>Basic (total)</i>	
PSA-PA	1.29	0.29	0.96	0.31	4.3
GACN	1.03	0.02	0.31	0.34	4.8

To complement the surface functionality characterization, XPS analysis was performed and the results are presented in Figure 6.2 and Table 6.4. The results showed that PSA-PA possesses a higher amount of oxygen than GACN. In fact, the XPS data indicate contents of 74.8 % of carbon, 17.3 % of oxygen and 2.3 % of nitrogen for PSA-PA, and 90.5 % of carbon and 7.3 % of oxygen for GACN. These results are coincident with those from the ultimate analysis (Table 6.2). By deconvolution of the C1s region, the prevalence of graphitic Csp^2 is evident (especially for GACN), along with the presence of C-Csp^3 bonds associated to phenolic, alcoholic and etheric carbons at the edge of the graphene layer (especially for PSA-PA) (Nielsen et al., 2014; Velo-Gala et al., 2014). These results are also in accordance with the ATR-FTIR spectra, presenting bands characteristic of alcohols (between 3800 cm^{-1} and 3600 cm^{-1}), mainly observed in PSA-PA spectrum. Peaks associated to carbonyl or quinones and to carboxyl or ether groups are present in relatively similar percentages for both GAC (peaks 3 and 4, respectively, for C1s). These results do not seem to be in agreement with the Boehm's titration data, where the calculated values for carboxylic groups were greater than for the phenol groups, especially in the case of GACN. These differences can be attributed to the fact that XPS is a surface technique while Boehm's titration is a bulk technique. Both spectra also present a peak at 291 eV, which can be associated to $\text{C } \pi\text{-}\pi^*$ transition (Velo-Gala et al., 2014). Concerning the O1s spectra, PSA-PA presents a peak at 535.5 (peak 3), which may be attributed to chemisorbed oxygen (Velo-Gala et al., 2014). Also, it presents a peak at 531 eV, which can be assigned to C=O bonding in quinones and carbonyl groups, and a peak around 533 eV assigned to oxygen atoms of hydroxyl groups and to lactones and anhydrides. These two peaks (at 531 eV and 533 eV) are likewise in the GACN XPS spectrum, which also presents a peak at

534.4 eV that may be associated to oxygen of carboxyl groups, which is coincident with the Boehm's titrations results.

For PSA-PA it was also performed the fitting of the peaks associated to N1s. In fact, comparing the overall spectra of the two GAC Figure 6.2, it is possible to clearly observe a peak in the N1s zone for PSA-PA, while for GACN this peak is not noticeable. This is consistent with the higher N content of PSA-PA in comparison with GACN, as revealed by the ultimate analysis (Table 6.2). The fitting indicates the presence of two peaks, at 398.0 eV and 400.1 eV, which might be attributed to pyridinic and pyrrolic N, respectively (Li et al., 2014; Wei et al., 2016).

Table 6.4. X-Ray photoelectron spectroscopy (XPS) results for PSA-PA and GACN.

	Peak	PSA-PA		GACN		Possible bond assignment
		Binding Energy (eV)	%	Binding Energy (eV)	%	
C1s	1	284.5	58.5	284.6	68.4	Csp ² ; graphitic carbon
	2	285.8	22.0	285.8	10.2	C-C sp ³ ; C-(O, N, H): phenolic, alcoholic, etheric carbon
	3	287.6	7.3	287	8.2	C=O: carbonyl or quinone
	4	289	6.3	288.9	5.4	O-C=O: carboxyl or ether
	5	291	5.9	291	7.7	π - π^* transition in C
O1s	1	531.1	20.1	531.2	24.4	C=O: carbonyl or quinone
	2	533	54.6	533	44.4	C=O: carboxyl/carbonyl or sulfoxides/sulfones; O-C: phenol/epoxy, ether, ester, anhydride, carboxyl
	3	-	-	534.4	22	-COOH or -COOR
	4	535.3	17.5	-	-	Water or chemisorbed oxygen
N1s	1	398	18.9	-	-	Pyridinic N (N-6)
	2	400.1	81.9	-	-	Pyrrolic N (N-5)

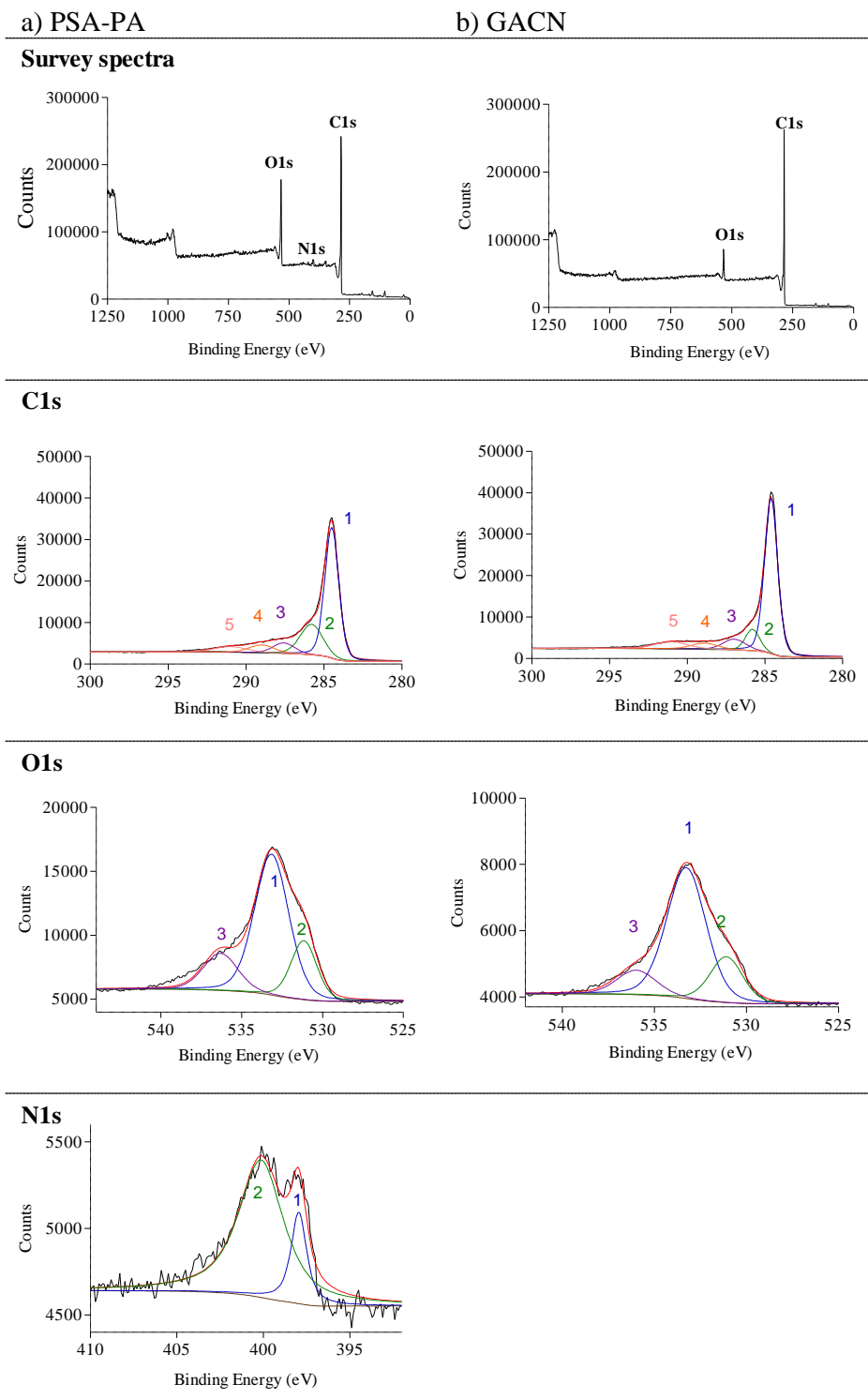


Figure 6.2. XPS survey spectra and high-resolution spectra for C1s, O1s, and N1s, of a) PSA-PA and b) GACN.

6.3.1.2. Physical characterization

For the study of the textural features of the materials, nitrogen adsorption isotherms and SEM were used as characterization techniques. The results of S_{BET} and Hg porosimetry are presented in Table 6.5. For both GAC, S_{BET} and micropore volume (W_0) values are very similar; however, GACN possesses larger total pore volume (V_p) and average pore diameter (D) values than PSA-PA, which might have important implications in the adsorptive performance of the materials, as explained below (section 6.3.2). Observing the pore size distribution (Figure 6.3), it is evident that PSA-PA possesses a narrower pore size with prevalence of pores with 5 nm of diameter and smaller, whilst GACN presents a broader distribution, including a significant amount of larger pore sizes in the mesopores' range (2-50 nm). This may be an interesting feature of PSA-PA considering the selective adsorption of molecules with different sizes. On the other hand, the apparent density is similar for both materials, although it is slightly superior in the case of GACN.

Table 6.5. Textural characterization of PSA-PA and GACN.

Sample	ρ_{Hg} (g cm ⁻³)	N ₂ adsorption at -196 °C						
		S_{BET} (m ² g ⁻¹)	V_p (cm ³ g ⁻¹)	Dubinin-Radushkevich (DR)		D (nm)	Dubinin-Astakhov (DA)	
				W_0 (cm ³ g ⁻¹)	L (nm)		W_0 (cm ³ g ⁻¹)	L (nm)
PSA-PA	0.61	671	0.37	0.27	1.44	1.11	0.28	1.58
GACN	0.65	629	0.75	0.27	-	2.38	0.30	1.71

ρ_{Hg} - apparent density; V_p - total pore volume; W_0 - micropore volume; L - average micropore width; D - average pore diameter ($2V_p/S_{\text{BET}}$, assuming slit-shaped pores)

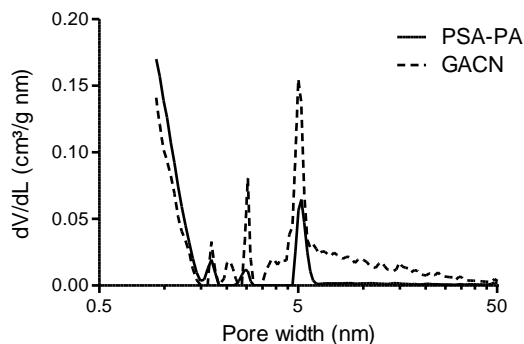


Figure 6.3. Pore size distribution of PSA-PA and GACN.

The surface morphological structure of the two GAC was analyzed by SEM (Figure 6.4). It is interesting to observe that, at the lowest magnifications, GACN appears to have a more homogeneous morphology but, at higher magnifications, the structure becomes rougher and the porosity is revealed. In the case of PSA-PA, at the lowest magnifications, a more disordered structure (possibly due to fragments of fibers that have not been destroyed) can be observed, but at higher magnification, porosity is also clearly observed.

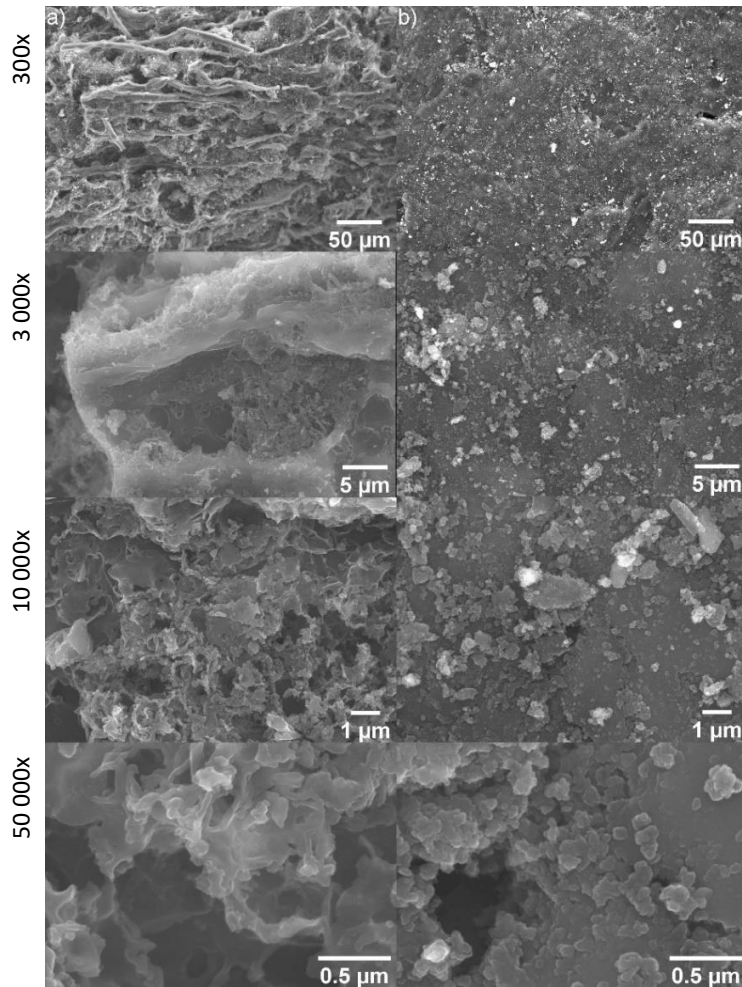


Figure 6.4. Scanning electron microscopy (SEM) images for a) PSA-PA and b) GACN at magnifications of 300x, 3 000x, 10 000x and 50 000x.

6.3.2. Batch adsorption experiments with the produced granular activated carbon (PSA-PA) and the commercial granular activated carbon (GACN)

6.3.2.1. Wastewater samples' characterization

Results on the characterization of wastewater concerning the five collection campaigns, namely, pH, conductivity and TOC are depicted in Table 6.6.

Table 6.6. Properties of the wastewater samples.

	Sample 1	Sample 2	Sample 3	Sample 4	Sample 5
pH	7.7	7.8	7.9	8.0	7.7
Conductivity (mS cm⁻¹)	8.5	9.2	5.8	5.7	3.4
TOC (%)	16.9	17	18.5	12.8	24.3

The analyzed parameters showed that the wastewater collected during different campaigns maintained similar properties. Therefore, the stability of the wastewater matrix for the adsorption experiments may be assumed.

6.3.2.2. Kinetic studies

The graphical representation of experimental and model results, and the parameters of the fitted models for the adsorption kinetics of CBZ, SMX, and PAR onto the two studied GAC (PSA-PA and GACN) in ultrapure water and in wastewater are presented in Figure 6.5 and Table 6.7, respectively. The kinetic models used to describe the experimental data were the pseudo-first order and pseudo-second order models (chapter 5, Table 5.1).

As it may be seen in Table 6.7, the fittings to the pseudo-first order and the pseudo-second models presented R^2 values above 0.90, except for the adsorption kinetics of PAR onto GACN, in ultrapure water. Therefore, both models (pseudo-first and pseudo-second order) were considered to reasonably describe the experimental data. In general terms, it may be said that, for CBZ and SMX, the results were slightly better described by the pseudo-second order model, while pseudo-first order model was the most adequate to describe the adsorption kinetics of PAR.

In relation to the rate constants k_1 and k_2 , the values vary between 10^{-6} and 10^{-3} (min^{-1} or $\text{g mg}^{-1} \text{min}^{-1}$, respectively). These low values are in agreement with the relatively long equilibrium times (above

24 h) here determined. It must be taken into account that, due to the particle size of GAC, adsorption kinetics are usually slower than onto powdered materials. Nevertheless, it is possible to observe that GACN presents a slightly faster adsorption rate than PSA-PA for CBZ in ultrapure water (2 times higher k_2), and for PAR in ultrapure and wastewater (3.6 and 3.25 times higher k_1 , respectively), while PSA-PA presents a faster adsorption rate than GACN in the case of CBZ in wastewater (4 times higher k_2) and SMX in both matrices (3.5 times higher k_2 in ultrapure water and 22 times higher k_2 in wastewater).

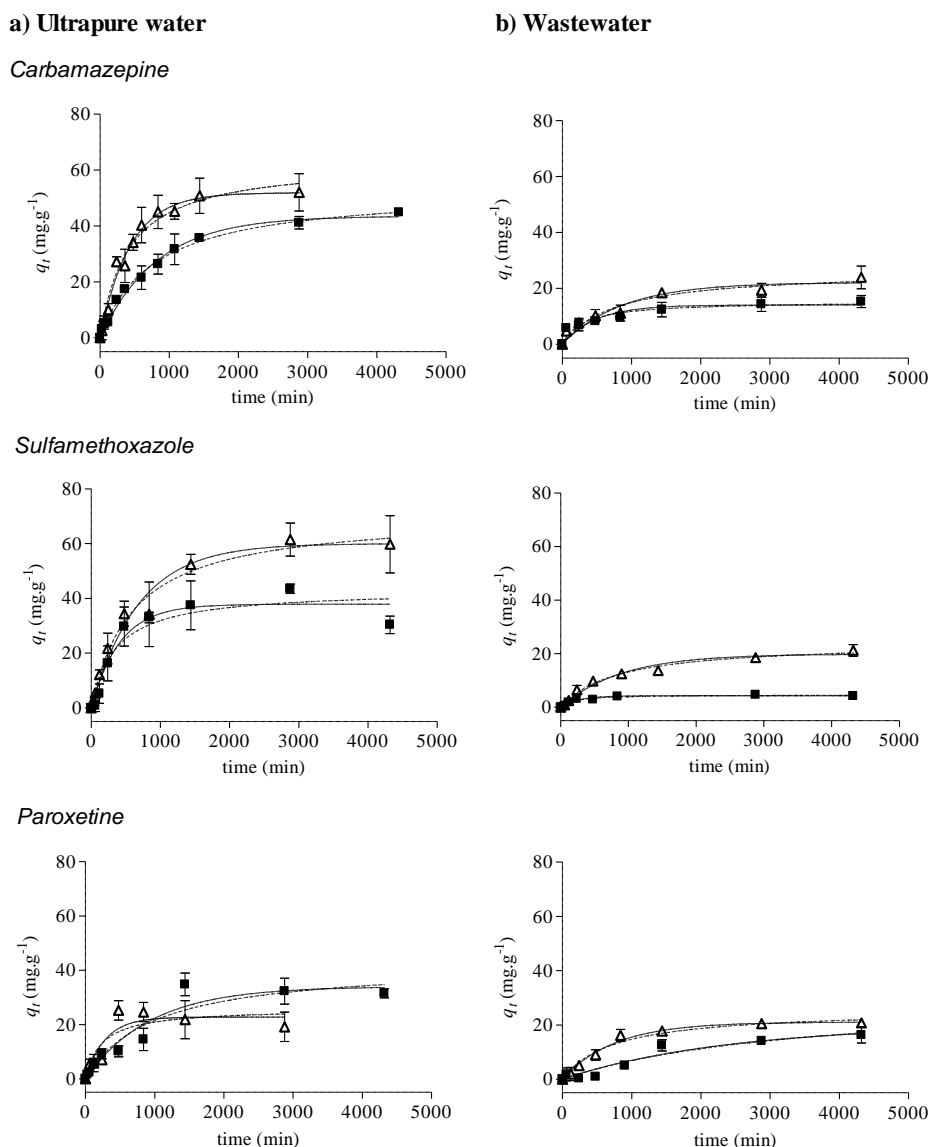


Figure 6.5. Kinetic study of the adsorption of CBZ, SMX and PAR onto PSA-PA (■) and GACN (Δ) in a) ultrapure water and in b) wastewater. Results were fitted to pseudo-first (full line) and pseudo-second (dash line) order kinetic models.

Table 6.7. Fitting parameters of pseudo-first and pseudo-second order kinetic models to the experimental data for both carbons (PSA-PA and GACN) and the three pharmaceuticals (CBZ, SMX, and PAR) in ultrapure water and wastewater.

		<i>Pseudo-first order</i>		<i>Pseudo-second order</i>			
		q_e	k_1	R^2	q_e	k_2	R^2
<i>ultrapure water</i>							
CBZ	PSA-PA	44 ± 1	(1.22 ± 0.08) x10 ⁻³	0.991	53 ± 2	(2.4 ± 0.2) x10 ⁻⁵	0.995
	GACN	52 ± 2	(2.3 ± 0.2) x10 ⁻³	0.986	63 ± 4	(3.9 ± 0.8) x10 ⁻⁵	0.980
SMX	PSA-PA	38 ± 3	(2.4 ± 0.6) x10 ⁻³	0.936	43 ± 5	(7 ± 3) x10 ⁻⁵	0.901
	GACN	60 ± 3	(1.5 ± 0.2) x10 ⁻³	0.977	71 ± 4	(2.4 ± 0.5) x10 ⁻⁵	0.983
PAR	PSA-PA	34 ± 3	(1.1 ± 0.3) x10 ⁻³	0.928	43 ± 7	(2 ± 1) x10 ⁻⁵	0.913
	GACN	23 ± 3	(4 ± 1) x10 ⁻³	0.847	26 ± 5	(2 ± 1) x10 ⁻⁴	0.790
<i>wastewater</i>							
CBZ	PSA-PA	14 ± 1	(2.0 ± 0.6) x10 ⁻³	0.863	15 ± 1	(2.1 ± 0.9) x10 ⁻⁴	0.916
	GACN	22 ± 2	(1.1 ± 0.3) x10 ⁻³	0.932	26 ± 3	(5 ± 2) x10 ⁻⁵	0.950
SMX	PSA-PA	4.3 ± 0.3	(3.8 ± 0.8) x10 ⁻³	0.944	4.8 ± 0.3	(1.1 ± 0.3) x10 ⁻³	0.952
	GACN	20 ± 1	(1.1 ± 0.2) x10 ⁻³	0.971	24 ± 1	(5 ± 1) x10 ⁻⁵	0.986
PAR	PSA-PA	20 ± 5	(4 ± 2) x10 ⁻⁴	0.923	31 ± 12	(9 ± 10) x10 ⁻⁶	0.918
	GACN	21.0 ± 0.8	(1.3 ± 0.1) x10 ⁻³	0.986	26 ± 2	(5 ± 2) x10 ⁻⁵	0.972

q_e – amount adsorbed at equilibrium (mg g⁻¹); k_1 – rate constant of pseudo-first order (min⁻¹); k_2 – rate constant of pseudo-second order (g mg⁻¹ min⁻¹); R^2 – coefficient of correlation

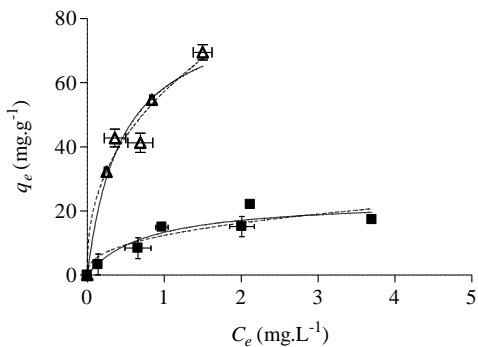
6.3.2.3. Equilibrium studies

Experimental equilibrium and model results, and the corresponding parameters of the non-linear fittings, for the adsorption of CBZ, SMX, and PAR onto PSA-PA and GACN in ultrapure water and in wastewater are presented in Figure 6.6 and Table 6.8, respectively. The isotherm models used to describe the equilibrium experimental results were Langmuir and Freundlich models (chapter 5, Table 5.2), and Sips model (equation 6.1, section 6.2.5).

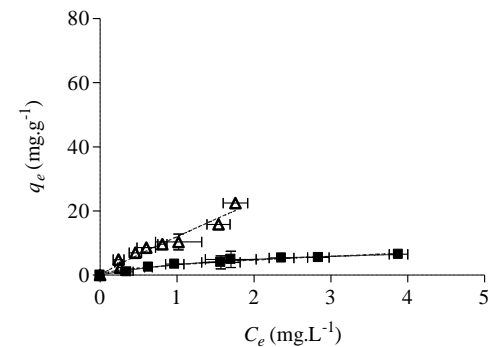
Equilibrium results of the three pharmaceuticals onto PSA-PA, either in ultrapure or wastewater, were better described by the Langmuir and the Sips models than by the Freundlich model. In the case of GACN, the Sips model revealed to be not suitable to model the experimental data, with most of the fittings being ambiguous. Considering the other tested models, even though the Freundlich equation has presented fittings with R^2 values slightly higher in some cases, it can be said that the equilibrium results were mostly best fitted by the Langmuir isotherm. Thus, to allow the comparison of the results of all the studied systems, the Langmuir model was selected.

a) Ultrapure water

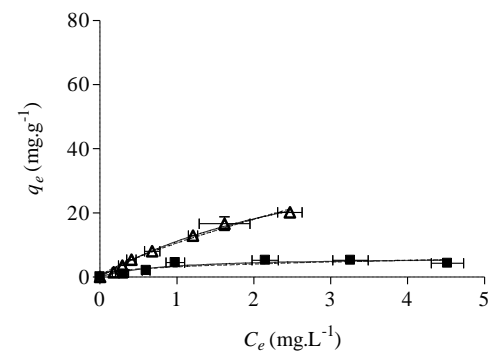
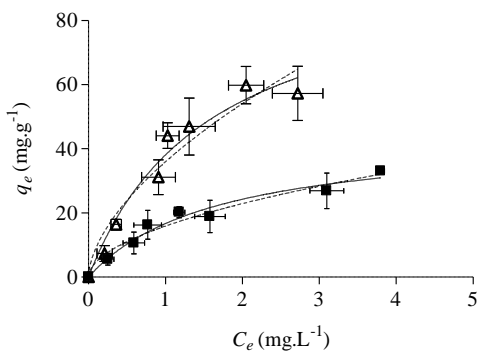
Carbamazepine



b) Wastewater



Sulfamethoxazole



Paroxetine

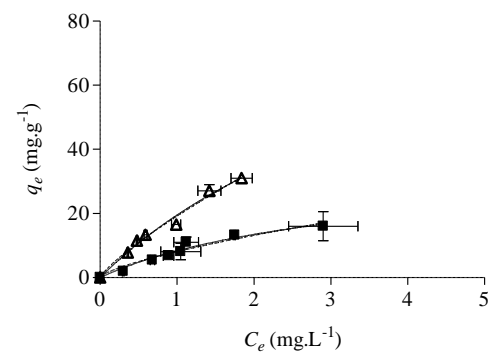
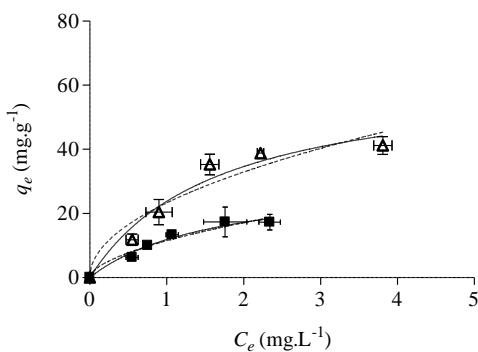


Figure 6.6. Equilibrium study of the adsorption of CBZ, SMX and PAR onto PSA-PA (■) and GACN (Δ) in a) ultrapure water and in b) wastewater. Results considering the fitting to Langmuir (full line) and Freundlich (dash line) models are presented.

The Langmuir maximum adsorption capacity (q_m) of GACN is higher than that of PSA-PA. For the latter, q_m values range from $(24 \pm 5) \text{ mg g}^{-1}$ to $(44 \pm 5) \text{ mg g}^{-1}$ and from $(6 \pm 1) \text{ mg g}^{-1}$ to $(34 \pm 9) \text{ mg g}^{-1}$, in ultrapure water and wastewater, respectively. Meanwhile, for GACN, the q_m range from $(64 \pm 12) \text{ mg g}^{-1}$ to $(98 \pm 17) \text{ mg g}^{-1}$ and from $(49 \pm 6) \text{ mg g}^{-1}$ to $(106 \pm 40) \text{ mg g}^{-1}$, in ultrapure water and wastewater, respectively. Both GAC present better performance for CBZ and SMX in ultrapure water than in wastewater. However, the effect of the aqueous matrix in q_m was not remarkable for the adsorption of PAR, particularly in the case of PSA-PA.

Table 6.8. Fitting parameters of Langmuir, Freundlich, and Sips isotherm models to the experimental data for both carbons (PSA-PA and GACN) and the three pharmaceuticals (CBZ, SMX, and PAR) in ultrapure water and wastewater.

		<i>Langmuir</i>			<i>Freundlich</i>			<i>Sips</i>			
		q_m	K_L	R^2	K_F	n	R^2	q_m	K_S	N	R^2
<i>Ultrapure water</i>											
CBZ	PSA-PA	24 ± 5	1.3 ± 0.8	0.895	12 ± 2	3 ± 1	0.845	20 ± 4	2 ± 2	0.6 ± 0.4	0.905
	GACN	85 ± 14	2.2 ± 0.9	0.946	57 ± 3	2.4 ± 0.4	0.966	Ambiguous fitting			
SMX	PSA-PA	44 ± 5	0.6 ± 0.2	0.970	16 ± 1	1.9 ± 0.2	0.968	58 ± 45	0.4 ± 0.4	1.2 ± 0.6	0.971
	GACN	98 ± 17	0.6 ± 0.2	0.967	36 ± 3	1.6 ± 0.3	0.937	70 ± 10	1.3 ± 0.5	0.6 ± 0.1	0.979
PAR	PSA-PA	31 ± 6	0.6 ± 0.2	0.973	12 ± 1	1.7 ± 0.3	0.958	18.5 ± 0.6	2.4 ± 0.4	0.39 ± 0.04	0.998
	GACN	64 ± 12	0.6 ± 0.2	0.960	23 ± 3	2.0 ± 0.5	0.923	43 ± 2	1.3 ± 0.2	0.43 ± 0.06	0.996
<i>Wastewater</i>											
CBZ	PSA-PA	10 ± 1	0.5 ± 0.1	0.984	3.2 ± 0.2	1.8 ± 0.2	0.969	8 ± 1	0.7 ± 0.2	0.8 ± 0.2	0.986
	GACN	Not Converged			12 ± 1	1.1 ± 0.1	0.950	Ambiguous fitting			
SMX	PSA-PA	6 ± 1	1 ± 1	0.866	3.2 ± 0.5	3 ± 1	0.781	5.0 ± 0.3	5 ± 4	0.3 ± 0.1	0.959
	GACN	49 ± 6	0.30 ± 0.06	0.995	10.6 ± 0.4	1.3 ± 0.1	0.986	Ambiguous fitting			
PAR	PSA-PA	34 ± 9	0.3 ± 0.1	0.967	8 ± 1	1.4 ± 0.2	0.947	19 ± 2	0.8 ± 0.2	0.5 ± 0.1	0.982
	GACN	106 ± 40	0.2 ± 0.1	0.982	19 ± 1	1.2 ± 0.1	0.984	Ambiguous fitting			

q_m – maximum adsorption capacity (mg g^{-1}); K_L – Langmuir equilibrium constant related to the rate of adsorption (L mg^{-1}); K_F – Freundlich adsorption constant ($\text{mg}^{1-1/n} \text{L}^{1/n} \text{g}^{-1}$); n – constant related with the degree of non-linearity of the equation; K_S – Sips constant ($\text{L mg}^{-1} \text{N}$); N – Sips parameter associated to the heterogeneity of the surface; R^2 – coefficient of correlation

As it may be seen in Figure 6.6, the adsorption of CBZ onto GACN was much lower in wastewater than in ultrapure water. The decrease was not so evident in the adsorption of CBZ onto PSA-PA, but, still, q_m decreased from $(24 \pm 5) \text{ mg g}^{-1}$ (in ultrapure water) to $(10 \pm 1) \text{ mg g}^{-1}$ (in wastewater).

The q_m determined for the adsorption of SMX onto both carbons in wastewater was lower than in ultrapure water. However, while in the case of GACN the adsorption capacity decreased to a half (from (98 ± 17) mg g⁻¹ to (49 ± 6) mg g⁻¹), the decrease was more accentuated for PSA-PA (from (44 ± 5) mg g⁻¹ to (6 ± 1) mg g⁻¹). Finally, as evidenced in Figure 6.6 and confirmed by the parameters in Table 6.8, the adsorption of PAR onto both carbons remained mostly the same in wastewater and in ultrapure water. This was also verified in the adsorption of PAR onto the PS-based PAC (AC3, in chapter 5), where wastewater matrix did not negatively influenced the adsorption capacity of AC3 for PAR, being even higher in that matrix than in ultrapure water.

Analyzing the textural properties of both carbons (Table 6.5), it is possible to see that S_{BET} and W_0 are very similar, indicating that these parameters are probably not the main factors influencing the differences observed between the GAC with respect to the adsorption of the studied pharmaceuticals. However, V_p and D of GACN are significantly superior to those of PSA-PA. Taking into account the similar value of the W_0 for both GAC, a larger V_p in GACN indicates that this carbon has a higher presence of mesopores in its porous structure. Furthermore, the pore size distribution (Figure 6.3) clearly evidences that GACN has a broader distribution of the pore sizes in the range of mesopores (2-50 nm), while PSA-PA has a higher presence of pores below 5 nm. Therefore, the mesoporous character of the GACN could explain to a certain extent the better results of the adsorption experiments for this adsorbent. This might be due not only to the importance of mesopores as channels that guarantee the accessibility to micropores but also to the molecular sizes of the studied pharmaceuticals, which are very close to the PSA-PA average pore diameter (between 0.653 nm and 1.174 nm for CBZ and between 0.623 nm and 1.362 nm for SMX (Nielsen et al., 2014). The influence of these parameters in the adsorption of pharmaceuticals onto waste-based activated carbons has also been reported by Mestre et al. (2009). On the other hand, for PSA-PA, which possesses a higher amount of functional groups (Table 6.3), surface interactions are more likely to be present.

Considering the adsorption of CBZ, for both GAC and matrices, the compound is mainly in the neutral form (see pK_a values in Table 1.1, chapter 1), which indicates that electrostatic forces might not have a significant role in the adsorption process of this pharmaceutical. Also, CBZ has a low solubility in water at 25 °C and a high log K_{ow} , and therefore, hydrophobic interactions may play an important role mainly in ultrapure water. Considering that the adsorption of CBZ onto GACN is higher than in PSA-PA, GACN might be more hydrophobic than PSA-PA, since it possesses fewer surface functional groups and higher prevalence of graphitic carbon and thus a higher degree of aromaticity (Tables 6.2 and 6.4). In this context, and particularly for GACN, π - π interactions may occur between CBZ benzene rings (that act as a π -electron acceptor due to the amide functionality, which functions as an electron withdrawing

group (Cai and Larese-Casanova, 2014)) and the aromatic benzene rings of the graphitic part of the carbon that can act as π -electron donor groups, forming a π - π electron donor-acceptor complex.

Relative to the adsorption of SMX, and similarly to CBZ, π - π interactions can occur between the π -donor hydroxyl substituent groups of the benzene rings and the π -acceptor of SMX amino group and N-heteroaromatic rings (Zhang et al., 2010). This last interaction may have contributed, to the higher adsorption capacity of SMX onto GACN, since according to the H/C ratio (Table 6.2) and as above referred, this carbon presents a higher degree of aromaticity and, therefore, of graphitic carbon (as confirmed by the XPS results (Table 6.4)). The reduction of the adsorption capacity of the GAC towards SMX from ultrapure water to wastewater can be explained by the pH change. In the case of the wastewater matrix (pH between 7.7 and 8.0), both GAC present a negative net charge (pH_{pzc} between 4 and 5) and SMX species are mostly present in the anionic form (see $\text{p}K_a$ values in Table 1.1, chapter 1), and therefore, electrostatic repulsion is likely to occur. Besides, SMX is the pharmaceutical possessing the lowest $\log K_{ow}$ value, being the less adsorbed pharmaceutical in this condition.

For the adsorption of PAR onto both GAC, no significant differences were verified between adsorption capacities in ultrapure water and wastewater (Figure 6.6 and Table 6.8). In fact, PAR is mostly present in its positive form in both matrices (see $\text{p}K_a$ values in Table 1.1, chapter 1) and thus, in the case of wastewater, electrostatic interactions have certainly an important role in the adsorption process, balancing competitive effects that may affect the carbons' adsorption capacity. Also, PAR possesses a high value of $\log K_{ow}$, which is considered to positively influence the adsorption onto the nonpolar surface of activated carbons (Çeçen and Aktaş, 2011).

All the target pharmaceuticals possess hydrogen-bonding acceptors, namely, three H bond acceptors in CBZ, four in PAR and six in SMX (Table 1.1, chapter 1). Analyzing the q_m values for the three pharmaceuticals in ultrapure water for PSA-PA, it is possible to observe some correlation with the number of hydrogen-bonding acceptors as PSA-PA shows a higher adsorption capacity for SMX (the pharmaceutical with more hydrogen bond acceptors), and a smaller adsorption capacity for CBZ (the one possessing fewer hydrogen bond acceptors). This can point out hydrogen bonding as one of the possible mechanisms occurring in the adsorption of these pharmaceuticals in ultrapure water onto PSA-PA. This tendency, however, is not maintained in the wastewater matrix, where the highest adsorption capacity is obtained for PAR, followed by CBZ, and SMX. Thus, as referred above, pH effects and electrostatic interactions appear to be important factors ruling the adsorption of the studied pharmaceuticals in wastewater.

6.4. Conclusions

In this work, fourteen different procedures were tested to accomplish the challenge of producing a GAC from a cellulosic industrial waste. The production of a GAC was only possible using AL as binder agent and it was successfully achieved by a procedure involving a two-step pyrolysis. Then, the resulting material (PSA-PA) was applied for the adsorptive removal of CBZ, SMX, and PAR from water. It was found that PSA-PA exhibits very similar physicochemical properties to the commercial GAC (GACN) used as reference in what concerns S_{BET} , micropore volumes, predominance of surface phenol and carboxylic groups and acidic pH_{pzc} . However, the total pore volume and an average pore diameter of PSA-PA are approximately half those of GACN, indicating a significantly higher presence of mesopores in GACN, which may be responsible for the lower adsorption capacity of PSA-PA towards the considered pharmaceuticals. On the other hand, the adsorption capacity of PSA-PA and GACN was strongly affected by the matrix, with a significant decrease in the adsorption of CBZ and SMX from wastewater as compared with ultrapure water. However, the same effect was not verified for the adsorption of PAR, which could be explained by pH effects and electrostatic interactions. Overall, this study represents a step forward in the utilization of PS as raw material for GAC production, enabling its application in fixed-bed systems for the adsorption of pharmaceuticals, which will be considered in the next chapter.

6.5. References

- Ahmed, M.J., Dhedan, S.K., 2012. Equilibrium isotherms and kinetics modeling of methylene blue adsorption on agricultural wastes-based activated carbons. *Fluid Phase Equilib.* 317, 9-14.
- Aygün, A., Yeniso-y-Karakas, S., Duman, I., 2003. Production of granular activated carbon from fruit stones and nutshells and evaluation of their physical, chemical and adsorption properties. *Micropor. Mesopor. Mat.* 66, 189-195.
- Bae, W., Kim, J., Chung, J., 2014. Production of granular activated carbon from food processing wastes (walnut shells and jujube seeds) and its adsorptive properties. *J. Air Waste Manage.* 64, 879-886.
- Blackmore, K.A.E., 1988. Lignosulfonate/urea binder for particulate composites. US Patent 4,786,438, filed August 10, 1987 and issued November 22, 1988.
- Cai, N., Larese-Casanova, P., 2014. Sorption of carbamazepine by commercial graphene oxides: a comparative study with granular activated carbon and multiwalled carbon nanotubes. *J. Colloid. Interf. Sci.* 426, 152-161.
- Calisto, V., Ferreira, C.I., Santos, S.M., Gil, M.V., Otero, M., Esteves, V.I., 2014. Production of adsorbents by pyrolysis of paper mill sludge and application on the removal of citalopram from water. *Bioresource Technol.* 166, 335-344.
- Carvalho, A.P., Mestre, A.S., Pires, J., Pinto, M.L., Rosa, M.E., 2006. Granular activated carbons from powdered samples using clays as binders for the adsorption of organic vapours. *Micropor. Mesopor. Mat.* 93, 226-231.
- Çeçen, F., Aktaş, Ö., 2011. Integration of Activated Carbon Adsorption and Biological Processes in Wastewater Treatment, in *Activated Carbon for Water and Wastewater Treatment: Integration of Adsorption and Biological Treatment*. Wiley-VCH Verlag GmbH & Co. KGaA, Weinheim, Germany.
- Coates, J., 2000. *Interpretation of Infrared Spectra, A Practical Approach*. John Wiley & Sons Ltd, Chichester.
- Ferreira, C.I.A., Calisto, V., Otero, M., Nadais, H., Esteves, V.I., 2017. Fixed-bed adsorption of Tricaine Methanesulfonate onto pyrolysed paper mill sludge. *Aquacult. Eng.* 77, 53-60.
- Franco, M.A.E.d., Carvalho, C.B., Bonetto, M.M., Soares, R.d.P., Féris, L.A., 2017. Removal of amoxicillin from water by adsorption onto activated carbon in batch process and fixed bed column: Kinetics, isotherms, experimental design and breakthrough curves modelling. *J. Clean. Prod.* 161, 947-956.
- Heschel, W., Klose, E., 1995. On the suitability of agricultural by-products for the manufacture of granular activated carbon. *Fuel* 74, 1786-1791.
- Kårelid, V., Larsson, G., Björleinius, B., 2017. Pilot-scale removal of pharmaceuticals in municipal wastewater: Comparison of granular and powdered activated carbon treatment at three wastewater treatment plants. *J. Environ. Manage.* 193, 491-502.

- Kim, J.-W., Sohn, M.-H., Kim, D.-S., Sohn, S.-M., Kwon, Y.-S., 2001. Production of granular activated carbon from waste walnut shell and its adsorption characteristics for Cu²⁺ ion. *J. Hazard. Mater. B* 85, 301-315.
- Kovach, Julius Louis. 1975. Hard Granular Activated Carbon and Preparation from a Carbonaceous Material a Binder and a Inorganic Activating Agent. US Patent 3,864, 277, filed August 14, 1972, and issued at February 4 1975.
- Krahnstöver, T., Wintgens, T., 2018. Separating powdered activated carbon (PAC) from wastewater – Technical process options and assessment of removal efficien. *J. Environ. Chem. Eng.* 6, 5744-5762.
- Li, Z., Xu, Z., Wang, H., Ding, J., Zahiri, B., Holt, C.M.B., Tan, X., Mitlin, D., 2014. Colossal pseudocapacitance in a high functionality–high surface area carbon anode doubles the energy of an asymmetric supercapacitor. *Energ. Environ. Sci.* 7, 1708.
- Lozano-Castelló, D., Cazorla-Amorós, D., Linares-Solano, A., Quinn, D.F., 2002. Activated carbon monoliths for methane storage: influence of binder. *Carbon* 40, 2817-2825.
- Marsh, H., Rodríguez-Reinoso, F., 2006. Activated Carbon, First ed. Elsevier, England.
- Mestre, A.S., Pires, J., Nogueira, J.M., Parra, J.B., Carvalho, A.P., Ania, C.O., 2009. Waste-derived activated carbons for removal of ibuprofen from solution: role of surface chemistry and pore structure. *Bioresource Technol.* 100, 1720-1726.
- Nielsen, L., Biggs, M.J., Skinner, W., Bandosz, T.J., 2014. The effects of activated carbon surface features on the reactive adsorption of carbamazepine and sulfamethoxazole. *Carbon* 80, 419-432.
- Sips, R., 1948. On the structure of a catalyst surface. *J. Chem. Phys.* 16, 490.
- Smith, K.M., Fowler, G.D., Pullket, S., Graham, N.J.D., 2012. The production of attrition resistant, sewage–sludge derived, granular activated carbon. *Sep. Purif. Technol.* 98, 240-248.
- Stuart, B., 2004. Infrared Spectroscopy: Fundamentals and Applications. John Wiley & Sons.
- Velo-Gala, I., López-Peñalver, J.J., Sánchez-Polo, M., Rivera-Utrilla, J., 2014. Surface modifications of activated carbon by gamma irradiation. *Carbon* 67, 236-249.
- Wei, T., Zhang, Q., Wei, X., Gao, Y., Li, H., 2016. A Facile and Low-Cost Route to Heteroatom Doped Porous Carbon Derived from Broussonetia Papyrifera Bark with Excellent Supercapacitance and CO₂ Capture Performance. *Sci. Rep.* 6, 2-10.
- Zhang, D., Pan, B., Zhang, H., Ning, P., Xing, B., 2010. Contribution of Different Sulfamethoxazole Species to Their Overall Adsorption on Functionalized Carbon Nanotubes. *Environ. Sci. Technol.* 44, 3806-3811.

7

FIXED-BED PERFORMANCE OF PRIMARY PAPER MILL SLUDGE-BASED GRANULAR ACTIVATED CARBON FOR REMOVAL OF PHARMACEUTICALS FROM WATER

Abstract

This work aimed to assess the fixed-bed adsorptive performance of a primary paper mill sludge-based granular activated carbon (PSA-PA) for the removal of pharmaceuticals, namely carbamazepine (CBZ), sulfamethoxazole (SMX), and paroxetine (PAR), from water. The breakthrough curves corresponding to the adsorption of CBZ at different flow rates and in two different matrices (distilled water and municipal wastewater) were firstly determined, which allowed to select the most favorable flow rate for the subsequent experiments. Subsequently, the fixed-bed adsorption of CBZ, SMX, and PAR from single and ternary solutions in wastewater were evaluated and the results showed that the performance of PSA-PA was different for each pharmaceutical. According to the obtained breakthrough curves, the poorest bed adsorption capacity, either from single or ternary solution, was observed for SMX, which may be related with electrostatic repulsion at the pH of the wastewater used (pH ~ 7.3-7.7). Also, the bed adsorption capacity of PSA-PA for SMX, in the ternary solution, was notoriously lower compared to the single solution, while it slightly decreased for CBZ and even increased for PAR. The regeneration studies showed that the CBZ adsorption capacity of the PSA-PA bed decreased about 38 % and 71 % after the first and the second thermal regeneration stages, respectively. This decline was comparatively larger than the corresponding reduction of the PSA-PA specific surface area (S_{BET}), which decreased only 5 % and 25 % for the first and second regeneration stages, respectively, and pointed to the lack of viability of more than one regeneration stage.

This chapter was based on the published article:

Jaria, G., Calisto, V., Silva, C.P., Gil, M.V., Otero, M., Esteves, V.I., 2019. Fixed-bed performance of a waste-derived granular activated carbon for the removal of micropollutants from municipal wastewater. *Sci. Total Environ.* 683, 699-708.

7.1. Contextualization

As previously mentioned, one of the main sources of pharmaceuticals in water systems is the discharge of wastewater treatment plants' (WWTP) effluents into the environment (Yang et al., 2017) due to their inefficiency in the removal of these compounds, since they were not originally designed for that purpose (Patel et al., 2019). Also, as referred in the previous chapter (chapter 6), granular forms of activated carbon (GAC) are frequently applied in the removal of organic compounds from water and wastewater (Franco et al., 2017) and they can be used both in stirred-tank and column (fixed-bed) reactors, with fixed-bed columns being the most commonly applied in this context (Metcalf and Eddy, 2003). This type of reactor presents several advantages, namely, simple operation mode, effectiveness, capacity of adsorbent regeneration, and easiness of scaling-up for industrial applications (Franco et al., 2017; Ahmed and Hameed, 2018). Therefore, fixed-bed studies are very important before planning the application of GAC in a treatment facility, allowing to determine the breakthrough curves and to obtain information for the design of the system, so to define a rational scale for practical operation (Petech et al., 2006; Xu et al., 2013). After fixed-bed saturation, GAC can be subjected to regeneration (so minimizing the demand of virgin adsorbents), which may be advantageous in terms of economic viability, environmental and energetic sustainability (Radhika et al., 2018).

In the literature there are many studies on the adsorption of pharmaceuticals under batch operation in stirred reactors, using different adsorbents, which are mainly powdered materials. However, a smaller number of works have been published on the application of continuous fixed-bed adsorption in the removal of pharmaceuticals from water (Ahmed and Hameed, 2018). On the other hand, although some adsorbents from agriculture wastes (such as raspberry, olive stones, walnut shell, coffee residue or peach stones) have been used in fixed-bed adsorption of pharmaceuticals (Ahmed and Hameed, 2018), the utilization of industrial waste-based materials is very scarce.

The production of a waste-derived GAC (named as PSA-PA) using two industrial residues, namely primary paper mill sludge (as raw material) and ammonium lignosulfonate (as binder agent), and its application for the removal of carbamazepine (CBZ), sulfamethoxazole (SMX), and paroxetine (PAR) in batch system was described in the previous chapter (chapter 6). In this chapter, the performance of PSA-PA in column reactors is analyzed in order to assess the fixed-bed continuous adsorption of the three referred pharmaceuticals from single and ternary solutions. Firstly, different flow rates were tested for single component systems, for the adsorption of CBZ in distilled and wastewater matrices. Then, the

adsorption of the three pharmaceuticals onto PSA-PA in the fixed-bed system at constant flow rate was studied in single and ternary solutions using a wastewater matrix, and the thermal regeneration of PSA-PA was also fulfilled to evaluate its life cycle.

7.2. *Materials and Methods*

7.2.1. *Chemicals and reagents*

The pharmaceuticals used for the adsorption experiments were CBZ (Sigma-Aldrich, 99 %), SMX (TCI, > 98 %), and PAR (paroxetine-hydrochloride, TCI, > 98 %), which were prepared in distilled water or in wastewater (details on wastewater collection and characterization are presented in section 8.2.2). The analytical quantification of the pharmaceuticals was performed by Micellar Electrokinetic Chromatography (MEKC) as described in Appendix B (section B2.). Solutions were all prepared using ultrapure water, obtained from a Milli-Q Millipore system (Milli-Q plus 185).

7.2.2. *Wastewater sampling*

Wastewater was collected from the outlet of the local WWTP described in chapter 5 (section 5.2.4). After collection, the wastewater was filtered and characterized as described in chapter 5 (section 5.2.4). Five collection campaigns were carried out between Mars and June 2018. Characterization results are presented in Table 7.2 (section 7.3.1), where it may be seen that the properties of the collected wastewater remained quite stable between campaigns.

7.2.3. *Adsorption studies in fixed-bed systems using the granular activated carbon PSA-PA as adsorbent*

The adsorbent used in this work was a GAC (PSA-PA) produced from primary paper mill sludge (PS) and ammonium lignosulfonate (AL), which production and characterization were described in the previous chapter (chapter 6). The fixed-bed performance of PSA-PA in the removal of pharmaceuticals under continuous operation mode was evaluated using column reactors, as described in the following sub-sections. All the fixed-bed experiments were performed in a CHROMAFLEX® glass column (13 cm total height, 2.5 cm internal diameter), with an acrylic jacket, at a constant temperature of (25 ± 1) °C using a thermostatic recirculating bath (HAAKE A10, Thermo Scientific). The column was packed with PSA-PA with a constant bed depth (Z) of 2.6 cm, corresponding to 3.6 g of PSA-PA, using a flow adapter, with a 20 μm porosity HDPE bed support on the top of the column.

Before each experiment, the system was equilibrated for about 24 h with a continuous flow of distilled water. This time of equilibration was chosen according to the results obtained from an experiment where PSA-PA fixed-bed column was fed with distilled water, at a flow rate of 4.3 L d^{-1} , and samples were collected from the outlet. The samples were analyzed in terms of conductivity (WTW meter) and TOC (Shimadzu, model TOC-V_{CPH}, SSM-5000A). After 24 h of equilibration the conductivity and TOC values indicated the stability of the effluent with negligible variations.

After equilibrating the system, the corresponding pharmaceutical(s) solution was up-flow pumped into the column with a peristaltic pump (BT100-2J/DG15-28, 2 channels, Longer Pump). Wastewater samples were collected at set time intervals until the concentration of pharmaceutical remained constant by using a programmable fraction collector (IS-95 Interval Sampler, Spectra/Chrom®). The concentration of the pharmaceuticals after filtration in the column effluent was determined by capillary electrophoresis using a micellar electrokinetic chromatography (MEKC) method, described in Appendix B, Section B2.

7.2.3.1. Fixed-bed adsorption of pharmaceuticals

Fixed-bed studies on the adsorptive removal of pharmaceuticals by PSA-PA under continuous operation mode were carried out in two subsequent stages:

- i) Study of the effect of flow rate on the adsorption of CBZ using distilled water and wastewater as matrices. For this purpose, the fixed-bed column was fed with a single solution of CBZ (5 mg L^{-1}) at flow rates of 4.3, 8.4, and 13.0 L d^{-1} . CBZ solution was prepared either in distilled water or in wastewater and fed at the three different flow rates mentioned above.
- ii) Study of the adsorption of CBZ, SMX, and PAR from single (5 mg L^{-1}) and ternary (5 mg L^{-1} of each pharmaceutical) solutions in wastewater. These experiments were carried out at the most favorable flow rate (4.3 L d^{-1}), as selected from results obtained for CBZ in *i*).

7.2.3.2. Regeneration of exhausted granular activated carbon PSA-PA

Thermal regeneration of PSA-PA saturated with CBZ (after adsorption from distilled water) was performed at $500 \text{ }^\circ\text{C}$ under nitrogen atmosphere for 90 min. The chosen temperature was based on the results from obtained by Ullah et al. (2015) on the thermogravimetric analysis of CBZ, which showed that this pharmaceutical is completely degraded at around $300 \text{ }^\circ\text{C}$. After regeneration, PSA-PA was re-

packed into the column and the fixed-bed adsorption of CBZ, dissolved in distilled water, under a flow rate of 4.3 L d⁻¹, was determined (cycle 1). Subsequently, the exhausted regenerated PSA-PA was subjected to a second thermal regeneration and the fixed-bed adsorption was repeated using the same conditions (cycle 2). The specific surface area (S_{BET}) of the PSA-PA used in each fixed-bed adsorption cycle and of PSA-PA after the cycle 2 was determined by nitrogen adsorption isotherms, as described in Appendix A (section A1).

7.2.3.3. Fixed-bed column data analysis and mathematical breakthrough fitting models

To evaluate the adsorption of the pharmaceuticals onto PSA-PA in a fixed-bed system, breakthrough curves were obtained by plotting C/C_0 (where C is the pharmaceutical concentration at the outlet of the column at time t and C_0 is the initial concentration of the pharmaceutical) as a function of operating time (t , min). Breakthrough curves allow to determine the breakthrough point, which is the time when the effluent concentration reaches a determined percentage relatively to the influent concentration. This percentage can be defined according to legislated thresholds (when existent) or an operator defined value, frequently between 5 % and 10% (Metcalf and Eddy, 2003). The breakthrough point is an important parameter as it allows to determine the volume of treated effluent by the system (Ferreira et al., 2017). In the case of the studied pharmaceuticals, no maximum limit is established yet for the discharge of these compounds into the environment; therefore, a 10% ($C/C_0 \approx 0.1$) was considered to define the breakthrough point ($t_{10\%}$).

The area above the breakthrough curve allows to determine the bed adsorption capacity, q_{total} (mg g⁻¹) for a determined feed concentration (C_0 , mg L⁻¹), and was calculated according to equation (7.1):

$$q_{total} = \frac{Q}{1000} \frac{C_0 A}{m} = \frac{Q}{1000} \frac{C_0}{m} \int_0^t \left(1 - \frac{C}{C_0}\right) dt \quad (\text{equation 7.1})$$

where Q the flow rate (L d⁻¹); A is the area above the breakthrough curve; m is the dry weight of adsorbent in the column (g); C is the concentration of pharmaceutical at the outlet of the column at a time t (mg L⁻¹) and t_{total} is the total flow time (d) (Ferreira et al., 2017).

The height of the mass transfer zone (h_{MTZ}) is used as a parameter to select the best operating flow rate since the lowest h_{MTZ} , the closer is the system to ideality (Lima et al., 2017). The calculation of h_{MTZ} is done by the following expression:

$$h_{MTZ} = \left(1 - \frac{q_t}{q_{total}}\right) h \quad (\text{equation 7.2})$$

where q_t is the mass of adsorbate adsorbed at time t per gram of adsorbent (mg g^{-1}), q_{total} is the maximum mass of adsorbate adsorbed at saturation time per gram of adsorbent (mg g^{-1}) and h is the bed height (cm).

Also, the empty bed contact time (EBCT), the adsorbent usage rate (U_r), and the fraction of bed utilization (FBU) are useful parameters for the analysis of breakthrough curves. FBU is related to h_{MTZ} , and EBCT or residence time influences the volume of influent treated and the nature of the breakthrough curve (Deokar and Mandavgane, 2015). The expression used for the calculation of the referred parameters are as follows:

$$EBCT = \frac{V_c}{Q} \quad (\text{equation 7.3})$$

$$U_r = \frac{m}{V_b} \quad (\text{equation 7.4})$$

$$FBU = \frac{q_b}{q_{\text{total}}} \quad (\text{equation 7.5})$$

where V_c is the fixed-bed volume (L); Q is the flow rate (L d^{-1}); V_b is the volume treated at breakthrough (L); m is the mass of adsorbent (g); and q_b is the mass of adsorbate adsorbed per gram of adsorbent at breakthrough time ($t_{10\%}$), equivalent to $q_{10\%}$ (mg g^{-1}) (Deokar and Mandavgane, 2015).

For the modelling of the experimental breakthrough curves, three models were used, namely, the Thomas model, the Yoon-Nelson and the Yan model (Table 7.1).

Table 7.1. Breakthrough models considered for the description of fixed-bed column studies.

Model	Equation	Assumptions	References
Yan	$\frac{C_t}{C_0} = 1 - \frac{1}{1 + \left(\frac{C_0 Q t}{q_Y m}\right)^{\alpha^Y}}$	Also known as Modified Dose Response (MDR); minimize the deviation between experimental data and the predicted breakthrough curve from Thomas model (especially at very small or very large operation times).	Yan et al. (2001); Franco et al. (2017)
Thomas	$\frac{C_t}{C_0} = \frac{1}{1 + \exp\left(\frac{k_T q_0 m}{Q} - k_T C_0 t\right)}$	Assumes second-order “reversible reaction kinetics, Langmuir isotherm and no axial dispersion”.	Thomas (1944); Saadi et al. (2013); Xu et al. (2013)
Yoon-Nelson	$\frac{C_t}{C_0} = \frac{\exp(k_{YN} t - t_{50\%} k_{YN})}{1 + \exp(k_{YN} t - t_{50\%} k_{YN})}$	The decrease in the probability of each adsorbate to be adsorbed is proportional to the probability of its adsorption and breakthrough on the adsorbent.	Yoon and James, (1984); Xu et al. (2013); Deokar and Mandavgane (2015); Singh and Thakur, (2016)

C_0 – influent compound concentration (mg L^{-1}); C_t – effluent concentration at time t (mg L^{-1}); q_Y – the amount of solute adsorbed (mg g^{-1}); α^Y – is a model parameter; k_T - Thomas constant rate ($\text{mL min}^{-1} \text{mg}^{-1}$); q_0 – sorption capacity of the adsorbent per unit mass of the adsorbent (mg g^{-1}); m – amount of adsorbent in the column (g); k_{YN} – rate constant (h^{-1}); $t_{50\%}$ – time required for 50% adsorbate breakthrough (h).

7.3. Results and Discussion

7.3.1. Wastewater sample's characterization

The characterization results, namely, pH, conductivity, and TOC, of wastewater from the six collection campaigns are depicted in Table 7.2. According to the results obtained for the analyzed parameters, it is possible to assume the consistency of the properties of the wastewater matrix for the adsorption experiments.

Table 7.2. Properties of the wastewater samples.

	Sample 1	Sample 2	Sample 3	Sample 4	Sample 5	Sample 6
pH	7.4	7.7	7.4	7.4	7.6	7.3
Conductivity (mS cm⁻¹)	1.4	1.0	3.0	3.9	4.6	2.9
TOC (%)	7.5	6.5	9.95	10.3	12.1	10.4
Collected volume (L)	100	60	100	100	80	50

7.3.2. Fixed-bed adsorption experiments with the granular activated carbon PSA-PA

7.3.2.1. Adsorption of carbamazepine from distilled water and wastewater at different flow rates

The experimental breakthrough curves of the fixed-bed adsorption of CBZ onto PSA-PA from distilled water and wastewater are presented in Figure 7.1. The breakthrough curves represent the ratio of concentration at a time t and the initial concentration (C/C_0) versus time (in days).

The results displayed in Figure 7.1 show that fixed-bed adsorption of CBZ onto PSA-PA was affected by the flow rate and the aqueous matrix. As it may be seen, in both matrices, the largest the flow rate, the steeper the breakthrough curve, possibly because an increase in the flow rate implies a decrease of the contact time between the adsorbent (PSA-PA) and the adsorbate (CBZ), which leads to a reduction in the bed adsorption capacity and service time. With respect to the matrix, steeper curves were determined in wastewater than in distilled water, which must be associated with competition effects in wastewater. On the other hand, as it may be seen in Figure 7.1, asymmetric breakthrough curves were obtained under the experimental conditions used. The breakthrough curves are skewed and steeper at the initial part of the experiment, which may be associated, at least partially, to heterogeneity within the bed. Even small differences in the particle size of the granular PSA-PA may result in some heterogeneity in packing densities within the bed. Furthermore, the shape of the breakthrough curves is highly influenced

by the adsorption rate or mass transfer from the aqueous phase to the adsorption sites inside the PSA-PA particles. Curves in Figure 7.1 show that, especially at the highest flow rate, breakthrough occurs very quickly, and it is almost spontaneous, which indicates that the CBZ molecules move through the packed bed and reach the outlet before they can enter the pores of the PSA-PA particles. Then, the exhaustion of the bed ($C/C_0 = 1$) is not attained within the duration of the experiments. This behavior has already been observed by other authors in fixed-bed studies involving the adsorption of pharmaceuticals (Nazari et al., 2016; Darweesh and Ahmed, 2017). In this specific study, such a pattern must be related to the slow adsorption kinetics of CBZ onto PSA-PA, which possesses very narrow pores (chapter 6, section 6.3.1.2).

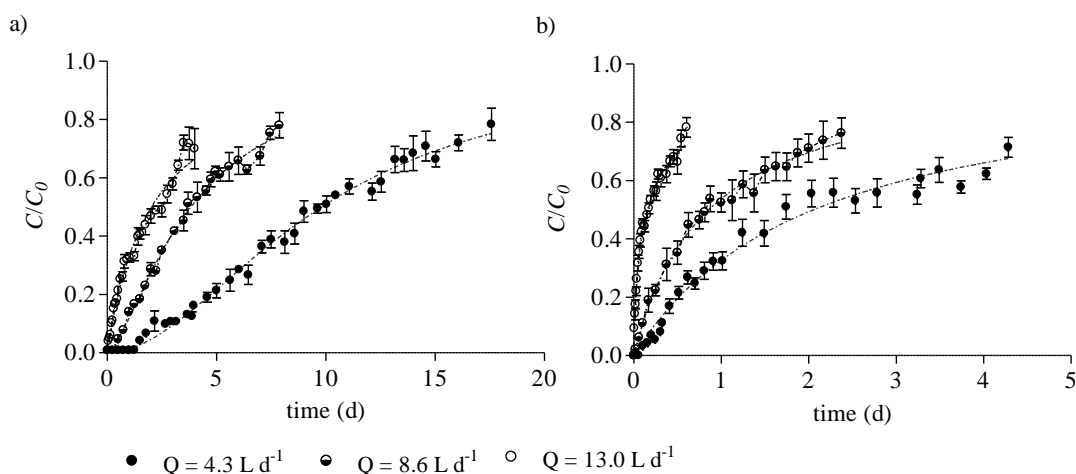


Figure 7.1. Breakthrough curves and fittings of the experimental data to the Yan model for the adsorption of CBZ onto PSA-PA at flow rates of 4.3 L d^{-1} , 8.6 L d^{-1} , and 13 L d^{-1} , in a) distilled water and b) wastewater.

Efficiency and mass transfer parameters derived from experimental breakthrough curves on the fixed-bed adsorption of CBZ from distilled and wastewater are presented in Table 7.3. These parameters evidence that, for both aqueous matrices, the lowest flow rate (4.3 L d^{-1}) is the one presenting a longer operation time (breakthrough time), defined as the time for which 10 % of saturation ($t_{10\%}$) of the adsorbent is attained, and a larger treated volume. Also, at this flow rate (4.3 L d^{-1}), FBU, which express the relation between the amount of CBZ adsorbed at breakthrough point and at saturation, is higher. By increasing the flow rate, a decrease in $t_{10\%}$ and in the total mass of CBZ adsorbed onto PSA-PA (q_{total}) is obtained. In fact, the correlations between the flow rates and these two parameters are quite linear, except for q_{total} in wastewater, which is quite similar at the flow rates of 4.3 L d^{-1} and 8.6 L d^{-1} , but notoriously

decreases at 13.0 L d^{-1} . The decrease in the q_{total} and $t_{10\%}$ with the increase in the flow rate can be attributed to the insufficient contact time between the CBZ and PSA-PA, which has already been observed in other systems (Deokar and Mandavgane, 2015; Tor et al., 2009). The h_{MTZ} value is equal to the fixed-bed height under the three different flow rates and in the two aqueous matrices, which further confirms that CBZ molecules move quickly towards the outlet of the column. Concerning U_r , its value increases with the increase in the flow rate: in wastewater, this increase is very accentuated, being 10 times higher when changing from a flow rate of 8.6 L d^{-1} to 13.0 L d^{-1} . According to Sánchez-Machado et al. (2016), high flow rates reduce the thickness of liquid film around adsorbent particles leading to low mass transfer resistance and high rate of mass transfer, explaining the increase in U_r with the increase in the flow rate.

Table 7.4 depicts the parameters from the fittings of breakthrough experimental curves in Figure 7.1 to the considered models. As evidenced by the R^2 , the Yan model is the one that best fits the fixed-bed adsorption of CBZ onto PSA-PA at the three flow rates and both in distilled and wastewater matrices. Fittings to the Yan model are shown together with experimental results in Figure 7.1, while, for comparison purposes, fittings to the three models here considered are represented in Figures C7.1 and C7.2 in Appendix C7 (please, note that the fittings to the Thomas and Yoon-Nelson are superimposed in Figures C7.1 and C7.2). Regarding parameters in Table 7.4, the predicted values for the maximum adsorption capacity determined by the Thomas and the Yan models (q_{Th} and q_Y , respectively) are, except for $Q = 13.0 \text{ L d}^{-1}$ in wastewater, quite higher than the experimentally calculated one (q_{total} in Table 7.3). In any case, q_Y is, as expected due to the best fitting, closer to the experimentally calculated values than q_{Th} , especially in distilled water. Comparing the values of the batch studies (chapter 6) with these results, it may be seen that for CBZ in distilled water, the maximum adsorption capacity at saturation in batch system ($q_m = (24 \pm 5) \text{ mg g}^{-1}$) is less than half of that estimated by the Yan model for the continuous system at $Q = 4.3 \text{ L d}^{-1}$ ($q_Y = (59.6 \pm 0.6) \text{ mg g}^{-1}$). In wastewater matrix, the difference is not so accentuated, with $q_m = (10 \pm 1) \text{ mg g}^{-1}$ for batch system (chapter 6) and $q_Y = (12.5 \pm 0.4) \text{ mg g}^{-1}$ for the fixed-bed column. The same tendency is verified for $Q = 8.6 \text{ L d}^{-1}$. According to Tor et al. (2009), differences on maximum adsorption capacities between batch and continuous modes, for the same initial concentration of adsorbate, have been observed in other studies and they may be due to the textural properties of the adsorbent, namely the characteristics of the porous structure. In this case, the microporous structure of PSA-PA may lead to difficulties in the retention of CBZ molecules under the fixed-bed experimental conditions used.

Table 7.3. Efficiency and mass transfer parameters determined from the breakthrough curves corresponding to the fixed-bed adsorption of pharmaceuticals onto PSA-PA in distilled water and wastewater.

	Q (L d ⁻¹)	Mass of adsorbent (g)	$t_{10\%}$ (d)	V_b (L)	$q_{10\%}$ (mg g ⁻¹)	t_{total} (d)	q_{total} (mg g ⁻¹)	h_{MTZ} (cm)	EBC _T (d)	U_r (g L ⁻¹)	FBU
<i>Distilled water (single solution)</i>											
CBZ	4.3	3.55	2.92	12.61	1.01	17.58	39.91	2.49	0.0029	0.28	0.0252
	8.6	3.61	0.83	7.17	0.79	8.72	31.66	2.49	0.0014	0.50	0.0251
	13.0	3.56	0.21	2.72	0.20	4.00	19.95	2.53	0.0010	1.31	0.0099
<i>Wastewater (single solution)</i>											
CBZ	4.3	3.56	0.33	1.41	0.14	4.28	6.65	2.50	0.0029	2.52	0.0206
	8.6		0.10	0.90	0.07	2.38	7.00	2.52	0.0014	3.96	0.0104
	13		0.01	0.09	0.01	0.60	2.34	2.54	0.0010	39.18	0.0028
SMX	4.3	3.56	0.10	0.45	0.03	1.46	2.23	2.52	0.0029	7.91	0.0136
PAR	4.3	3.56	0.01	0.04	0.00	4.00	4.46	2.55	0.0029	82.29	0.0000
<i>Wastewater (ternary solution)</i>											
CBZ	4.3	3.56	0.03	0.14	0.01	3.17	5.58	2.55	0.0029	26.34	0.0014
SMX			0.06	0.24	0.02	1.88	0.67	2.46	0.0029	14.80	0.0337
PAR			0.00	0.00	0.00	4.21	8.57	2.55	0.0029	-	-
<i>Distilled water after regeneration</i>											
CBZ	-	4.3	3.56	1.54	0.62	10.38	24.95	2.49	0.0029	0.53	0.0249
cycle 1											
CBZ	-	4.3	3.56	0.29	0.14	6.88	11.49	2.52	0.0029	2.82	0.0124
cycle 2											

Q – flow rate; $t_{10\%}$ – breakthrough time; V_b – volume treated at breakthrough; $q_{10\%}$ – mass of adsorbate adsorbed at breakthrough per gram of adsorbent; q_{total} – total flow time; q_{total} – maximum mass of adsorbate adsorbed at saturation per gram of adsorbent; h_{MTZ} – height of the mass transfer zone; EBC_T – Empty bed contact time; U_r – usage rate; FBU – Fraction bed utilization

Table 7.4. Fitting parameters of the Thomas, Yoon-Nelson and Yan models to the experimental data of the fixed-bed adsorption of CBZ onto PSA-PA, at different flow rates.

Model	Parameters	CBZ in distilled water			CBZ in wastewater		
		Flow rate (L d ⁻¹)					
		4.3	8.6	13.0	4.3	8.6	13.0
<i>Yan</i>	q_Y	59.6 ± 0.6	45.9 ± 0.7	36.8 ± 1.2	12.5 ± 0.4	10.4 ± 0.2	2.83 ± 0.08
	α^Y	1.91 ± 0.05	1.49 ± 0.04	1.01 ± 0.04	1.00 ± 0.04	0.98 ± 0.03	0.72 ± 0.02
	R ²	0.993	0.993	0.978	0.980	0.992	0.990
<i>Thomas</i>	q_{Th}	64.3 ± 1.2	52.1 ± 1.8	43.1 ± 1.7	15.5 ± 0.9	13.6 ± 0.8	4.3 ± 0.4
	k_{Th}	0.049 ± 0.002	0.094 ± 0.007	0.15 ± 0.01	0.14 ± 0.02	0.27 ± 0.03	0.9 ± 0.1
	R ²	0.964	0.931	0.920	0.831	0.874	0.808
<i>Yoon-Nelson</i>	$t_{50\% \text{ pred}}$	10.6 ± 0.2	4.3 ± 0.2	2.37 ± 0.09	2.6 ± 0.2	1.12 ± 0.07	0.23 ± 0.02
	$t_{50\% \text{ exp}}$	10	3.7	2.5	1.7	0.8	0.2
	k_{YN}	0.25 ± 0.01	0.47 ± 0.04	0.76 ± 0.05	0.71 ± 0.08	1.4 ± 0.2	4.6 ± 0.6
	R ²	0.964	0.931	0.920	0.831	0.874	0.808

q_{Th} - theoretical saturation adsorption capacity (mg g⁻¹); k_{Th} - Thomas model rate constant (L d⁻¹ mg⁻¹); $t_{50\% \text{ pred}}$ - time required for 50 % of the adsorbate breakthroughs predicted by the model (d); $t_{50\% \text{ exp}}$ - experimental time required for 50 % of the adsorbate breakthroughs (d); k_{YN} - Yoon-Nelson model rate constant (d⁻¹); q_Y - amount of solute adsorbed (mg g⁻¹); α^Y - Yan model parameter; R² - coefficient of correlation

As referred, Yan model is the one that best describes the adsorption of CBZ onto PSA-PA in the studied fixed-bed continuous adsorption systems. However, apart from the maximum adsorption capacity, no other theoretical information can be deduced from the model. On the other hand, Thomas model allows to observe that the predicted adsorption rate constant increases with increasing flow rate, meaning that the mass transfer resistance decreases and, proportionally, the axial dispersion and thickness of the liquid film on the particle surface also decrease (Tor et al., 2009). Additionally, the Yoon-Nelson model gives the predicted time for the 50 % of fixed-bed saturation ($t_{50\%}$) which is, for CBZ in distilled water, very close to the experimental values, only showing a variation between 5 and 16% relatively to the experimental value (Table 7.3). For wastewater, the differences are greater, with $t_{50\%}$ being highly overestimated by the model, except for the flow rate of 13.0 L d⁻¹.

Considering the obtained results for the fixed-bed adsorption of CBZ onto PSA-PA, the flow rate of 4.3 L d⁻¹ was chosen as the most favorable in terms of $t_{10\%}$, FBU and U_r , and hence used in the subsequent experiments in wastewater.

7.3.2.2. Adsorption of carbamazepine, sulfamethoxazole, and paroxetine from single and ternary solutions in wastewater

The experimental breakthrough curves on the adsorption of CBZ, SMX and PAR from their single and ternary wastewater solutions are presented in Figure 7.2 a) and b), respectively. Regarding the single adsorption, it is evident that the breakthrough curve for SMX is steeper than those of PAR and CBZ. Still, the initial elution of PAR from the PSA-PA packed bed is almost immediate, while that of CBZ and SMX takes a bit longer. As already mentioned for CBZ, under the used experimental conditions, the fast elution together with asymmetric skewed curves not reaching exhaustion within the duration of the experiments point to adsorption kinetic limitations in the retention of these pharmaceuticals in the PSA-PA active sites. Also, in the wastewater matrix and, particularly, in the case of PAR, some biodegradation might be occurring simultaneously with adsorption, meaning further depletion of the pharmaceuticals' concentration (Metcalf and Eddy, 2003). This hypothesis is mainly viable for PAR once this pharmaceutical is liable to degrade by autochthonous microorganisms present in activated sludge and estuarine sediments (Duarte et al., 2019). Regarding the adsorption of the considered pharmaceuticals from their ternary solution in wastewater (Figure 7.2b), and comparatively with their respective single adsorption (Figure 7.2a), steeper and higher breakthrough curves were obtained for CBZ and SMX while the contrary was observed for PAR.

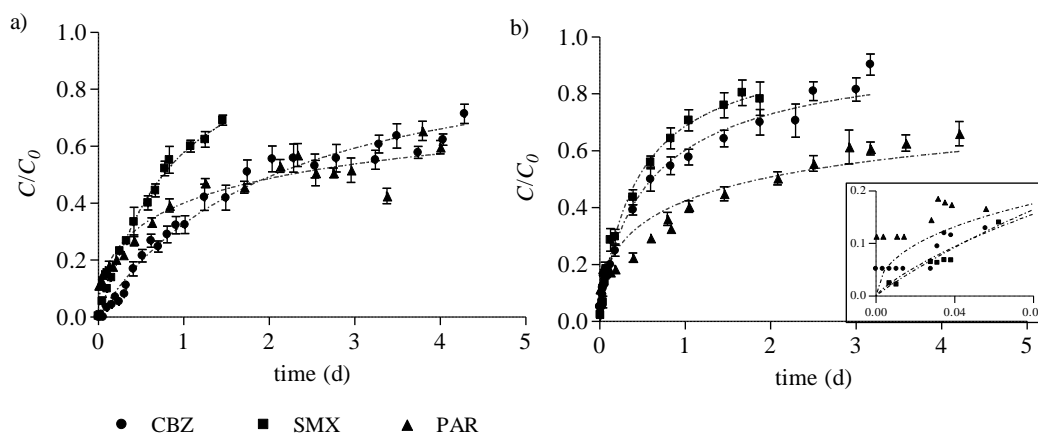


Figure 7.2. Breakthrough curves and fittings of the experimental data to the Yan model for the fixed-bed adsorption of CBZ, SMX, and PAR onto PSA-PA at a flow rate of 4.3 L d^{-1} from a) single and b) ternary solutions in wastewater.

Efficiency and mass transfer parameters in Table 7.3 evidence that, for the single adsorption in wastewater, the breakthrough time ($t_{10\%}$) and the corresponding adsorption capacity ($q_{10\%}$) of each

pharmaceutical are very distinct, diminishing in the order $CBZ > SMX > PAR$. This must be related to the almost spontaneous elution of PAR from the PSA-PA fixed-bed. However, the order of the total mass adsorbed (q_{total}) does not coincide with the breakthrough order, with PSA-PA showing greater adsorption for CBZ, followed by PAR and SMX. The latter is in agreement with previous results obtained under batch conditions (chapter 6), which pointed to the relatively low SMX adsorption capacity of PSA-PA in wastewater (as compared with CBZ and PAR). This was related with the pH of wastewater, which implies a negative charge for both PSA-PA and SMX, leading to some electrostatic repulsion between adsorbate and adsorbent (chapter 6). This, together with competitive and possible exclusion effects (due to the high presence of pores below 5 nm and a low presence of mesoporosity in PSA-PA), might have also negatively affected the adsorption of PAR from the ternary solution. In fact, under competition with other pharmaceuticals in the ternary solution, the $t_{10\%}$ determined for PAR was zero, with $t_{10\%}$ decreasing relatively to the single solution also for SMX and, especially, for CBZ. Interestingly, the largest capacity (q_{total}) for the adsorption from the ternary solution was obtained for PAR, followed by CBZ, and then by SMX. This behavior can be explained by the slower kinetics of PAR adsorption onto PSA-PA compared to CBZ and SMX, as observed in the batch stirred system in chapter 6. Concerning U_r determined for the fixed-bed adsorption from wastewater single solution, its value increases in the order $CBZ < SMX < PAR$, as well as for the corresponding decreasing volume treated at the breakthrough (V_b). Adsorption from the ternary solution meant a notorious decrease in the volume treated at breakthrough, V_b , for the three pharmaceuticals, increasing in the order $PAR < CBZ < SMX$. In the case of ternary solution, this may be related with competitive effects, which resulted in a lower U_r value for SMX than for CBZ.

The parameters from the fitting of the experimental results to the considered mathematical models for the adsorption of CBZ, SMX and PAR from their single and ternary solutions in wastewater are depicted in Table 7.5. As for the corresponding R^2 , it is evident that the Yan model continues to be the model that best describes the experimental data and the corresponding fittings are shown together with experimental results in Figure 7.2. For comparison purposes, fittings to the three models here considered are displayed along with experimental results in Figure C7.3 and C7.4 in Appendix C7 (please, note that fittings to the Thomas and Yoon-Nelson models are superimposed). Regarding the fitting parameters (Table 7.5), it is to highlight that the q_Y for the fixed-bed adsorption from single solution is overestimated as compared with the experimental maximum adsorption capacity (q_{total} in Table 7.3) for CBZ, SMX, and PAR. However, for adsorption from the ternary solution, q_Y is slightly smaller than q_{total} for CBZ, while it is larger than q_{total} for PAR and, especially, for SMX. Divergences are possibly related to deviations of the Yan fitting from experimental results at the end of the experimental curve, which does not reach exhaustion.

Table 7.5. Fitting parameters of the Thomas, Yoon-Nelson and Yan models to the experimental data of the fixed-bed adsorption of CBZ, SMX and PAR onto PSA-PA from single and ternary solutions in wastewater at a flow rate of 4.3 L d⁻¹.

Model	Parameters	Pharmaceutical					
		Single solution			Ternary solution		
		CBZ ^a	SMX	PAR	CBZ	SMX	PAR
Yan	q_Y	12.5 ± 0.4	4.61 ± 0.08	13.5 ± 1.5	3.7 ± 0.2	2.67 ± 0.08	11.4 ± 1.6
	α^Y	1.00 ± 0.04	1.15 ± 0.03	0.51 ± 0.04	0.83 ± 0.04	0.95 ± 0.03	0.49 ± 0.04
	R ²	0.980	0.996	0.929	0.986	0.996	0.916
Thomas	q_{Th}	15.5 ± 0.9	5.3 ± 0.3	16.1 ± 1.1	6.9 ± 0.7	4.3 ± 0.5	14.3 ± 0.7
	k_{Th}	0.14 ± 0.02	0.45 ± 0.06	0.11 ± 0.01	0.30 ± 0.04	0.56 ± 0.08	0.126 ± 0.009
	R ²	0.831	0.898	0.820	0.889	0.875	0.915
Yoon-Nelson	$t_{50\% \text{ pred}}$	2.6 ± 0.2	0.86 ± 0.05	2.6 ± 0.2	1.1 ± 0.1	0.70 ± 0.07	2.4 ± 0.1
	$t_{50\% \text{ exp}}$	1.7	0.8	1.3	0.6	0.6	2.1
	k_{YN}	0.71 ± 0.08	2.3 ± 0.3	0.54 ± 0.06	1.5 ± 0.2	2.8 ± 0.4	0.63 ± 0.05
	R ²	0.831	0.898	0.820	0.889	0.875	0.915

q_Y – amount of solute adsorbed (mg g⁻¹); α^Y – Yan model parameter; q_{Th} – theoretical saturation adsorption capacity (mg g⁻¹); k_{Th} – Thomas model rate constant (L d⁻¹ mg⁻¹); $t_{50\% \text{ pred}}$ – time required for 50 % of the adsorbate breakthroughs predicted by the model (d); $t_{50\% \text{ exp}}$ – experimental time required for 50% of the adsorbate breakthroughs (d); k_{YN} – Yoon-Nelson model rate constant (d⁻¹); R²– coefficient of correlation

^a Values from Table 7.4.

7.3.3. Regeneration and adsorption onto granular activated carbon PSA-PA

The experimental breakthrough curves corresponding to the fixed-bed adsorption of CBZ onto PSA-PA ($Q = 4.3 \text{ L d}^{-1}$) in subsequent cycles after regeneration are depicted in Figure 7.3. As it may be seen, steeper curves are obtained from cycle 0 to cycle 2, accompanied by a reduction of the PSA-PA capacity during regeneration. This is further confirmed by the corresponding efficiency and mass transfer parameters in Table 7.3. Observing the parameters for the cycles 0 (virgin PSA-PA), 1 (after first regeneration) and 2 (after second regeneration), it is possible to see that the $q_{10\%}$ was reduced by 39 % and 86 %, while the q_{total} decreased in 38 % and 71 %, after regeneration cycles 1 and 2, respectively. This decrease in the adsorption capacity of the regenerated PSA-PA may be related to a decrease in the S_{BET} after the thermal regeneration. Table 7.6 presents the textural parameters of the virgin and regenerated PSA-PA used in the subsequent cycles and of the exhausted PSA-PA after use in cycle 2. These results show a decrease in the S_{BET} after regeneration, along with a decrease of the total pore volume (V_p) and the micropore volume (W_0), which is more notorious after the second thermal

regeneration. Meanwhile, the average pore diameter (D) and average pore width (L) increase in the thermal regeneration treatments, due to the destruction of the micropore structure of the adsorbent. Still, the decrease in S_{BET} and W_0 , is not so relevant as the adsorption capacity reduction, especially in the cycle 1, which indicates that other factors are probably affecting the adsorption of CBZ in subsequent cycles. For instance, a change in the surface functionality of the regenerated adsorbent could also be an important factor influencing the results, since it was already observed that chemical interactions are determinant in the adsorption of CBZ onto PSA-PA (chapter 6).

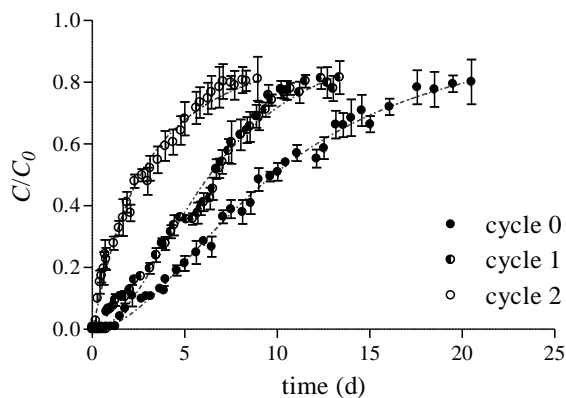


Figure 7.3. Breakthrough curves and fittings of the experimental data to the Yan model for the fixed-bed adsorption of CBZ from distilled water for 3 cycles of PSA-PA utilization: cycle 0 – virgin PSA-PA; cycle 1 – after first regeneration; and cycle 2 – after second regeneration.

Table 7.6. Textural characterization of PSA-PA used in the subsequent fixed-bed adsorption cycles: cycle 0 (virgin PSA-PA), cycle 1 (after first regeneration) and cycle 2 (after second regeneration) and of PSA-PA after use in the cycle 2.

	N ₂ adsorption at -196 °C						
	S_{BET} (m ² g ⁻¹)	V_p (cm ³ g ⁻¹)	Dubinin-Radushkevich (DR)		Dubinin-Astakhov (DA)		
			W_0 (cm ³ g ⁻¹)	L (nm)	D (nm)	W_0 (cm ³ g ⁻¹)	L (nm)
<i>Cycle 0^a</i>	671	0.37	0.27	1.44	1.11	0.28	1.58
<i>Cycle 1</i>	617	0.35	0.25	1.34	1.12	0.27	1.62
<i>Cycle 2</i>	463	0.29	0.19	1.65	1.25	0.20	1.69
After use in <i>cycle 2</i>	391	0.24	0.16	-	1.25	0.17	1.77

V_p = total pore volume; W_0 = micropore volume; L = average micropore width; D = average pore diameter

^aValues presented in chapter 6, Table 6.5 in section 6.3.1.2.

Parameters corresponding to the fittings of the experimental breakthrough curves to the Thomas, Yoon-Nelson and Yan models are depicted in Table 7.7. As for the largest R^2 , the Yan model is again the one providing the best fittings, which are shown in Figure 7.3 together with the experimental results. For comparison purposes, Figure C7.5 in Appendix C7 represents the fittings to the three models considered (note that fittings to Thomas and Yoon-Nelson models are superimposed). Regarding the q_Y values in Table 7.7 overestimate the experimental q_{total} values in Table 7.3. Anyhow, the q_Y values further confirm the depletion of the CBZ adsorption capacity in subsequent utilization cycles after PSA-PA thermal regeneration.

Based on the above-mentioned results, no more than one cycle of utilization of PSA-PA after regeneration should be set, particularly taking into account the energy consumption associated to thermal regeneration together with the loss of adsorption capacity. Moreover, given that the production of PSA-PA is based on the use of two residues as raw materials, obtaining new PSA-PA could be also equated.

Table 7.7. Fitting parameters of the Thomas, Yoon-Nelson and Yan models to the experimental data of the fixed-bed adsorption of CBZ onto PSA-PA from distilled water after regeneration stages 1 and 2, at a flow rate of 4.3 L d⁻¹.

Model	Parameters	Fixed-bed adsorption cycles		
		Cycle 0 ^a	Cycle 1	Cycle 2
<i>Yan</i>	q_Y	59.6 ± 0.6	38.8 ± 0.6	16.1 ± 0.5
	α^Y	1.91 ± 0.05	2.03 ± 0.09	1.11 ± 0.05
	R^2	0.993	0.981	0.984
<i>Thomas</i>	q_{Th}	64.3 ± 1.2	41.3 ± 0.5	20.62 ± 0.99
	k_{Th}	0.049 ± 0.002	0.082 ± 0.003	0.103 ± 0.009
	R^2	0.964	0.979	0.902
<i>Yoon-Nelson</i>	$t_{50\% \text{ pred}}$	10.6 ± 0.2	6.80 ± 0.08	3.4 ± 0.2
	$t_{50\% \text{ exp}}$	10	6.7	2.7
	k_{YN}	0.25 ± 0.01	0.41 ± 0.01	0.52 ± 0.04
	R^2	0.964	0.979	0.902

q_Y – amount of solute adsorbed (mg g⁻¹); α^Y – Yan model parameter; q_{Th} – theoretical saturation adsorption capacity (mg g⁻¹); k_{Th} – Thomas model rate constant (L d⁻¹ mg⁻¹); $t_{50\% \text{ pred}}$ – time required for 50 % of the adsorbate breakthroughs predicted by the model (d); $t_{50\% \text{ exp}}$ – experimental time required for 50 % of the adsorbate breakthroughs (d); k_{YN} – Yoon-Nelson model rate constant (d⁻¹); R^2 – coefficient of correlation

^a values from Table 7.4

7.3.4. Comparison with other studies assessing the removal of carbamazepine, sulfamethoxazole, and paroxetine in fixed-bed reactors

To the best of the authors' knowledge, only a few studies evaluated the adsorptive removal of CBZ and SMX in fixed-bed reactors, with most of studies being focused on the adsorption in batch mode. Moreover, in relation to PAR, there are no literature data on its adsorption in fixed-bed systems. Furthermore, the existing works concerning the adsorption of pharmaceuticals onto AC using fixed-bed reactors were carried out under very distinct operational conditions, making extremely difficult to establish valid comparisons between them (Yu et al., 2009; Sotelo et al., 2013; Ek et al., 2014; Torrellas et al., 2015; Hu et al., 2016; Zuo et al., 2016; Sperlich et al., 2017; Ahmed and Hameed, 2018). Notwithstanding, some of the most relevant studies are commented below.

Concerning the use of GAC in fixed-bed reactors, Sotelo et al. (2013), Sperlich et al. (2017), and Yu et al. (2009) addressed the adsorptive removal of CBZ from water using commercial GAC, while Torrellas et al. (2015) used a GAC produced from peach stones activated with H_3PO_4 . In the latter study, 0.6 g of three GAC (the originally produced from the peach stones with H_3PO_4 activation, and two that were subsequently obtained from the modification of the original) were used. The operational conditions applied consisted of an initial concentration of 15 mg L^{-1} of CBZ and a flow rate of 3 mL min^{-1} (corresponding to a flow rate of 4.3 L d^{-1} , as used in this study), and the amount of CBZ adsorbed at breakthrough time varied between 5.8 mg g^{-1} and 24.4 mg g^{-1} with the breakthrough times obtained from C/C_0 of 0.30 and 0.52. The total amount adsorbed (at saturation time) varied between 69.7 mg g^{-1} and 235.1 mg g^{-1} . In a work performed by Ek et al. (2014), a pilot study for the application of sequential column reactors, using commercial GAC for wastewater treatment was studied, and CBZ was one of the emerging contaminants addressed, using environmentally realistic concentrations.

Other studies refer to the removal of CBZ and SMX in fixed-bed systems, however with other adsorbent materials than AC, such as resins (Wang et al., 2016), montmorillonite modified with ionic liquid (Lawal and Moodley, 2018), modified Y-zeolites (Cabrera-Lafaurie et al., 2014; Cabrera-Lafaurie et al., 2015), and carbon nanotubes (Tian et al., 2013). Besides the scarcity of publications regarding the adsorption of these pharmaceuticals in fixed-bed reactors, the use of industrial residues as precursors for the production of GAC to be used in these systems is, as far as it concerns the authors' knowledge, inexistent.

7.4. Conclusions

The fixed-bed adsorption performance of CBZ using PSA-PA, a primary paper mill sludge-based GAC, was higher in distilled water than in wastewater, possibly due to the competitive effects in the latter. In both matrices, the larger the flow rate, the steeper the breakthrough curves, with the most favorable flow rate being 4.3 L d^{-1} . Under this flow rate, the fixed-bed adsorption of CBZ, SMX and PAR from their single solution in wastewater showed that the bed capacity decreased in the order $\text{CBZ} > \text{PAR} > \text{SMX}$. However, from the ternary solution, it decreased following the order $\text{PAR} > \text{CBZ} > \text{SMX}$ since the bed capacity for CBZ and, especially, for SMX decreased under the competition of the other pharmaceuticals. Contrarily, and despite being eluted instantaneously from the column, PAR showed an enhanced bed capacity in the ternary solution. The Yan model was the one that generally best described the experimental breakthrough curves for the adsorption of the considered pharmaceuticals under the tested experimental conditions. Finally, although the thermal regeneration of PSA-PA involved a relatively low decrease in its S_{BET} , it resulted in a reduction of the CBZ bed adsorption capacity of around 39 % and 71 % in the first and second regeneration stages, respectively. Therefore, no more than one regeneration stage is recommended for the fixed-bed utilization of PSA-PA in the removal of CBZ.

Studies assessing the removal of these pharmaceuticals using GAC produced from industrial residues in fixed-bed systems are very scarce and, therefore, the present study is a relevant contribution to this field.

7.5. References

- Ahmed, M.J., Hameed, B.H., 2018. Removal of emerging pharmaceutical contaminants by adsorption in a fixed-bed column: A review. *Ecotoxicol. Environ. Saf.* 149, 257-266.
- Cabrera-Lafaurie, W.A., R., F.R., Hernández-Maldonado, A.J., 2014. Removal of salicylic acid and carbamazepine from aqueous solution with Y-zeolites modified with extraframework transition metal and surfactant cations: Equilibrium and fixed-bed adsorption. *J. Environ. Chem. Eng.* 2, 899-906.
- Cabrera-Lafaurie, W.A., Román, F.R., Hernández-Maldonado, A.J., 2015. Single and multi-component adsorption of salicylic acid, clofibrac acid, carbamazepine and caffeine from water onto transition metal modified and partially calcined inorganic-organic pillared clay fixed beds. *J. Hazard. Mater.* 282, 174-182.
- Darweesh, T.M., Ahmed, M.J., 2017. Adsorption of ciprofloxacin and norfloxacin from aqueous solution onto granular activated carbon in fixed bed column. *Ecotoxicol. Environ. Saf.* 138, 139-145.
- Deokar, S.K., Mandavgane, S.A., 2015. Estimation of packed-bed parameters and prediction of breakthrough curves for adsorptive removal of 2,4-dichlorophenoxyacetic acid using rice husk ash. *Journal of Environmental Chemical Engineering* 3, 1827-1836.
- Duarte, P., Almeida, C.M.R., Fernandes, J.P., Morais, D., Lino, M., Gomes, C.R., Carvalho, M.F., Mucha, A.P., 2019. Bioremediation of bezafibrate and paroxetine by microorganisms from estuarine sediment and activated sludge of an associated wastewater treatment plant. *Sci. Total Environ.* 655, 796-806.
- Ek, M., Baresel, C., Magnér, J., Bergstroöm, R., Harding, M., 2014. Activated carbon for the removal of pharmaceutical residues from treated wastewater. *Water Sci. Technol.* 69, 2372-2380.
- Ferreira, C.I.A., Calisto, V., Otero, M., Nadais, H., Esteves, V.I., 2017. Fixed-bed adsorption of Tricaine Methanesulfonate onto pyrolysed paper mill sludge. *Aquacult. Eng.* 77, 53-60.
- Franco, M.A.E.d., Carvalho, C.B., Bonetto, M.M., Soares, R.d.P., Féris, L.A., 2017. Removal of amoxicillin from water by adsorption onto activated carbon in batch process and fixed bed column: Kinetics, isotherms, experimental design and breakthrough curves modelling. *J. Clean. Prod.* 161, 947-956.
- Hu, J., Aarts, A., Shang, R., Heijman, B., Rietveld, L., 2016. Integrating powdered activated carbon into wastewater tertiary filter for micro-pollutant removal. *J. Environ. Manage.* 177, 45-52.
- Lawal, I.A., Moodley, B., 2018. Fixed-Bed and Batch Adsorption of Pharmaceuticals from Aqueous Solutions on Ionic Liquid-Modified Montmorillonite. *Chem. Eng. Technol.* 41, 983-993.
- Lima, L.F., de Andrade, J.R., da Silva, M.G.C., Vieira, M.G.A., 2017. Fixed Bed Adsorption of Benzene, Toluene, and Xylene (BTX) Contaminants from Monocomponent and Multicomponent Solutions Using a Commercial Organoclay. *Ind. Eng. Chem. Res.* 56, 6326-6336.
- Metcalf, Eddy, I., 2003. *Wastewater Engineering : Treatment and Reuse*, Fourth ed. McGraw-Hill.

- Nazari, G., Abolghasemi, H., Esmaili, M., Sadeghi Pouya, E., 2016. Aqueous phase adsorption of cephalexin by walnut shell-based activated carbon: A fixed-bed column study. *Appl. Surf. Sci.* 375, 144-153.
- Patel, M., Kumar, R., Kishor, K., Mlsna, T., Pittman, C. U., Mohan, D., 2019. Pharmaceuticals of Emerging Concern in Aquatic Systems: Chemistry, Occurrence, Effects, and Removal Methods. *Chem. Rev.* 119, 3510-3673.
- Pelech, R., Milchert, E., Bartkowiak, M., 2006. Fixed-bed adsorption of chlorinated hydrocarbons from multicomponent aqueous solution onto activated carbon: Equilibrium column model. *J. Colloid. Interf. Sci.* 296, 458-464.
- Radhika, R., Jayalatha, T., Rekha Krishnan, G., Jacob, S., Rajeev, R., George, B.K., 2018. Adsorption performance of packed bed column for the removal of perchlorate using modified activated carbon. *Process Saf. Environ.* 117, 350-362.
- Saadi, Z., Saadi, R., Fazaeli, R., 2013. Fixed-bed adsorption dynamics of Pb (II) adsorption from aqueous solution using nanostructured γ -alumina. *Journal Of Nanostructure in Chemistry* 3, 1-8.
- Sánchez-Machado, D.I., López-Cervantes, J., Correa-Murrieta, M.A., Sánchez-Duarte, R.G., 2016. Modeling of breakthrough curves for aqueous iron (III) adsorption on chitosan-sodium tripolyphosphate. *Water Sci. Technol.* 74, 2297-2304.
- Singh, B., Thakur, V., Bhatia, G., Verma, D., Singh, K., 2016. Eco-friendly and Cost-effective Use of Rice Straw in the Form of Fixed Bed Column to Remove Water Pollutants. *J. Bioremed. Biodegrad.* 7, 374.
- Sotelo, J.L., Ovejero, G., Rodríguez, A., Álvarez, S., García, J., 2013. Adsorption of Carbamazepine in Fixed Bed Columns: Experimental and Modeling Studies. *Sep. Sci. Technol.* 48, 2626-2637.
- Sperlich, A., Harder, M., Zietzschmann, F., Gnirss, R., 2017. Fate of trace organic compounds in granular activated carbon (GAC) adsorbers for drinking water treatment. *Water* 9, 479.
- Thomas, H.C., 1944. Heterogeneous Ion Exchange in a Flowing System. *J. Am. Chem. Soc.* 66, 1664-1666.
- Tian, Y., Gao, B., Morales, V.L., Chen, H., Wang, Y., Li, H., 2013. Removal of sulfamethoxazole and sulfapyridine by carbon nanotubes in fixed-bed columns. *Chemosphere* 90, 2597-2605.
- Tor, A., Danaoglu, N., Arslan, G., Cengeloglu, Y., 2009. Removal of fluoride from water by using granular red mud: Batch and column studies. *J. Hazard. Mater.* 164, 271-278.
- Torrellas, S.Á., García Lovera, R., Escalona, N., Sepúlveda, C., Sotelo, J.L., García, J., 2015. Chemical-activated carbons from peach stones for the adsorption of emerging contaminants in aqueous solutions. *Chem. Eng. J.* 279, 788-798.
- Ullah, M., Ullah, H., Murtaza, G., Mahmood, Q., Hussain, I., 2015. Evaluation of influence of various polymers on dissolution and phase behavior of carbamazepine-succinic acid cocrystal in matrix tablets. *BioMed Res. Int.* 2015, 870656.

- Wang, W., Li, X., Yuan, S., Sun, J., Zheng, S., 2016. Effect of resin charged functional group, porosity, and chemical matrix on the long-term pharmaceutical removal mechanism by conventional ion exchange resins. *Chemosphere* 160, 71-79.
- Xu, Z., Cai, J.-g., Pan, B.-c., 2013. Mathematically modeling fixed-bed adsorption in aqueous systems. *Journal of Zhejiang University Science A* 14, 155-176.
- Yan, G., Viraraghavan, T., Chen, M., 2001. A New Model for Heavy Metal Removal in a Biosorption Column. *Adsorpt. Sci. Technology* 19, 25-43.
- Yang, Y., Ok, Y.S., Kim, K.H., Kwon, E.E., Tsang, Y.F., 2017. Occurrences and removal of pharmaceuticals and personal care products (PPCPs) in drinking water and water/sewage treatment plants: A review. *Sci. Total Environ.* 596-597, 303-320.
- Yoon, Y.H., James, H.N., 1984. Application of gas adsorption kinetics I. A theoretical model for respirator cartridge service life. *The American Industrial Hygiene Association Journal* 45, 509-516.
- Yu, Z., Peldszus, S., Huck, P.M., 2009. Adsorption of Selected Pharmaceuticals and an Endocrine Disrupting Compound by Granular Activated Carbon. 1. Adsorption Capacity and Kinetics. *Environ. Sci. Technol.* 43, 1467-1473.
- Zuo, L., Ai, J., Fu, H., Chen, W., Zheng, S., Xu, Z., Zhu, D., 2016. Enhanced removal of sulfonamide antibiotics by KOH-activated anthracite coal: Batch and fixed-bed studies. *Environ. Pollut.* 211, 425-434.

8

SURFACE FUNCTIONALIZATION OF WASTE-BASED ACTIVATED CARBON AND ITS EFFECT ON THE REMOVAL OF SIX PHARMACEUTICALS FROM WATER

Abstract

The functionalization of a paper mill sludge-based activated carbon (AC3) was addressed in this work. Four different procedures have been accomplished in order to introduce amine functional groups (AC-NH₂ and AC-APTES), thiol functional groups (AC-MPTMS), and a covalent organic polymer (AC-COP) onto the activated carbon (AC) surface. The materials were characterized showing that the functionalization was succeeded but implying a reduction of the specific surface area (S_{BET}), except for AC-MPTMS. The produced AC were tested for the removal of six pharmaceuticals - carbamazepine (CBZ), lorazepam (LOR), sulfamethoxazole (SMX), piroxicam (PIR), paroxetine (PAR), and venlafaxine (VEN) - from different matrices (ultrapure water, ultrapure water with pH adjusted to 7.6, and wastewater (effluent) from a municipal wastewater treatment plant (WWTP). The results indicated textural parameters, S_{BET} , micropore area and micropore volume, as the main factors influencing the adsorption, except for AC-NH₂ which showed a great specificity for PAR and VEN. Also, AC-MPTMS presented a high removal percentage of the antibiotic SMX in wastewater. Overall, AC-MPTMS and AC-APTES provided, respectively, the best and the poorest adsorptive performance. Although the functionalization did not result in the enhancement of pharmaceuticals' adsorption as compared with the parent AC3, the selectivity for some pharmaceuticals seems to be improved.

This chapter was based on the published article:

Jaria, G., Lourenço, M.A.O., Silva, C.P., Ferreira, P., Otero, M., Calisto, V., Esteves, V.I., 2020. Effect of the surface functionalization of a waste-derived activated carbon on pharmaceuticals' adsorption from water. *J. Mol. Liq.* 299, 112098.

8.1. Contextualization

The previous chapters (chapters 4 to 6) showed the potential of primary paper mill sludge (PS) to produce activated carbon (AC) in both powdered (PAC) and granular (GAC) forms, with the PAC AC3 presenting an interesting specific surface area (S_{BET}) and adsorption performance, for the pharmaceuticals carbamazepine (CBZ), sulfamethoxazole (SMX), and paroxetine (PAR) in ultrapure water. In chapter 5, the performance of AC3, was evaluated through kinetic and equilibrium adsorption studies for the removal of the three pharmaceuticals in study (CBZ, SMX, and PAR) from ultrapure water and wastewater matrices. The results showed that the behavior of AC3 was greatly influenced by the matrix, mainly in the case of SMX, for which the adsorption capacity of AC3 decreased from (194 ± 10) mg g⁻¹ in ultrapure water to (47 ± 1) mg g⁻¹ in wastewater. On the other hand, an increase in the adsorption of PAR in wastewater matrix was observed for AC3. This behavior could be, in part, explained by the effect of electrostatic interactions in the adsorption process, influenced by both the point of zero charge (pH_{pzc}) of AC3 and the $\text{p}K_a$ of the pharmaceuticals. Considering the results of the study presented in chapter 5, and as it has been mentioned in chapter 2, not only surface area (S_{BET}) is responsible to the adsorption effectiveness of the material, being also important other physicochemical characteristics of the AC, namely pH_{pzc} and its surface chemistry. Hence, introducing specific chemical features onto the AC surface for interaction with the target pharmaceuticals could be beneficial for increasing the efficiency of these materials in drug adsorption-separation. As referred in chapter 2 (section 2.2.2.2), in general, the modification of the AC surface has been mainly addressed in terms of oxidation, acidic or basic treatments (Yin et al., 2007; Stavropoulos et al., 2008; Rivera-Utrilla et al., 2011; Bhatnagar et al., 2013). The resulting materials, applied to water treatment, have been used for the removal of several compounds, namely, metal ions or organic pollutants such as dyes, phenols, naphthalenesulphonic acids, dibenzothiophene, benazolin, 2,4-dichlorophenoxy acetic acid, and atrazine (Bhatnagar et al., 2013). Therefore, there are few examples concerning the application for the removal of pharmaceuticals from water, which include the work by Guedidi et al. (2017), who studied the adsorption of ibuprofen onto AC cloths modified by NaOCl oxidation and thermal treatment under nitrogen atmosphere, and that by Bhadra et al. (2016), who carried out an AC modification by oxidation with further application in the adsorption of diclofenac. Also, some biologically modified AC were tested for the removal of organic contaminants, such as methyl tert-butyl ether, natural organic matter and organic micropollutants (17 β -estradiol, pesticides and bromate) (Bhatnagar et al., 2013). Mines et al.

(2017), who highlighted the relevance of AC functionalization for expanding their application for a wider range of pollutants, grafted a covalent organic polymer (COP) on the surface of an AC and tested the functionalized material in the removal of an azo dye and cadmium from water, resulting in a significant increase in the adsorption of the first. Besides these examples, the functionalization of AC has been mostly studied for catalytic applications (Radkevich et al., 2008; Figueiredo, 2013) and carbon electrodes (Pognon et al., 2011; Lebègue et al., 2013a), to get some insights on reaction mechanisms (Lebègue et al., 2011; Lebègue et al., 2013b).

In this context, the main aim of this work was to evaluate the effects of different chemical functionalization methodologies on the properties and adsorptive performance of AC3, for application in the removal of pharmaceuticals from water and wastewater. For this purpose, AC3 was modified recurring to four different functionalization methods, namely: direct amination to enhance the percentage of amine functional group (Lourenço et al., 2016), organosilane grafting with (3-aminopropyl)triethoxysilane (APTES), with impact on the nitrogen content; organosilane grafting with (3-mercaptopropyl)trimethoxysilane (MPTMS), influencing the sulfur content (Lourenço et al., 2017); and functionalization with a covalent organic polymer (COP) (Mines et al., 2017). After a full characterization of the produced materials, they were tested for the adsorption of 6 pharmaceuticals from different classes and with different physicochemical properties in order to assess the impact of functionalization and allowing to select the most promissory modification route(s) for the target application.

8.2. *Materials and Methods*

8.2.1. *Chemicals and reagents*

The AC3 chemical functionalization was achieved using the following reagents: ethanol (99.9 %, Riedel-de Haën), hydrochloric acid (HCl, 37 % v/v, Carlo Erba), sulfuric acid (H₂SO₄, 95-97 % v/v, PanReac), tin chloride (SnCl₂, 98 %, Sigma-Aldrich), isopropylamine (99.5 %, Aldrich), (3-mercaptopropyl)trimethoxysilane (MPTMS, 95 %, Aldrich), (3-aminopropyl)triethoxysilane (APTES, 95 %, Aldrich), toluene (99.8 %, Aldrich), dichloromethane (CH₂Cl₂, 99.9 %, Sigma-Aldrich), thionyl chloride (SOCl₂, 99 %, Fluka), melamine (C₃H₆N₆, 99 %, Aldrich), dimethyl sulfoxide (DMSO, ≥ 99.5 %, Sigma-Aldrich), diisopropylethylamine (DIPEA, 99 %, Aldrich), terephthalaldehyde (> 98.0 %, TCI). The pharmaceuticals used for the adsorption experiments were carbamazepine (CBZ, Sigma-Aldrich, 99 %), sulfamethoxazole (SMX, TCI, > 98 %), paroxetine (paroxetine-hydrochloride, PAR, TCI, > 98 %),

lorazepam (LOR, Sigma-Aldrich, 99 %), piroxicam (PIR, Sigma-Aldrich, 99 %) and venlafaxine (VEN, TCI, > 98 %).

8.2.2. Material synthesis

8.2.2.1. Waste-based activated carbon (AC3) synthesis

The AC3 synthesis was performed as described in chapter 4 (production conditions of experiment 3 of the full factorial design). Briefly, primary paper mill sludge (PS) was impregnated with a chemical activating agent (potassium hydroxide at a *w:w* ratio of 1:1). The impregnated PS was sonicated during 1 h in an ultrasound bath, dried at room temperature and then in an oven overnight at 105 °C. Subsequently, the material was subjected to pyrolysis under inert atmosphere, at 800 °C and for 150 min. The obtained carbon was then washed with hydrochloric acid (1.2 M), for the removal of ashes, and distilled water until the washing leachate reach neutral pH. The resulting material was oven dried at 105 °C and stored in a sealed container. A new batch of material was exclusively produced for this work.

8.2.2.2. Functionalization of the alternative activated carbon (AC3)

The material from the previous step was used as precursor to produce 4 different functionalized AC: AC-NH₂, AC-APTES, AC-MPTMS and AC-COP. The procedures for obtaining these functionalized AC are next described and summarized in Figure 8.1.

Direct amination

In order to yield AC-NH₂, the introduction of the amine functionalities into the phenylene moieties of the produced AC3 was reached using a two-step procedure described by Inagaki *et al.* for periodic mesoporous organosilica (PMO) materials (Inagaki *et al.*, 2002; Ohashi *et al.*, 2008; Lourenço *et al.*, 2016). In a typical synthesis, the phenylene groups of AC (0.125 g) were first nitrated using very strong acid solutions of HNO₃ (0.7 mL) and H₂SO₄ (2.2 mL). After stirring at room temperature during 72 h, the obtained AC-NO₂ was filtered-off, washed with distilled water and dried at 60 °C. Then, the AC-NO₂ (0.102 g) was treated with SnCl₂ (0.338 g) and HCl (3.2 mL) solution in order to reduce the nitro group to amine functionalities. The mixture was stirred at room temperature during 72 h. The obtained AC-NH₂ was filtered-off, washed with distilled water followed by isopropylamine-ethanol solution, and finally it was dried overnight at 60 °C (Figure 8.1A).

Organosilane grafting

The AC-APTES and AC-MPTMS materials were obtained from AC3 using a similar procedure used to functionalize PMO materials (Lourenço et al., 2017). After the activation of the pores of AC3 (0.125 g), dry toluene (5 mL) was added. Then APTES (0.192 mL) or MPTMS (0.154 mL) were added drop wise to the suspension to obtain AC-APTES and AC-MPTMS, respectively. The mixtures were vigorously stirred for 24 h. The functionalized AC were filtered off, washed with toluene to remove unreacted species and further washed with a large amount of distilled water and oven dried at 60 °C overnight (Figure 8.1 B and C).

Functionalization with an organic polymer

The covalent organic polymer attached AC3 (AC-COP) was synthesized using a procedure similar to that reported by Mines et al. (2017). First, the oxidation of the AC3 (resulting in AC-Ox) was made by refluxing 5 g of AC3 with 50 mL of HNO₃ during 24 h. The AC-Ox was further washed with large amount of ultrapure water until reaching neutral pH. Then the AC-Ox was oven dried at 110 °C for 72 h. After activation of AC-Ox in vacuum at 110 °C, 1 g of this material was refluxed under nitrogen atmosphere with a mixture of 40 mL of CH₂Cl₂, and 20 mL SOCl₂. After 24 h, the acyl chloride modified AC (AC-Thio) was obtained by removing the solvent by vacuum distillation. Finally, a melamine modified AC material (AC-Mel) was obtained as follows. Under inert conditions, 2 g of AC-Thio were treated with a sonicated solution of 0.150 g of melamine dissolved in 60 mL of DMSO and 1 mL of DIPEA. The mixture was heated to 120 °C for 24 h. The AC-Mel material was filtered, washed three times each with DMSO, ultrapure water and ethanol and dried in a vacuum for 8 h at 110 °C. The preparation of AC-COP was made in a typical synthesis, where 0.368 g of melamine and 0.23 g of terephthalaldehyde were sonicated with 69 mL of DMSO under N₂ atmosphere. Then, 0.460 g of AC-Mel were added into the solution, under inert atmosphere. The obtained mixture was stirred under reflux for 48 h. The AC-COP was filtered-off, further washed three times with DMSO, acetone, ultrapure water and ethanol and finally, it was dried (Figure 8.1D).

Surface functionalization of waste-based activated carbon and its effect on the removal of six pharmaceuticals from water

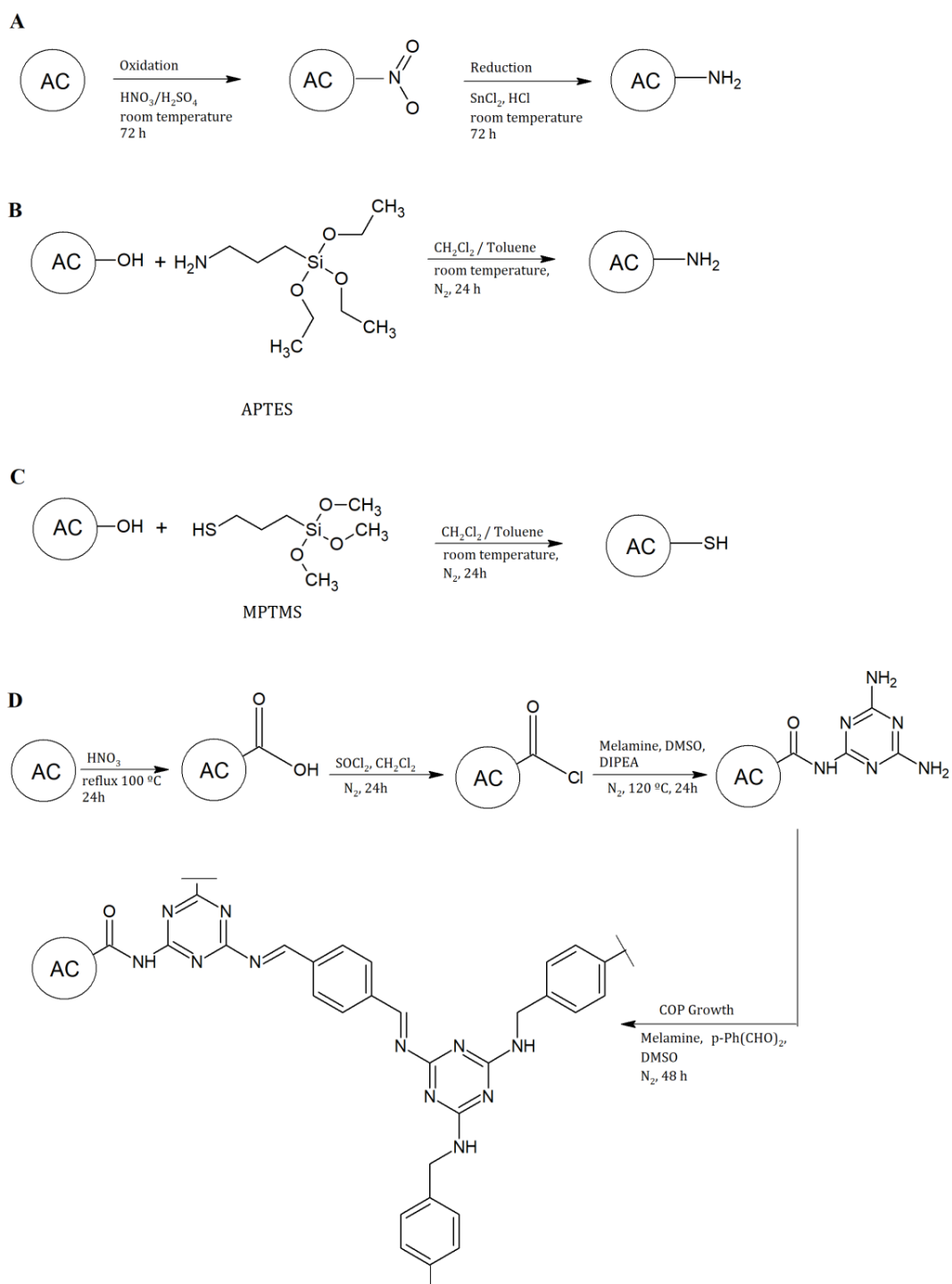


Figure 8.1. Schematic representation of the functionalization procedures: A - Direct amination; B - Organosilane grafting with APTES; C - Organosilane grafting with MPTMS; and D - functionalization with an organic polymer (COP-19, based on Mines et al. (2017)).

8.2.3. *Methods for characterization of the synthesized materials*

The AC3 and functionalized AC were characterized by $-196\text{ }^{\circ}\text{C}$ N_2 -sorption isotherms, elemental analysis, Fourier transformed infrared (ATR-FTIR) spectroscopy, Raman spectroscopy, thermogravimetric analysis (TGA), and determination of the point of zero charge (pH_{pzc}). Also, AC-NH₂ and AC-MPTMS, which were the functionalized AC presenting the most interesting results in terms of adsorption percentage, were further analyzed by X-Ray photoelectron spectroscopy (XPS) and scanning electron microscopy (SEM). More information concerning the used characterization techniques (specific methods, equipment models and conditions used) can be found in the Appendix A, Sections A1, A2, A3.2 and A5.

8.2.4. *Adsorptive removal of pharmaceuticals from water*

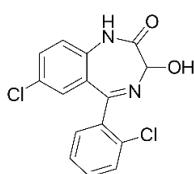
Batch adsorption experiments were performed to evaluate the efficiency of the AC3 and functionalized AC for the removal of six different pharmaceuticals from water. Besides the adsorption of CBZ, SMX, and PAR, also the anxiolytic LOR, the non-steroidal anti-inflammatory PIR, and the antidepressant VEN were studied. The adsorption studies of these additional three pharmaceuticals were addressed mostly for comparison purposes concerning the differences in the structure of pharmaceuticals from the same class or with the same net charge at the pH medium. This selection aimed at finding out possible connections between adsorption behavior, pharmaceuticals properties and the features of the AC. The physicochemical properties of CBZ, SMX and PAR are presented in Table 1.1 (in chapter 1) and those of LOR, PIR and VEN are presented in Table 8.1.

Single component pharmaceuticals solutions, with an initial concentration of 5 mg L^{-1} , were prepared and put in contact with each produced material (at a dosage of 25 mg L^{-1}) in 50 mL polypropylene tubes. This dose of material, based on preliminary studies, was selected in order to have a quantifiable removal percentage of each pharmaceutical under the studied conditions. In this way, it was avoided using different doses for different systems, which would imply the impossibility of a direct comparison of the results. The tubes were shaken in a head-over-head shaker for 24 h, at 80 rpm and controlled temperature ($(25.0 \pm 0.1)\text{ }^{\circ}\text{C}$) since, on the basis of previous studies, it was possible to attain equilibrium in these conditions (chapter 5). All the experiments were run in triplicate. Control experiments, consisting of the pharmaceutical solutions in the absence of the adsorbent, were also run. After the defined contact time, the solutions with the suspended AC were filtered through $0.22\text{ }\mu\text{m}$ PVDF

filters (Whatman) and the remaining concentration of the pharmaceutical in the aqueous solution was determined by Micellar Electrokinetic Chromatography (MEKC) as described in the Appendix B2.

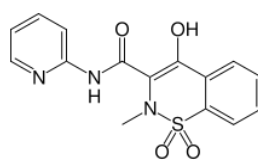
Table 8.1. Physicochemical properties of the additional studied pharmaceuticals (based on PubChem, accessed in February 2019).

<i>Pharmaceutical</i>	<i>MW</i> (<i>g mol⁻¹</i>)	<i>S_w</i> (<i>mg L⁻¹</i>)	<i>pK_a</i>	<i>log K_{ow}</i>	<i>Polar surface area /Å²</i>	<i>H bond acceptors</i>
Lorazepam (4)	321.157	80	1.3; 11.5	2.4	61.7	3
Piroxicam (5)	331.346	23 (22 °C)	6.3	1.7	108	7
Venlafaxine (6)	277.408	267 (25 °C)	10.09	2.9	32.7	3



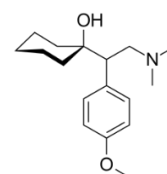
(4)

C₁₅H₁₀Cl₂N₂O₂



(5)

C₁₅H₁₃N₃O₄S



(6)

C₁₇H₂₇NO₂

All the adsorption experiments were performed in three different matrices: ultrapure water without pH adjustment (pH ~ 5.5 to 6), ultrapure water with pH adjusted to 7.6 (adjusted with sodium hydroxide 1 M and hydrochloric acid 1M) and wastewater from an urban wastewater treatment plant (WWTP) (pH ~ 7.6). The pH for the experiments run in ultrapure water with adjusted pH was selected according to the pH of the collected WWTP wastewater. This pH was considered to be representative of urban WWTP final effluents, which would be the target application of the developed materials. The use of different aqueous media aimed at evaluating the effects of the pH and matrix complexity in the adsorption performance.

The wastewater for the adsorption experiments was collected between July and September 2018 at the outlet (after biological treatment) of the local urban WWTP described in chapter 5 (section 5.2.4). After collection, wastewater was filtered and characterized as described in chapter 5 (section 5.2.4).

8.3. Results and Discussion

The results obtained for the functionalization of AC3 and their discussion are presented in two parts: the first one considers the physicochemical characterization of the AC3 and functionalized AC

(section 8.3.1), and the second part (section 8.3.2) addresses the results related with the adsorption removal of the six studied pharmaceuticals by the produced materials, in the 3 different aqueous matrices. The characterization results presented are related to the batches of AC3, AC-NH₂, AC-APTES, AC-MPTMS, and AC-COP produced for and used in this work.

8.3.1. Characterization of the synthesized materials

The physical and textural properties of the AC3 and functionalized AC were studied by low temperature N₂ adsorption-desorption isotherms, and the results are presented in Table 8.2. The presence of different micro, meso and macropores was verified. The majority of the synthesized materials present an isotherm resembling a Type Ib (IUPAC classification) (Sing et al., 1985), usually observed for microporous materials with wide micropores and possibly narrow mesopores (≤ 2.5 nm). Nonetheless, the AC-NH₂ presents a Type Ia isotherm (IUPAC classification) (Sing et al., 1985), typically observed in microporous materials presenting mainly narrow micropores (≤ 1 nm). In all cases, some Type II (IUPAC classification) (Sing et al., 1985) character is also observed and can be associated to the presence of non-porous or macroporous fractions. All materials show a H4 hysteresis, which is often found in micro-mesoporous carbons. As can be seen in Table 8.2, the unmodified AC3 presents the highest S_{BET} of approximately $1000 \text{ m}^2 \text{ g}^{-1}$ and the highest t-plot micropore area (S_{micro}) of above $442 \text{ m}^2 \text{ g}^{-1}$. The modification of the AC3 with different functionalities led to a reduction of both S_{BET} and S_{micro} for all materials with exception of AC-MPTMS, where only the S_{micro} was reduced. The S_{BET} decreased in the way $\text{AC3} > \text{AC-MPTMS} > \text{AC-APTES} > \text{AC-COP} > \text{AC-NH}_2$. Thus, AC-NH₂ is the material with the lowest values of both S_{BET} and S_{micro} , $195 \text{ m}^2 \text{ g}^{-1}$ and $101 \text{ m}^2 \text{ g}^{-1}$, respectively. This can be explained by the size and diffusion of the functionalization reactants into the pores of the non-functionalized AC3. For example, the NH₂ group is the smallest introduced functionality, thus it is expected to be the one that has better diffusion into the pore channels of the AC3, which is confirmed by the highest reduction in the pore volume (V_p), from $0.49 \text{ cm}^3 \text{ g}^{-1}$ (AC3) to $0.12 \text{ cm}^3 \text{ g}^{-1}$ (AC-NH₂).

Figure 8.2 shows a comparison of the pore size distribution (PSD) curves of AC3 and functionalized AC. All modifications in the AC3 led to a reduction of the mesopores, more pronounced in the AC-NH₂. Also, the modification of the AC3 promotes a slight shift to left in the pores between 1.2 nm and 5 nm, confirming the introduction of some functional groups into the pore channels of the parent AC3. A slight reduction in the volume adsorbed into the bigger micropores (between 1.2 nm and 2 nm) is also observed for the functionalized AC with exception of AC-MPTMS.

Table 8.2. Textural properties of AC3 and functionalized AC.

Sample	S_{BET} ($\text{m}^2 \text{g}^{-1}$)	$S_{\text{micro}}^{\text{a}}$ ($\text{m}^2 \text{g}^{-1}$)	V_{p}^{a} ($\text{cm}^3 \text{g}^{-1\text{a}}$)	W_0^{a} ($\text{cm}^3 \text{g}^{-1\text{a}}$)	Isotherm type (hysteresis)
AC3	994	442	0.49	0.19	Ib + II (H4)
AC-NH ₂	195	101	0.12	0.04	Ia + II (H3)
AC-APTES	650	207	0.43	0.09	Ib + II (H4)
AC-MPTMS	993	379	0.56	0.17	Ib + II (H4)
AC-COP	410	98	0.34	0.06	Ib + II (H4+H3)

^a S_{micro} (microporous area) and W_0 (micropore volume) values were determined by the t-plot method.

^b V_{p} corresponds to the Barret-Joyner-Halenda (BJH) adsorption cumulative pore volume applying the Kruk-Jaroniec-Sayari correction.

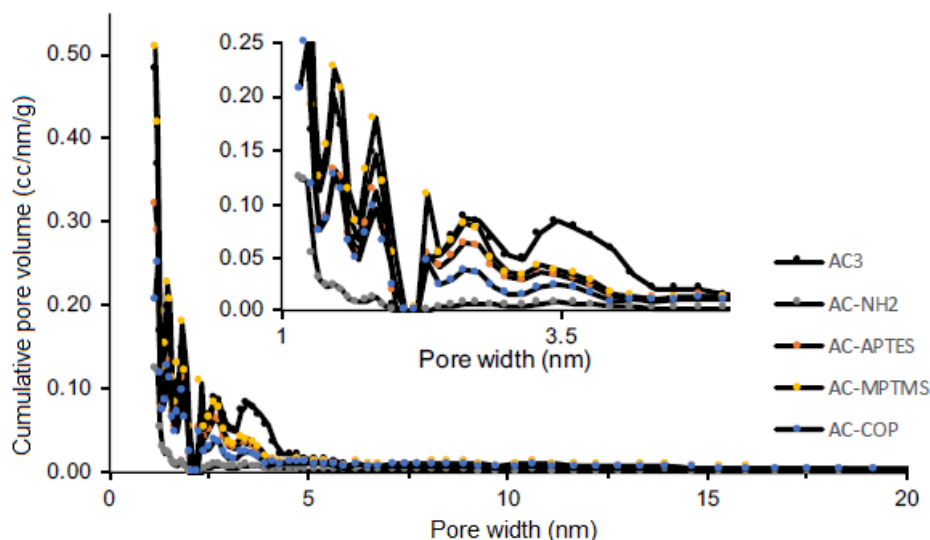


Figure 8.2. Pore size distribution of AC3 and functionalized AC. Pore width was obtained from the non-linear density functional theory (NLDFT).

SEM micrograph images, depicted in Figure 8.3, show the morphological characteristics of AC3, AC-NH₂ and AC-MPTMS. AC3 and AC-NH₂ seem to be in large aggregates of smooth surface particles almost without visible macroporosity (Figure 8.3a-b) while AC-MPTMS display a roughness surface particle full of macropores (Figure 8.3c). These characteristics are in agreement with the type II character detected in the N₂-sorption isotherms (Table 8.2).

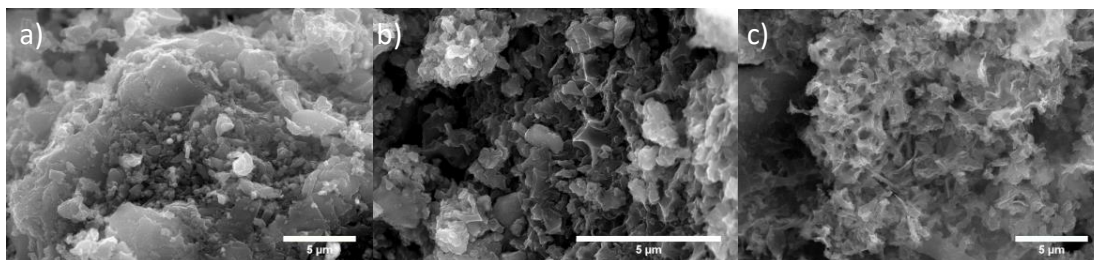


Figure 8.3. SEM images of crushed samples of a) AC3, b) AC-NH₂, and c) AC-MPTMS.

The chemical composition of the AC was verified by FTIR spectroscopy, elemental analyses and XPS. In Figure 8.4 it is possible to observe the FTIR spectra of the parent AC3 material, where no distinguishable peaks are noticed, settling the absence of significant functionalities. The direct amine modification of the phenylene groups of the AC3 can be detected by the presence of two peaks at 1556 and 1197 cm⁻¹ attributed to the formation of N-H and C-N bonds, respectively. The grafting of APTES and MPTMS reactants to the surface of the AC3 was also confirmed by FTIR (Figure 8.4). The AC-COP shows peaks at 1722, 1581, 1506, 1336, 1205, 1093, 790, and 786 cm⁻¹, similar to those observed by Mines et al. (2017) in their functionalized AC, as for the COP contained within the matrix.

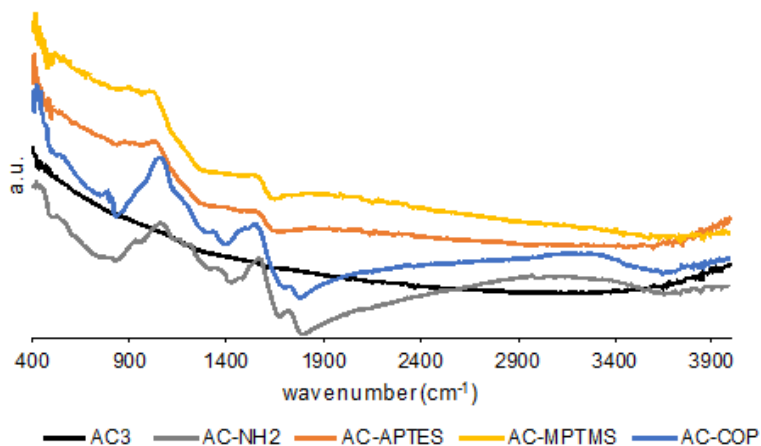


Figure 8.4. ATR-FTIR spectra of AC3 and functionalized AC.

In Raman spectra (Figure 8.5), one can observe that all the materials present two pronounced bands around 1300-1350 cm⁻¹ and 1600 cm⁻¹ that may be attributed to D and G bands, respectively, which are typical of AC (Glonek et al., 2017; Alcaraz et al., 2018). The D band is related to the disorder of the carbon atoms, highlighting the defects in the carbon structure. The G band is associated to the graphitic carbon, therefore, to the more ordered, symmetrical, and crystalline part of the structure

(Alcaraz et al., 2018). The materials are very similar, with the D band being more intense than the G band. Additionally, all AC present a broad band at the far wave number side (represented as the 2D or G' region, 2400 cm^{-1} to 3250 cm^{-1}). This can be related with the presence of graphitic species. Both S–H and N–H stretching bands are difficult to be identified in the functionalized AC and should appear between 2500 cm^{-1} and 2700 cm^{-1} and between 3100 cm^{-1} and 3400 cm^{-1} , respectively. Both pristine AC3 and AC-MPTMS also show an intense band at 3450 cm^{-1} , assigned to the presence of O–H stretching modes of the phenolic or hydroxyl groups (Larkin, 2011; Adar, 2016).

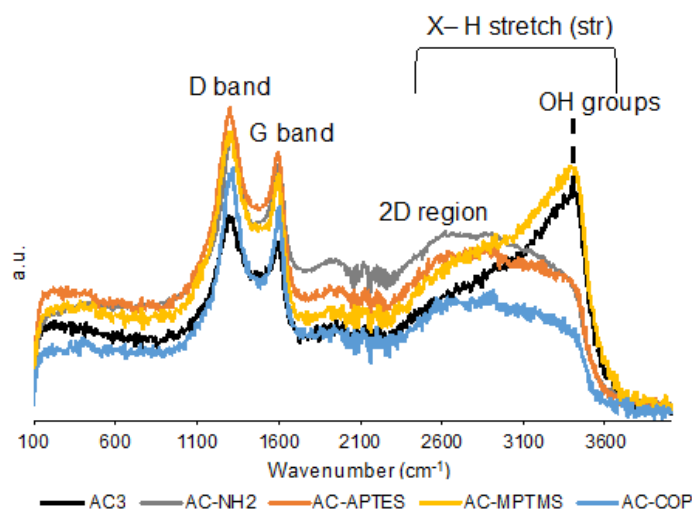


Figure 8.5. Raman spectra of AC3 and functionalized AC. X can be C, S, N or O atoms.

Table 8.3 shows the elemental analysis results for AC3 and functionalized AC. The aromatic amination of the phenylene moieties of the parent AC3 (AC-NH₂) was successfully achieved by incorporation of 3.3 % of nitrogen content. The AC-APTES and AC-MPTMS display 2.6 % and 2.7 % of N and S, respectively, demonstrating that the grafting reaction of APTES and MPTMS functionalities with the free OH groups of the AC3 was effectively accomplished. These results are in agreement with those obtained by FTIR analysis (Figure 8.4). The AC-COP has the highest N content (11.2 %) among the materials produced in this work while its S content is negligible (0.2 %).

The point of zero charge (pH_{pzc}) of each of the produced materials is also depicted in Table 8.3. As it may be seen, the lowest pH_{pzc} is that of AC3 ($\text{pH}_{pzc} = 3.9$), while the functionalized materials displayed values between 4.9 (AC-COP) and 6.6 (AC-APTES).

Table 8.3. Elemental analyses and point of zero charge (pH_{pzc}) results for AC3 and functionalized AC.

Sample	% C	% H	% N	% S	H/C	pH_{pzc}
AC3	58.2	1.1	0.6	0.3	0.019	3.9
AC-NH ₂	50.1	3.2	3.3	0.5	0.064	5.2
AC-APTES	54.1	2.2	2.6	0.6	0.040	6.6
AC-MPTMS	55.7	1.0	0.4	2.7	0.018	5.2
AC-COP	51.3	2.9	11.2	0.2	0.057	4.9

The survey XPS spectra for AC-NH₂, AC-MPTMS, and AC3 are shown in Figure 8.6 along with the respective high-resolution spectra for C1s, O1s, N1s and S2p+Si2s. The results regarding the fittings and the possible bond assignments are presented in Table 8.4.

The overview spectra (Figure 8.6) show that all carbon materials present a high content in carbon followed by oxygen. In the AC-NH₂ overview spectrum it is possible to observe a peak in the N1s region, and in the AC-MPTMS spectrum a double peak in the S2p+Si2s region is observed, confirming that the functionalization of the AC3 succeeded. Also, in the case of AC-NH₂, a peak associated to the presence of Sn (around 490-488 eV) can be observed, possibly due to the use of SnCl₂ in the synthesis process.

The high-resolution spectra for C1s show that the majority of the carbon is in the graphitic form (sp^2) and as C–C and C–H (sp^3) on the edge of graphene sheets (Velo-Gala et al., 2014). The peak at 287.2 eV is generally associated to carbon-oxygen bonds, however, some authors also ascribed this peak to C=N and C–N bonds (Gaspar et al., 2011; Velo-Gala et al., 2014; Susi et al., 2015; Lee et al., 2016). The appearance or increase of this peak is expected in silylated materials (AC-MPTMS) and have been attributed to the new C–O bonds due to the unreacted alkoxy groups in organosilane (Gaspar et al., 2011). The peaks at 288-289 eV can be attributed to O–C=O from carboxylic groups, anhydrides and esters (Velo-Gala et al., 2014; Lee et al., 2016) and in the case of AC-MPTMS, may be due to the presence of unreacted carboxyls.

In the N1s spectrum of AC-NH₂, the peaks at 399.6 eV and 400.3 eV are in accordance with the peak at 286.2 eV in C1s (Gaspar et al., 2011; Figueiredo, 2013; Lee et al., 2016). Also, the peak at 402.8 eV, attributed to the presence of some oxidized forms of nitrogen (Figueiredo and Pereira, 2010; Gaspar et al., 2011; Velo-Gala et al., 2014; Susi et al., 2015; Lee et al., 2016; Wei et al., 2016), may be due to residual unreactive C–NO₂ species from the reduction step of the synthesis.

The O1s spectra of the different materials are very distinct from each other, indicating the presence of the same functionalities but at very different relative intensities. The peaks at 531-532 eV present a higher relative intensity for AC-MPTMS, which may be due to residual components of the synthesis.

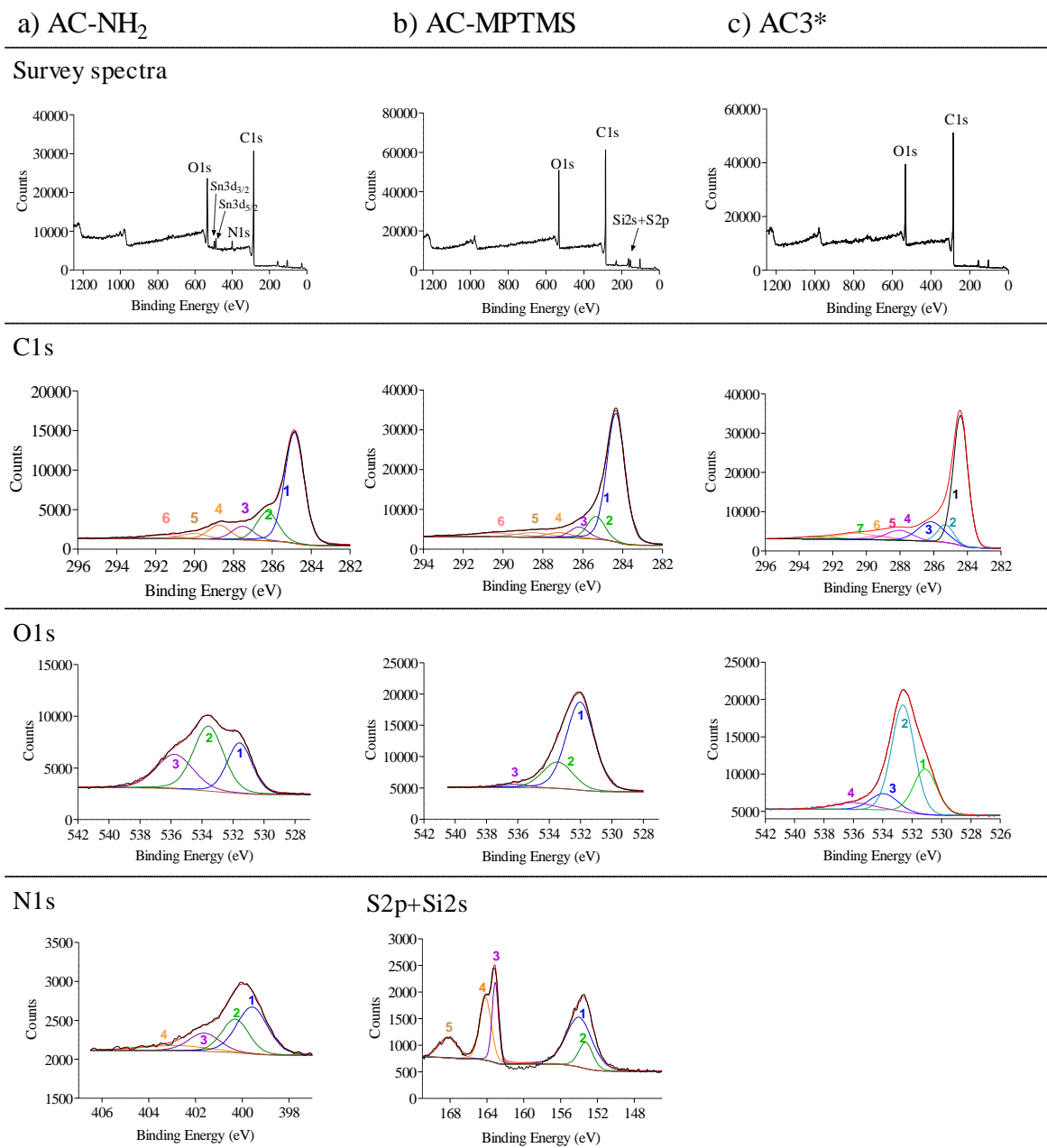


Figure 8.6. XPS survey spectra and high-resolution XPS spectra of C1s, N1s, S2p+Si2s, and O1s for: a) AC-NH₂, b) AC-MPTMS, and c) AC3* (results from chapter 5).

Table 8.4. X-Ray photoelectron spectroscopy (XPS) results for AC3*, AC-NH₂, and AC-MPTMS.

		AC-NH ₂	AC-MPTMS	AC3*	Possible bond assignment
C 1s	1	284.9	284.3	284.4	Graphitic C (sp ²) ^a
	2		285.3	285.3	C–C on the edge of graphene sheets (sp ³) C–H ^a
		286.2			Single bond C–O (phenolic or hydroxyl groups) ^{a,b}
	3		286.2	286.1	C–C bonds from the organosilane alkyl chain ^c (for AC-MPTMS)
		287.2			C–N bonds of aliphatic amines groups or due to the incomplete reduction of C–NO ₂ in the synthesis step ^{c,d} (in particular for AC-NH ₂)
	4	288.7	287.2		Carbon-oxygen bonds; C=N and C–N bonds ^{a,c,e,f}
5		288.5	289.2	C–O bonds due to the unreacted alkoxy groups in organosilane ^c (for AC-MPTMS)	
	290.0			O–C=O from carboxylic groups, anhydrides and esters ^{a,e}	
6		290.4	290.5	π - π^* transitions in C ^a	
	291.7			Plasmon band in C ^g	
O 1s	1	531.6	532.0	531.1	Carbonyl (–C=O) oxygen atoms in lactones, anhydrides and oxygen atoms in hydroxyl groups ^{a,h}
	2	533.6	533.5	532.6	–C–O–C– in ether and phenol groups ^c
	3			533.9	Oxygen in carboxylic groups (–COOH or –COOR) ^a
	4	535.8	536.1		Chemisorbed water or oxygen ^a
			536		
N 1s	1	399.6		397.7	Nitrogen from amine, imine or amide groups (–NH ₂ , C=N, N–C=O) ^{c,e,h}
	2	400.3		399.6	Pyridonic or pyrrolic nitrogen (N5) ^{a,c–f,i}
	3	401.6		401.5	Quaternary nitrogen (N–Q) ^{a,c–f,i}
	4	402.9		402.9	Nitrogen oxides or nitrates (N–X) ^{a,c–f,i}
Si2s+S2p	1		153.3		Silanes ⁱ
	2		154.0		
	3		163.1		Thiol moieties (–SH) ^{c,j}
	4		164.1		Sulfur-carbon (S–C) bonds ^{c,j}
	5		168.2		Sulfoxide groups ^k

* results from chapter 5

^a Velo-Gala et al., 2014^b Ma et al., 2014^c Gaspar et al., 2011^d Figueiredo and Pereira, 2010^e Lee et al., 2016^f Susi et al., 2015^g Zhu et al., 2008^h Figueiredo et al., 1999ⁱ Wei et al., 2016^j Martín-García et al., 2015^k Roberts et al., 2015

The thermal stability of the materials was assessed by TGA up to 800 °C and both the TGA and derivative TGA (DrTGA) results are presented in Figure 8.7. The first weight loss observed below 150 °C is related to desorption of physisorbed water. The parent AC3 presents a second decomposition at 210 °C of 3 % that can be assigned to the decomposition and release of hydroxyl and carboxylic acid groups of the AC3 surface. The decomposition and release of other organic moieties of the AC3 starts around 350 °C. The modification of the phenylene moieties of the AC3 with the NH₂ groups was confirmed by TGA. The functional groups produced by the nitration/oxidation of the AC3 material and amine functionalization decompose at temperatures below 400 °C. The organic moieties' degradation and release of the AC material occurs below 615 °C (with maximum at 535 °C). The grafting modification of the AC3 with APTES and MPTMS leads to a slight increase in the thermal stability of the material, with the decomposition and release of amino-propyl ($\approx 9\%$) and mercapto-propyl ($\approx 6\%$) groups at 220 °C and 265 °C, respectively, followed by the decomposition of the materials that starts at approximately 390 °C. In the case of AC-COP, it presents a TGA curve that is very similar to that observed by Mines et al. (2017) for a COP functionalized AC.

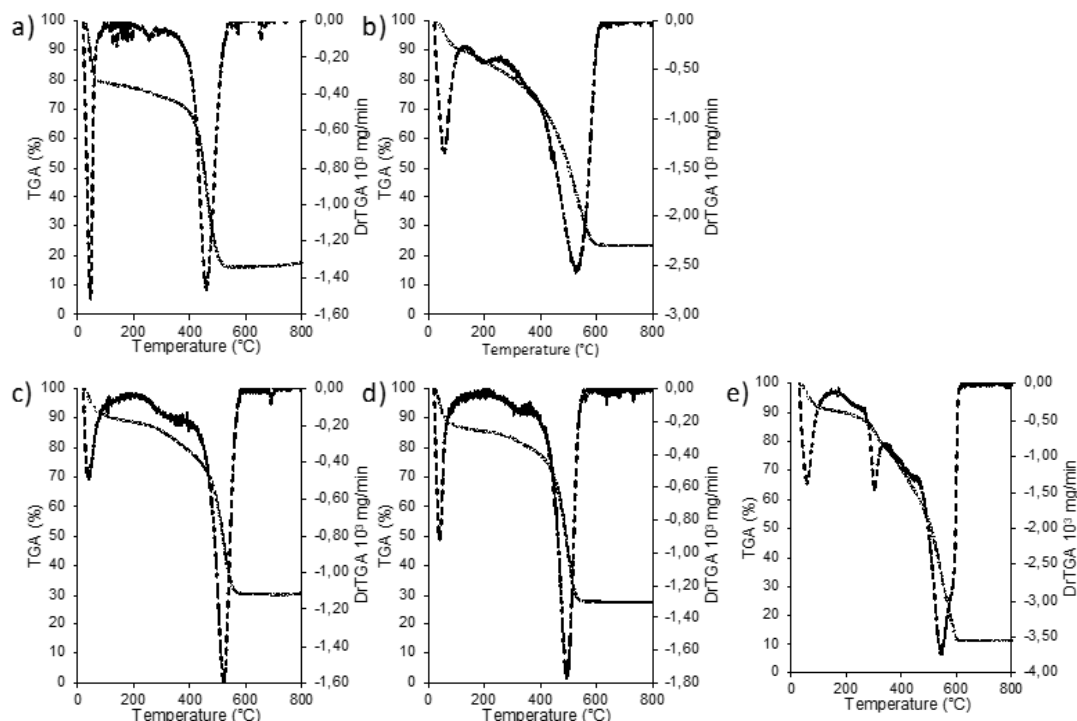


Figure 8.7. TGA and DrTGA of a) AC3, b) AC-NH₂, c) AC-APTES, d) AC-MPTMS, and e) AC-COP. Note: Different scales in the secondary yy axis (DrTGA) were chosen in each figure for a better visualization of results.

8.3.2. Adsorptive removal of pharmaceuticals from water

The results concerning the single adsorption of the pharmaceuticals onto AC3 and the functionalized materials are presented in Figure 8.8. Overall, among all the materials, AC-APTES is the one that presents lower adsorption percentages while AC3 and AC-MPTMS display the greater efficiencies for the pharmaceuticals considered. In any case, the adsorption of each pharmaceutical was very different, with PAR being the most adsorbed one, except for AC-MPTMS in ultrapure water and AC-APTES in ultrapure water and ultrapure water at pH 7.6. Contrarily, SMX was generally poorly adsorbed, except for AC-MPTMS, which furthermore showed larger SMX adsorption in the wastewater than in the other matrixes.

PAR presents, in all matrices, a positive net charge, which means that, in ultrapure water, π -cation interactions can be present, and in the matrices at pH 7.6 electrostatic interactions are likely to highly favor adsorption due to the negative net charge of the materials at this pH (as for the pH_{pzc} in Table 8.3). Furthermore, PAR has a fluorine atom, the most electronegative halogen, which may potentiate hydrogen bonds with hydrogen bond donors such as C–H, N–H, and O–H present in the AC surfaces in the form of amines, hydroxyls and carboxyls. This may explain the differences in the adsorption of VEN, which is also positively charged in all matrices, but is consistently less adsorbed by all the AC.

Regarding CBZ and LOR, they are in their non-ionizable form ($pK_{a,CBZ} = 2.3$ and 13.9 ; $pK_{a,LOR} = 1.3$ and 11.5) in the three matrices, hence electrostatic interactions may not play a significant role in their adsorption. Some authors (Cai and Larese-Casanova, 2014; Hofman-Caris et al., 2015; Baghdadi et al., 2016; Chen et al., 2017) have suggested that the adsorption of CBZ onto carbon materials (such as AC, graphene, carbon nanotubes) is ruled by aromatic-aromatic interactions due to the formation of π - π electron donor-acceptor (EDA) complex between CBZ benzene ring (π -electron acceptor) and the aromatic benzene rings of AC or electron-rich carbonyl groups (π -electron donors).

SMX and PIR adsorption from ultrapure water is quite larger onto AC3 than onto the functionalized materials, except for AC-MPTMS. If just affected by pH related electrostatic interactions, the adsorption of these two pharmaceuticals would be expected to decrease in ultrapure water at pH 7.6 and wastewater, where they are mainly in their negative form and AC also have a negative net charge. However, this is not fully verified for the adsorption of SMX onto AC3 and AC-MPTMS and so some specific interactions may be underneath. It has been referred that when the interactions between adsorbate and adsorbent include repulsive electrostatic forces, the increase in the ionic strength may

favor adsorption (Reguyal and Sarmah, 2018), which could explain the relatively high adsorption of SMX onto AC-MPTMS in wastewater matrix.

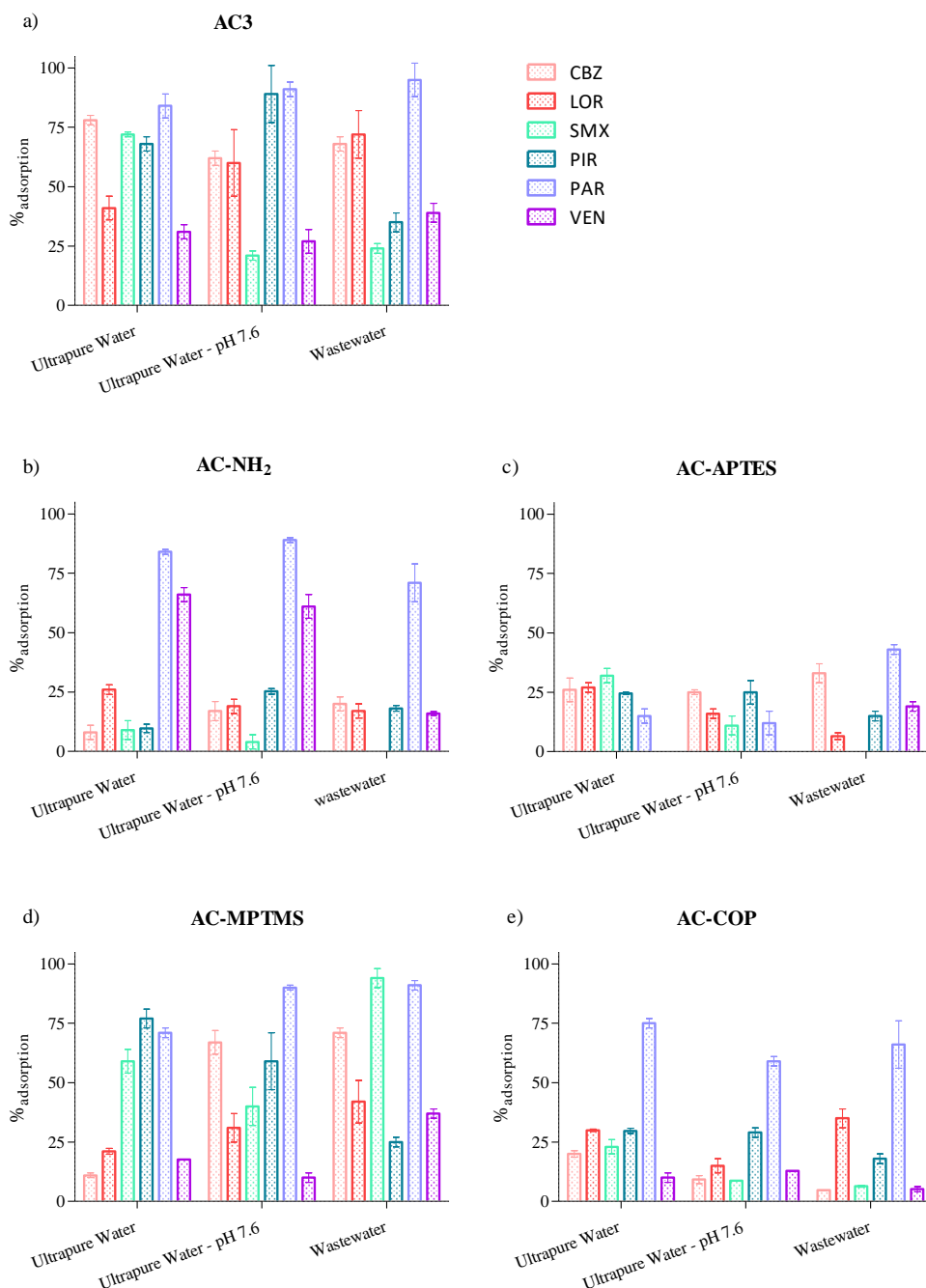


Figure 8.8. Adsorption of the six studied pharmaceuticals (CBZ, LOR, SMX, PIR, PAR and VEN) in different matrices (ultrapure water, ultrapure water at pH 7.6 and wastewater) onto the AC3 and the functionalized AC. Error bars correspond to the standard deviation (n=3).

It is important to note that the adsorption process in wastewater matrix may be influenced by the presence of organic matter and also the ionic strength (Arafat et al., 1999; Reguyal and Sarmah, 2018), which can either positively or negatively influence the adsorption depending on the adsorbent and the adsorbate. This can be clearly seen in this study, where no apparent similar pattern is observed when changing the test matrix from ultrapure water to wastewater.

A principal component analysis (PCA) was carried out in order to find out possible correlations between the normalized adsorption percentages and the physicochemical properties of the studied pharmaceuticals. Results are shown in Figure 8.9, which evidences that the pharmaceuticals are assembled in three groups: (i) SMX and PIR; (ii) CBZ, LOR and VEN; (iii) PAR. Adsorption onto AC-NH₂ appears to be especially affected by the pharmaceuticals hydrophobicity ($\log K_{ow}$) and solubility (S_w) while onto AC-COP, S_w is the most relevant property. Meanwhile, for AC-MPTMS and AC-APTES, the polar surface area (PSA) and the number of H bond acceptors (Hbond-ac) are generally the main properties influencing the pharmaceuticals adsorption.

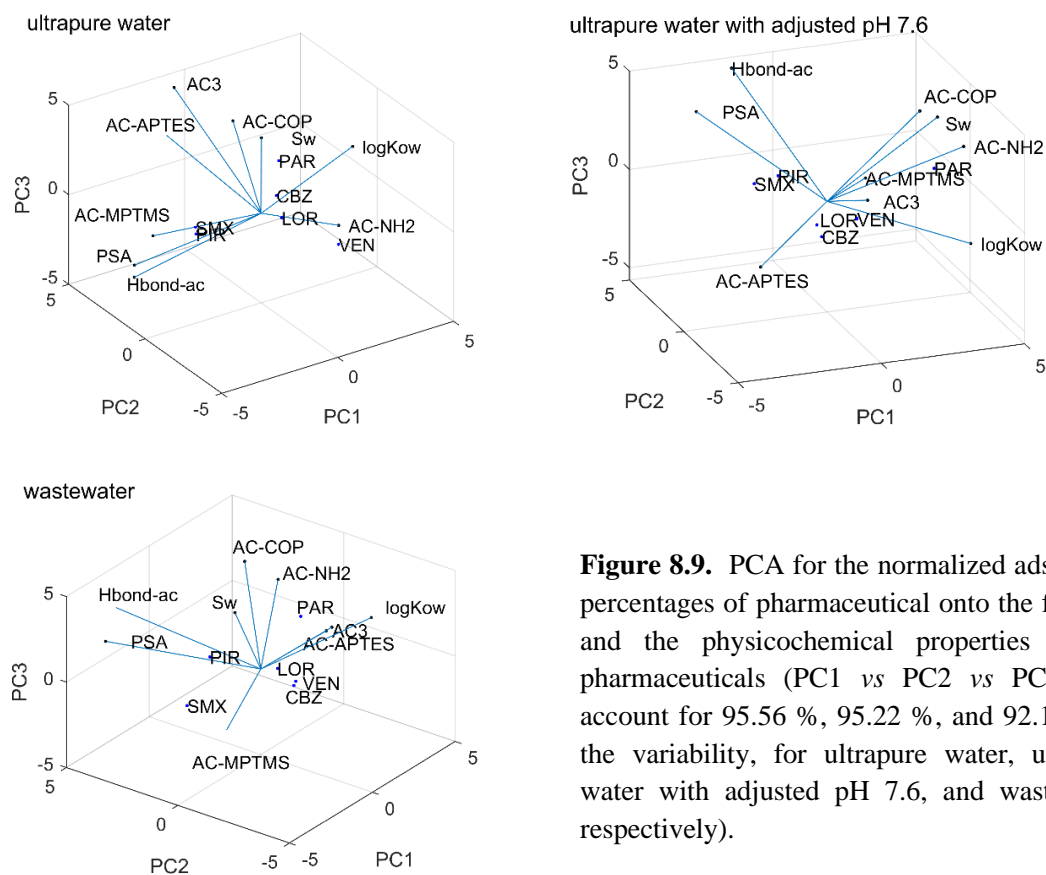


Figure 8.9. PCA for the normalized adsorption percentages of pharmaceutical onto the five AC and the physicochemical properties of the pharmaceuticals (PC1 vs PC2 vs PC3 plots account for 95.56 %, 95.22 %, and 92.17 % of the variability, for ultrapure water, ultrapure water with adjusted pH 7.6, and wastewater, respectively).

In order to find out if there was any relation between the adsorption of pharmaceuticals and the S_{BET} , data on the adsorption percentage were normalized for the S_{BET} of the materials, as depicted in Figure 8.10. The normalization shows that the AC-NH₂ is the material having the largest adsorption regarding its S_{BET} . Also, Figure 8.10 further evidences the selectivity of AC-NH₂ for the antidepressants PAR and VEN for both ultrapure water matrices (no pH adjustment and pH adjusted to 7.6) and for PAR in wastewater matrix, that was intuited in Figure 8.8, so indicating that the S_{BET} is not the main factor influencing the adsorption of these two drugs. Some selectivity not related with S_{BET} may be also perceived for the adsorption of PAR by AC-COP (Figure 8.10). For a more comprehensive analysis of the results, a PCA concerning the AC properties and the adsorption percentage of the pharmaceuticals was applied to the experimental data (results are presented in Figure 8.11). The first and second principal components (PC1 and PC2, respectively) account for 80.5 % of the variability while the three components (PC1, PC2, and PC3) account for 93.7 % of the variability, therefore, the three components were considered for the analysis.

The PCA plots (Figure 8.11), in particular those concerning PC1, evidence that the adsorption of the considered pharmaceuticals from the three matrices is mostly influenced by the S_{BET} , S_{micro} and W_0 of the AC. However, and despite AC3 and AC-MPTMS having similar S_{BET} , the adsorption percentages of all pharmaceuticals, except SMX, is mostly equal or higher onto AC3. Therefore, other factors may be influencing the adsorption of these pharmaceuticals in these matrices. One of those factors may be related to the pore size distribution (Figure 8.2). AC3 has a higher cumulative pore volume in the range of 3-5 nm (mesopores) while AC-MPTMS has a greater prevalence of pores in the range of 1-2 nm (micropores). This difference can be an important factor concerning the adsorption of pharmaceuticals, which, in principle, is favored by the presence of mesopores due to their large molecular size.

As illustrated by Figure 8.11, total pore volume (V_p) and surface functionality, namely, the amount of sulfur heteroatoms (% S) also seem to play a role in the adsorption of the studied pharmaceuticals while the content in nitrogen (% N) looks as having little influence (Figure 8.11, plots PC1 vs PC2 and PC1 vs PC3). The latter is evidenced by the fact that AC-APTES, which is the material with the highest % N, displays visibly lower adsorption for all systems. In fact, even AC-NH₂, which possesses the smallest S_{BET} , shows greater adsorption percentages, in particular for positively charged pharmaceuticals (PAR and VEN), in comparison with AC-APTES. The higher adsorption of PAR and VEN onto AC-NH₂ as compared with AC-APTES, which is especially interesting since these materials are both aminated, cannot be explained by the textural properties. Therefore, it may be related to differences in the surface chemistry of the materials. AC-NH₂ has aromatic amino groups at the surface, while AC-APTES has propyl amino groups. Additionally, AC-NH₂ also presents tin oxide (SnO₂)

nanoparticles that can influence the interaction with PAR and VEN (Figure 8.6a). Thus, this improvement in the adsorption properties of the AC-NH₂ can be also related to acid–base and electrostatic interactions of PAR and VEN drugs with the Lewis acid sites of SnO₂ (Shamsizadeh et al., 2014; Vidal et al., 2015).

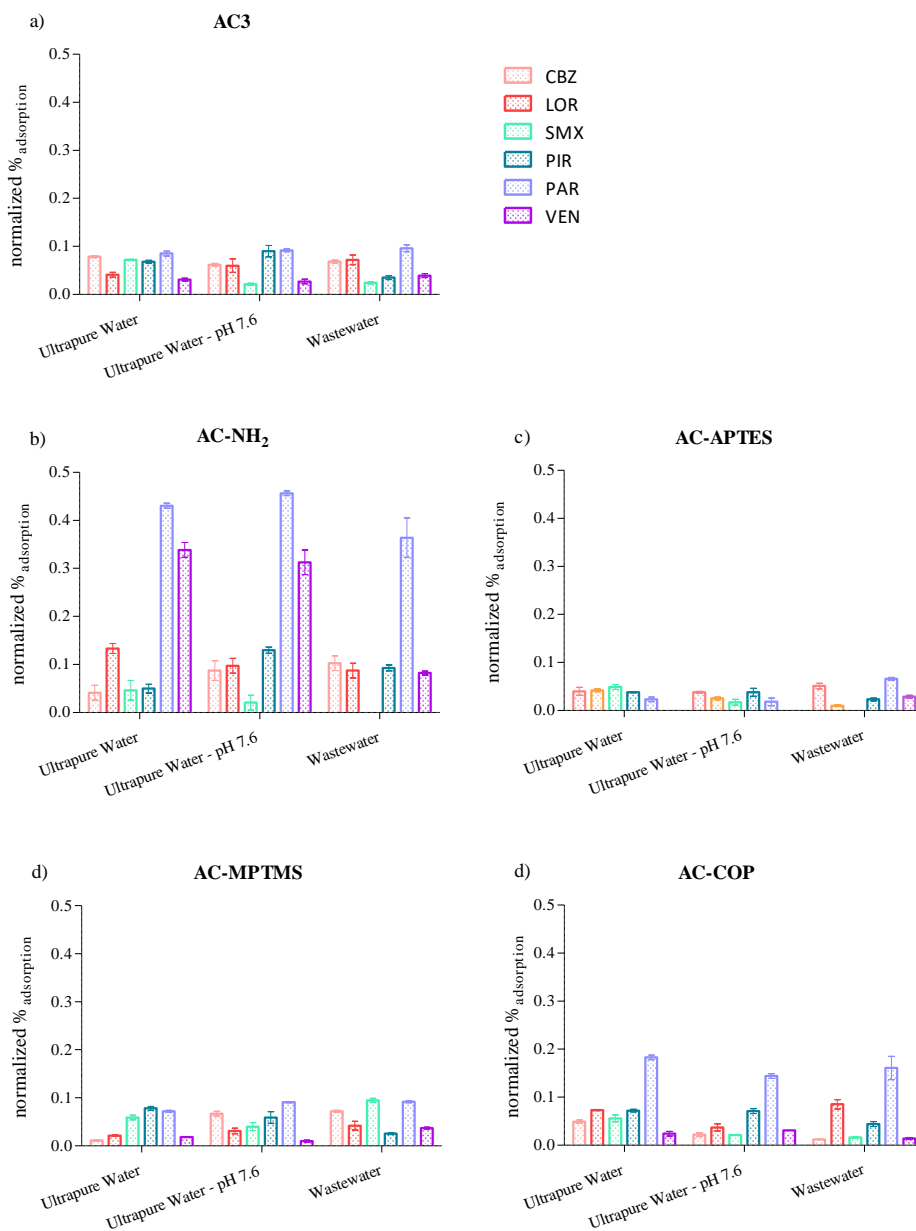


Figure 8.10. Adsorption of the six studied pharmaceuticals in different matrices onto the AC3 and the functionalized AC, normalized to the S_{BET} for each AC. Error bars correspond to standard deviations ($n = 3$).

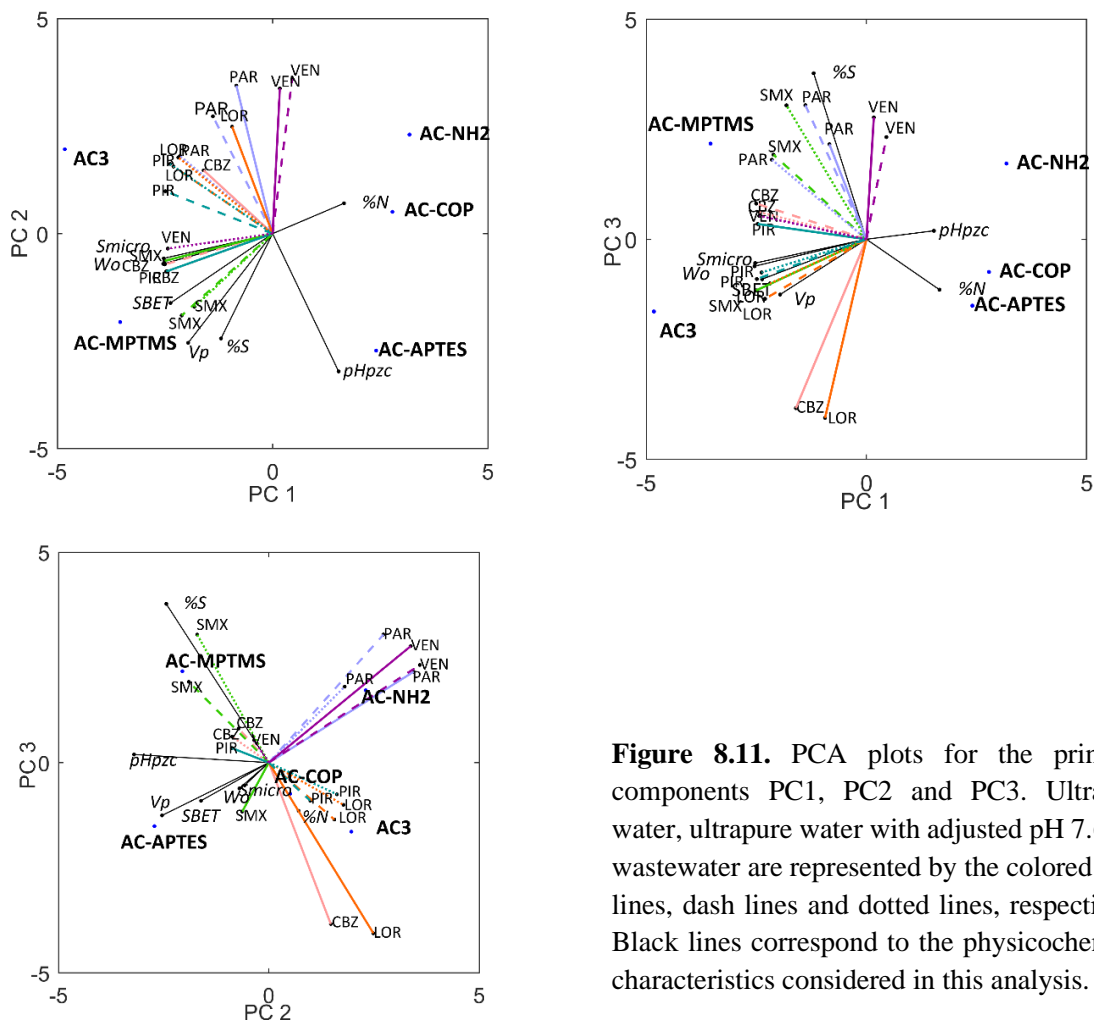


Figure 8.11. PCA plots for the principal components PC1, PC2 and PC3. Ultrapure water, ultrapure water with adjusted pH 7.6 and wastewater are represented by the colored solid lines, dash lines and dotted lines, respectively. Black lines correspond to the physicochemical characteristics considered in this analysis.

Apart from the previously commented, another materials' property included in the PCA was pH_{pzc} . pH is known to have an important role in the adsorption mechanism as it affects the protonation or deprotonation of the adsorbates and the surface charge of the AC (Song et al., 2017). The introduction of different functionalities onto the AC3 surface resulted in materials with different pH_{pzc} (between 3.9 and 6.6, Table 8.3). Still, in each matrix, all the AC are in the same protonation state. Thereupon, as for the PCA results (Figure 8.11), pH_{pzc} appears to have no relevant influence in the adsorption of the studied pharmaceuticals.

In view of the above results, it may be stated that, globally, the parent AC3 followed by AC-MPTMS were the materials providing the best adsorptive performance for the considered

pharmaceuticals and matrices. This must be related with the reduction in S_{BET} that resulted from functionalization (except for AC-MPTMS). Still, it was here observed that some functionalized AC shown remarkable properties and/or a distinct behavior that may be useful for specific applications. Considering that this is a pioneer work on the functionalization of waste derived AC, the obtained results are the basis for a novel research line. In order to further elucidate the mechanistic aspects that rule the adsorption process, in particular for the materials that presented the best removal percentages, kinetic, equilibrium and thermodynamic studies will be the focus of the following chapter.

8.4. Conclusions

The functionalization of a PS-based AC was successfully achieved considering the addition of the specific functional groups onto the AC3: amine groups (AC-NH₂ and AC-APTES), sulfonic groups (AC-MPTMS), and a covalent organic polymer (AC-COP). Comparatively with the parent AC3, this addition resulted in the reduction of both S_{BET} and S_{micro} for all materials with exception of AC-MPTMS, for which just S_{micro} decreased. The application of the functionalized AC in the removal of the six pharmaceuticals considered in this study (CBZ, LOR, SMX, PIR, PAR, and VEN) from ultrapure water, ultrapure water at pH 7.6 and wastewater revealed that the adsorption of each pharmaceutical in each matrix showed distinct patterns, with the non-functionalized AC3 mostly displaying the best performance. Textural parameters, namely S_{BET} , S_{micro} and W_0 had the greatest influence in the adsorption of these pharmaceuticals, with V_p and % S also playing a role and % N having little repercussion. On the other hand, according to their pH_{pzc} , the produced AC were all at the same protonation state in each matrix, making it difficult to infer if pH_{pzc} was a key property for the adsorption of the pharmaceuticals onto the studied AC.

Regarding the impacts of functionalization for the target application, it may be said that grafting the organic polymer is a time-consuming process and AC-COP did not present any enhancement in the adsorption of pharmaceuticals. When comparing AC-APTES with AC-NH₂, despite the former having highest S_{BET} , it showed a poorer performance than AC-NH₂. On the other hand, AC-NH₂ showed some specificity for the antidepressants PAR and VEN, which may be advantageous. As regards AC-MPTMS, it was the functionalized material providing the best global performance, which was almost comparable to that of the parent AC3. Moreover, the remarkable affinity of AC-MPTMS for SMX in wastewater may be a relevant feature for specific applications. Overall, despite the decrease of the adsorption

properties of the AC3 after functionalization, the selectivity of the AC3 modified with MPTMS and aromatic amino groups increases, which is advantageous for the selective removal of pharmaceuticals.

8.5. References

- Adar, F., 2016. Introduction to Interpretation of Raman Spectra Using Database Searching and Functional Group Detection and Identification. pp. 16-23.
- Alcaraz, L., Lopez Fernández, A., García-Díaz, I., Lix, F., Lopez, A.L., 2018. Preparation and characterization of activated carbons from winemaking wastes and their adsorption of methylene blue. *Adsorpt. Sci. Technol.* 36, 1331-1351.
- Arafat, H.A., Franz, M., Pinto, N.G., 1999. Effect of Salt on the Mechanism of Adsorption of Aromatics on Activated Carbon. *Langmuir* 15, 5997-6003.
- Baghdadi, M., Ghaffari, E., Aminzadeh, B., 2016. Removal of carbamazepine from municipal wastewater effluent using optimally synthesized magnetic activated carbon: Adsorption and sedimentation kinetic studies. *J. Environ. Chem. Eng.* 4, 3309-3321.
- Bhadra, B.N., Seo, P.W., Jung, S.H., 2016. Adsorption of diclofenac sodium from water using oxidized activated carbon. *Chem. Eng. J.* 301, 27-34.
- Bhatnagar, A., Hogland, W., Marques, M., Sillanpää, M., 2013. An overview of the modification methods of activated carbon for its water treatment applications. *Chem. Eng. J.* 219, 499-511.
- Cai, N., Larese-Casanova, P., 2014. Sorption of carbamazepine by commercial graphene oxides: a comparative study with granular activated carbon and multiwalled carbon nanotubes. *J. Colloid. Interf. Sci.* 426, 152-161.
- Chen, D., Xie, S., Chen, C., Quan, H., Hua, L., Luo, X., Guo, L., 2017. Activated biochar derived from pomelo peel as a high-capacity sorbent for removal of carbamazepine from aqueous solution. *RSC Adv.* 7, 54960-54979.
- Figueiredo, J.L., 2013. Functionalization of porous carbons for catalytic applications. *J. Mater. Chem. A* 1, 9351-9364.
- Figueiredo, J.L., Pereira, M.F.R., 2010. The role of surface chemistry in catalysis with carbons. *Catal. Today* 150, 2-7.
- Figueiredo, J.L., Pereira, M.F.R., Freitas, M.M.A., Órfão, J.J.M., 1999. Modification of the surface chemistry of activated carbons. *Carbon* 37, 1379-1389.
- Gaspar, H., Pereira, C., Rebelo, S.L.H., Pereira, M.F.R., Figueiredo, J.L., Freire, C., 2011. Understanding the silylation reaction of multi-walled carbon nanotubes. *Carbon* 49, 3441-3453.
- Glonek, K., Wróblewska, A., Makuch, E., Ulejczyk, B., Krawczyk, K., Wróbel, R.J., Koren, Z.C., Michalkiewicz, B., 2017. Oxidation of limonene using activated carbon modified in dielectric barrier discharge plasma. *Appl. Surf. Sci.* 420, 873-881.
- Guedidi, H., Reinert, L., Soneda, Y., Bellakhal, N., Duclaux, L., 2017. Adsorption of ibuprofen from aqueous solution on chemically surface-modified activated carbon cloths. *Arab. J. Chem.* 10, S3584-S3594.

- Hofman-Caris, C.H.M., Bauerlein, P.S., Siegers, W.G., Ziaie, J., Tolkamp, H.H., de Voogt, P., 2015. Affinity adsorption for the removal of organic micropollutants in drinking water sources; proof of principle. *Wa. Sci. Technol.* 15, 1207-1219.
- Inagaki, S., Guan, S., Ohsuna, T., Terasaki, O., 2002. An ordered mesoporous organosilica hybrid material with a crystal-like wall structure. *Nature* 416, 304-307.
- Larkin, P., 2011. Infrared and Raman Spectroscopy Principles and Spectral Interpretation, 1st ed. Elsevier, USA.
- Lebègue, E., Brousse, T., Gaubicher, J., Cougnon, C., 2013a. Chemical functionalization of activated carbon through radical and diradical intermediates. *Electrochem. Commun.* 34, 14-17.
- Lebègue, E., Brousse, T., Gaubicher, J., Cougnon, C., 2013b. Spontaneous arylation of activated carbon from aminobenzene organic acids as source of diazonium ions in mild conditions. *Electrochim. Acta* 88, 680-687.
- Lebègue, E., Madec, L., Brousse, T., Gaubicher, J., Levillain, E., Cougnon, C., 2011. Modification of activated carbons based on diazonium ions in situ produced from aminobenzene organic acid without addition of other acid. *J. Mater. Chem.* 21, 12221-12223.
- Lee, M.S., Park, M., Kim, H.Y., Park, S.J., 2016. Effects of Microporosity and Surface Chemistry on Separation Performances of N-Containing Pitch-Based Activated Carbons for CO₂/N₂ Binary Mixture. *Sci. Rep.* 6, 1-11.
- Lourenço, M.A.O., Figueira, P., Pereira, E., Gomes, J.R.B., Lopes, C.B., Ferreira, P., 2017. Simple, mono and bifunctional periodic mesoporous organosilicas for removal of priority hazardous substances from water: The case of mercury(II). *Chem. Eng. J.* 322, 263-274.
- Lourenço, M.A.O., Siquet, C., Santos, J., Jorge, M., Gomes, J.R.B., Ferreira, P., 2016. Insights into CO₂ and CH₄ Adsorption by Pristine and Aromatic Amine-Modified Periodic Mesoporous Phenylene-Silicas. *J. Phys. Chem. C* 120, 14236-14245.
- Ma, X., Yang, H., Yu, L., Chen, Y., Li, Y., 2014. Preparation, surface and pore structure of high surface area activated carbon fibers from bamboo by steam activation. *Materials* 7, 4431-4441.
- Martín-García, B., Polovitsyn, A., Prato, M., Moreels, I., 2015. Efficient charge transfer in solution-processed PbS quantum dot-reduced graphene oxide hybrid materials. *J. Mater. Chem. C* 3, 7088-7095.
- Mines, P.D., Thirion, D., Uthuppu, B., Hwang, Y., Jakobsen, M.H., Andersen, H.R., Yavuz, C.T., 2017. Covalent organic polymer functionalization of activated carbon surfaces through acyl chloride for environmental clean-up. *Chem. Eng. J.* 309, 766-771.
- Ohashi, M., Kapoor, M.P., Inagaki, S., 2008. Chemical modification of crystal-like mesoporous phenylene-silica with amino group. *Chem. Commun.*, 841-843.
- Pognon, G., Brousse, T., Bélanger, D., 2011. Effect of molecular grafting on the pore size distribution and the double layer capacitance of activated carbon for electrochemical double layer capacitors. *Carbon* 49, 1340-1348.

- PubChem online data base at <https://pubchem.ncbi.nlm.nih.gov>, accessed in February 7, 2019.
- Radkevich, V.Z., Senko, T.L., Wilson, K., Grishenko, L.M., Zaderko, A.N., Diyuk, V.Y., 2008. The influence of surface functionalization of activated carbon on palladium dispersion and catalytic activity in hydrogen oxidation. *Appl. Catal. A-Gen* 335, 241-251.
- Reguyal, F., Sarmah, A.K., 2018. Adsorption of sulfamethoxazole by magnetic biochar: Effects of pH, ionic strength, natural organic matter and 17alpha-ethinylestradiol. *Sci. Total Environ.* 628-629, 722-730.
- Rivera-Utrilla, J., Sánchez-Polo, M., Gómez-Serrano, V., Álvarez, P.M., Alvim-Ferraz, M.C.M., Dias, J.M., 2011. Activated carbon modifications to enhance its water treatment applications. An overview. *J. Hazard. Mater.* 187, 1-23.
- Roberts, A.D., Li, X., Zhang, H., 2015. Hierarchically porous sulfur-containing activated carbon monoliths via ice-templating and one-step pyrolysis. *Carbon* 95, 268-278.
- Shamsizadeh, A., Ghaedi, M., Ansari, A., Azizian, S., Purkait, M.K., 2014. Tin oxide nanoparticle loaded on activated carbon as new adsorbent for efficient removal of malachite green-oxalate: Non-linear kinetics and isotherm study. *J. Mol. Liq.* 195, 212-218.
- Sing, K.S.W., Everett, D.H., Haul, R.A.W., Moscou, L., Pierotti, R.A., Rouquerol, J., Siemieniewska, T., 1985. Reporting Physisorption Data for Gas/Solid Systems with Special Reference to the Determination of Surface Area and Porosity. *Pure Appl. Chem.* 57, 603-619.
- Song, J.Y., Bhadra, B.N., Jhung, S.H., 2017. Contribution of H-bond in adsorptive removal of pharmaceutical and personal care products from water using oxidized activated carbon. *Micropor. Mesopor. Mat.* 243, 221-228.
- Stavropoulos, G.G., Samaras, P., Sakellaropoulos, G.P., 2008. Effect of activated carbons modification on porosity, surface structure and phenol adsorption. *J. Hazard. Mater.* 151, 414-421.
- Susi, T., Pichler, T., Ayala, P., 2015. X-ray photoelectron spectroscopy of graphitic carbon nanomaterials doped with heteroatoms. *Beilstein J. Nanotechnol.* 6, 177-192.
- Velo-Gala, I., López-Peñalver, J.J., Sánchez-Polo, M., Rivera-Utrilla, J., 2014. Surface modifications of activated carbon by gamma irradiation. *Carbon* 67, 236-249.
- Vidal, C.B., dos Santos, A.B., do Nascimento, R.F., Bandosz, T.J., 2015. Reactive adsorption of pharmaceuticals on tin oxide pillared montmorillonite: Effect of visible light exposure. *Chem. Eng. J.* 259, 865-875.
- Wei, T., Zhang, Q., Wei, X., Gao, Y., Li, H., 2016. A Facile and Low-Cost Route to Heteroatom Doped Porous Carbon Derived from *Broussonetia Papyrifera* Bark with Excellent Supercapacitance and CO₂ Capture Performance. *Sci. Rep.* 6, 2-10.
- Yin, C.Y., Aroua, M.K., Daud, W.M.A.W., 2007. Review of modifications of activated carbon for enhancing contaminant uptakes from aqueous solutions. *Sep. Purif. Technol.* 52, 403-415.

Zhu, M., Weber, C.J., Yang, Y., Konuma, M., Starke, U., Kern, K., Bittner, A.M., 2008. Chemical and electrochemical ageing of carbon materials used in supercapacitor electrodes. *Carbon* 46, 1829-1840.

9

EFFECTS OF THIOL FUNCTIONALIZATION OF A WASTE-DERIVED ACTIVATED CARBON ON THE ADSORPTION OF SULFAMETHOXAZOLE FROM WATER: KINETIC, EQUILIBRIUM AND THERMODYNAMIC STUDIES

Abstract

An activated carbon (AC) was produced from paper mill sludge (AC3) and functionalized with thiol groups (AC-MPTMS) for the adsorptive removal of the antibiotic sulfamethoxazole (SMX) from ultrapure buffered solution (pH 8) and real wastewater. The physicochemical properties of the two materials showed some differences between them, mainly in specific surface area (S_{BET}), in the type of oxygen functional groups and in the relative percentage of sulphur groups. The adsorption results showed a decrease in the Langmuir adsorption capacity (q_m) upon an increase on temperature (15 °C, 25 °C and 35 °C), varying between $(113 \pm 7) \text{ mg g}^{-1}$ and $(42 \pm 1) \text{ mg g}^{-1}$ for AC3 and $(140 \pm 20) \text{ mg g}^{-1}$ and $(28.0 \pm 1.5) \text{ mg g}^{-1}$ for AC-MPTMS. Pseudo-second order model presented the best fit for the kinetic studies, with rate constants (k_2) increasing with temperature and varying from $(0.005 \pm 0.002) \text{ g mg}^{-1} \text{ min}^{-1}$ and $(0.013 \pm 0.004) \text{ g mg}^{-1} \text{ min}^{-1}$ for AC3 and $(0.006 \pm 0.002) \text{ g mg}^{-1} \text{ min}^{-1}$ and $(0.03 \pm 0.01) \text{ g mg}^{-1} \text{ min}^{-1}$ for AC-MPTMS. Both adsorbents showed very similar thermodynamic parameters, with the adsorption process being spontaneous ($-26 \text{ kJ mol}^{-1} < \Delta G^\circ < -40 \text{ kJ mol}^{-1}$), endothermic ($69 \text{ kJ mol}^{-1} < \Delta H^\circ < 78 \text{ kJ mol}^{-1}$) and entropically favorable ($356 \text{ J mol}^{-1} \text{ K}^{-1} < \Delta S^\circ < 365 \text{ J mol}^{-1} \text{ K}^{-1}$). The adsorption of SMX from real wastewater by AC-MPTMS showed a reduction of the adsorption velocity and capacity as compared with ultrapure buffered solution (pH 8), which was related with competitive effects by background organic matter.

This chapter was based on the published article:

Jaria, G., Calisto, V., Gil M. V., Ferreira, P., Santos, S., Otero, M., Esteves, V.I., 2021. Effects of thiol functionalization of a waste-derived activated carbon on the adsorption of sulfamethoxazole from water: kinetic, equilibrium and thermodynamic studies. *J. Mol. Liq.* 323, 115003.

9.1. Contextualization

The importance and influence of the physicochemical characteristics of activated carbons (AC) and the adsorbates properties in the adsorption process has been clearly observed along the previous chapters (chapters 5 and 8), where the removal of pharmaceuticals was highly dependent on the applied conditions. In chapter 8, it was observed that, in general, AC3 (a powdered activated carbon) produced from primary paper mill sludge (PS) and AC-MPTMS (an AC resulting from the thiol functionalization of AC3) presented the best results for the adsorption of the pharmaceuticals under study. The material AC-MPTMS appeared to present a higher affinity for the antibiotic sulfamethoxazole (SMX), even in wastewater (chapter 8), while AC3 had its adsorptive performance greatly reduced in the same matrix (chapters 5 and 8). Taking into account that SMX is a pharmaceutical which adsorption from wastewater is quite difficult (Guillossou et al., 2019; Patel et al., 2019), and that special attention should be given to its removal in order to restrict bacterial resistance issues, it was selected as target pharmaceutical for this study. For instance, in the work of Guillossou et al. (2019), where an AC adsorption pilot strategy was applied as tertiary treatment, it was verified that in the particular case of SMX, the removal percentage by conventional WWTP treatments was $-29 (\pm 53) \%$, increasing only to $34 (\pm 19) \%$ with the pilot advanced treatment with activated carbon (Guillossou et al., 2019).

Hence, considering the results of chapter 5 and 8, in this work, AC3 and AC-MPTMS were applied in the adsorption of SMX from water and wastewater. Kinetic and equilibrium adsorption experiments were carried out at different temperatures and the thermodynamic parameters involved in the process were analyzed aiming to gain some insights concerning the adsorption mechanism.

9.2. Materials and Methods

9.2.1. Chemicals and reagents

The production of the AC3 was achieved using potassium hydroxide (KOH, EKA PELLETS, $\geq 86 \%$) as activating agent. For the chemical functionalization, the following reagents were used: (3-mercaptopropyl)trimethoxysilane (MPTMS, Aldrich, 95 %) and toluene (Aldrich, 99.8 %). The pharmaceutical SMX ($> 98 \%$) was purchased from TCI. Di-potassium hydrogen (K_2HPO_4 , PanReac AppliChem, 99.0 %), potassium dihydrogen phosphate (KH_2PO_4 , MERCK, 99.5 %), and ortho-phosphoric acid (H_3PO_4 , Panreac, 85.0 %) were used for pH adjustment and control.

For the analytical determination of SMX in the aqueous phase by Micellar Electrokinetic Chromatography (MEKC), as described in Appendix B2.

All the solutions were prepared in ultrapure water obtained from a Milli-Q Millipore system (Milli-Q plus 185).

9.2.2. Material synthesis and characterization

9.2.2.1. Production of the alternative activated carbon (AC3) and thiol functionalized AC3 (AC-MPTMS)

AC3 synthesis

In this chapter the production of the parent AC was performed according to the production conditions of experiment 3 of the full factorial design, described in chapter 4 (AC3). A new batch of material was exclusively produced for this work. Briefly, PS was impregnated with KOH in a 1:1 ratio (*w/w*), air dried and pyrolysed at 800 °C for 150 min. The obtained carbon material was washed with hydrochloric acid 1.2 M and then with distilled water until neutral pH of the washing leachate. After filtration, AC3 was oven dried at 105 °C for 24 h.

Synthesis of AC-MPTMS by organosilane grafting

Organosilane grafting of the produced AC3 with (3-mercaptopropyl)trimethoxysilane was performed as described in chapter 8 in order to produce AC-MPTMS. A new batch of material was exclusively produced for this work. Briefly, AC3 was first activated in vacuum, and then 10 mL of dry toluene were added to 0.250 g of the material. Next, 0.308 mL of MPTMS were added drop wise to the suspension to obtain AC-MPTMS. The mixture was vigorously stirred for 24 h under nitrogen atmosphere. The functionalized AC was filtered, washed with toluene, and further washed with distilled water. The filtered material was oven dried at 60 °C overnight.

9.2.2.2. Methods for physicochemical characterization of the synthesized materials

The physicochemical characterization of AC3 and AC-MPTMS was performed by the determination of S_{BET} and microporous volume (W_0), X-ray photoelectron spectroscopy (XPS), and scanning electron microscopy (SEM). More information concerning the used characterization techniques (specific methods, equipment models and conditions used) can be found in the APPENDIX A, sections A1, A2.1, and A2.2. The characterization results presented are related to the batches of AC3 and AC-MPTMS produced for and used in this work.

9.2.3. Adsorption experiments

Using AC3 and AC-MPTMS as adsorbents, kinetic and equilibrium studies on the adsorption of SMX were performed in batch mode and under stirring at 80 rpm in an overhead shaker (Heidolph, Reax 2). Experiments with ultrapure water solutions were carried out at three different temperatures (15 °C, 25 °C and 35 °C) and at buffered pH 8, which was chosen to be close to the pH of wastewater. For the pH adjustment, SMX solutions were prepared in phosphate buffer 0.01 M using 94 mL of 0.1 M K_2HPO_4 and 6 mL of 0.1 M KH_2PO_4 for 1 L of solution. When necessary, H_3PO_4 1M or KOH 1M were used to tune the final pH.

The adsorptive performance of AC-MPTMS was also assessed in a real matrix, namely the effluent from the local WWTP (described in chapter 5, section 5.2.4). For that purpose, batch adsorption experiments under stirring (80 rpm) were carried out at 25 °C using SMX solutions prepared in wastewater collected in May 2019 at the outlet of the WWTP, namely after secondary decanting, which corresponds to the effluent that is discharged into the aquatic environment. After collection, wastewater was filtered and characterized as described in chapter 5 (section 5.2.4). and analyzed by micellar electrokinetic chromatography (MEKC) as described on Appendix B, section B2.

9.2.3.1. Kinetic studies

Kinetic studies were performed to determine the time necessary to reach the equilibrium (t_e) for the adsorption of SMX onto AC3 and AC-MPTMS. For experiments in buffered solutions prepared in ultrapure water (pH 8), solutions of SMX with an initial concentration of 5 mg L⁻¹ were placed in polypropylene tubes in the presence of the adsorbent at a concentration of 0.040 g L⁻¹. The polypropylene tubes were stirred under controlled temperature, for different time intervals ranging from 5 min to 480 min. Regarding the study on the SMX adsorption onto AC-MPTMS from wastewater, kinetic experiments were performed as above described but with an adsorbent concentration of 0.060 g L⁻¹ and stirring times between 15 min and 1440 min. At the end of each time interval, stirring was stopped and the solutions were filtered through 0.22 µm PVDF filters (Whatman) and analyzed for the residual concentration of SMX. All the adsorption kinetic experiments were performed in triplicate and in parallel with controls (tubes without adsorbent).

The adsorbed concentration of SMX onto AC3 or AC-MPTMS at a time t , q_t (mg g⁻¹), was calculated using equation 5.1 in chapter 5 (section 5.2.5.1). The experimental results were fit to the

kinetic pseudo-first order model (equation 5.2) and pseudo-second order models (equation 5.3), presented in Table 5.1 in chapter 5 (section 5.2.5.1).

9.2.3.2. Equilibrium studies

Equilibrium studies were carried out to determine the adsorbents behavior and capacities at the equilibrium and the corresponding equilibrium constant. Hence, for experiments from buffered solutions prepared in ultrapure water (pH 8), predefined volumes of SMX solution with an initial concentration of 5 mg L⁻¹ were placed in polypropylene tubes together with different concentrations of AC3 or AC-MPTMS, ranging from 0.020 g L⁻¹ to 0.300 g L⁻¹. The polypropylene tubes were stirred under controlled temperature during the equilibrium time determined in the previous kinetic studies. Regarding the SMX adsorption onto AC-MPTMS from wastewater, the equilibrium study was performed as described above but with adsorbent concentrations ranging from 0.040 g L⁻¹ to 0.400 g L⁻¹. Then, stirring was stopped and solutions were filtered through 0.22 µm PVDF filters (Whatman) and analyzed for the residual concentration of SMX by MEKC. All the adsorption equilibrium experiments were performed in triplicate, together with control tubes without adsorbent.

The adsorbed concentration of SMX onto each adsorbent at the equilibrium, q_e (mg g⁻¹), was calculated using equation 5.4 in chapter 5 (section 5.2.5.2) and the equilibrium experimental results were fit to the isotherm models of Langmuir (equation 5.5) and Freundlich (equation 5.6) (Table 5.2 in chapter 5, section 5.2.5.2).

9.2.3.3. Adsorption activation energy and thermodynamic parameters

Activation energy (E_a) is an important thermodynamic parameter representing the minimum energy necessary for a specific interaction between the adsorbate and the adsorbent to occur (Limousin et al., 2007). The calculation of E_a allows one to determine the dependence of the adsorption reaction rate on temperature (Saha and Chowdhury, 2011). E_a can be determined by applying the Arrhenius equation (equation 9.1) (Saha and Chowdhury, 2011):

$$\ln k = -\frac{E_a}{R} \frac{1}{T} + \ln F \quad (9.1)$$

where k is the adsorption rate constant, T (K) is the temperature, R is the universal gas constant (8.314 J K⁻¹ mol⁻¹), and F is the frequency factor or collision probability factor (Limousin et al., 2007; Mourid et al., 2019). By plotting $\ln k$ vs $1/T$, E_a was determined from the slope and F from the intercept.

Thermodynamic parameters, namely the standard Gibbs energy (ΔG° , J mol⁻¹), standard enthalpy (ΔH° , J mol⁻¹) and standard entropy (ΔS° , J mol⁻¹ K⁻¹), associated to the adsorption of SMX onto AC3 and AC-MPTMS were calculated on the basis of the third principle of thermodynamics (equation 9.2) and the van't Hoff equation (equation 9.3) (Atkins, 1999; Lima et al., 2019):

$$\Delta G^\circ = \Delta H^\circ - T\Delta S^\circ \quad (9.2)$$

$$\Delta G^\circ = -RT \ln (K_e^\circ) \quad (9.3)$$

where K_e is the thermodynamic equilibrium constant (dimensionless) (Atkins, 1999; Lima et al., 2019). The combination of the equations above (9.2 and 9.3) results in equation 9.4, which allows for the determination of the thermodynamic parameters ΔH° and ΔS° (Atkins, 1999; Ghosal and Gupta, 2017).

$$\ln K_e^\circ = -\frac{\Delta H^\circ}{R} \frac{1}{T} + \frac{\Delta S^\circ}{R} \quad (9.4)$$

By plotting $\ln K_e$ versus $1/T$, ΔH° was determined from the slope and ΔS° from the intercept. The adsorption equilibrium constant derived from the fittings of experimental results to isotherm models must become dimensionless, so to be possible its utilization in the van't Hoff equation. Thus, K_e° (dimensionless) was calculated using equation 9.5, as proposed by Lima et al. (2019).

$$K_e^\circ = \frac{1000.K_g.MW.[Adsorbate]^\circ}{\gamma} \quad (9.5)$$

where K_g (L mg⁻¹) is the Langmuir equilibrium constant for the best equilibrium fitting; MW (g mol⁻¹) is the molecular weight of the adsorbate; $[Adsorbate]^\circ$ is the standard concentration of the adsorbate (1 mol L⁻¹); and γ is the coefficient of activity of the adsorbate (dimensionless) (Lima et al., 2019). In general, the standard concentration of a solute in a solution is considered 1 mol L⁻¹, and the activity coefficient is considered unitary for diluted solutions (Lima et al., 2019; Spessato et al., 2019). Considering that the initial concentration of SMX is 5 mg L⁻¹, which is equivalent to 1.974 x 10⁻⁵ mol L⁻¹, and that a solution is considered diluted when its molar concentration is not higher than 0.01 M (Atkins, 1999), the SMX solution used can be seen as a very diluted solution and, therefore, the activity coefficient was considered unitary.

9.3. Results and Discussion

9.3.1. Physicochemical characterization of the alternative activated carbon (AC3) and thiol functionalized AC3 (AC-MPTMS)

9.3.1.1. Specific Surface Area (S_{BET})

The S_{BET} values of the produced materials are presented in Table 9.1 and the pore size distribution (PSD) is represented in Figure 9.1. It can be observed that the functionalization of AC3 with thiol groups led to a reduction in the S_{BET} of around 19 %, and that both AC3 and AC-MPTMS show a high degree of microporosity (Table 9.1), as previously observed in chapter 8. Regarding the PSD of the materials (Figure 9.1), AC3 and AC-MPTMS showed very similar patterns, with most of the pore volume in the range of 2 to 4 nm. Still, AC-MPTMS displayed a slight decrease in this range as compared with AC3, which was also observed in chapter 8, and related with the introduction of functional groups into the pore channels of AC3.

Table 9.1. Textural characterization of AC3 and AC-MPTMS.

Material	N_2 adsorption at -196°C						
	S_{BET} ($\text{m}^2\text{ g}^{-1}$)	V_p ($\text{cm}^3\text{ g}^{-1}$)	Dubinin-Radushkevich (DR)			Dubinin-Astakhov (DA)	
			W_0 ($\text{cm}^3\text{ g}^{-1}$)	L (nm)	D (nm)	W_0 ($\text{cm}^3\text{ g}^{-1}$)	L (nm)
AC3	1433	0.98	0.57	-	1.37	0.70	1.78
AC-MPTMS	1164	0.85	0.47	-	1.46	0.57	1.81

V_p – total pore volume; W_0 – micropore volume; L – average pore width; D – average pore diameter

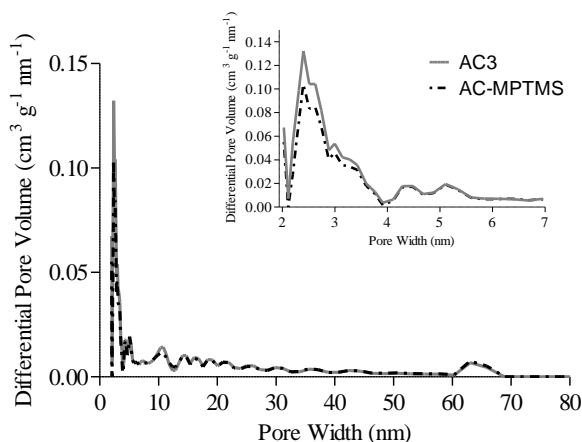


Figure 9.1. Pore size distribution determined for AC3 (grey line) and AC-MPTMS (dash black line).

9.3.1.2. Scanning electron microscopy (SEM)

The SEM images for AC3 and AC-MPTMS are depicted in Figure 9.2. Both materials present a high degree of porosity, which agrees with the S_{BET} results, with AC3 presenting a rougher and more porous surface than AC-MPTMS. This last observation may be related to the surface modification with organosilane precursor, which smooth the AC surface.

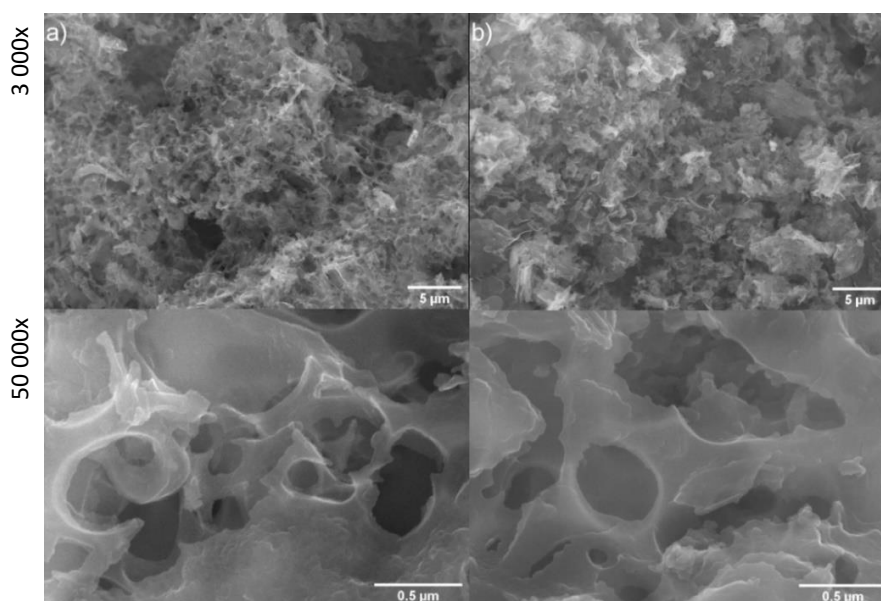


Figure 9.2. SEM images obtained for a) AC3 and b) AC-MPTMS at magnifications of 3 000x and 50 000x.

9.3.1.3. X-Ray photoelectron spectroscopy (XPS)

XPS survey and high-resolution spectra are presented in Figure 9.3. Inspection of the XPS survey spectra and the high-resolution spectra for C1s, N1s and Si2s+S2p, it is possible to observe that AC3 and AC-MPTMS present similar profiles, just with the Si2s+S2p spectra revealing differences on the intensities of the peaks associated to sulphur bonds (around 163 eV and 164 eV). In what concerns the high-resolution spectra, and for C1s, both materials present a main peak at 284.5 eV assigned to the graphitic carbon (sp^2) (Velo-Gala et al., 2014), followed by a peak around 285.3-285.5 eV attributed to C–C on the edge of graphene sheets (sp^3) and C–H bonds (Velo-Gala et al., 2014). The other peaks may

be associated to other functionalities such as carbon-oxygen single bond in ether and alcohol groups (~ 286 eV) (Ma et al., 2014; Velo-Gala et al., 2014); double bond carbon-oxygen groups (-C=O) (Velo-Gala et al., 2014; Wang et al., 2014) or -C=N- species (Lee et al., 2016) around 287 eV; carbon in carboxyl, lactone or ester groups (~ 288 eV) (Ma et al., 2014); and carbon in carbonate groups (Ma et al., 2014) (Figure 9.3). In the case of nitrogen, it is possible to observe in the survey spectra, that the peak associated to the nitrogen core-level is very small, nearly imperceptible. Nevertheless, the high-resolution N1s spectra show the same pattern for both AC3 and AC-MPTMS, presenting three peaks that can be assigned to pyridinic nitrogen ($\sim 397\text{-}398$ eV); pyrrolic or pyridonic nitrogen (~ 400 eV); and quaternary nitrogen ($\sim 401\text{-}402$ eV) (Li et al., 2014; Lee et al., 2016). The main differences are in the relative percentage of each group, with AC3 presenting a higher percentage for pyridinic and pyrrolic nitrogen than AC-MPTMS, while AC-MPTMS has a greater percentage of quaternary nitrogen than AC3 (Figure 9.3). For the Si2s+S2p high-resolution spectra, it is evident the relatively large peak associated to the sulphur binding energies for AC-MPTMS (Figure 9.3). Furthermore, both AC3 and AC-MPTMS present a high peak corresponding to silanes around 154 eV (Martín-García et al., 2015); two peaks around 163 eV and 164 eV, which have a higher relative percentage for AC-MPTMS, and may be respectively attributed to S–H, S–C bonds and thiol moieties (Roberts et al., 2015), and to S–S bonds (Martín-García et al., 2015), elemental S and thiol groups (Roberts et al., 2015); and a fourth peak at 168–169 eV, which may be assigned to sulfoxide groups (Roberts et al., 2015). In what concerns the high resolution O1s spectra, large differences may be observed between the materials, with AC-MPTMS presenting only one peak at 532.3 eV, which is mostly associated to single bond carbon-oxygen groups (C-O-C and C-OH) (Li et al., 2014; Lee et al., 2016). In the case of AC3, the O1s spectrum shows a peak at 532.8 eV, with the highest relative percentage (71.6 %); another at 531.0 eV, which is possibly due to the presence of double bond oxygen groups (C=O) (Li et al., 2014) in quinones (Velo-Gala et al., 2014) or carbonyl groups (Velo-Gala et al., 2014); and a third one at 534.0 eV, which can be assigned to oxygen in carboxyl groups (-COOH or COOR) (Velo-Gala et al., 2014) (Figure 9.3).

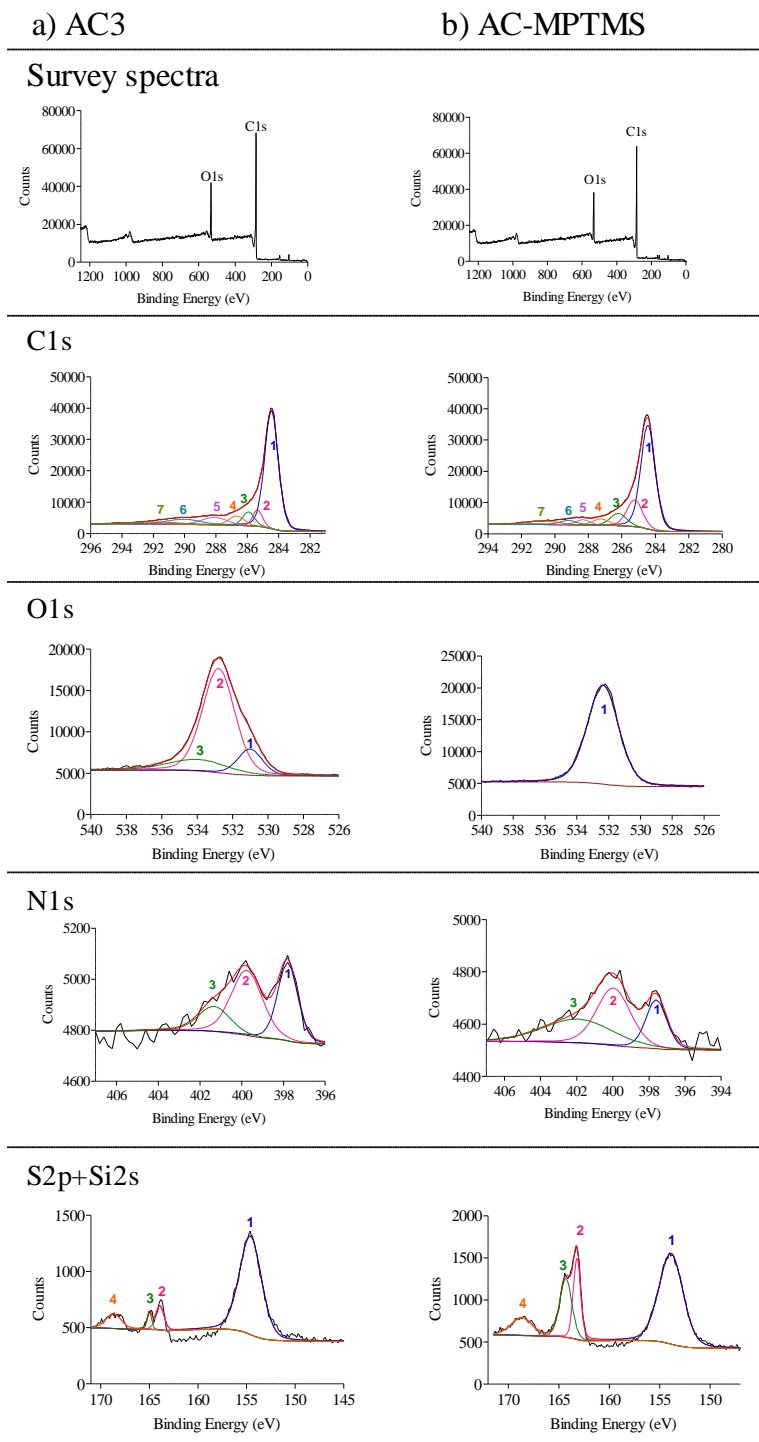


Figure 9.3. XPS survey spectra and high-resolution spectra (with deconvolution) of C1s, O1s, N1s and Si2s+S2p determined for a) AC3 and b) AC-MPTMS.

9.3.2. Adsorption of sulfamethoxazole onto the alternative activated carbon (AC3) and thiol functionalized AC3 (AC-MPTMS) – studies in buffered solutions at pH 8 prepared ultrapure water

9.3.2.1. Kinetic and equilibrium studies

The results of the kinetic studies on the adsorption of SMX onto AC3 and AC-MPTMS from buffered solutions prepared in ultrapure water (pH 8) at different temperatures and the respective fittings for the two models used (pseudo-first and pseudo-second order) are presented in Figure 9.4 and Table 9.2.

As it may be seen in Figure 9.4, kinetic curves showed a quite fast adsorption of SMX onto AC3 and AC-MPTMS, with a steep initial slope and q_t values rapidly reaching stabilization at the corresponding q_e . As for the effect of temperature, slightly steeper slopes may be observed for increasing temperature. Also, an increase in temperature resulted in a decrease in q_e . For all the studied systems, equilibrium was attained within 120 min, which was considered as the minimum t_e for the subsequent equilibrium studies.

According to results in Table 9.2, pseudo-second order model presented best correlation coefficients (R^2) in the fitting of kinetic results. This model points to a strong interaction between adsorbate and adsorbent, not only due to the microporosity, but also due to the complementary interaction in both entities (Acosta et al., 2016). Parameters in Table 9.2 evidence that, under the experimental conditions used, the fitted values of q_e decrease with temperature for both adsorbents, with those of AC3 being larger than those of AC-MPTMS. Meanwhile, the kinetic constant rates (k_2) increase with temperature, indicating a decrease in the time required to reach equilibrium (Sekulic et al., 2019), and are very similar for both adsorbents, being only slightly higher for AC-MPTMS. In any case, the determined values of k_2 are similar to values recently obtained by other authors for the adsorption of SMX onto AC. For example, the adsorption of SMX at 25 °C occurred with a k_2 of 0.008 g mg⁻¹ min⁻¹ onto a core-shell activated carbon (Ndagijimana et al., 2019), and of 0.0039 g mg⁻¹ min⁻¹ onto a cetyltrimethylammonium bromide (CTAB) modified AC (Liu et al., 2019). On the other hand, Tonucci et al. (2015) determined increasing k_2 with temperature for the adsorption of SMX onto an AC produced from pine tree, with values 0.001 g mg⁻¹ min⁻¹ < k_2 < 0.01 g mg⁻¹ min⁻¹ in the temperature range of 15 °C to 45 °C. Such an increase is in agreement with Arrhenius equation (7.1) and must be related to the increased mobility of SMX molecules and the increasing number of molecules with sufficient energy to undergo interaction with active sites on the adsorbents surface.

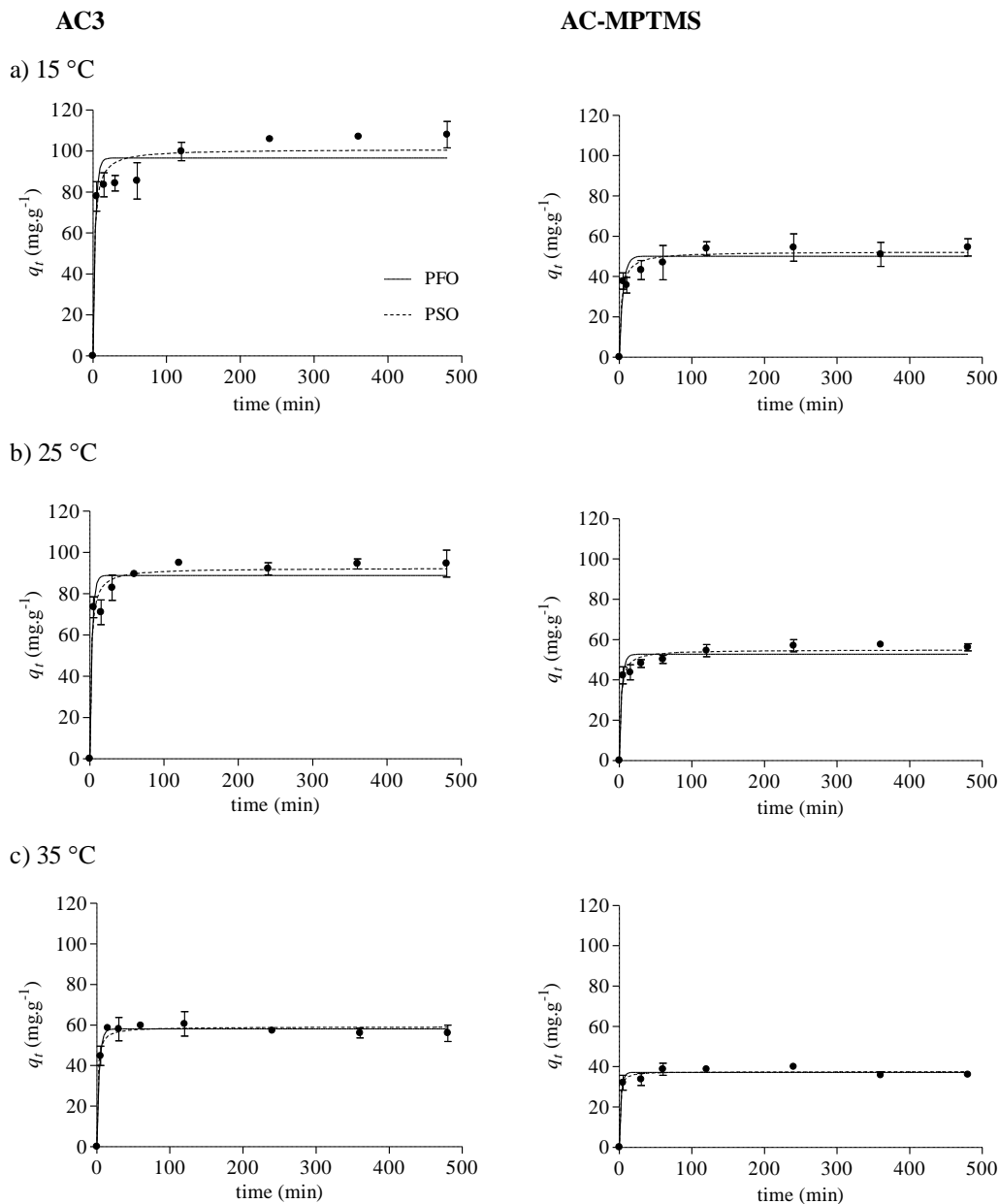


Figure 9.4. Fitting results from the kinetic studies on the adsorption of SMX onto AC3 and AC-MPTMS from buffered solution prepared in ultrapure water (pH 8) at three different temperatures: a) 15 °C, b) 25 °C, and c) 35 °C. Results were fitted to pseudo-first (full line) and pseudo-second (dash line) order kinetic models.

Table 9.2. Fitting results from the kinetic studies on the adsorption of SMX onto AC3 and AC-MPTMS from buffered solution prepared in ultrapure water (pH 8) at three different temperatures (15 °C, 25 °C and 35 °C).

Model / Parameter	Adsorbent					
	AC3			AC-MPTMS		
	Temperature			Temperature		
	288 K (15 °C)	298 K (25 °C)	308 K (35 °C)	288 K (15 °C)	298 K (25 °C)	308 K (35 °C)
<i>Pseudo-first order</i>						
q_e	97 ± 4	89 ± 3	58 ± 1	50 ± 2	53 ± 2	37 ± 1
k_1	0.3 ± 0.1	0.3 ± 0.1	0.30 ± 0.03	0.20 ± 0.05	0.3 ± 0.1	0.4 ± 0.1
R^2	0.915	0.939	0.994	0.914	0.940	0.977
<i>Pseudo-second order</i>						
q_e	101 ± 4	93 ± 2	59 ± 1	52 ± 2	55 ± 1	38 ± 1
k_2	0.005 ± 0.002	0.006 ± 0.002	0.013 ± 0.004	0.006 ± 0.002	0.009 ± 0.003	0.03 ± 0.01
R^2	0.950	0.971	0.983	0.959	0.974	0.980

q_e - amount of pharmaceutical adsorbed at equilibrium (mg g^{-1}); k_1 - rate constant of pseudo-first order (min^{-1}); k_2 - rate constant of pseudo-second order ($\text{g mg}^{-1} \text{min}^{-1}$); R^2 - coefficient of correlation

The results from the equilibrium studies on the adsorption of SMX onto AC3 and AC-MPTMS from buffered solution prepared with ultrapure water (pH 8), at different temperatures, and the respective fitting to Langmuir and Freundlich models are presented in Figure 9.5 and Table 9.3. Observing Figure 9.5, AC3 and AC-MPTMS show distinct patterns, with AC3 isotherms achieving a clear *plateau*, which is not so well defined for AC-MPTMS, especially at 15 °C. This is reflected in the fitting results (Table 9.3), since AC-MPTMS at 15 °C is the only system where the Freundlich isotherm model presents a slightly better correlation coefficient (R^2) than the Langmuir model. Also, it can be seen in Figure 9.5, that in the low range of C_e ($< 1 \text{ mg L}^{-1}$), AC-MPTMS displayed similar q_e at the different temperatures, while that was not the case of AC3 (Figure 9.5).

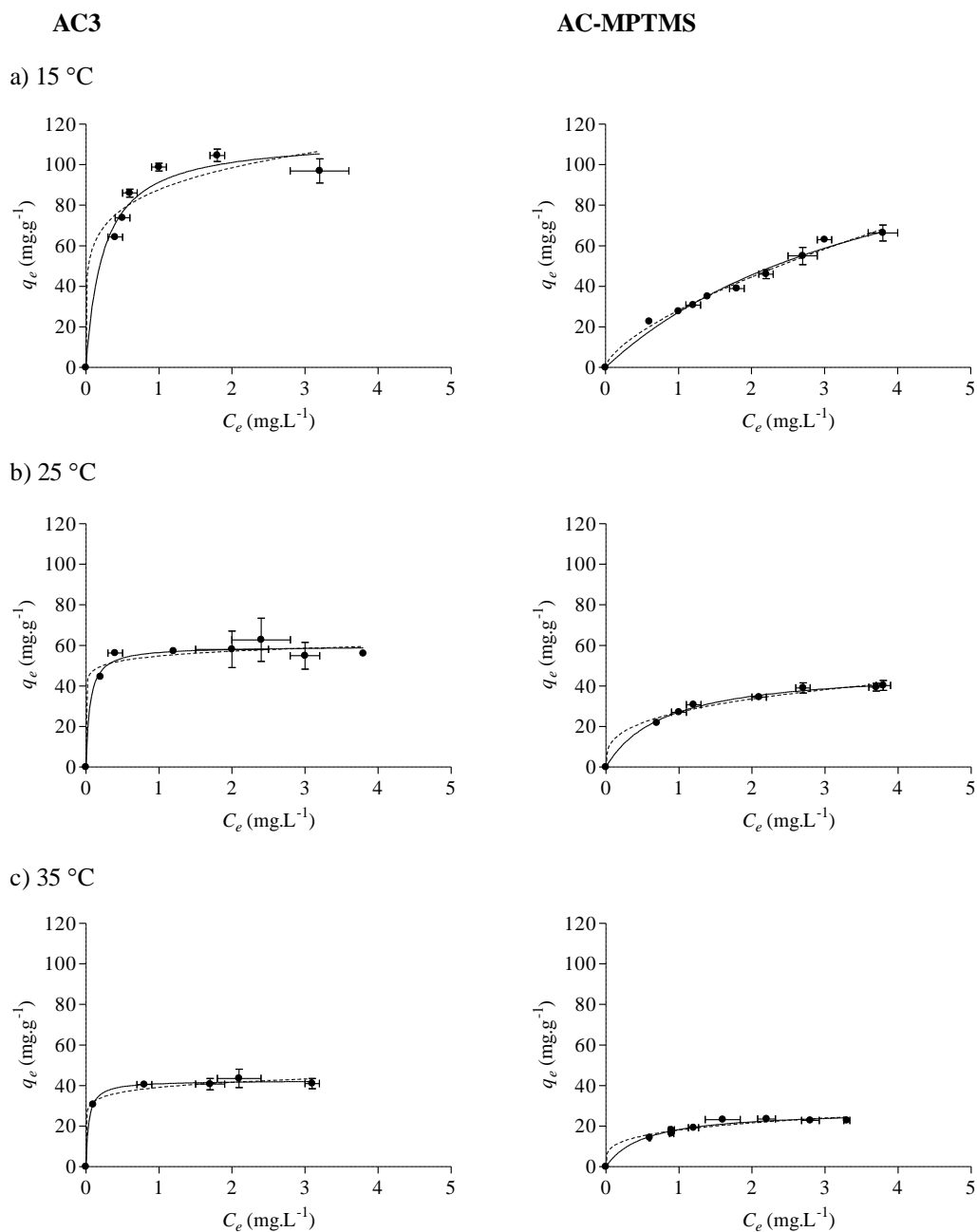


Figure 9.5. Fitting results from the equilibrium studies on the adsorption of SMX onto AC3 and AC-MPTMS from buffered solution prepared in ultrapure water (pH 8) at three different temperatures: a) 15 °C, b) 25 °C, and c) 35 °C. Results were fitted to Langmuir (full line) and Freundlich (dash line) models.

Table 9.3. Fitting results from the equilibrium studies on the adsorption of SMX onto AC3 and AC-MPTMS from buffered solution prepared in ultrapure water (pH 8) at three different temperatures (15 °C, 25 °C and 35 °C).

Model / Parameter	Adsorbent					
	AC3			AC-MPTMS		
	Temperature			Temperature		
	288 K (15 °C)	298 K (25 °C)	308 K (35 °C)	288 K (15 °C)	298 K (25 °C)	308 K (35 °C)
Langmuir						
q_m	113 ± 7	62 ± 3	42 ± 1	140 ± 20	49 ± 1	28.0 ± 1.5
K_L	4 ± 1	19 ± 6	26 ± 4	0.2 ± 0.1	1.3 ± 0.1	1.9 ± 0.4
R^2	0.971	0.960	0.997	0.983	0.996	0.978
Freundlich						
n	6 ± 2	16 ± 8	11 ± 3	1.5 ± 0.1	3.2 ± 0.3	4 ± 1
K_F	88 ± 4	55 ± 2	39 ± 1	28 ± 1	27 ± 1	18 ± 1
R^2	0.943	0.940	0.989	0.988	0.987	0.961

q_m – maximum adsorption capacity (mg g⁻¹); K_L – Langmuir equilibrium constant related to the rate of adsorption (L mg⁻¹); K_F – Freundlich adsorption constant (mg^{1-1/n} L^{1/n} g⁻¹); n – constant related with the degree of non-linearity of the equation; R^2 – coefficient of correlation

Considering the fitting results depicted in Table 9.3, Langmuir model was selected as the most adequate for subsequent considerations on the equilibrium of the studied systems. For both AC3 and AC-MPTMS, the Langmuir constant (K_L) increases with temperature while the maximum adsorption capacity decreases. Therefore, although the affinity between SMX molecules and these adsorbents increases with temperature, such temperature increase implies a reduction of the monolayer capacity. Comparing the adsorbents produced in this work, the K_L values determined for AC3 are higher than those of AC-MPTMS (Table 9.3), and steeper isotherms were observed for AC3 comparatively to AC-MPTMS (Figure 9.5). With respect to the q_m values determined for AC3 at 25 °C and 35 °C, these are higher than those determined for AC-MPTMS. Meanwhile, at 15 °C, and due to the high standard deviation of the q_m values determined for AC-MPTMS, there are not significant differences between the monolayer capacity of both materials.

Differences in the obtained results on the adsorption of SMX onto AC3 and AC-MPTMS may be related with the larger S_{BET} of the former. Also, the larger K_L and q_m determined for AC3 may be associated to the larger number of available oxygen functional groups, like carbonyl and carboxyl groups, in comparison with AC-MPTMS. These additional groups will likely stabilize the interaction of AC with

SMX by $n-\pi$ electron donor-acceptor interactions and dipole-dipole H-bond (Sekulic et al., 2019). As for the sulphur functional groups in AC-MPTMS, they do not seem to have significantly influenced the adsorption of SMX.

For comparison purposes, published results on the adsorption of SMX by different AC in the literature are depicted in Table 9.4. Among the referred works, Sekulic et al. (2019) used a lignocellulosic waste-based functionalized AC and determined a q_m of 17 mg L^{-1} (at pH 6-7 and $22 \text{ }^\circ\text{C}$), which is lower than that attained by AC-MPTMS under similar conditions (at pH 8 and $25 \text{ }^\circ\text{C}$). However, the commercial GAC used in the work of Moral-Rodríguez et al. (2016) provided a q_m of 213 mg L^{-1} , 269 mg L^{-1} and 317 mg L^{-1} at pH 7, 9 and 11, respectively (at $25 \text{ }^\circ\text{C}$), which are significantly higher than those obtained in this work for both AC3 and AC-MPTMS (Table 9.4).

9.3.2.2. Estimation of the activation energy and thermodynamic parameters

The E_a values associated to the adsorption of SMX onto AC3 and AC-MPTMS, which were calculated by plotting $\ln k_2$ vs. $1/T$ (according to equation 9.1; Figure 9.6) and are depicted in Table 9.5, were $(36 \pm 13) \text{ kJ mol}^{-1}$ and $(61 \pm 17) \text{ kJ mol}^{-1}$, respectively. These values imply that the energy needed for the SMX adsorption onto AC-MPTMS was slightly higher than onto AC3. Yet, and despite these values being quite close to each other, SMX adsorption onto AC3 is mostly a physisorption process (5 kJ mol^{-1} to 40 kJ mol^{-1}) as suggested by the respective E_a , whereas chemisorption is the dominant process for adsorption onto AC-MPTMS (40 kJ mol^{-1} to 120 kJ mol^{-1}) (Mourid et al., 2019). With respect to the pre-exponential factor A , which can be regarded as a collision probability factor (Limousin et al., 2007), it has a very high value for AC-MPTMS ($6 \times 10^8 \pm 6 \times 10^4$) comparing to that of AC3 ($2 \times 10^4 \pm 3 \times 10^2$) (Table 9.5).

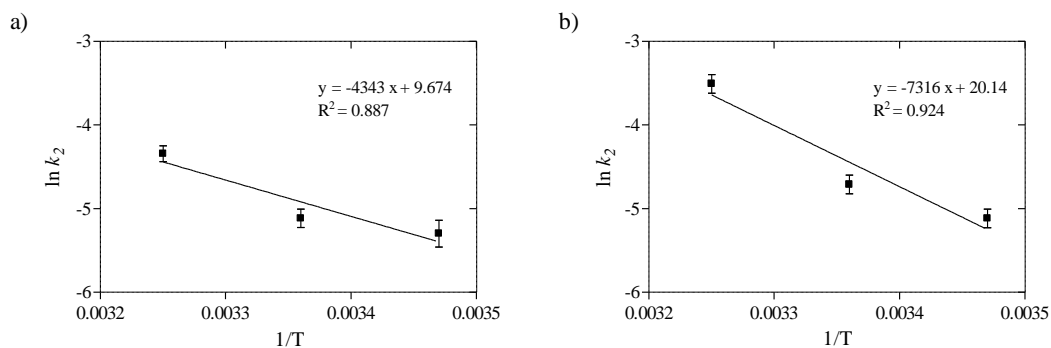


Figure 9.6. Plots of $\ln k_2$ versus $1/T$ for the adsorption of SMX onto a) AC3 and b) AC-MPTMS.

Table 9.4. Studies involving the adsorption of sulfamethoxazole (SMX) onto powdered (PAC) or granular (GAC) activated carbons.

AC	S _{BET} (m ² g ⁻¹)	Matrix	Temperature and pH conditions	Langmuir isotherm parameters		Thermodynamic parameters			Reference
				q _m (mg g ⁻¹)	K _L (L mg ⁻¹)	ΔG° (kJ mol ⁻¹)	ΔH° (kJ mol ⁻¹)	ΔS° (J mol ⁻¹ K ⁻¹)	
Commercial coal- based PAC	851	distilled water	20 °C	—	—	-2.68	-18.984	-0.05547	Çalışkan and Göktürk (2010)
			25 °C	185.19	0.351	-2.242			
			30 °C	—	—	-1.587			
			40 °C	—	—	-1.295			
PAC from pine tree (PAC-I)	452.6	—	pH 7; 15 °C	130.4	11.97	-38.8	-36.73	7.179	Tonucci et al. (2015)
			pH 7; 25 °C	130.37	4.64	-38.87			
			pH 7; 35 °C	162.56	3.21	-38.94			
			pH 7; 45 °C	146.48	2.26	-39.01			
PAC from coal (PAC-II)	781.4	—	pH 7; 25 °C	58.35	12.57	—	—	—	
PAC from coconut shell (PAC-III)	374	—	pH 7; 25 °C	—	—	—	—	—	
commercial GAC (F-400)	919	deionized water	pH 3; 25 °C	400.2 ^a	0.194 ^b	—	—	—	Moral- Rodríguez et al. (2016)
			pH 5; 25 °C	445.8 ^a	0.060 ^b	—	—	—	
			pH 6; 25 °C	283.7 ^a	0.454 ^b	—	—	—	
			pH 7; 10 °C	212.8 ^a	0.131 ^b	—	7.1	—	
			pH 7; 25 °C	268.5 ^a	0.092 ^b	—	—	—	
			pH 7; 40 °C	316.6 ^a	0.132 ^b	—	—	—	
			pH 9; 25 °C	220.4 ^a	0.037 ^b	—	—	—	
			pH 11; 25 °C	126.6 ^a	0.043 ^b	—	—	—	
AC	70.96	—	25 °C	10.965	0.258	-23.05	-20.32	9.02	Liu et al. (2019)
			35 °C	—	—	-23.02			
			45 °C	—	—	-23.23			

^a The values were presented in mmol g⁻¹ units, hence q_m (mg g⁻¹) were calculated by: q_m (mmol g⁻¹) x MW (SMX, 253.28 g mol⁻¹)

^b The values were presented in L mmol⁻¹ units, hence K_L (L mg⁻¹) were calculated by: K_L (L mmol⁻¹) / MW (SMX, 253.28 g mol⁻¹)

Table 9.4. (Continued)

AC	S_{BET} ($\text{m}^2 \text{g}^{-1}$)	Matrix	Temperature and pH conditions	Langmuir parameters		isotherm			Thermodynamic parameters			Reference
				q_m (mg g^{-1})	K_L (L mg^{-1})	K_L (L mg^{-1})	ΔG° (kJ mol^{-1})	ΔH° (kJ mol^{-1})	ΔS° ($\text{J mol}^{-1} \text{K}^{-1}$)			
AC modified with hexadecyl trimethyl ammonium (MAC)	36.67	—	25 °C	17.513	0.299	—	-24.21	-11.21	43.79	Liu et al. (2019)		
			35 °C	—	—	-24.81	—	—				
			45 °C	—	—	-25.08	—	—				
AC (from waste lignocellulosic biomass functionalized with phosphorous groups (PPhA)	1230.6	ultrapure water	pH 6-7; 22 °C	17.19	10.812	—	—	—	—	Sekulic et al. (2019)		
			—	—	—	—	—	—				
PAC commercial (CAC)	996	ultrapure water wastewater	25 °C	118 ± 7	1.8 ± 0.6	—	—	—	—	Silva et al. (2019)		
			25 °C	123 ± 5	8.4 ± 2.5	—	—	—				
PAC from paper mill sludge (AAC)	1627	ultrapure water wastewater	25 °C	194 ± 10	3.2 ± 0.7	—	—	—	—	—		
			25 °C	47 ± 1	7.3 ± 1.2	—	—	—				
PAC from paper mill sludge (AC3)	1433	buffered ultra-pure water (pH 8)	pH 8; 15 °C	113 ± 7	4.2 ± 1.2	—	-33.2 ± 0.2	68.9 ± 0.4	356 ± 88	This study		
			pH 8; 25 °C	62 ± 3	19 ± 6	—	-38.1 ± 0.3	—	—			
			pH 8; 35 °C	42.5 ± 0.6	26 ± 4	—	-40.20 ± 0.06	—	—			
PAC from paper mill sludge functionalized with thiol groups (AC- MPTMS)	1164	buffered ultra-pure water (pH 8)	pH 8; 15 °C	140 ± 20	0.24 ± 0.06	—	-26.4 ± 0.2	78.2 ± 0.4	365 ± 96	—		
			pH 8; 25 °C	48.9 ± 1.4	1.3 ± 0.1	—	-31.48 ± 0.02	—	—			
			pH 8; 35 °C	28.0 ± 1.5	1.9 ± 0.4	—	-33.5 ± 0.1	—	—			
			pH 7.99; 25 °C	16.1 ± 0.3	3.8 ± 0.4	—	—	—	—			

^a The values were presented in mmol g^{-1} units, hence q_m (mg g^{-1}) were calculated by: q_m (mmol g^{-1}) x MW (SMX, 253.28 g mol^{-1})

^b The values were presented in L mmol^{-1} units, hence K_L (L mg^{-1}) were calculated by: K_L (L mmol^{-1}) / MW (SMX, 253.28 g mol^{-1})

Table 9.5. Thermodynamic parameters calculated for the adsorption of SMX onto AC3 and AC-MPTMS.

Carbon material	Temperature (K)	Activation energy, E_a (kJ mol ⁻¹)	Pre-exponential factor, F (g mg ⁻¹ min ⁻¹)	Isotherm model	ΔG° (kJ mol ⁻¹) *	ΔH° (kJ mol ⁻¹)	ΔS° (J mol ⁻¹ K ⁻¹)
AC3	288				-33.2 ± 0.2		
	298	36 ± 13	2x10 ⁴ ± 3x10 ²	Langmuir	-38.1 ± 0.3	68.9 ± 0.4	356 ± 88
	308				-40.2 ± 0.1		
AC-MPTMS	288				-26.4 ± 0.2		
	298	61 ± 17	6x10 ⁸ ± 6x10 ⁴	Langmuir	-31.48 ± 0.02	78.2 ± 0.4	365 ± 96
	308				-33.5 ± 0.1		

* The value of ΔG° was calculated by equation (9.3) $\Delta G^\circ = -RT \ln K_e^\circ$

For the determination of thermodynamic parameters, the calculation of K_e° was performed according to equation (9.5), where, considering the selection of Langmuir fittings to describe the experimental data (section 9.3.2.1), K_g was equaled to K_L . Then, K_e was plotted vs. $1/T$ (according to equation 9.4; Figure 9.7). These plots allowed for the determination of ΔH° , ΔS° and then ΔG° , which are depicted in Table 9.5. As it may be observed, for both AC3 and AC-MPTMS, the adsorption of SMX is a spontaneous process at the temperatures considered, as ΔG° presented negative values (Hong et al., 2009; Subramani and Thinakaran, 2017). Furthermore, for both materials, a slight decrease of the ΔG° values with the temperature was observed, indicating that the increase of the temperature is favorable for the spontaneity of SMX adsorption. ΔH° presented positive values, viz. 68.9 kJ mol⁻¹ and 78.2 kJ mol⁻¹, respectively for AC3 and AC-MPTMS, indicating the endothermic nature of the adsorption of SMX onto these materials. On the other hand, ΔH° values here determined are between 40 kJ mol⁻¹ and 80 kJ mol⁻¹, which indicates that both physisorption and chemisorption can be taking place in the adsorptive removal of SMX by both AC3 and AC-MPTMS (Spessato et al., 2019). Nevertheless, ΔH° value for the adsorption of SMX onto AC-MPTMS is closer to 80 kJ mol⁻¹ and its E_a (Table 9.5) is larger than onto AC3, which points to the greater influence of chemisorption on the adsorption of SMX onto AC-MPTMS than onto AC3. This is further supported by the ΔG° value, which is not clearly within the range of physisorption (between -20 kJ mol⁻¹ and 0 kJ mol⁻¹), nor of chemisorption (between -400 kJ mol⁻¹ and -80 kJ mol⁻¹) (Spessato et al., 2019). ΔS° also presented positive values for both systems, (356 ± 88) J mol⁻¹ K⁻¹ and (365 ± 96) J mol⁻¹ K⁻¹ for AC3 and AC-MPTMS, respectively, indicating an entropically favorable process.

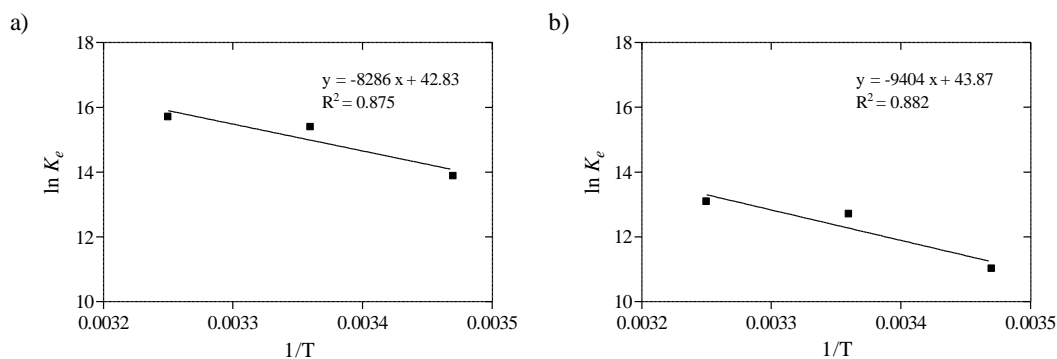


Figure 9.7. Plots of $\ln K_e$ versus $1/T$ for the adsorption of SMX onto a) AC3 and b) AC-MPTMS.

ΔG° values similar to those obtained in this work, namely around -38 kJ mol^{-1} (Tonucci et al., 2015) and -24 kJ mol^{-1} (Liu et al., 2019), have been respectively published for the adsorption of SMX onto pine tree AC and CTAB modified AC at temperatures within 288 K and 318 K (Table 9.4). These authors (Tonucci et al., 2015; Liu et al., 2019) also found that SMX adsorption onto the produced adsorbents implied an increase of entropy, but, contrarily to this work, the process was exothermic.

9.3.3. Evaluation of the functionalized activated carbon (AC-MPTMS) performance in the adsorption of sulfamethoxazole from wastewater

The thiol functionalized material AC-MPTMS was tested for the adsorption of SMX from the effluent from a local WWTP. Follows the characterization of the wastewater used: pH of 7.99, conductivity of 3.03 mS cm^{-1} , and a total organic content of 21.5 mg L^{-1} .

Kinetic and equilibrium results on the adsorption of SMX from the real matrix onto AC-MPTMS are presented in Figure 9.8 together with fittings to the considered models, while the fitted parameters are depicted in Table 9.6. By the kinetic fitting in Figure 9.8, it may be observed that q_t rapidly increases at the initial part of the curve and that the adsorption equilibrium is attained at around 240 min. Comparing with the results obtained in buffered solution prepared with ultrapure water (Figure 9.4), the increase in the time necessary for reaching the equilibrium in the effluent is clear. This is also seen by the value estimated for the rate constant, k_2 , of pseudo-second order model (presenting the best fit correlation (Table 9.6), which is around half of the value obtained in buffered solution (pH 8) at 25°C (Table 9.2). The values obtained for q_e by the pseudo-second order model in wastewater were also smaller than the ones obtained in buffered solution prepared in ultrapure water (pH 8). Such decreases

of both q_e and k_2 may be related with the matrix effects in wastewater, namely, due to the presence of dissolved organic matter (DOM) (Prasannamedha and Kumar, 2020). A decrease of the fitted q_e accompanied by an increase of k_2 has been observed in some studies for the adsorption of other pharmaceuticals (Coimbra et al., 2019) and specifically for SMX (chapter 5) from wastewater, as compared with ultrapure water and for waste-based adsorbents. In any case, the k_2 and fitted q_e depicted in Table 9.6 show that the adsorption of SMX onto AC-MPTMS from wastewater was faster than the SMX adsorption onto the functionalized biochar produced by Ahmed et al. (2017) when used in synthetic wastewater at pH 4-4.25 ($k_2 = 0.0002 \text{ g mg}^{-1} \text{ min}^{-1}$, $q_e = 12.15 \text{ mg g}^{-1}$).

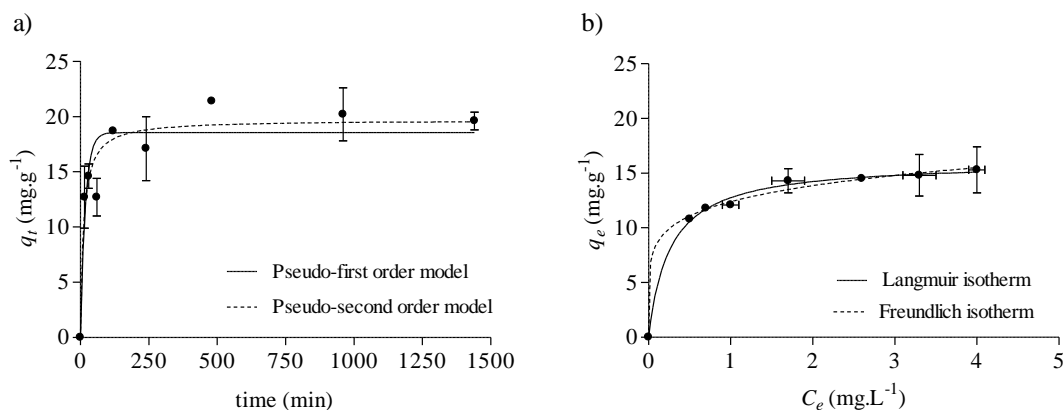


Figure 9.8. Experimental results from the a) kinetic and b) equilibrium studies on the adsorption of SMX onto AC-MPTMS from wastewater (at 25 °C) together with fittings to the considered models.

Table 9.6. Fitting results for the kinetic and equilibrium studies on the adsorption of SMX onto AC-MPTMS from wastewater (at 25 °C).

Kinetic fittings		Isotherm fittings	
Model/parameter		Model/parameter	
Pseudo-first order		Langmuir	
q_e	19 ± 1	q_m	16.1 ± 0.3
k_1	0.06 ± 0.02	K_L	3.8 ± 0.4
R^2	0.866	R^2	0.996
Pseudo-second order		Freundlich	
q_e	20 ± 1	n	6 ± 1
k_2	0.004 ± 0.002	K_F	12.4 ± 0.2
R^2	0.925	R^2	0.995

q_e - amount of pharmaceutical adsorbed at equilibrium (mg g^{-1}); k_1 - rate constant of pseudo-first order (min^{-1}); k_2 - rate constant of pseudo-second order ($\text{g mg}^{-1} \text{ min}^{-1}$); q_m - maximum adsorption capacity (mg g^{-1}); K_L - Langmuir equilibrium constant related to the rate of adsorption (L mg^{-1}); K_F - Freundlich adsorption constant ($\text{mg}^{1-1/n} \text{ L}^{1/n} \text{ g}^{-1}$); n - constant related with the degree of non-linearity of the equation; R^2 - coefficient of correlation

Relatively to the equilibrium study, the best isotherm model that fits the experimental data is the Langmuir model, predicting a maximum adsorption capacity of $(16.1 \pm 0.3) \text{ mg g}^{-1}$ and a K_L of $(3.8 \pm 0.4) \text{ L mg}^{-1}$ (Table 9.6 and Figure 9.8). In Figure 9.8, the tendency for the formation of a *plateau* can be observed, corresponding to the monolayer adsorption. It is observed a great reduction in the Langmuir adsorption capacity in wastewater as compared with buffered solution at pH 8, namely from $(49 \pm 1) \text{ mg g}^{-1}$ (Table 9.3) to $(16.1 \pm 0.3) \text{ mg g}^{-1}$ (Table 9.6). Despite the lower value obtained in the wastewater matrix, this q_m is in the same range as the determined for the functionalized AC produced by Sekulic et al. (2019), which was applied in ultrapure water at pH 6-7 (Table 9.4). The decrease of micropollutants (including SMX) adsorption capacity of AC in wastewater as compared with ultrapure water has already been verified in chapter 5 and by Bonvin et al. (2016), Oliveira et al. (2018), Coimbra et al. (2019), and Sousa et al. (2020); and associated to adverse effects of competing wastewater matrix components on the adsorption of target micropollutants. Using ultrapure buffered water (pH 8.1) as reference, Bonvin et al. (2016) verified two to three-fold lower adsorption capacities for the adsorption of pharmaceuticals onto powder AC from wastewater effluent (pH 7.8 ± 0.2). This reduction was especially evident in the case of pharmaceuticals showing a low carbon affinity, such as SMX (Bonvin et al., 2016). Even at acidic pH, which favors SMX adsorption, Akpotu and Moodley (2018) observed a decrease in the percentage of adsorption of this antibiotic by silica nanotubes graphene oxide (SNTGO) from real matrices, namely lake water and WWTP effluent. As already pointed out, background organic matter in wastewater reduces the number of adsorption sites available for micropollutants, either through direct competition for adsorption sites and/or pore blocking, and consequently decreases the adsorption efficiency of AC (Bonvin et al., 2016; Prasannamedha and Kumar, 2020).

9.4. Conclusions

In this work a functionalization of a waste-based activated carbon (AC3) was performed in order to introduce thiol groups onto its surface, so to obtain AC-MPTMS, and to study the effect of such functionalization on the adsorption of SMX. The physicochemical characterization of AC3 and AC-MPTMS showed slight differences between the materials, mostly in what concerns S_{BET} , types of oxygen functional groups and in the relative percentage of sulphur groups. The kinetic adsorption results in buffered solutions prepared in ultrapure water (pH 8) were described by the pseudo-second order model, with k_2 values varying between $0.005 \text{ g mg}^{-1} \text{ min}^{-1}$ and $0.013 \text{ g mg}^{-1} \text{ min}^{-1}$ for the adsorption of SMX

onto AC3 and between $0.006 \text{ g mg}^{-1} \text{ min}^{-1}$ and $0.03 \text{ g mg}^{-1} \text{ min}^{-1}$ for the adsorption of SMX onto AC-MPTMS. These values allowed for the estimation the SMX adsorption activation energy as 36 kJ mol^{-1} and 61 kJ mol^{-1} for AC3 and AC-MPTMS, respectively. The equilibrium results were described by the Langmuir model, with AC3 presenting maximum adsorption capacities at $15 \text{ }^\circ\text{C}$, $25 \text{ }^\circ\text{C}$ and $35 \text{ }^\circ\text{C}$, of 113 mg g^{-1} , 62 mg g^{-1} , and 42 mg g^{-1} , respectively; and for AC-MPTMS of 140 mg g^{-1} , 49 mg g^{-1} , and 28.0 mg g^{-1} , respectively. The thermodynamic parameters ΔG° , ΔH° and ΔS° , estimated from the equilibrium constants, showed comparable results for AC3 and AC-MPTMS, with both presenting a spontaneous, endothermic, and entropically favorable adsorption of SMX. The application of AC-MPTMS to real wastewater matrix showed a decrease of the performance of this material in the adsorption of SMX as compared with buffered solutions prepared in ultrapure water (pH 8). Hence, this study revealed that S_{BET} was determinant in the performance of the produced materials regarding the adsorption of SMX. Indeed, the applied functionalization did not allow for overcoming the competitive effects of background organic matter in the adsorption of SMX from wastewater.

9.5. References

- Acosta, R., Fierro, V., Yuso, A.M.d., Nabarlantz, D., Celzard, A., 2016. Tetracycline adsorption onto activated carbons produced by KOH activation of tyre pyrolysis char. *Chemosphere* 149, 168-176.
- Ahmed, M.B., Zhou, J.L., Ngo, H.H., Guo, W., Johir, M.A.H., Belhaj, D., 2017. Competitive sorption affinity of sulfonamides and chloramphenicol antibiotics toward functionalized biochar for water and wastewater treatment. *Bioresour. Technol.* 238, 306-312.
- Akpotu, S.O., Moodley, B., 2018. Encapsulation of Silica Nanotubes from Elephant Grass with Graphene Oxide/Reduced Graphene Oxide and Its Application in Remediation of Sulfamethoxazole from Aqueous Media. *ACS Sustain. Chem. Eng.* 6, 4539-4548.
- Atkins, P.W., 1999. Físico-Química (Tradução: Horacio Macedo), 6 ed. LTC Editora, Rio de Janeiro, Brazil.
- Bonvin, F., Jost, L., Randin, L., Bonvin, E., Kohn, T., 2016. Super-fine powdered activated carbon (SPAC) for efficient removal of micropollutants from wastewater treatment plant effluent. *Water Res.* 90, 90-99.
- Çalışkan, E., Göktürk, S., 2010. Adsorption Characteristics of Sulfamethoxazole and Metronidazole on Activated Carbon. *Sep. Sci. Technol.* 45, 244-255.
- Coimbra, R.N., Calisto, V., Ferreira, C.I.A., Esteves, V.I., Otero, M., 2019. Removal of pharmaceuticals from municipal wastewater by adsorption onto pyrolyzed pulp mill sludge. *Arab. J. Chem.* 12, 3611-3620.
- Ghosal, P.S., Gupta, A.K., 2017. Determination of thermodynamic parameters from Langmuir isotherm constant-revisited. *J. Mol. Liq.* 225, 137-146.
- Guillossou, R., Le Roux, J., Mailler, R., Vulliet, E., Morlay, C., Nauleau, F., Gasperi, J., Rocher, V., 2019. Organic micropollutants in a large wastewater treatment plant: What are the benefits of an advanced treatment by activated carbon adsorption in comparison to conventional treatment? *Chemosphere* 218, 1050-1060.
- Hong, S., Wen, C., He, J., Gan, F., Ho, Y.S., 2009. Adsorption thermodynamics of Methylene Blue onto bentonite. *J. Hazard. Mater.* 167, 630-633.
- Lee, M.S., Park, M., Kim, H.Y., Park, S.J., 2016. Effects of Microporosity and Surface Chemistry on Separation Performances of N-Containing Pitch-Based Activated Carbons for CO₂/N₂ Binary Mixture. *Sci. Rep.* 6, 1-11.
- Li, Z., Xu, Z., Wang, H., Ding, J., Zahiri, B., Holt, C.M.B., Tan, X., Mitlin, D., 2014. Colossal pseudocapacitance in a high functionality–high surface area carbon anode doubles the energy of an asymmetric supercapacitor. *Energ. Environ. Sci.* 7, 1708.
- Lima, E.C., Hosseini-Bandegharaei, A., Moreno-Piraján, J.C., Anastopoulos, I., 2019. A critical review of the estimation of the thermodynamic parameters on adsorption equilibria. Wrong use of

- equilibrium constant in the Van't Hoof equation for calculation of thermodynamic parameters of adsorption. *J. Mol. Liq.* 273, 425-434.
- Limousin, G., Gaudet, J.P., Charlet, L., Szenknect, S., Barthès, V., Krimissa, M., 2007. Sorption isotherms: A review on physical bases, modeling and measurement. *Appl. Geochem.* 22, 249-275.
- Liu, Y., Liu, X., Zhang, G., Du, T.M.T., Yang, Y., Lu, S., Wang, W., 2019. Adsorptive removal of sulfamethazine and sulfamethoxazole from aqueous solution by hexadecyl trimethyl ammonium bromide modified activated carbon. *Colloid. Surface. A* 564, 131-141.
- Ma, X., Yang, H., Yu, L., Chen, Y., Li, Y., 2014. Preparation, surface and pore structure of high surface area activated carbon fibers from bamboo by steam activation. *Materials* 7, 4431-4441.
- Martín-García, B., Polovitsyn, A., Prato, M., Moreels, I., 2015. Efficient charge transfer in solution-processed PbS quantum dot–reduced graphene oxide hybrid materials. *J. Mater. Chem. C* 3, 7088-7095.
- Moral-Rodríguez, A.I., Leyva-Ramos, R., Ocampo-Pérez, R., Mendoza-Barron, J., Serratos-Alvarez, I.N., Salazar-Rabago, 2016. Removal of ronidazole and sulfamethoxazole from water solutions by adsorption on granular activated carbon: equilibrium and intraparticle diffusion mechanisms. *Adsorption* 22, 89-103.
- Mourid, E.H., Lakraimi, M., Benaziz, L., Elkhatabi, E.H., Legrouri, A., 2019. Wastewater treatment test by removal of the sulfamethoxazole antibiotic by a calcined layered double hydroxide. *Appl. Clay Sci.* 168, 87-95.
- Ndagijimana, P., Liu, X., Yu, G., Wang, Y., 2019. Synthesis of a novel core-shell-structure activated carbon material and its application in sulfamethoxazole adsorption. *J. Hazard. Mater.* 368, 602-612.
- Oliveira, G., Calisto, V., Santos, S.M., Otero, M., Esteves, V.I., 2018. Paper pulp-based adsorbents for the removal of pharmaceuticals from wastewater: a novel approach towards diversification. *Sci. Total Environ.* 631-632, 1018-1028.
- Patel, M., Kumar, R., Kishor, K., Mlsna, T., Pittman, C. U., Mohan, D., 2019. Pharmaceuticals of Emerging Concern in Aquatic Systems: Chemistry, Occurrence, Effects, and Removal Methods. *Chem. Rev.* 119, 3510–3673.
- Prasannamedha, G., Kumar, P.S., 2020. A review on contamination and removal of sulfamethoxazole from aqueous solution using cleaner techniques: Present and future perspective. *J. Clean. Prod.* 250, 119553.
- Roberts, A.D., Li, X., Zhang, H., 2015. Hierarchically porous sulfur-containing activated carbon monoliths via ice-templating and one-step pyrolysis. *Carbon* 95, 268-278.
- Saha, P., Chowdhury, S., 2011. Insight Into Adsorption Thermodynamics, Thermodynamics, Mizutani Tadashi, IntechOpen, DOI: 10.5772/13474. Available from: <https://www.intechopen.com/books/thermodynamics/insight-into-adsorption-thermodynamics>.

- Sekulic, M.T., Boskovic, N., Slavkovic, A., Garunovic, J., Kolakovic, S., Pap, S., 2019. Surface functionalised adsorbent for emerging pharmaceutical removal: Adsorption performance and mechanisms. *Process. Saf. Environ.* 125, 50-63.
- Silva, C.P., Jaria, G., Otero, M., Esteves, V.I., Calisto, V., 2019. Adsorption of pharmaceuticals from biologically treated municipal wastewater using paper mill sludge-based activated carbon. *Environ. Sci. Pollut. R.* 26, 13173-13184.
- Sousa, A.F.C., Gil, M.V., Calisto, V., 2020. Upcycling spent brewery grains through the production of carbon adsorbents - application to the removal of carbamazepine from water. *Environ. Sci. Pollut. R.* 27, 36463-36475.
- Spessato, L., Bedin, K.C., Cazetta, A.L., Souza, I.P.A.F., Duarte, V.A., Crespo, L.H.S., Silva, M.C., Pontes, R.M., Almeida, V.C., 2019. KOH-super activated carbon from biomass waste: Insights into the paracetamol adsorption mechanism and thermal regeneration cycles. *J. Hazard. Mater.* 371, 499-505.
- Subramani, S.E., Thinakaran, N., 2017. Isotherm, kinetic and thermodynamic studies on the adsorption behaviour of textile dyes onto chitosan. *Process. Saf. Environ.* 106, 1-10.
- Tonucci, M.C., Gurgel, L.V.A., Aquino, S.F.d., 2015. Activated carbons from agricultural byproducts (pine tree and coconut shell), coal, and carbon nanotubes as adsorbents for removal of sulfamethoxazole from spiked aqueous solutions: Kinetic and thermodynamic studies. *Ind. Crop. Prod.* 74, 111-121.
- Velo-Gala, I., López-Peñalver, J.J., Sánchez-Polo, M., Rivera-Utrilla, J., 2014. Surface modifications of activated carbon by gamma irradiation. *Carbon* 67, 236-249.
- Wang, G., Wang, H., Lu, X., Ling, Y., Yu, M., Zhai, T., Tong, Y., Li, Y., 2014. Solid-State Supercapacitor Based on Activated Carbon Cloths Exhibits Excellent Rate Capability. *Adv. Mater.* 26, 2676-2682.

10

FINAL REMARKS AND FUTURE WORK

In this chapter, the general conclusions obtained from this work are highlighted and some suggestions for future work to be developed are presented.

10.1. Final remarks

The main objective of this work was to evaluate the potential of pulp and paper mill sludge to produce activated carbon (AC) and the performance of the produced AC on the removal of pharmaceuticals from water.

The possibility of using primary (PS) and biological (BS) paper mill sludge as raw materials to produce alternative activated carbon (AC) was evaluated and showed that PS, as compared to BS, is a more adequate precursor to produce carbon-based materials, since its pyrolysis resulted in biochar with consistent properties, namely, surface area (S_{BET}), total organic carbon (TOC) and inorganic carbon (IC). Subsequently, the optimization study on the production of AC using PS and a chemical activation process consisting of its impregnation with KOH or K_2CO_3 before pyrolysis, revealed that pyrolysis temperature and activating agent ratio were the main factors influencing the final characteristics of the AC. Pyrolysis at 800 °C and a precursor:activating agent ratio ($w:w$) of 1:1 with KOH resulted in AC (named AC3) with S_{BET} around 1600 m^2g^{-1} and with very good adsorption percentages for carbamazepine (CBZ), sulfamethoxazole (SMX) and paroxetine (PAR) in ultrapure water (between 81 % and 90 %). Adsorption studies with AC3 indicated good adsorption kinetics and adsorption capacities for the three pharmaceuticals, CBZ, SMX, and PAR, in ultrapure water, comparable to a commercial PAC. However, in wastewater matrices, and particularly for SMX, the efficiency of AC3 decreased, which was attributed mainly to electrostatic repulsive forces between adsorbent and adsorbate.

The production of a granular AC (GAC), using PS was also assessed in this work. The obtained GAC under optimized conditions (PSA-PA) showed some physicochemical characteristics similar to a commercial GAC (GACN) used for comparison, namely, in what concerns S_{BET} (around 670 $\text{m}^2 \text{g}^{-1}$). However, PSA-PA revealed a lower adsorption kinetics and adsorption capacity than GACN, behavior attributed to the microporosity of PSA-PA and to the molecular size of the adsorbate molecules. The fixed-bed studies have also shown a decrease in the efficiency of PSA-PA as the complexity of the matrix increased from distilled to wastewater, due to competitive effects in the latter. The thermal regeneration studies indicated an accentuated decrease in the S_{BET} and in the adsorption capacity of PSA-PA from the first regeneration cycle, indicating that more than one cycle of regeneration was not a viable option.

Finally, the modification of the surface chemistry of the PS-based AC, AC3, conducted through four functionalization methodologies, aiming the introduction of amine groups (AC-NH₂ and AC-APTES), the introduction of thiol groups (AC-MPTMS), and the introduction of a covalent organic polymer (AC-COP), showed that the surface enrichment in amine or sulfur containing groups was

successfully achieved. Despite the increase in the nitrogen content verified for AC-NH₂, AC-APTES, and AC-COP, this had no significant expression in the point of zero charge (pH_{pzc}) of the materials. Also, a general reduction of the S_{BET} of the nitrogen-functionalized materials was observed as well as a reduction of the overall adsorption percentages of the pharmaceuticals. The study revealed that, regardless the functionalization, S_{BET} and microporous volume (W_0) remain the main factors contributing to the adsorption of the pharmaceuticals. Interesting was the case of AC-MPTMS, that showed the lowest S_{BET} reduction and comparable adsorption percentages to the non-functionalized AC precursor (AC3), and presented apparently a distinctive behavior in the particular case of SMX adsorption from wastewater matrix, with enhanced adsorption percentage of this compound when compared to AC3, at 25 °C. However, the study on the adsorption of SMX from buffered solutions at pH 8 and from wastewater onto AC-MPTMS, at 25 °C, showed a reduction on the adsorption capacity of AC-MPTMS for SMX in wastewater, possibly due to matrix effects. Also, the determination of the thermodynamic parameters of the adsorption of SMX onto AC3 and AC-MPTMS showed that no great differences in the adsorption thermodynamics of the two materials, both presenting spontaneous and endothermic adsorption processes. Therefore, the functionalization of AC3 did not result in a practical increase of pharmaceuticals adsorption. Still, this work was pioneer on the functionalization of waste-derived AC, with novel results on the properties and application of the functionalized materials that opens a new research line in this field.

Overall, these results demonstrated that PS is an interesting material to be used as precursor to produce powdered AC (PAC) for its application in the removal of pharmaceuticals from water. The produced AC3 presented high S_{BET} and high adsorption efficiency for CBZ, SMX and PAR, mostly in ultrapure water. The increase of the complexity of the matrices led to a reduction in the effectiveness of the produced materials due to the competitive effects of other compounds present, the adsorption conditions like pH, and also the physicochemical properties of both the adsorbent and adsorbates. The production of GAC revealed to be more difficult, once this was not possible without an agglomeration process. Also, the adsorption results obtained for this material, as comparable to the commercial GAC, were less attractive.

These studies provide a possible direction toward the valorization of PS as precursor for the production of carbon adsorbents, mainly PAC, and a possible alternative way of PS management, contributing to a more circular economy approach, without forgetting the possibility of water remediation concerning the removal of pharmaceuticals from water.

10.2. Future work

The obtained results in this work point to the use of PS to produce, mostly, PAC materials. Considering this, further work is to be carried out focusing on the improvement of some of the physicochemical properties of the waste-based AC to enhance their adsorption capacity for pharmaceuticals in wastewater matrices. A possible direction to achieve this goal may be through the exploration of other activation and pyrolysis methodologies, which must also lead to higher product yields. In this sense, microwave pyrolysis may be an interesting approach to this purpose also, possibly, allowing for a more efficient energetic process which can be more economic and environmentally friendly. Additionally, an evaluation of the application of the PAC in large scale and in continuous treatment systems is crucial, being essential to address methods of efficient recovery of the materials, for instance, through the introduction of magnetic properties to the PAC adsorbents permitting their collection by the application of a magnetic field. Finally, it is important to assess to the costs associated to the production of the waste-based AC in large scale and the environmental effects associated to this production and to the real application of the materials.

APPENDIX

Contents

Appendix A

<i>Analytical methodologies applied to the physicochemical characterization of the materials</i>	217
A1. Nitrogen adsorption-desorption isotherms for the determination of S_{BET} and porosity.....	217
A2. Spectroscopic and microscopic techniques	
A2.1. X-Ray Photoelectron Spectroscopy (XPS).....	217
A2.2. Scanning electron microscopy (SEM).....	218
A2.3. Fourier transform infrared (FTIR) spectroscopy with attenuated total reflectance (ATR-FTIR)	218
A2.4. Raman spectroscopy	218
A3. Proximate and ultimate analysis.....	218
A3.1. Proximate analysis.....	218
A3.2. Ultimate analysis	219
A4. Total organic carbon (TOC) and inorganic carbon (IC).....	219
A5. Determination of the point of zero charge (pH_{pzc}).....	219
A6. Boehm's titrations	220

Appendix B

<i>Analytical methodology for the quantification of the pharmaceuticals in solution</i>	221
B1. UV-Vis	221
B2. Micellar Electrokinetic Electrochromatography method.....	221

Appendix C

<i>Supplementary information for the results and discussion sections of the different chapters</i>	223
C3. Supplementary information for CHAPTER 3	223
Figure C3.1. FTIR-ATR spectra of PS and the corresponding carbon adsorbents (P and PW materials) produced from them. F1 and F2 correspond to Factory 1 and Factory 2, respectively; PS1, PS2, PS3, and PS4 indicates lots 1, 2, 3, and 4 of primary sludge, respectively; the P and PW suffix are for pyrolyzed and pyrolyzed + washed materials, respectively.	224/225

Figure C3.2. ATR-FTIR spectra of BS and corresponding carbon adsorbents (P and PW materials) produced from them. F1 and F2 correspond to Factory 1 and Factory 2, respectively; BS1, BS2, BS3, and BS4 indicates lots 1, 2, 3, and 4 of biological sludge respectively; the P and PW suffix are for pyrolyzed and pyrolyzed+washed materials, respectively.....226/227

C7. Supplementary information for CHAPTER 7.....228

Figure C7.1. Breakthrough curves' fittings using the Thomas, Yoon-Nelson and Yan models (Thomas and Yoon-Nelson models are superimposed), for the fixed-bed adsorption of CBZ onto PSA-PA from distilled water using a flow rate ($L d^{-1}$) of a) 4.3, b) 8.6, and c) 13.0.228

Figure C7.2. Breakthrough curves' fittings using the Thomas, Yoon-Nelson, and Yan models (Thomas and Yoon-Nelson models are superimposed), for the fixed-bed adsorption of CBZ onto PSA-PA from wastewater using a flow rate ($L d^{-1}$) of a) 4.3, b) 8.6, and c) 13.0.228

Figure C7.3. Breakthrough curves' fitting using the Thomas, Yoon-Nelson, and Yan models (Thomas and Yoon-Nelson models are superimposed), for the fixed-bed adsorption of a) CBZ, b) SMX, and c) PAR onto PSA-PA from single solutions in wastewater at a flow rate of $4.3 L d^{-1}$229

Figure C7.4. Breakthrough curves' fitting using the Thomas, Yoon-Nelson, and Yan models (Thomas and Yoon-Nelson models are superimposed), for the fixed-bed adsorption of a) CBZ, b) SMX, and c) PAR onto PSA-PA from ternary solutions in wastewater at a flow rate of $4.3 L d^{-1}$229

Figure C7.5. Breakthrough curves' fitting using the Thomas, Yoon-Nelson, and Yan models (Thomas and Yoon-Nelson models are superimposed), for the fixed-bed adsorption of CBZ onto PSA-PA from distilled water for a) cycle 1 (after the first thermal regeneration stage) and b) cycle 2 (after the second thermal regeneration stage).230

References231

APPENDIX A

ANALYTICAL METHODOLOGIES APPLIED TO THE PHYSICOCHEMICAL CHARACTERIZATION OF THE MATERIALS

A1. Nitrogen adsorption-desorption isotherms for the determination of S_{BET} and porosity

For the materials studied in chapters 3, 4, 6, 7, and 9, the nitrogen adsorption isotherms were acquired at $-196\text{ }^{\circ}\text{C}$ using a Micromeritics Instrument, Gemini VII 2380. Before analysis, the materials were outgassed overnight at $120\text{ }^{\circ}\text{C}$. For the materials studied in chapter 8, the nitrogen adsorption isotherms were measured at $-196\text{ }^{\circ}\text{C}$ using a Gemini V 2.00 instrument model 2380. All materials were dehydrated overnight at $200\text{ }^{\circ}\text{C}$ to an ultimate pressure of 1024 mbar and then cooled to room temperature prior to adsorption.

S_{BET} was calculated from the Brunauer–Emmett–Teller equation (Brunauer et al., 1938) in the relative pressure range 0.01–0.1. Pore volume (V_p) was estimated from the amount of nitrogen adsorbed at a relative pressure of 0.99. The micropore volume (W_0) was determined by applying the Dubinin–Radushkevich equation (Dubinin, 1966) or the Dubinin–Astakhov (DA) equation to the lower relative pressure zone of the nitrogen adsorption isotherm.

A2. Spectroscopic and microscopic techniques

A2.1. X-Ray Photoelectron Spectroscopy (XPS)

XPS analysis was performed in an ultra-high vacuum (UHV) system with a base pressure of 2×10^{-10} mbar and equipped with a hemispherical electron energy analyser (SPECS Phoibos 150), a delay-line detector and a monochromatic Al $K\alpha$ (1486.74 eV) X-ray source. High resolution spectra were recorded at normal emission take-off angle and with a pass-energy of 20 eV, providing an overall instrumental peak broadening of 0.5 eV. This technique was applied to the materials produced in chapters 5, 6, 8, and 9.

A2.2. Scanning electron microscopy (SEM)

The superficial morphology of the selected ACs was analyzed by scanning electron microscopy (SEM) using a Hitachi SU-70. The images were obtained at magnitudes between 300 and 50 000x. This technique was applied to the materials produced in chapters 4, 6, 8, and 9. In chapter 8 a Bruker silicon drift detector was used.

A2.3. Fourier transform infrared (FTIR) spectroscopy with attenuated total reflectance (ATR-FTIR)

In chapters 3 and 6, the attenuated total reflectance Fourier transform infrared spectroscopy (ATR-FTIR) spectra were obtained by a Shimadzu-IRaffinity-1 equipment, using an ATR module, under a nitrogen purge. The measurements were recorded in the range 600–4000 cm^{-1} , 4.0 of resolution, 128 scans (chapters 3), 256 scans (chapter 6) and with atmosphere and background correction. In chapter 3, ATR-FTIR was measured on the raw materials (PS and BS) and all the P and PW materials produced from them. In chapter 6, FTIR-ATR was obtained by film deposition, the AC samples were suspended in ultra-pure water and a small drop of the suspension was placed on the top of the ATR crystal and dried with a nitrogen purge, prior to the spectra collection.

In chapter 8, ATR-FTIR was carried out in a FTIR Bruker Tensor 27 instrument with a Golden Gate ATR. AC based materials were dehydrated at 110 °C overnight before FTIR analysis. The ATR-FTIR spectra were recorded in Absorbance mode from 400 cm^{-1} to 4000 cm^{-1} by accumulation of 256 scans.

A2.4. RAMAN spectroscopy

In chapter 8 the RAMAN spectra were acquired in a RAMAN-FT Bruker RFS/100S instrument equipped with a Nd:YAG (1064 nm) laser.

A3. Proximate and ultimate analysis

A3.1. Proximate analysis

In chapters 3, 4, and 6, proximate analysis was performed by thermogravimetric analysis (TGA). The analysis was carried out in a thermogravimetric balance Setsys Evolution 1750, Setaram, TGA mode (S type sensor). Standard methods to determine the moisture (UNE 32002) (AENOR, 1995), volatile matter (UNE 32019) (AENOR, 1985) and ash content (UNE 32004) (AENOR, 1984) were employed.

The experimental procedure for TGA consisted of the sample heating, under nitrogen atmosphere, from room temperature to 105 °C (heating rate of 10 °C min⁻¹); sample was kept at this temperature until total stabilization of the sample mass (approximately 30 min); next, temperature was increased from 105 °C to 950 °C (10 °C min⁻¹), keeping the sample at 950 °C until total stabilization of the sample mass (approximately 30 min); finally, at 950 °C, the carrier gas was automatically switched to air and the sample was maintained at 950 °C until total stabilization of the sample mass. The mass loss observed around 105 °C is attributed to moisture; the mass loss registered from the end of this first step up to the switching of the carrier gas corresponds to volatile matter; the mass loss comprised between the introduction of the air flow and the stabilization of the mass is attributed to fixed carbon content; and lastly the final residue corresponds to ash content.

In chapter 8, thermogravimetric analyses (TGA) were performed on a Shimadzu TGA-50 instrument with a program rate of 5 °C min⁻¹ in air.

A3.2. Ultimate analysis

In chapters 4 and 6 ultimate analysis to determine C, H, N and S was performed in a LECO CHNS-932 elemental analyzer. The oxygen content was calculated by difference in dry basis. Samples' masses used in each analysis ranged from 1 to 2 mg. The carrier gas used was helium (200 mL min⁻¹) and the samples were subjected to combustion at 975 °C using 15 mL of oxygen. Sulfamethazine was used as a standard. In chapter 8, the ultimate analysis was made with a TruSpec 630-200-200 CNHS Analyzer, using the following analysis parameters: sample mass between 1 mg and 2 mg; combustion furnace temperature = 1075 °C; afterburner temperature = 850 °C, and detection method: carbon, infrared absorption; hydrogen, infrared absorption; nitrogen, thermal conductivity.

A4. Total organic carbon (TOC) and inorganic carbon (IC)

Total carbon (TC) and inorganic carbon (IC) analyses in chapters 3, 4, and 6 were performed using a TOC analyzer (Shimadzu, model TOC-V_{CPH}, SSM-5000A, Japan). All the materials were analyzed in triplicate. TOC was calculated by difference between TC and IC.

A5. Determination of the point of zero charge (pH_{pzc})

The point of zero charge (pH_{pzc}) was determined by pH drift method (Prola et al., 2013). For each AC, a predetermined mass of adsorbent was shaken in a polypropylene tube with 0.1 M NaCl

solutions at 10 different initial pH (pH_i) in the range of 2 to 11. The dosage of AC were 0.01 g L^{-1} (chapter 4), 0.05 g L^{-1} (chapter 6), and 0.1 g L^{-1} (chapter 8). The initial pH values were adjusted with NaOH or HCl (0.1 M). The polypropylene tubes were shaken for 24 h at $25 \text{ }^\circ\text{C}$ and the final pH (pH_f) of each tube was measured. The pH_{pzc} was determined by plotting the difference of pH_f and pH_i (ΔpH) versus pH_i and the value corresponding to the pH_{pzc} is where the curve crosses the x-axis ($\Delta\text{pH} = 0$) (Prola et al., 2013).

A6. Determination of acidic and basic groups by Boehm's titrations

The determination of the main surface functional groups of the AC, in chapters 4 and 6, was performed through Boehm's titration method (Boehm, 1994; Ferreira et al., 2016). For that, 35 mL of each reactive bases NaOH, Na_2CO_3 and NaHCO_3 0.05 M, and an acid, HCl 0.05 M, were separately equilibrated with about 350 mg of AC and stirred at 80 rpm during 24 hours at $25 \text{ }^\circ\text{C}$. Then, the solutions were filtered, and 20 mL of each filtrate was titrated with standardized solutions of HCl, in the case of the reactive bases, and NaOH in the case of HCl, to quantify the respective reactants that were neutralized during the initial equilibration. All the solutions were purged with a N_2 flow prior and during the titrations in order to remove the dissolved CO_2 from the solutions. The different acidic groups were estimated as follows: the amount of carboxylic groups was determined by neutralization with NaHCO_3 solution; the amount of lactones was determined by the difference between the neutralization with Na_2CO_3 solution and that determined for the NaHCO_3 solution; the amount of phenols was determined by the difference between the neutralization with NaOH solution and that determined for Na_2CO_3 solution. The amount of total basic groups was estimated by neutralization with HCl solution (Ferreira et al., 2016).

APPENDIX B

ANALYTICAL METHODOLOGY FOR THE QUANTIFICATION OF THE PHARMACEUTICALS IN SOLUTION

B1. UV-Vis

In chapter 4, the quantification of pharmaceuticals in the aqueous phase was carried out by UV–visible spectrometry (T90+UV/visible Spectrometer) at 214 nm for carbamazepine (CBZ) and at 200 nm for sulfamethoxazole (SMX) and for paroxetine (PAR). The calibration curves were applied to a concentration range between 0.5 mg L⁻¹ and 5 mg L⁻¹. All experiments were performed in triplicate. Also, control experiments (pharmaceutical solution without the adsorbent) were carried out simultaneously with adsorption experiments and used as reference for the calculation of adsorption percentages.

B2. Micellar Electrokinetic Electrochromatography method

For the quantification of the pharmaceuticals studied, a micellar electrokinetic chromatography method (MEKC) was used, adapted from the procedure described in Calisto et al. (2011) and (Calisto et al., 2015). The MEKC was performed in a Beckman P/ACE MDQ instrument (Fullerton, CA, USA), equipped with a UV-Vis detector or a photodiode array detection system.

A fused-silica capillary with 75 µm of internal diameter x 375 µm of external diameter, with 40 cm (30 cm to the detector) was dynamically coated. The conditioning of each new capillary was performed as follow:

1. Rinse at 20 psi with 1M of sodium hydroxide (NaOH) for 30 min;
2. Rinse at 20 psi with ultrapure water for 15 min;
3. Rinse at 20 psi with a solution of (hexadimethrine bromide (polybrene) 0.5 % (w/v) in 0.5 M NaCl for 20 min;
4. Rinse at 20 psi with ultra-pure water for 5 min;
5. Rinse at 20 psi with running buffer for 20 min

At the beginning of each working day, the coated capillary was washed with running buffer for 20 min. At the end of the working day the capillary was washed with ultra-pure water for 10 min and the extremities were immersed in ultrapure water.

The sample preparation consisted of the addition of ethylvanillin as internal standard, which was spiked to all samples and standard solutions at a final concentration of 3.34 mg L^{-1} . Also, sodium tetraborate, at a final concentration of 10 mM , was also added to all samples and standard solutions, in order to obtain better peak shape and resolution and higher repeatability (except for the solutions prepared in chapter 9).

The running (separation) buffer consisted of 15 mM of sodium tetraborate and 30 mM of sodium dodecyl sulphate (SDS). Capillary was washed between each run with ultrapure water for 1 min and separation buffer for 1.5 min at 20 psi , and the running buffer was renewed every six runs. The electrophoretic separation was accomplished at $25 \text{ }^\circ\text{C}$, in direct polarity mode at 25 kV , during no longer than 5 min runs.

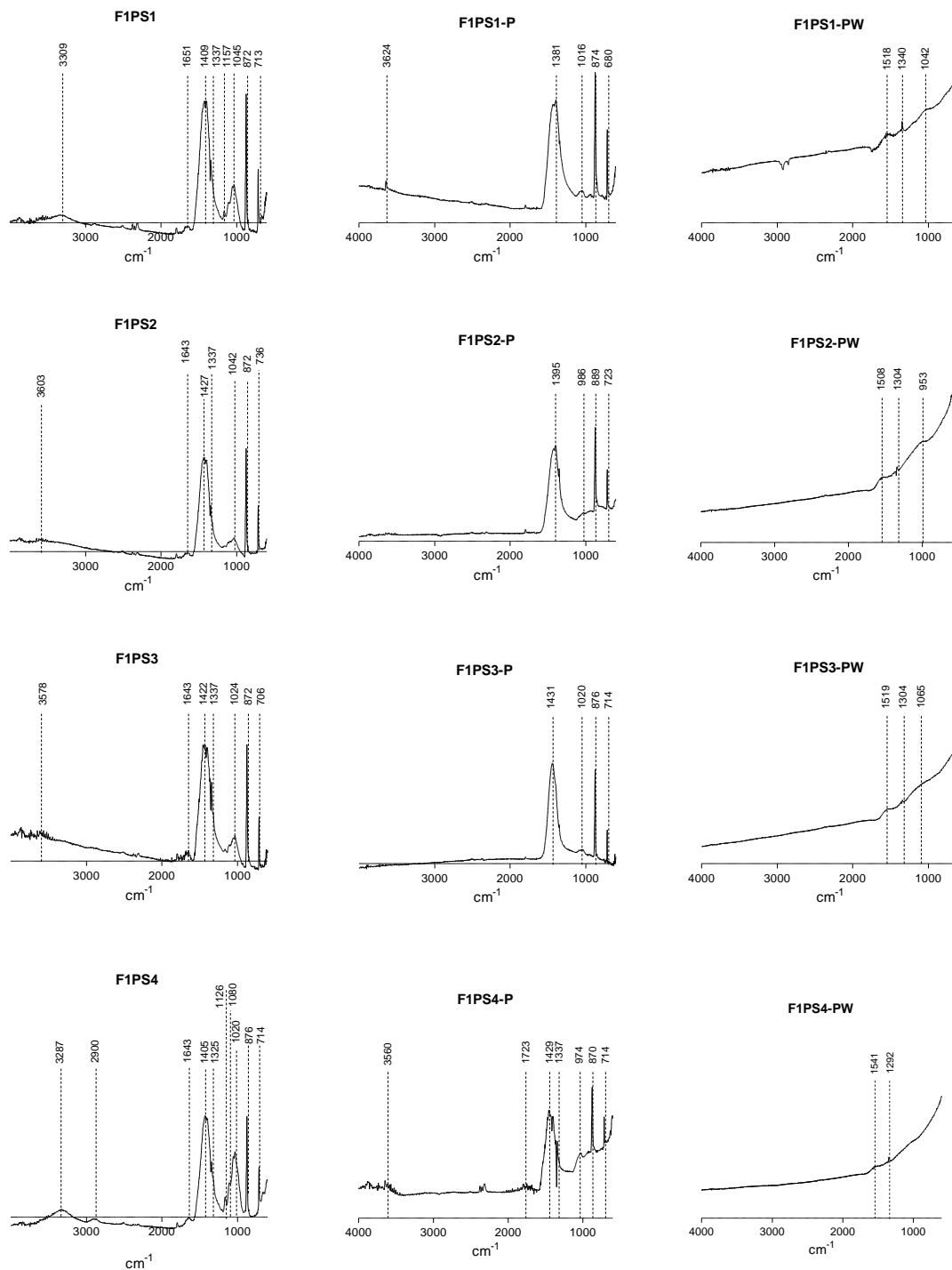
Detection was monitored at 200 nm for sulfamethoxazole (SMX), paroxetine (PAR), lorazepam (LOR), piroxicam (PIR) and venlafaxine (VEN) and at 214 nm for carbamazepine (CBZ).

For each pharmaceutical, calibration was performed by analysing standard solutions with concentrations ranging from 0.25 mg L^{-1} and 5.0 mg L^{-1} . Standards were analysed in quadruplicate and samples in triplicate.

APPENDIX C

SUPPLEMENTARY INFORMATIONS FOR THE RESULTS AND DISCUSSION SECTIONS OF THE DIFFERENT CHAPTERS

C3. Supplementary Information for CHAPTER 3



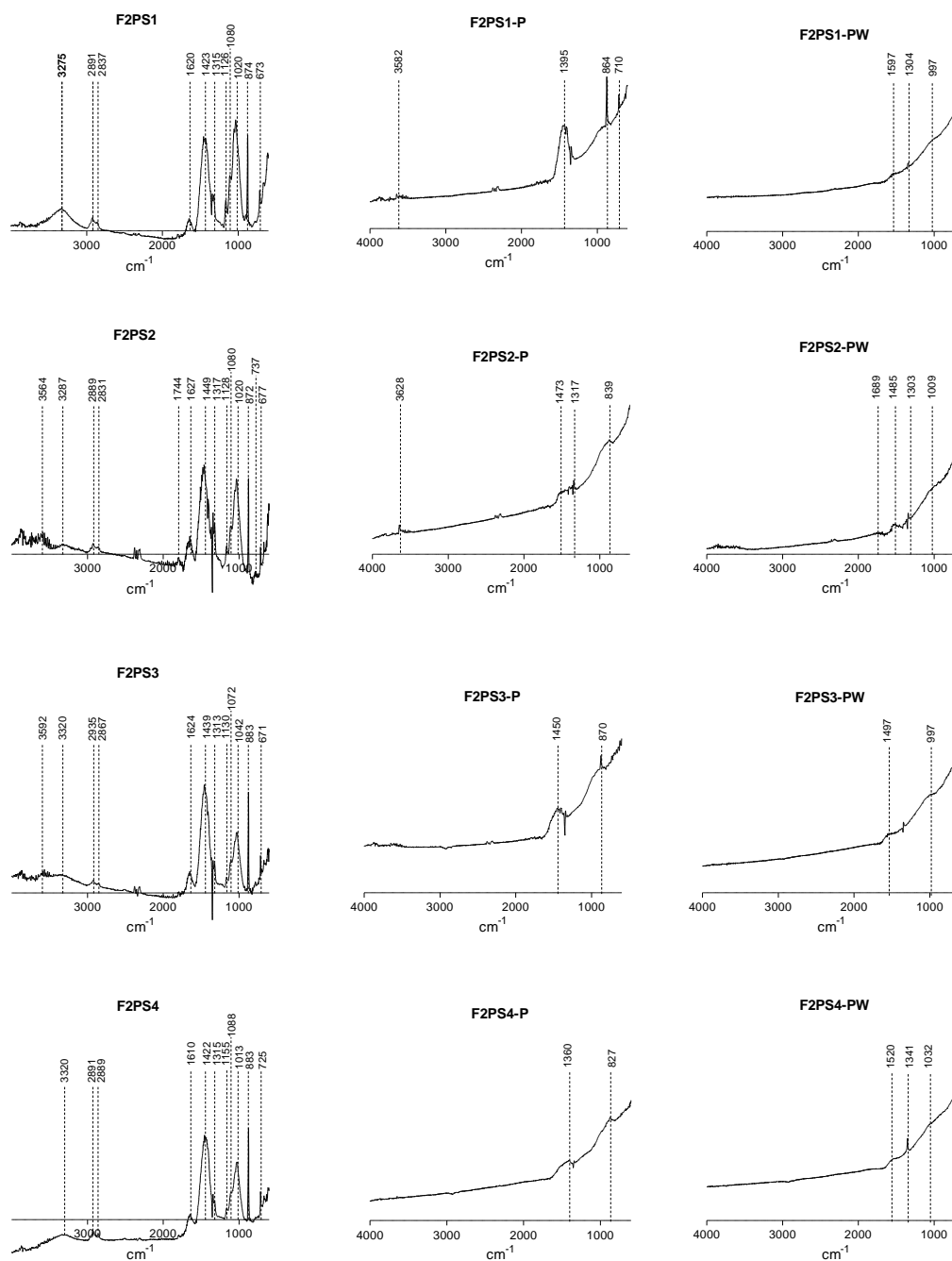
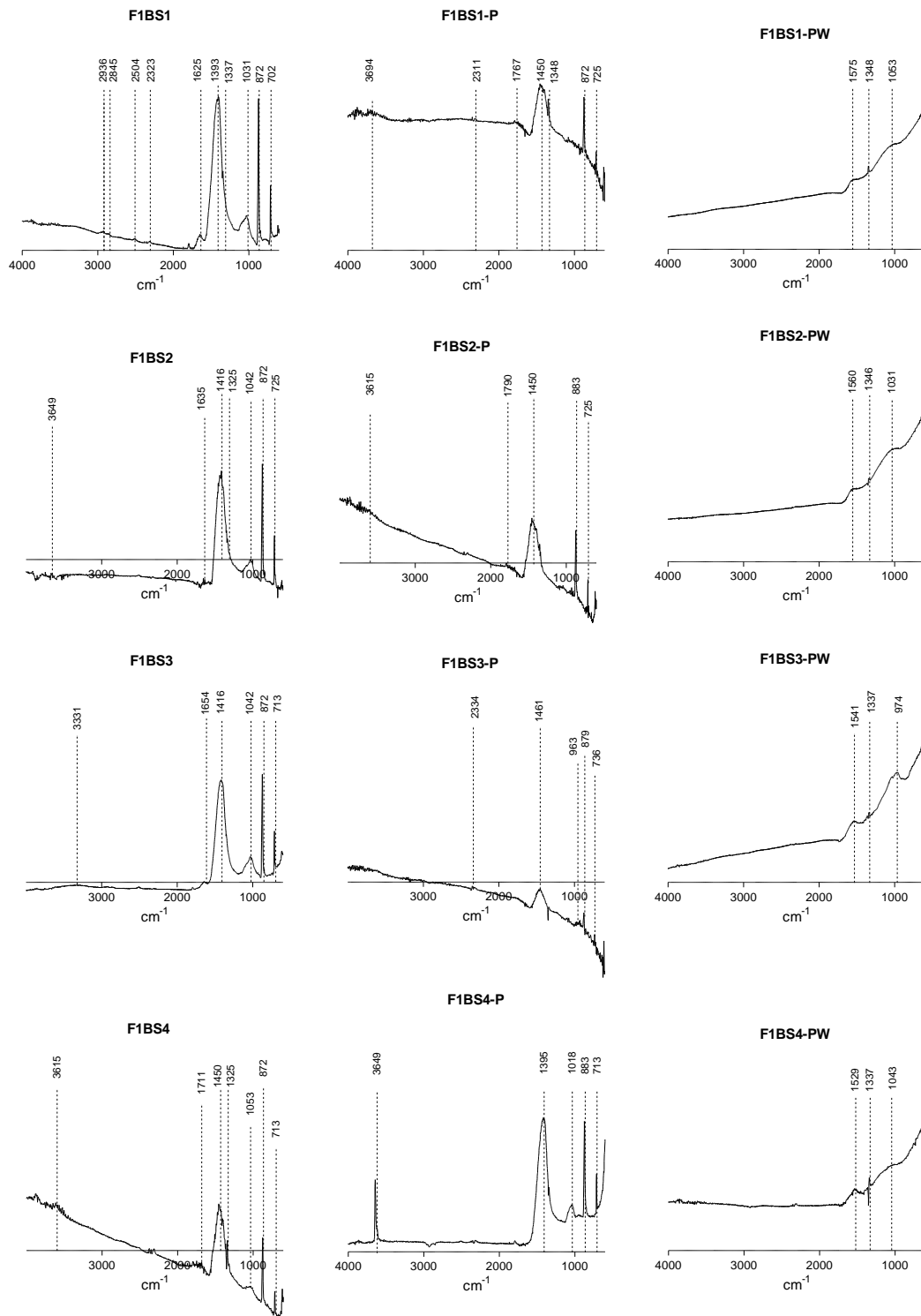


Figure C3.1. ATR-FTIR spectra of PS raw materials and carbon adsorbents (P and PW materials) produced from them. F1 and F2 correspond to Factory 1 and Factory 2, respectively; PS1, PS2, PS3, and PS4 indicates that is the primary sludge, lot 1, 2, 3, and 4, respectively; The P and PW suffix are for pyrolyzed and pyrolyzed + washed materials, respectively.



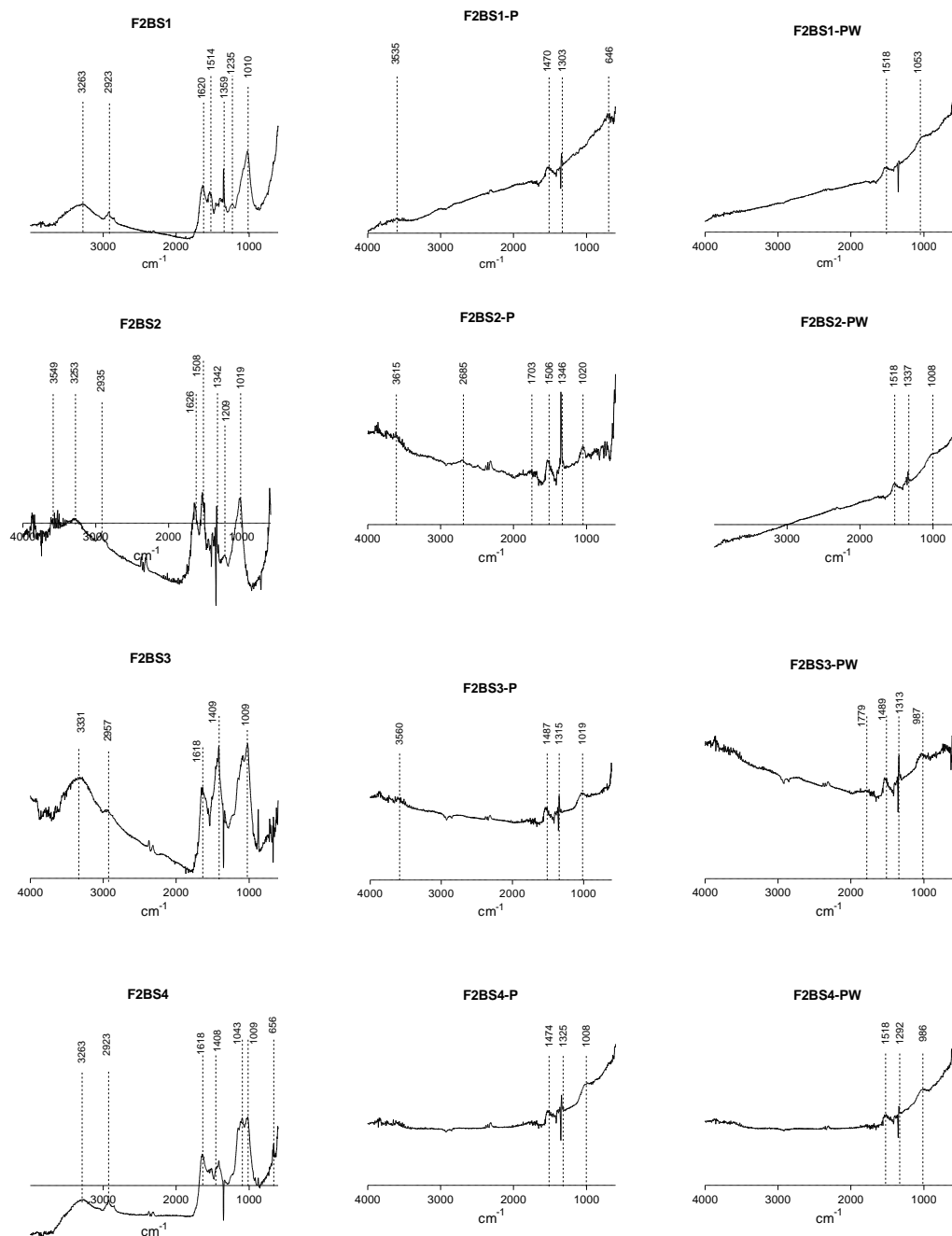


Figure C3.2. ATR-FTIR spectra of BS raw materials and adsorbent carbons (P and PW materials) produced from them. F1 and F2 correspond to Factory 1 and Factory 2, respectively; BS1, BS2, BS3, and BS4 indicates that is the biological sludge, lot 1, 2, 3, and 4, respectively; The P and PW suffix are for pyrolyzed and pyrolyzed + washed materials, respectively.

C7. Supplementary Information for CHAPTER 7

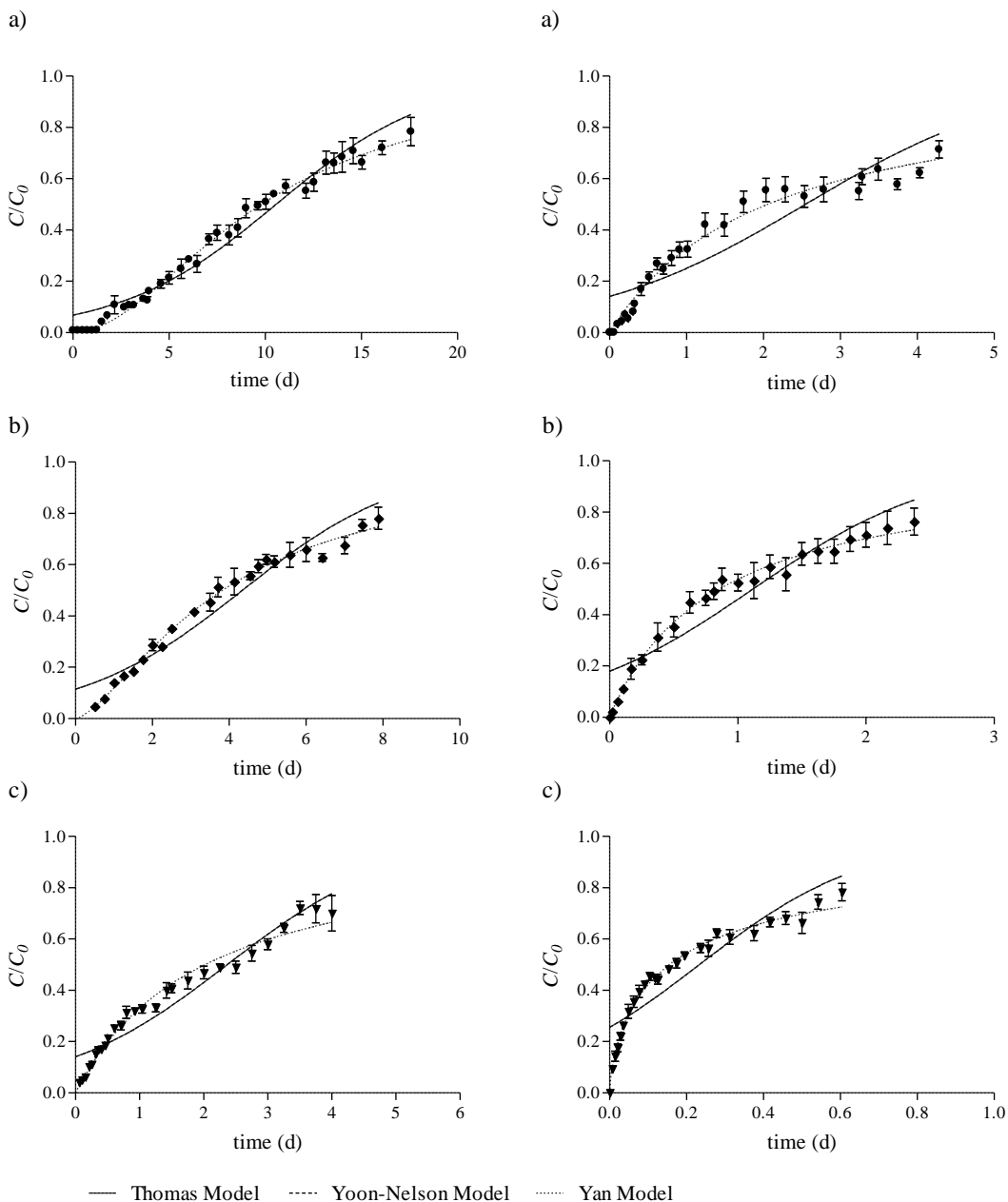


Figure C7.1. Breakthrough curves' fittings using the Thomas, Yoon-Nelson and Yan models (Thomas and Yoon-Nelson models are superimposed), for the fixed-bed adsorption of CBZ onto PSA-PA from distilled water using a flow rate ($L d^{-1}$) of a) 4.3, b) 8.6, and c) 13.0.

Figure C7.2. Breakthrough curves' fittings using the Thomas, Yoon-Nelson, and Yan models (Thomas and Yoon-Nelson models are superimposed), for the fixed-bed adsorption of CBZ onto PSA-PA from wastewater using a flow rate ($L d^{-1}$) of a) 4.3, b) 8.6, and c) 13.0.

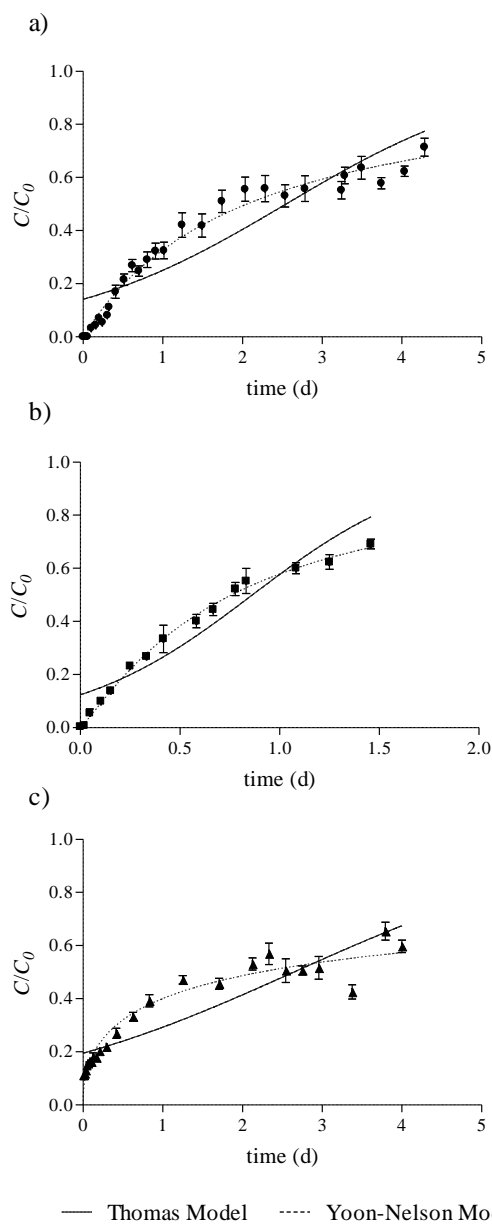


Figure C7.3. Breakthrough curves' fitting using the Thomas, Yoon-Nelson, and Yan models (Thomas and Yoon-Nelson models are superimposed), for the fixed-bed adsorption of a) CBZ, b) SMX, and c) PAR onto PSA-PA from single solutions in wastewater at a flow rate of 4.3 L d⁻¹.

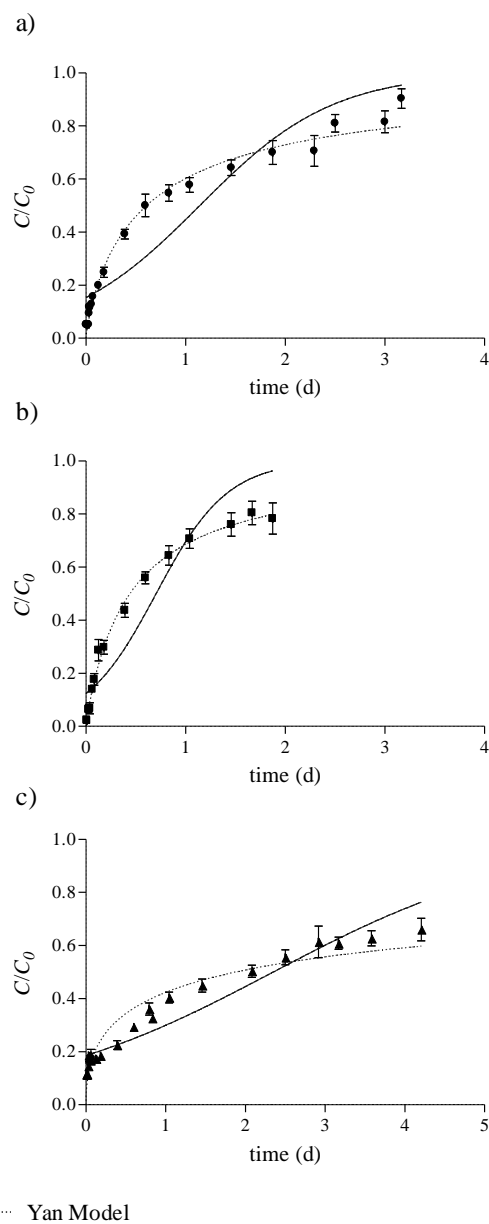


Figure C7.4. Breakthrough curves' fitting using the Thomas, Yoon-Nelson, and Yan models (Thomas and Yoon-Nelson models are superimposed), for the fixed-bed adsorption of a) CBZ, b) SMX, and c) PAR onto PSA-PA from ternary solutions in wastewater at a flow rate of 4.3 L d⁻¹.

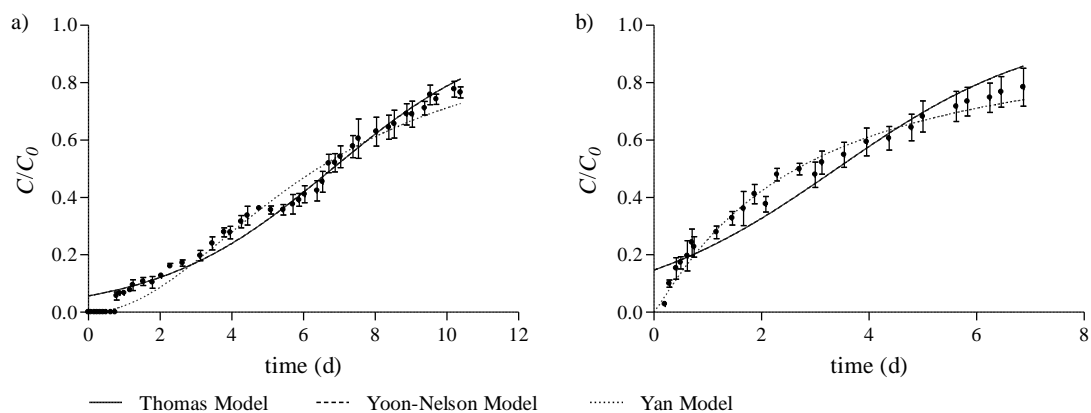


Figure C7.5. Breakthrough curves' fitting using the Thomas, Yoon-Nelson, and Yan models (Thomas and Yoon-Nelson models are superimposed), for the fixed-bed adsorption of CBZ onto PSA-PA from distilled water for a) cycle 1 (after the first thermal regeneration stage) and b) cycle 2 (after the second thermal regeneration stage).

References

- AENOR, 1984. Solid mineral fuels. Determination of ash. Asociación Española de Normalización y Certificación.
- AENOR, 1985. Hard coal and coke. Determination of volatile matter content. Asociación Española de Normalización y Certificación.
- AENOR, 1995. Solid mineral fuels. Determination of moisture in the analysis sample. Asociación Española de Normalización y Certificación.
- Boehm, H.P., 1994. Some aspects of the surface chemistry of carbon blacks and other carbons. *Carbon* 32, 759–769.
- Brunauer, S., Emmett, P.H., Teller, E., 1938. Adsorption of Gases in Multimolecular Layers. *J. Am. Chem. Soc.* 60, 309-319.
- Calisto, V., Domingues, M.R.M., Erny, G.L., Esteves, V.I., 2011. Direct photodegradation of carbamazepine followed by micellar electrokinetic chromatography and mass spectrometry. *Water Res.* 45, 1095-1104.
- Calisto, V., Ferreira, C.I., Oliveira, J.A., Otero, M., Esteves, V.I., 2015. Adsorptive removal of pharmaceuticals from water by commercial and waste-based carbons. *J. Environ. Manage.* 152, 83-90.
- Dubinin, M.M., 1966. Porous structure and adsorption properties of active carbons. In: Walker PL (ed) *Chemistry and Physics of Carbon*. Marcel Dekker Inc., New York, pp 51–120.
- Ferreira, C.I.A., Calisto, V., Otero, M., Nadais, H., Esteves, V.I., 2016. Comparative adsorption evaluation of biochars from paper mill sludge with commercial activated carbon for the removal of fish anaesthetics from water in Recirculating Aquaculture Systems. *Aquacult. Eng.* 74, 76-83.
- Prola, L.D.T., Acayanka, E., Lima, E.C., Umpierrez, C.S., Vaghetti, J.C.P., Santos, W.O., Laminsi, S., Djifon, P.T., 2013. Comparison of *Jatropha curcas* shells in natural form and treated by non-thermal plasma as biosorbents for removal of Reactive Red 120 textile dye from aqueous solution. *Ind. Crop. Prod.* 46, 328-340.

